ISSN 1007-9327 (print)
ISSN 2219-2840 (online)

World Journal of *Gastroenterology*

Weekly Volume 31 Number 19 May 21, 2025

Published by Baishideng Publishing Group Inc

World Journal of Gastroenterology

Contents

Weekly Volume 31 Number 19 May 21, 2025

EDITORIAL

REVIEW

MINIREVIEWS

ORIGINAL ARTICLE

Retrospective Study

LETTER TO THE EDITOR

CORRECTION

ABOUT COVER

AIMS AND SCOPE

The primary aim of *World Journal of Gastroenterology* (*WJG*, *World J Gastroenterol*) is to provide scholars and readers from various fields of gastroenterology and hepatology with a platform to publish high-quality basic and clinical research articles and communicate their research findings online. *WJG* mainly publishes articles reporting research results and findings obtained in the field of gastroenterology and hepatology and covering a wide range of topics including gastroenterology, hepatology, gastrointestinal endoscopy, gastrointestinal surgery, gastrointestinal oncology, and pediatric gastroenterology.

INDEXING/ABSTRACTING

The *WJG* is now abstracted and indexed in Science Citation Index Expanded (SCIE), MEDLINE, PubMed, PubMed Central, Scopus, Reference Citation Analysis, China Science and Technology Journal Database, and Superstar Journals Database. The 2024 edition of Journal Citation Reports® cites the 2023 journal impact factor (JIF) for *WJG* as 4.3; Quartile: Q1. The *WJG*'s CiteScore for 2023 is 7.8.

RESPONSIBLE EDITORS FOR THIS ISSUE

Production Editor: *Si Zhao*; **Production Department Director:** *Xu Guo*; **Cover Editor:** *Jia-Ru Fan.*

NAME OF JOURNAL
World Journal of Gastroenterology

ISSN
ISSN 1007-9327 (print) ISSN 2219-2840 (online)

LAUNCH DATE
October 1, 1995

FREQUENCY
Weekly

EDITORS-IN-CHIEF
Andrzej S Tarnawski

EXECUTIVE ASSOCIATE EDITORS-IN-CHIEF
Xian-Jun Yu, Jian-Gao Fan, Hou-Bao Liu

EDITORIAL BOARD MEMBERS
http://www.wjgnet.com/1007-9327/editorialboard.htm

PUBLICATION DATE
May 21, 2025

PUBLISHING PARTNER
Shanghai Pancreatic Cancer Institute and Pancreatic Cancer Institute, Fudan University
Biliary Tract Disease Institute, Fudan University

INSTRUCTIONS TO AUTHORS
https://www.wjgnet.com/bpg/gerinfo/204

GUIDELINES FOR ETHICS DOCUMENTS
https://www.wjgnet.com/bpg/GerInfo/287

GUIDELINES FOR NON-NATIVE SPEAKERS OF ENGLISH
https://www.wjgnet.com/bpg/gerinfo/240

PUBLICATION ETHICS
https://www.wjgnet.com/bpg/GerInfo/288

PUBLICATION MISCONDUCT
https://www.wjgnet.com/bpg/gerinfo/208

POLICY OF CO-AUTHORS
https://www.wjgnet.com/bpg/GerInfo/310

ARTICLE PROCESSING CHARGE
https://www.wjgnet.com/bpg/gerinfo/242

STEPS FOR SUBMITTING MANUSCRIPTS
https://www.wjgnet.com/bpg/GerInfo/239

ONLINE SUBMISSION
https://www.f6publishing.com

PUBLISHING PARTNER's OFFICIAL WEBSITE
https://www.shca.org.cn
https://www.zs-hospital.sh.cn

World Journal of Gastroenterology

Submit a Manuscript: https://www.f6publishing.com

World J Gastroenterol 2025 May 21; 31(19): 106628

DOI: 10.3748/wjg.v31.i19.106628

ISSN 1007-9327 (print) ISSN 2219-2840 (online)

EDITORIAL

Machine learning in colorectal polyp surveillance: A paradigm shift in post-endoscopic mucosal resection follow-up

Vasily Isakov

Specialty type: Gastroenterology and hepatology

Provenance and peer review: Invited article; Externally peer reviewed.

Peer-review model: Single blind

Peer-review report's classification

Scientific Quality: Grade B, Grade B, Grade C

Novelty: Grade B, Grade B, Grade D

Creativity or Innovation: Grade B, Grade B, Grade C

Scientific Significance: Grade B, Grade B, Grade C

P-Reviewer: Gadour E; Mubarak M; Yang S

Received: March 4, 2025

Revised: April 6, 2025

Accepted: May 6, 2025

Published online: May 21, 2025

Processing time: 78 Days and 21.3 Hours

Vasily Isakov, Department of Gastroenterology and Hepatology, Federal Research Center of Nutrition, Biotechnology and Food Safety, Moscow 115446, Russia

Corresponding author: Vasily Isakov, MD, PhD, Professor, Department of Gastroenterology and Hepatology, Federal Research Center of Nutrition, Biotechnology and Food Safety, 21 Kashirskoye Shosse, Moscow 115446, Russia. vasily.isakov@gmail.com

Abstract

Colorectal cancer remains a major health concern, with colorectal polyps as key precursors. Endoscopic mucosal resection (EMR) is a common treatment, but recurrence rates remain high. Traditional surveillance strategies rely on polyp characteristics and completeness of the resection potentially missing key risk factors. Machine learning (ML) offers a transformative approach by integrating patient-specific data to refine risk stratification. Recent studies highlight ML models, such as Extreme Gradient Boosting, which outperform conventional methods in predicting polyp recurrence within one-year post-EMR. These models incorporate factors like age, smoking status, family history, and pathology, optimizing follow-up recommendations and minimizing unnecessary procedures. Artificial intelligence (AI)-driven tools and web-based calculators enhance clinical workflow by providing real-time, personalized risk assessments. However, challenges remain in external validation, model interpretability, and clinical integration. Future surveillance strategies should combine expert judgment with AI insights to optimize patient outcomes. As gastroenterology embraces AI, ML-driven surveillance represents a paradigm shift, advancing precision medicine in colorectal polyp management. This editorial explores AI's role in transforming post-EMR follow-up, addressing benefits, limitations, and future directions.

Key Words: Colorectal polyps; Endoscopic mucosal resection; Colorectal polyp recurrence; Machine learning; Artificial intelligence; Recurrence risk assessment; Surveillance strategies

Core Tip: The recurrence rates of colorectal polyps after endoscopic mucosal resection remain high. Traditional surveillance strategies rely only on polyp characteristics, potentially missing important risk factors. Machine learning-based models leveraging patient- and polyp-related factors may accurately predict polyp recurrence. Personalized machine-learning-driven risk stratification may optimize surveillance, reduce unnecessary procedures, and improve early cancer detection and cost-effectiveness. Future models should be validated across diverse populations.

Citation: Isakov V. Machine learning in colorectal polyp surveillance: A paradigm shift in post-endoscopic mucosal resection follow-up. *World J Gastroenterol* 2025; 31(19): 106628
URL: https://www.wjgnet.com/1007-9327/full/v31/i19/106628.htm
DOI: https://dx.doi.org/10.3748/wjg.v31.i19.106628

INTRODUCTION

The use of artificial intelligence (AI) and machine learning (ML) in the medical field has shown promising advancements, particularly in the detection and prediction of colorectal polyps and colorectal cancer. These technologies are being integrated into colonoscopy procedures to enhance the detection rates of polyps, which are precursors to colorectal cancer, and to predict the recurrence of colorectal cancer after treatment. By leveraging electronic health records, imaging data, and histopathological features, ML models aim to enhance the early detection of colonic polyps and improve patient outcomes. A new way to use ML was demonstrated in the study by Shi *et al*[1] recently published in the *World Journal of Gastroenterology*, in which they tried to predict polyp recurrence within one year after polypectomy.

Several studies have developed ML models to predict the presence of colorectal polyps using noninvasive methods. For instance, a study utilized electronic health records to create a diagnostic model using the adaptive boosting machine algorithm, achieving an area under curve (AUC) of 0.675, indicating moderate predictive performance for colorectal polyps[2]. Another study focused on deep learning algorithms for real-time polyp detection during colonoscopies, achieving high sensitivity and specificity with an AUC of 0.984, demonstrating the potential of ML in enhancing colonoscopy accuracy[3]. ML has also been used to differentiate between benign and premalignant polyps by using computed tomography colonography. A random forest model achieved an AUC of 0.91, showing promise in noninvasively distinguishing polyp types, which is crucial for determining appropriate treatment strategies[4].

According to recent meta-analyses, AI-based systems have significantly improved the detection rates of adenomas and polyps during colonoscopy. Studies have shown that colonoscopies utilizing AI have higher adenoma detection rates and polyp detection rates than colonoscopies without AI. Specifically, AI systems increased adenoma detection rates to 29.6% compared to 19.3% without AI, and polyp detection rates to 45.4% compared to 30.6% without AI, demonstrating a substantial improvement in detection capabilities[5,6]. These systems are particularly effective in identifying small non-advanced adenomas, although they do not show a significant difference in detecting advanced adenomas[5]. Moreover, these systems have demonstrated high accuracy in histology prediction, with an AUC of 0.96, and have outperformed non-expert endoscopists in both detection and characterization tasks[7]. Timely detection and removal of colonic polyps with subsequent appropriate surveillance programs are crucial for reducing mortality due to colon cancer. The recurrence rate of colonic polyps after endoscopic mucosal resection (EMR) varies depending on the technique. Generally, recurrence rates are higher with standard EMR than with advanced techniques. The local recurrence rate for polyps ≥ 10 mm removed with standard EMR varies between 11% and 20% up to 12 months follow-up according to different meta-analyses[8,9]. Advanced EMR techniques, such as cold snare EMR[10], argon plasma coagulation, snare tip soft coagulation[11], and endoscopic submucosal dissection[12] significantly reduce recurrence rates.

Unfortunately, the high risk of metachronous polyps after bowel screening polypectomy requires a surveillance program that is determined by the characteristics of the removed polyp, such as size, number, and morphology. According to these criteria, patients are classified as high-risk, intermediate/low-risk, and corresponding intervals for surveillance are established by guidelines[13-18]. In addition to the obvious impact of surveillance on the early diagnosis and curative treatment of colon cancer, it has been widely criticized for its poor cost efficacy, low compliance, high demand for resources, and underestimation of patient characteristics for the risk of metachronous polyps after bowel screening polypectomy. Up to 20% of total colonoscopies are performed for surveillance after polypectomy, but only 36,6% of them were prescribed correctly[19]; however, during the same period, the demand for colonoscopy for average-risk screening increased nearly 3-fold[20]. This means that more resources will be necessary for screening, but at least the 1/5 of them are already used for surveillance programs that are often non-compliant. The compliance with surveillance guidelines varies significantly. In Israel, only 57.4% of the recommendations for surveillance were compatible with the guidelines, whereas 37% of the recommendations were for shorter interval[21]. Some studies reported high adherence rates, such as 86.5% compliance with British guidelines[22], while others indicated much lower adherence, such as 13.8% compliance with American guidelines[23]. Interestingly, in this study, 25.5% of the patients underwent surveillance endoscopy earlier than recommended, and none were diagnosed with malignancy. However, 45.8% of the patients had surveillance scopes later than recommended or were lost to follow-up. Among these patients, two actually were diagnosed with malignancy 3 and 5 years after their recommended surveillance scope date, respectively[23]. A recent meta-analysis showed that 38% of surveillance colonoscopies were performed earlier than their respective national clinical guidelines suggested[24]. Analysis of Medicare beneficiaries in the United States showed that at five years after bowel

screening polypectomy only 45.7% received another colonoscopy, with 32.3% of procedures including polypectomy[25]. Moreover, the use of colonoscopy for surveillance has decreased over the four-year study period. Coupled with other data showing the overuse of follow-up colonoscopy in patients without polyps, there appears to be a significant discordance between guidelines and actual practice. Compliance variability may contribute to the poor cost-efficacy of surveillance programs, which is one of the clear disadvantages that have become evident in recent years. A decision analysis model comparing strategies for performing or not performing one-year endoscopic surveillance in 60-year-old patients who underwent an initial endoscopic polypectomy demonstrated that 345 colonoscopies per year are needed to detect one colorectal cancer case and 1437 colonoscopies to prevent one colorectal cancer-related death[26].

Extending intervals for surveillance colonoscopy for high-risk patients for 3 years, which is accepted in the majority of guidelines, definitely reduces costs but does not seem to increase the efficacy of surveillance. A retrospective analysis involving 33011 patients who had adenomas removed during colonoscopies at 17 hospitals in the United Kingdom revealed that, in the absence of surveillance, the incidence of colorectal cancer was comparable to that of the general population for both low-risk [standardized incidence ratios: 0.86, 95% confidence interval (CI): 0.73-1.02] and intermediate-risk (1.16, 0.97-1.37) groups. However, it was notably higher among high-risk patients (1.91, 1.39-2.56)[27]. However, only 9% of the study population was classified as high-risk. The authors concluded that low- or intermediate-risk patients could be managed by screening rather than surveillance. According to these data updated guidelines in many countries simplify the findings of an index colonoscopy into two categories: "low-risk" in which surveillance is not needed and "high-risk" for which surveillance is recommended[13,18,28]. However, the United States Multi-Society Task Force classifies them into six risk categories with different recommendations[17].

A multicentered study which was conducted in United Kingdom and including patients who underwent polypectomy during screening colonoscopy (2009-2016) followed by surveillance retrospective analysis showed that the rate of non-advanced and advanced metachronous polyps was higher in British Society of Gastroenterology (BSG) 2020 high-risk *vs* low-risk patients (44.4% *vs* 35.4% for non-advanced and 15.7% *vs* 11.8% for advanced, $P < 0.001$), but the colorectal cancer rate was similar (0.6% *vs* 1.2%)[29]. This means that the BSG 2020 criteria correlated with metachronous polyps but did not differentiate between advanced and non-advanced lesions and were not predictive of cancer. The results of these studies indicated that risk stratification may benefit from refinement. It seems logical to evaluate the addition of a panel of novel risk factors for metachronous lesion development to the existing risk scores based on polyp number and morphology. Multiple factors such as patient characteristics or proteomic and genomic features of the index polyp tissue may be used[30], with the aim of increasing the positive yield of surveillance colonoscopy and reducing unnecessary procedures for those at a lower risk.

According to a meta-analysis, the detection of colorectal cancer and advanced polyps during surveillance colonoscopy in older individuals was higher than that in younger controls; however, the absolute risk increase for both was small[31]. In most guidelines, the age of the patient is used as a rule for restriction of surveillance rather than a risk factor for polyp recurrence. Thus, the guidelines of the BSG indicate that surveillance should only be performed in people whose life expectancy is greater than 10 years, and in general not in people older than 75 years[13]. The European Society of Gastrointestinal Endoscopy guidelines recommend cessation of surveillance at the age of 80 years or if the expected life expectancy is short due to comorbidities[28]. In contrast, in Japanese guidelines, the age of patients was not mentioned as surveillance endoscopy continued even in the 80s due to the longest life expectancy in the world[14].

Obesity and metabolic syndrome components are also considered important risk factors for metachronous polyps after bowel screening polypectomies. Thus, in a retrospective cohort study including 7473 participants with a median follow-up of 8,5 years after index polypectomy, 619 participants (8.3%) developed advanced colorectal neoplasms. Weight gain of ≥ 3% from baseline was reported as an independent risk factor for metachronous advanced colorectal neoplasm in both men and women, regardless of age[32]. Interestingly, weight loss due to bariatric surgery mitigates the risk of metachronous polyps, mainly in men, coincided with improvement in metabolic syndrome parameters[33,34]. However, components of metabolic syndrome may be associated with different types of lesions. A case-control study of 828 subjects without diabetes and no family or personal history of colorectal cancer showed that abdominal obesity, hypertension, and high HbA1c percentage were independently associated with adenomas, whereas a high triglyceride to high-density lipoprotein cholesterol ratio was associated with serrated polyps[35]. These patient characteristics [such as body mass index (BMI), metabolic syndrome components, and routine blood analyses] are easily accessible through electronic health records and may help select high-risk patients for metachronous polyps after bowel screening polypectomy.

Smoking is a significant risk factor for recurrence of colon polyps after polypectomy. The risk is notably higher in those with a history of heavy smoking, as indicated by pack-years[36-38]. Current smokers also show increased odds of developing hyperplastic polyps, particularly in the distal colon[39]. While smoking cessation reduces the risk slightly, former smokers still face a higher risk of recurrence than never-smokers[36,40]. This finding suggests that the effects of smoking on polyp recurrence are not entirely reversible and underscores the importance of smoking cessation programs as part of post-polypectomy care to mitigate the risk of recurrence.

Whether adding these or more patient characteristics to the established risk factors for metachronous polyps after bowel screening polypectomy will improve the efficacy of surveillance is unknown. However, the results of a study recently published in *World Journal of Gastroenterology*, in which Shi *et al*[1] constructed an ML-based predictive model for the relapse of the colonic polys one year after polypectomy clarify this point. Data from 1694 patients who underwent their first EMR for colorectal polyp removal with a one-year follow-up colonoscopy were retrospectively collected at three medical centers. In addition, 166 patients were prospectively enrolled to test the generalizability of the model. The dataset from the retrospective cohort was randomly divided into the training and validation sets. The training set was used to develop the model, allowing it to learn data patterns and extract effective features, whereas the validation set was used to evaluate the model's performance and identify any overfitting challenges. To build the predictive models, various ML algorithms were utilized, including support vector machine, random forest, decision trees, and Extreme Gradient

Boosting (XGBoost). Finally, an interactive and visual web-based calculator was developed.

Authors used in the model constructing process polyp-related features which were typical for all modern guidelines for surveillance and patient-related variables like age, sex, family history, BMI, *Helicobacter pylori* (*H. pylori*) infection, smoking, hematochezia, constipation, diarrhea, diabetes, hypertension, coronary heart disease, hyperlipidemia, and alcohol consumption. They also used serum levels of uric acid, total bilirubin, total bile acid, hypersensitive C-reactive protein, carcinoembryonic antigen, and carbohydrate antigens (CA, including CA724, CA199, and CA242). Multivariate analysis revealed that eight variables were independent predictors of colorectal polyp recurrence one year after EMR. These variables included age, family history, smoking, diarrhea, polyp size, number of polyps, *H. pylori* infection, and hazard classification (non-neoplastic polyps as reference, non-progressive adenoma, and progressive adenoma). Among the models, XGBoost demonstrated the highest AUC in the training, internal validation, and prospective validation sets, with AUCs of 0.909 (95%CI: 0.89-0.92), 0.921 (95%CI: 0.90-0.94), and 0.963 (95%CI: 0.94-0.99), respectively. The importance ranking of the feature variables in the XGBoost model, from highest to lowest, was as follows: Smoking, family history, age, number of polyps ≥ 3, progressive adenoma, diarrhea, *H. pylori* infection, polyp size > 1 cm, non-progressive adenoma, and polyp size 0.5-1 cm.

Among the four ML algorithms used by the authors, XGBoost demonstrated the highest AUCs for all datasets. However, different ML models have been used successfully in other studies. The random forest ML model demonstrated good performance, with an AUC of 0.859 for young-onset colorectal cancer risk stratification[41]. The Light Gradient Boosting Machine algorithm was successfully used for the development and internal validation of an ML-based colorectal cancer risk prediction model[42]. The adaptive boosting machine model exhibits the best performance among the nine ML models in the development and validation of ML algorithms for the prediction of colorectal polyps based on electronic health records[2]. Therefore, it is a good approach to test as many ML algorithms as possible, which are suitable for the selected task and choose the one that demonstrates the best performance.

High accuracy for the prediction of recurrent polyps is based on the unique approach in which ML provides a weighted importance rank of all risk factors against each other[1]. This can be clearly demonstrated when you try to use the developed application (https://webcalculatorsyh.shinyapps.io/XGBoost/) to put different values for patient variables (Figure 1). From Figure 1, it is clear that patient of 60 years old with less than three non-neoplastic polyps (≥ 0.5 cm has a chance of recurrence of 10% after 1 year. However, patients with the same polyp features and age, but who are *H. pylori*-positive smokers with diarrhea, have a higher chance of recurrence (> 86%). Smokers that were different only by age (60 years old *vs* 30 years old) demonstrate the 3 times difference in recurrence chance (39.1% *vs* 12.8%). Interestingly, the importance rank of the variables related to patients in some scenarios was higher than that of the variables related to polyps.

A clear advantage of this approach is the opportunity to personalize surveillance. According to the guidelines based only on polyp features, all patients shown in Figure 1 will be excluded from the surveillance program and move to screening, even when the prediction of recurrence is 86%. The limitation of this model is the datasets that were used by ML. This model provides excellent results in predicting recurrent colonic polyps in a Chinese population dataset on which the model was trained, but will it be also effective in other population? In China, a large multicenter study found that the majority of recurrent polyps after removal occur almost entirely within the first year, with a rate approaching 60%[43]. Therefore, the surveillance intervals recommended by the Chinese expert consensus on colonoscopy are significantly shorter than those recommended by other guidelines. If a similar model is developed for other populations, it will be necessary to create representative datasets and it is highly likely that the list of independent predictors of polyp recurrence will be different, and its importance rank will not be similar to this model. For example, in economically developed countries in the western hemisphere, the prevalence of *H. pylori* is much lower than that in China, and the prevalence of obesity and metabolic syndrome is higher, which may change their importance rank in prediction models for colonic polyp recurrence.

Developing ML models for medical applications faces several significant barriers to generalization, such as the ability of a model to perform effectively across diverse patient populations and clinical settings. Medical data often exhibit substantial variability due to differences in patient demographics, disease prevalence, and clinical practices across institutions. This heterogeneity can lead to models that perform well on training data but fail to generalize to new settings. In addition, issues such as incomplete or inconsistent data impede model reliability[44]. Variations in data collection methods, equipment, and electronic health record systems across healthcare institutions introduce inconsistencies that hinder model generalization. Differences in coding definitions, laboratory assays, and imaging protocols can result in models that are not transferable between settings[45]. Fortunately, for the ML model in predicting the recurrence of colonic polyps, some barriers are not irresistible. Endoscopic equipment in many countries is comparable in terms of technical abilities, guidelines for colon preparation, colonoscopy procedure protocols, and polyp description and classification are well standardized, making at least a part of the ML algorithm, which uses polyp-related features, less hindered for generalization. If the training data are not representative of the broader patient population, ML models may perpetuate existing biases, leading to disparities in healthcare outcomes. For example, models trained predominantly on data from one demographic or ethnic group may underperform when applied to under-represented populations. However, this type of barrier is possible to overcome only by collected new dataset from representative population and repeat the protocol of Shi *et al*[1]. In other words, distributing toolkits or shareable data science notebooks as long as researchers can train and validate local models locally seems the only way to effectively implement ML models for predicting the recurrence of colonic polyps in different settings.

Integrating AI into medical decision making raises several important ethical considerations that must be carefully addressed to ensure patient safety, equity, and trust within healthcare systems. First of all, patient privacy and data security have emerged as significant concerns owing to the large volumes of sensitive patient data required by ML. Current data protection frameworks may not fully safeguard against unauthorized access or misuse, highlighting the

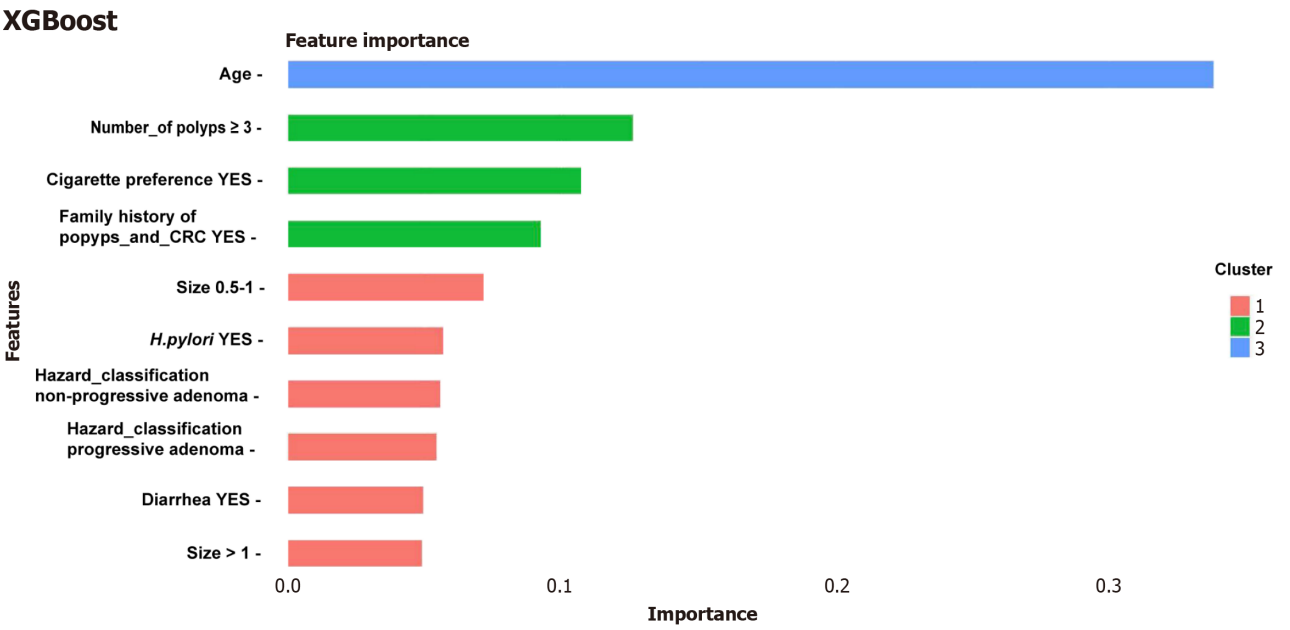

Age	Number of polyps	Size	Hazard classification	*H.pylori*	Family history of polyps/CRC	Cigarette preference	Diarrhea	Prediction
60	< 3	< 0.5	Non-neoplastic polyp	NO	NO	NO	NO	10.1%
60	< 3	< 0.5	Non-neoplastic polyp	YES	NO	YES	YES	86.31%
60	< 3	< 0.5	Non-neoplastic polyp	NO	NO	YES	NO	39.18%
30	< 3	< 0.5	Non-neoplastic polyp	NO	NO	YES	NO	12.8%

Figure 1 Colonic polyps recurrence risk prediction simulation using web-based calculator. Generated at: https://webcalculatorsyh.shinyapps.io/XGBoost/.

need for stronger protection to prevent privacy breaches and data exploitation[46]. However, it is a major problem for any ML study in which patient factors are used, which sometimes extend far from the depersonalized results of the frequency food questionnaire or the number of cigarettes smoked. Thus, the concept of informed consent requires careful consideration. Patients should not only be explicitly informed about AI involvement in their care, including the role of AI, potential benefits, and associated risks, but should also decide what of their data may be used for ML training, ensuring respect for patient autonomy. However, more important for the implementation of the results of the study is the problem of dataset bias, as AI-driven systems have the potential to perpetuate biases found in historical healthcare data, leading to disparities in diagnosis, treatment, prediction of recurrence, and overall care[47]. Therefore, it is essential to develop and implement algorithms trained on diverse and representative datasets to mitigate these biases and promote fairness. Shi *et al*[1] attempted to reduce the dataset bias by randomly dividing the dataset from a retrospective cohort of 1694 patients into training and validation sets. However, it does not exclude the bias related to ethnically and geographically homogenous populations included in the dataset, and the time frame selected by the authors for retrospective inclusion of cases may be more important for dataset bias. Thus, endoscopic diagnostic techniques used during the last 2 years are far more sophisticated than those used 10 years ago; therefore, the bias may be related to different evaluations of the polyps, as the authors used in the model constructing process polyp-related features. Authors selected 5-year period of inclusion of cases from three hospitals in the dataset[1], which seems minimally acceptable considering the very fast implementation of innovations in endoscopy. For many AI-driven systems, the issue of transparency and explainability arises due to the "black box" nature of certain ML models, potentially limiting healthcare professionals' ability to interpret and trust AI-driven recommendations. Therefore, enhancing the interpretability of AI systems is critical for maintaining accountability and supporting informed clinical decision-making. Fortunately, for the ML model used by Shi *et al*[1], all factors selected by ML can be easily explained as to why they are associated with increased colonic polyp recurrence, as supported by a number of published studies. However, it is more interesting why other factors, such as BMI or metabolic syndrome components, which are known risk factors for colonic polyps, were not selected during the ML process. It is universally agreed that AI should function as a support rather than a replacement for healthcare professionals' judgment, and professional oversight remains crucial to ensure that clinical decisions integrate AI recommendations with clinical expertise and patient values[48]. In the case of the prediction of polyp recurrence, it is clear that the ML algorithm proposed by Shi *et al*[1] already includes polyp-related risk factors on which existing guidelines for surveillance are based, but it provides a more personalized and better risk assessment tool for healthcare professionals, rather than replacing existing standards of care.

The advent of ML techniques for colonic polyp detection has generated a significant shift towards enhancing the efficacy and cost-effectiveness of screening procedures. AI-assisted colonoscopy has consistently demonstrated the ability to increase adenoma detection rates and reduce adenoma miss rates compared with standard colonoscopy. Studies have shown that AI systems can detect more adenomas per colonoscopy and improve the polyp detection rate, particularly for diminutive and serrated lesions, which are often missed during conventional procedures[49-51]. By enhancing detection accuracy, AI reduces the likelihood of interval colorectal cancers, which develop between screening intervals, thereby lowering the long-term costs associated with cancer treatment[52]. AI systems enable real-time characterization of polyps, distinguishing between neoplastic and non-neoplastic lesions with high accuracy. This capability supports the adoption of "leave-in-situ" and "resect-and-discard" strategies, which avoid unnecessary polypectomies and histopathological examinations for benign lesions[53,54]. For instance, a study in Spain found that AI-assisted colonoscopy avoided 173 polypectomies and 370 histopathologies per 1000 patients, leading to significant cost savings[55].

AI systems provide real-time assistance during colonoscopy, reducing the time required for examination by optimizing lesion detection and characterization. This increased efficiency enables endoscopists to perform more procedures within the same timeframe, thereby improving productivity and reducing operational costs[56]. Additionally, AI can standardize quality metrics such as withdrawal time and bowel preparation adequacy, further enhancing the overall efficiency of colonoscopy services[57]. AI can enhance the performance of noninvasive screening tests, such as fecal immunochemical tests, by improving the detection of advanced adenomas and early-stage cancers. A novel AI-based algorithm combining stool biomarkers and fecal immunochemical tests analysis achieved high sensitivity (82.2%) for advanced adenomas and specificity (90.1%) for non-neoplastic lesions, reducing the need for unnecessary colonoscopies and optimizing the diagnostic workflow[58,59].

Multiple cost-effectiveness analyses have demonstrated that AI-assisted colonoscopy is a cost-effective strategy for colorectal cancer screening. For example, a Canadian study found that the incremental cost-effectiveness ratio for AI-assisted colonoscopy was dominant, meaning that it was both more effective and less costly than conventional colonoscopy[60]. Similarly, an Italian study reported that the implementation of AI systems resulted in cost savings per patient, primarily due to the reduced costs associated with colorectal cancer care[53]. AI-assisted surveillance programs can optimize the colonoscopy capacity by reducing the number of procedures required for low-risk patients. Personalized risk stratification based on polyp characteristics and patient risk factors allows for tailored surveillance intervals (increased or shortened) and is cost-effective[61]. This approach not only reduces healthcare costs but also alleviates the burden on endoscopic resources, making screening programs more scalable, especially in low-income and middle-income countries[54]. The study performed by Shi *et al*[1] is the first in which the ML algorithm was developed and validated for personalized surveillance. Only further studies can demonstrate whether it is cost-effective compared with existing surveillance programs. There are two possible scenarios: In countries such as China or Japan, where shorter intervals for colonoscopy after polyp removal are usually recommend ML-based surveillance programs may reduce the number of unnecessary colonoscopies. In contrast, in the United States and EU, where longer intervals for surveillance or even allocation of low-risk patients into screening programs are recommended, ML-based surveillance programs may achieve cost efficacy by decreasing colon cancer incidence due to a higher rate of detection of recurrent polyps. Despite the promising cost-effectiveness of AI-assisted screening and surveillance programs, several challenges remain. The high upfront costs of AI systems and the lack of reimbursement frameworks in many healthcare systems pose significant barriers to their widespread adoption[62]. Additionally, the long-term clinical benefits of AI in reducing colorectal cancer incidence and mortality have not yet been fully established, necessitating further research to validate its impact.

CONCLUSION

The study of Shi *et al*[1] demonstrates an important paradigm shift in future research aimed at increasing the positive yield of surveillance colonoscopy. In the past two decades, progress in surveillance programs was provided by the sophistication of endoscopic technologies (digital imaging, magnifying, narrow-band light spectrum, *etc.*) and standardization and improvement of bowel preparation, which allow the identification and evaluation of the majority of polyps in the colon. Therefore, it is not surprising that different polyp features have become the foundation of modern surveillance guidelines, and they are good, especially for high-risk patients. High-risk patients represent only 10% of the population in which polyps were found during colonoscopy; for the remaining patients, extending surveillance intervals were introduced or the risk for recurrence was considered low, and they are recommended screening rather than surveillance, because colorectal cancer incidence in these patients is similar to that of the general population. However, this argument sounds like a statistical joke, because the incidence of colorectal cancer in the general population is high and screening is ineffective. According to the National Cancer Institute in 2021 in the United States, 71.8% of adults aged 50-75 years had received colorectal cancer screening based on the most recent guidelines; however, the Centers for Disease Control and Prevention reported that from 2017 to 2021 only 32.8% of colorectal cancer cases were diagnosed at the localized stage [63]. The major difference of these "low-risk" patients from general population is that we already know that they had colonic polyps, but the huge pool of information is stored in their electronic medical records, which can be accessed and analyzed with AI for the development of the ML-driven surveillance programs which are accurate and hopefully will be cost-effective.

FOOTNOTES

Author contributions: Isakov V wrote and edited the manuscript and reviewed the literature.

Supported by Ministry of Science and Higher Education of the Russian Federation, No. FGMF-2025-0003.

Conflict-of-interest statement: The author reports no relevant conflicts of interest for this article.

Country of origin: Russia

ORCID number: Vasily Isakov 0000-0002-4417-8076.

S-Editor: Wei YF
L-Editor: A
P-Editor: Wang WB

REFERENCES

1 **Shi YH**, Liu JL, Cheng CC, Li WL, Sun H, Zhou XL, Wei H, Fei SJ. Construction and validation of machine learning-based predictive model for colorectal polyp recurrence one year after endoscopic mucosal resection. *World J Gastroenterol* 2025; **31**: 102387 [PMID: 40124266 DOI: 10.3748/wjg.v31.i11.102387]

2 **Ba Q**, Yuan X, Wang Y, Shen N, Xie H, Lu Y. Development and Validation of Machine Learning Algorithms for Prediction of Colorectal Polyps Based on Electronic Health Records. *Biomedicines* 2024; **12**: 1955 [PMID: 39335469 DOI: 10.3390/biomedicines12091955]

3 **Wang P**, Xiao X, Glissen Brown JR, Berzin TM, Tu M, Xiong F, Hu X, Liu P, Song Y, Zhang D, Yang X, Li L, He J, Yi X, Liu J, Liu X. Development and validation of a deep-learning algorithm for the detection of polyps during colonoscopy. *Nat Biomed Eng* 2018; **2**: 741-748 [PMID: 31015647 DOI: 10.1038/s41551-018-0301-3]

4 **Grosu S**, Wesp P, Graser A, Maurus S, Schulz C, Knösel T, Cyran CC, Ricke J, Ingrisch M, Kazmierczak PM. Machine Learning-based Differentiation of Benign and Premalignant Colorectal Polyps Detected with CT Colonography in an Asymptomatic Screening Population: A Proof-of-Concept Study. *Radiology* 2021; **299**: 326-335 [PMID: 33620287 DOI: 10.1148/radiol.2021202363]

5 **Barua I**, Vinsard DG, Jodal HC, Løberg M, Kalager M, Holme Ø, Misawa M, Bretthauer M, Mori Y. Artificial intelligence for polyp detection during colonoscopy: a systematic review and meta-analysis. *Endoscopy* 2021; **53**: 277-284 [PMID: 32557490 DOI: 10.1055/a-1201-7165]

6 **Nazarian S**, Glover B, Ashrafian H, Darzi A, Teare J. Diagnostic Accuracy of Artificial Intelligence and Computer-Aided Diagnosis for the Detection and Characterization of Colorectal Polyps: Systematic Review and Meta-analysis. *J Med Internet Res* 2021; **23**: e27370 [PMID: 34259645 DOI: 10.2196/27370]

7 **Lui TKL**, Guo CG, Leung WK. Accuracy of artificial intelligence on histology prediction and detection of colorectal polyps: a systematic review and meta-analysis. *Gastrointest Endosc* 2020; **92**: 11-22.e6 [PMID: 32119938 DOI: 10.1016/j.gie.2020.02.033]

8 **Rotermund C**, Djinbachian R, Taghiakbari M, Enderle MD, Eickhoff A, von Renteln D. Recurrence rates after endoscopic resection of large colorectal polyps: A systematic review and meta-analysis. *World J Gastroenterol* 2022; **28**: 4007-4018 [PMID: 36157546 DOI: 10.3748/wjg.v28.i29.4007]

9 **Haghbin H**, Zakirkhodjaev N, Fatima R, Kamal F, Aziz M. Efficacy and Safety of Thermal Ablation after Endoscopic Mucosal Resection: A Systematic Review and Network Meta-Analysis. *J Clin Med* 2024; **13**: 1298 [PMID: 38592137 DOI: 10.3390/jcm13051298]

10 **Abdallah M**, Ahmed K, Abbas D, Mohamed MFH, Suryawanshi G, McDonald N, Wilson N, Umar S, Shaukat A, Bilal M. Cold snare endoscopic mucosal resection for colon polyps: a systematic review and meta-analysis. *Endoscopy* 2023; **55**: 1083-1094 [PMID: 37451284 DOI: 10.1055/a-2129-5752]

11 **Klein A**, Tate DJ, Jayasekeran V, Hourigan L, Singh R, Brown G, Bahin FF, Burgess N, Williams SJ, Lee E, Sidhu M, Byth K, Bourke MJ. Thermal Ablation of Mucosal Defect Margins Reduces Adenoma Recurrence After Colonic Endoscopic Mucosal Resection. *Gastroenterology* 2019; **156**: 604-613.e3 [PMID: 30296436 DOI: 10.1053/j.gastro.2018.10.003]

12 **Li B**, Zheng W. The Impact of Endoscopic Mucosal Resection and Endoscopic Submucosal Dissection on Colonic Polyp Resection and Factors Influencing Recurrence. *Surg Laparosc Endosc Percutan Tech* 2024; **34**: 607-613 [PMID: 39632425 DOI: 10.1097/SLE.0000000000001329]

13 **Rutter MD**, East J, Rees CJ, Cripps N, Docherty J, Dolwani S, Kaye PV, Monahan KJ, Novelli MR, Plumb A, Saunders BP, Thomas-Gibson S, Tolan DJM, Whyte S, Bonnington S, Scope A, Wong R, Hibbert B, Marsh J, Moores B, Cross A, Sharp L. British Society of Gastroenterology/Association of Coloproctology of Great Britain and Ireland/Public Health England post-polypectomy and post-colorectal cancer resection surveillance guidelines. *Gut* 2020; **69**: 201-223 [PMID: 31776230 DOI: 10.1136/gutjnl-2019-319858]

14 **Saito Y**, Oka S, Kawamura T, Shimoda R, Sekiguchi M, Tamai N, Hotta K, Matsuda T, Misawa M, Tanaka S, Iriguchi Y, Nozaki R, Yamamoto H, Yoshida M, Fujimoto K, Inoue H. Colonoscopy screening and surveillance guidelines. *Dig Endosc* 2021; **33**: 486-519 [PMID: 33713493 DOI: 10.1111/den.13972]

15 **Tanaka S**, Saitoh Y, Matsuda T, Igarashi M, Matsumoto T, Iwao Y, Suzuki Y, Nozaki R, Sugai T, Oka S, Itabashi M, Sugihara KI, Tsuruta O, Hirata I, Nishida H, Miwa H, Enomoto N, Shimosegawa T, Koike K. Evidence-based clinical practice guidelines for management of colorectal polyps. *J Gastroenterol* 2021; **56**: 323-335 [PMID: 33710392 DOI: 10.1007/s00535-021-01776-1]

16 **Ferlitsch M**, Hassan C, Bisschops R, Bhandari P, Dinis-Ribeiro M, Risio M, Paspatis GA, Moss A, Libânio D, Lorenzo-Zúñiga V, Voiosu AM, Rutter MD, Pellisé M, Moons LMG, Probst A, Awadie H, Amato A, Takeuchi Y, Repici A, Rahmi G, Koecklin HU, Albéniz E,

Rockenbauer LM, Waldmann E, Messmann H, Triantafyllou K, Jover R, Gralnek IM, Dekker E, Bourke MJ. Colorectal polypectomy and endoscopic mucosal resection: European Society of Gastrointestinal Endoscopy (ESGE) Guideline - Update 2024. *Endoscopy* 2024; **56**: 516-545 [PMID: 38670139 DOI: 10.1055/a-2304-3219]

17 **Gupta S**, Lieberman D, Anderson JC, Burke CA, Dominitz JA, Kaltenbach T, Robertson DJ, Shaukat A, Syngal S, Rex DK. Recommendations for Follow-Up After Colonoscopy and Polypectomy: A Consensus Update by the US Multi-Society Task Force on Colorectal Cancer. *Gastroenterology* 2020; **158**: 1131-1153.e5 [PMID: 32044092 DOI: 10.1053/j.gastro.2019.10.026]

18 **Mangas-Sanjuan C**, Jover R, Cubiella J, Marzo-Castillejo M, Balaguer F, Bessa X, Bujanda L, Bustamante M, Castells A, Diaz-Tasende J, Dí ez-Redondo P, Herráiz M, Mascort-Roca JJ, Pellisé M, Quintero E; Grupo de Cribado del Cáncer Colorrectal de la Sociedad Española de Epidemiología. Endoscopic surveillance after colonic polyps and colorrectal cancer resection. 2018 update. *Gastroenterol Hepatol* 2019; **42**: 188-201 [PMID: 30621911 DOI: 10.1016/j.gastrohep.2018.11.001]

19 **Radaelli F**, Paggi S, Bortoli A, De Pretis G; Italian Association of Hospital Gastroenterologists (AIGO). Overutilization of post-polypectomy surveillance colonoscopy in clinical practice: a prospective, multicentre study. *Dig Liver Dis* 2012; **44**: 748-753 [PMID: 22627070 DOI: 10.1016/j.dld.2012.04.015]

20 **Lieberman DA**, Williams JL, Holub JL, Morris CD, Logan JR, Eisen GM, Carney P. Colonoscopy utilization and outcomes 2000 to 2011. *Gastrointest Endosc* 2014; **80**: 133-143 [PMID: 24565067 DOI: 10.1016/j.gie.2014.01.014]

21 **Abu Freha N**, Abu Tailakh M, Elkrinawi J, Abu Kaf H, Philip A, Schwartz D, Yahia A, Etzion O. Post-polypectomy surveillance colonoscopy: are we following the guidelines? *Int J Colorectal Dis* 2020; **35**: 1343-1346 [PMID: 32152670 DOI: 10.1007/s00384-020-03556-4]

22 **Khattak MA**, Waheed A, Demetriou G, Bedford M. FP4.9 - Adherence to post Colonic polypectomy surveillance guidelines. *British J Surg* 2024; **111** [DOI: 10.1093/bjs/znae197.376]

23 **Koh FH**, Chan DKH, Ng J, Tan KK. Adherence to surveillance guidelines following colonic polypectomy is abysmal. *J Gastrointest Oncol* 2019; **10**: 166-170 [PMID: 31032081 DOI: 10.21037/jgo.2018.11.06]

24 **Ho YM**, Merollini KMD, Gordon LG. Frequency of colorectal surveillance colonoscopies for adenomatous polyps: systematic review and meta-analysis. *J Gastroenterol Hepatol* 2024; **39**: 37-46 [PMID: 37967829 DOI: 10.1111/jgh.16397]

25 **Cooper GS**, Kou TD, Barnholtz Sloan JS, Koroukian SM, Schluchter MD. Use of colonoscopy for polyp surveillance in Medicare beneficiaries. *Cancer* 2013; **119**: 1800-1807 [PMID: 23436321 DOI: 10.1002/cncr.27990]

26 **Hassan C**, Pickhardt PJ, Di Giulio E, Kim DH, Zullo A, Morini S. Cost-effectiveness of early one-year colonoscopy surveillance after polypectomy. *Dis Colon Rectum* 2009; **52**: 964-71; discussion 971 [PMID: 19502863 DOI: 10.1007/DCR.0b013e31819f244e]

27 **Cross AJ**, Robbins EC, Pack K, Stenson I, Kirby PL, Patel B, Rutter MD, Veitch AM, Saunders BP, Duffy SW, Wooldrage K. Long-term colorectal cancer incidence after adenoma removal and the effects of surveillance on incidence: a multicentre, retrospective, cohort study. *Gut* 2020; **69**: 1645-1658 [PMID: 31953252 DOI: 10.1136/gutjnl-2019-320036]

28 **Hassan C**, Antonelli G, Dumonceau JM, Regula J, Bretthauer M, Chaussade S, Dekker E, Ferlitsch M, Gimeno-Garcia A, Jover R, Kalager M, Pellisé M, Pox C, Ricciardiello L, Rutter M, Helsingen LM, Bleijenberg A, Senore C, van Hooft JE, Dinis-Ribeiro M, Quintero E. Post-polypectomy colonoscopy surveillance: European Society of Gastrointestinal Endoscopy (ESGE) Guideline - Update 2020. *Endoscopy* 2020; **52**: 687-700 [PMID: 32572858 DOI: 10.1055/a-1185-3109]

29 **Johnstone MS**, Stoops R, Lynch G, Hay J, Jawny J, Sloan W, Edwards J, McSorley ST. Risk stratification for the detection of metachronous polyps after bowel screening polypectomy: clinical outcomes from the Integrated Technologies for Improved Polyp Surveillance (INCISE) study cohort. *BJS Open* 2023; **7**: zrad034 [PMID: 37158435 DOI: 10.1093/bjsopen/zrad034]

30 **Ibáñez-Sanz G**, Sanz-Pamplona R, Garcia M; PhD on behalf of the MSIC-SC research group. Post-polypectomy colonoscopy surveillance: Can we improve the diagnostic yield? *Gastroenterol Hepatol* 2022; **45**: 474-487 [PMID: 34848307 DOI: 10.1016/j.gastrohep.2021.11.005]

31 **Williams GJ**, Hellerstedt ST, Scudder PN, Calderwood AH. Yield of Surveillance Colonoscopy in Older Adults with a History of Polyps: A Systematic Review and Meta-Analysis. *Dig Dis Sci* 2022; **67**: 4059-4069 [PMID: 34406584 DOI: 10.1007/s10620-021-07198-6]

32 **Lee S**, Do YS, Lee HJ, Kim GU, Park HW, Chang HS, Choe J, Byeon JS, Lee JY. Gastrointestinal: Weight gain increases the risk of metachronous advanced colorectal neoplasm observed in post-polypectomy surveillance colonoscopy. *J Gastroenterol Hepatol* 2024; **39**: 47-54 [PMID: 37743847 DOI: 10.1111/jgh.16360]

33 **Hussan H**, Ali MR, Hussain SK, Lyo V, McLaughlin E, Chiang C, Thompson HJ. The impact of surgical weight loss procedures on the risk of metachronous colorectal neoplasia: the differential effect of surgery type, sex, and anatomic location. *J Natl Cancer Inst Monogr* 2023; **2023**: 77-83 [PMID: 37139983 DOI: 10.1093/jncimonographs/lgac029]

34 **Hussan H**, McLaughlin E, Chiang C, Marsano JG, Lieberman D. The Risk of Colorectal Polyps after Weight Loss Therapy Versus Obesity: A Propensity-Matched Nationwide Cohort Study. *Cancers (Basel)* 2023; **15**: 4820 [PMID: 37835515 DOI: 10.3390/cancers15194820]

35 **Fliss-Isakov N**, Zelber-Sagi S, Webb M, Halpern Z, Shibolet O, Kariv R. Distinct Metabolic Profiles are Associated with Colorectal Adenomas and Serrated Polyps. *Obesity (Silver Spring)* 2017; **25** Suppl 2: S72-S80 [PMID: 29086511 DOI: 10.1002/oby.22001]

36 **Jacobson JS**, Neugut AI, Murray T, Garbowski GC, Forde KA, Treat MR, Waye JD, Santos J, Ahsan H. Cigarette smoking and other behavioral risk factors for recurrence of colorectal adenomatous polyps (New York City, NY, USA). *Cancer Causes Control* 1994; **5**: 215-220 [PMID: 8061168 DOI: 10.1007/BF01830239]

37 **Harrington LX**, Wei JW, Suriawinata AA, Mackenzie TA, Hassanpour S. Predicting colorectal polyp recurrence using time-to-event analysis of medical records. *AMIA Jt Summits Transl Sci Proc* 2020; **2020**: 211-220 [PMID: 32477640]

38 **Jang J**, Park J, Park SJ, Park JJ, Cheon JH, Kim TI. Clinical characteristics and risk factors related to polyposis recurrence and advanced neoplasm development among patients with non-hereditary colorectal polyposis. *Intest Res* 2023; **21**: 510-517 [PMID: 37248175 DOI: 10.5217/ir.2022.00139]

39 **Paskett ED**, Reeves KW, Pineau B, Albert PS, Caan B, Hasson M, Iber F, Kikendall JW, Lance P, Shike M, Slattery ML, Weissfeld J, Kahle L, Schatzkin A, Lanza E; Polyp Prevention Trial Study Group. The association between cigarette smoking and colorectal polyp recurrence (United States). *Cancer Causes Control* 2005; **16**: 1021-1033 [PMID: 16184467 DOI: 10.1007/s10552-005-0298-2]

40 **Jung YS**, Kim NH, Lee MY, Park JH, Park DI, Sohn CI. Effect of Cotinine-Verified Change in Smoking Status on Risk of Metachronous Colorectal Neoplasia After Polypectomy. *Clin Gastroenterol Hepatol* 2020; **18**: 163-170 [PMID: 30772586 DOI: 10.1016/j.cgh.2019.02.018]

41 **Zhen J**, Li J, Liao F, Zhang J, Liu C, Xie H, Tan C, Dong W. Development and validation of machine learning models for young-onset colorectal cancer risk stratification. *NPJ Precis Oncol* 2024; **8**: 239 [PMID: 39438621 DOI: 10.1038/s41698-024-00719-2]

42 **Herrera DJ**, Seibert DM, Feyen K, van Loo M, Van Hal G, van de Veerdonk W. Development and Internal Validation of a Machine Learning-

Based Colorectal Cancer Risk Prediction Model. *Gastrointest Disord* 2025; **7**: 26 [DOI: 10.3390/gidisord7020026]

43 **Gao QY**, Chen HM, Sheng JQ, Zheng P, Yu CG, Jiang B, Fang JY. The first year follow-up after colorectal adenoma polypectomy is important: a multiple-center study in symptomatic hospital-based individuals in China. *Front Med China* 2010; **4**: 436-442 [PMID: 21128011 DOI: 10.1007/s11684-010-0200-9]

44 **Goetz L**, Seedat N, Vandersluis R, van der Schaar M. Generalization-a key challenge for responsible AI in patient-facing clinical applications. *NPJ Digit Med* 2024; **7**: 126 [PMID: 38773304 DOI: 10.1038/s41746-024-01127-3]

45 **Kelly CJ**, Karthikesalingam A, Suleyman M, Corrado G, King D. Key challenges for delivering clinical impact with artificial intelligence. *BMC Med* 2019; **17**: 195 [PMID: 31665002 DOI: 10.1186/s12916-019-1426-2]

46 **Harishbhai Tilala M**, Kumar Chenchala P, Choppadandi A, Kaur J, Naguri S, Saoji R, Devaguptapu B. Ethical Considerations in the Use of Artificial Intelligence and Machine Learning in Health Care: A Comprehensive Review. *Cureus* 2024; **16**: e62443 [PMID: 39011215 DOI: 10.7759/cureus.62443]

47 **Dankwa-Mullan I**. Health Equity and Ethical Considerations in Using Artificial Intelligence in Public Health and Medicine. *Prev Chronic Dis* 2024; **21**: E64 [PMID: 39173183 DOI: 10.5888/pcd21.240245]

48 **Benzinger L**, Ursin F, Balke WT, Kacprowski T, Salloch S. Should Artificial Intelligence be used to support clinical ethical decision-making? A systematic review of reasons. *BMC Med Ethics* 2023; **24**: 48 [PMID: 37415172 DOI: 10.1186/s12910-023-00929-6]

49 **Adiwinata R**, Tandarto K, Arifputra J, Waleleng BJ, Gosal F, Rotty L, Winarta J, Waleleng A, Simadibrata P, Simadibrata M. The Impact of Artificial Intelligence in Improving Polyp and Adenoma Detection Rate During Colonoscopy: Systematic-Review and Meta-Analysis. *Asian Pac J Cancer Prev* 2023; **24**: 3655-3663 [PMID: 38019222 DOI: 10.31557/APJCP.2023.24.11.3655]

50 **Spadaccini M**, Hassan C, De Marco A, Mori Y, Facciorusso A, Gkolfakis P, Tziatzios G, Triantafyllou K, Antonelli G, Khalaf K, Rizkala T, Bretthauer M, Vandvik PO, Foroutan F, Fugazza A, Rondonotti E, Brown JG, Kamba S, Correale L, Bhandari P, Bisschops R, Dekker E, Kaminski MF, Jover R, Saito Y, Sharma P, Rex DK, Repici A. Real-time computer-aided detection of colorectal neoplasia during colonoscopy: systematic review and meta-analysis. *Gastrointest Endoscopy* 2023; **97**: AB715-AB716 [DOI: 10.1016/j.gie.2023.04.1180]

51 **Maas MHJ**, Neumann H, Shirin H, Katz LH, Benson AA, Kahloon A, Soons E, Hazzan R, Landsman MJ, Lebwohl B, Lewis SK, Sivanathan V, Ngamruengphong S, Jacob H, Siersema PD. A computer-aided polyp detection system in screening and surveillance colonoscopy: an international, multicentre, randomised, tandem trial. *Lancet Digit Health* 2024; **6**: e157-e165 [PMID: 38395537 DOI: 10.1016/S2589-7500(23)00242-X]

52 **Young E**, Edwards L, Singh R. The Role of Artificial Intelligence in Colorectal Cancer Screening: Lesion Detection and Lesion Characterization. *Cancers (Basel)* 2023; **15**: 5126 [PMID: 37958301 DOI: 10.3390/cancers15215126]

53 **Hassan C**, Povero M, Pradelli L, Spadaccini M, Repici A. Cost-utility analysis of real-time artificial intelligence-assisted colonoscopy in Italy. *Endosc Int Open* 2023; **11**: E1046-E1055 [PMID: 37954109 DOI: 10.1055/a-2136-3428]

54 **Rao HB**, Sastry NB, Venu RP, Pattanayak P. The role of artificial intelligence based systems for cost optimization in colorectal cancer prevention programs. *Front Artif Intell* 2022; **5**: 955399 [PMID: 36248620 DOI: 10.3389/frai.2022.955399]

55 **Bustamante-Balén M**, Merino Rodríguez B, Barranco L, Monje J, Álvarez M, de Pedro S, Oyagüez I, Van Lent N, Mareque M. Cost-effectiveness analysis of artificial intelligence-aided colonoscopy for adenoma detection and characterization in Spain. *Endosc Int Open* 2025; **13**: a25097278 [PMID: 40109314 DOI: 10.1055/a-2509-7278]

56 **Sinagra E**, Badalamenti M, Maida M, Spadaccini M, Maselli R, Rossi F, Conoscenti G, Raimondo D, Pallio S, Repici A, Anderloni A. Use of artificial intelligence in improving adenoma detection rate during colonoscopy: Might both endoscopists and pathologists be further helped. *World J Gastroenterol* 2020; **26**: 5911-5918 [PMID: 33132644 DOI: 10.3748/wjg.v26.i39.5911]

57 **Maida M**, Marasco G, Facciorusso A, Shahini E, Sinagra E, Pallio S, Ramai D, Murino A. Effectiveness and application of artificial intelligence for endoscopic screening of colorectal cancer: the future is now. *Expert Rev Anticancer Ther* 2023; **23**: 719-729 [PMID: 37194308 DOI: 10.1080/14737140.2023.2215436]

58 **Turgeon DK**, Krammes L, Mahmood H, Frondorf F, Königs V, Luther J, Schölz C, Becker P, Maharjan S, Sever A, Garapati S, Balasubramaniam A, Knabe M, Sharma G, Pham T, Preywisch R, Eidens M, Bresalier R, Dollinger M. A novel, noninvasive, multimodal screening test for the early detection of precancerous lesions and colorectal cancers using an artificial intelligence-based algorithm. *J Clin Oncol* 2024; **42**: 3627-3627 [DOI: 10.1200/jco.2024.42.16_suppl.3627]

59 **Fouladi A**, Asadi A, Sherer EA, Madadi M. Cost-effectiveness Analysis of Colorectal Cancer Screening Strategies Using Active Learning and Monte Carlo Simulation. *Med Decis Making* 2024; **44**: 554-571 [PMID: 38907706 DOI: 10.1177/0272989X241258224]

60 **Barkun AN**, von Renteln D, Sadri H. Cost-effectiveness of Artificial Intelligence-Aided Colonoscopy for Adenoma Detection in Colon Cancer Screening. *J Can Assoc Gastroenterol* 2023; **6**: 97-105 [PMID: 37273970 DOI: 10.1093/jcag/gwad014]

61 **Sekiguchi M**, Igarashi A, Sakamoto T, Saito Y, Esaki M, Matsuda T. Cost-effectiveness analysis of postpolypectomy colonoscopy surveillance using Japanese data. *Dig Endosc* 2019; **31**: 40-50 [PMID: 30062760 DOI: 10.1111/den.13250]

62 **Hassan C**, Repici A, Mori Y. Cost of artificial intelligence: Elephant in the room and its cage. *Dig Endosc* 2023; **35**: 900-901 [PMID: 37160614 DOI: 10.1111/den.14567]

63 **United States Cancer Statistics**. U.S. Cancer Statistics Colorectal Cancer Stat Bite. [cited 5 January 2025]. Available from: https://www.cdc.gov/united-states-cancer-statistics/publications/colorectal-cancer-stat-bite.html

World Journal of Gastroenterology

Submit a Manuscript: https://www.f6publishing.com

World J Gastroenterol 2025 May 21; 31(19): 106814

DOI: 10.3748/wjg.v31.i19.106814

ISSN 1007-9327 (print) ISSN 2219-2840 (online)

REVIEW

Current status of endoscopic resection for small rectal neuroendocrine tumors

Jian-Ning Liu, Hui Chen, Nian Fang

Specialty type: Gastroenterology and hepatology

Provenance and peer review: Invited article; Externally peer reviewed.

Peer-review model: Single blind

Peer-review report's classification

Scientific Quality: Grade B, Grade B, Grade B, Grade C

Novelty: Grade B, Grade C, Grade C, Grade D

Creativity or Innovation: Grade B, Grade C, Grade C, Grade D

Scientific Significance: Grade B, Grade B, Grade C, Grade D

P-Reviewer: Xie DY; Yang SK

Received: March 9, 2025

Revised: March 21, 2025

Accepted: April 27, 2025

Published online: May 21, 2025

Processing time: 74 Days and 14.1 Hours

Jian-Ning Liu, Nian Fang, Department of Gastroenterology, The Third Affiliated Hospital, Jiangxi Medical College, School of Queen Mary, Nanchang University, Nanchang 330009, Jiangxi Province, China

Hui Chen, Endoscopic Center, Xijing Hospital of Digestive Diseases, Air Force Medical University (Fourth Military Medical University), Xi'an 710032, Shaanxi Province, China

Nian Fang, Department of Gastroenterology, The First Hospital of Nanchang, Nanchang 330009, Jiangxi Province, China

Co-corresponding authors: Hui Chen and Nian Fang.

Corresponding author: Nian Fang, PhD, Professor, Department of Gastroenterology, The Third Affiliated Hospital, Jiangxi Medical College, School of Queen Mary, Nanchang University, No. 128 Xiangshan North Road, Nanchang 330009, Jiangxi Province, China.
nianfang_ncu@163.com

Abstract

Rectal neuroendocrine tumor (rNET) is an indolent malignancy often detected during colonoscopy screening. The incidence of rNET has increased approximately 10-fold over the past 30 years. Most rNETs detected during screening endoscopy are small, measuring < 10 mm. Current guidelines recommend endoscopic resection for small, well-differentiated rNET using modified endoscopic submucosal resection (mEMR) or endoscopic submucosal dissection. However, the optimal endoscopic treatment method remains uncertain. This paper summarizes the evidence on mEMR with submucosal stretching, mEMR without submucosal stretching, endoscopic submucosal dissection and endoscopic full-thickness resection. Given that rNETs often exhibit submucosal invasion, achieving adequate resection depth is crucial to ensure histological complete resection. mEMR with submucosal stretching appears favorable due to its high rate of histological complete resection, safety and convenience. Risk factors associated with lymph node and distant metastases are also discussed. A treatment algorithm is proposed to facilitate clinical decision-making.

Key Words: Rectal neuroendocrine tumor; Endoscopic resection; Endoscopic submucosal dissection; Modified endoscopic mucosal resection; Histological complete resection; Resection depth; Risk factor; Treatment algorithm

Core Tip: The initial evaluation of small rectal neuroendocrine tumors should thoroughly assess endoscopic features, including size, location, surface pit pattern and atypical changes. Imaging modalities should be used to rule out possible lymph node involvement and distant metastasis. Cold biopsy or polypectomy should be avoided, and modified endoscopic mucosal resection with submucosal stretching should be chosen as a priority. For small incompletely resected tumors without other risk factors, salvage resection can be carefully considered. Long-term follow-up is necessary if patients decline additional treatment. For patients with complete resection and risk factors, extended follow-up should be considered.

Citation: Liu JN, Chen H, Fang N. Current status of endoscopic resection for small rectal neuroendocrine tumors. *World J Gastroenterol* 2025; 31(19): 106814
URL: https://www.wjgnet.com/1007-9327/full/v31/i19/106814.htm
DOI: https://dx.doi.org/10.3748/wjg.v31.i19.106814

INTRODUCTION

Rectal neuroendocrine tumors (rNETs) are typically small and have low malignant potential, but the risk of metastasis exists[1]. Unlike neuroendocrine tumors (NETs) in other locations, carcinoid syndrome of rNETs is rare because tumors usually do not produce serotonin[2]. The majority of rNETs are < 10 mm, largely due to increased detection through screening colonoscopy[3]. Local excision, including endoscopic techniques and transanal surgery, is usually recommended for rNETs confined to the mucosal or submucosal layers. However, even tumors measuring ≤ 10 mm carry a 2%-3% risk of metastasis, underscoring the importance of developing robust strategies for optimal management of these tumors[4]. Currently, there are no clear guidelines for the optimal treatment or follow-up plan for small rNETs. This review aims to address these issues based on the most recent literature.

EPIDEMIOLOGY

The incidence of rNETs is about 1.04 per 100000 persons per year, accounting for about 1% of rectal neoplastic lesions[5,6]. Most patients are relatively young at diagnosis compared to those with mucosal malignancy, who are typically in their sixth decade with a slight male dominance[7]. rNETs are the third most common type of NET, representing about 15% of all gastroenteropancreatic-NETs[7]. There are global variations in the incidence of rNETs, with a high prevalence in Asian countries where they may account for up to 80% of all gastroenteropancreatic-NETs[8]. Racial disparities also exist, with higher rates observed in Black and Asian populations compared to White populations[9]. Risk factors for development of rNETs include low levels of high-density lipoprotein-cholesterol, elevated cholesterol and ferritin levels, and the presence of metabolic syndrome[10,11]. Other risk factors, including family history of cancer, smoking, alcohol consumption and body mass index, have not been consistently associated with the prevalence of rNETs in meta-analysis[12].

The incidence of NETs has been increasing across all sites, but rectal tumors have seen one of the most significant rises, likely due to increased recognition and the more frequent use of colonoscopy in screening[13]. In analysis of the Surveillance, Epidemiology, and End Results (SEER) database (SEER registry of the National Cancer Institute, United States), the age-adjusted incidence of rNETs has increased approximately 10-fold over the past 30 years[7]. In a large-scale observational study from Japan, colorectal NETs were identified in 67 of 82005 colonoscopies, yielding a detection rate of 82 per 100000 procedures[14]. However, age-adjusted incidence rate of rNETs has plateaued since 2015, possibly indicating the maximal benefit of colonoscopy screening[7]. According to the United States Cancer Statistics, rNET incidence rates during 2001 and 2020 have increased in younger adults (< 55 years) but not in older adults[15].

ENDOSCOPIC DIAGNOSIS

The presentation of rNETs ranges from asymptomatic, indolent tumors to aggressive metastatic disease. Resection can be either endoscopic or surgical, and the choice of technique depends on tumor characteristics such as size, grade, invasion into the muscularis propria (MP) layer, and the presence of lymph node involvement or distant metastases[8]. These factors should be thoroughly considered at the initial diagnosis.

Routine endoscopy

Recognizing rNETs during initial endoscopy is crucial for appropriate management[16,17]. Polypectomy or biopsy is commonly performed if the lesion is mistaken as a common polyp rather than an rNET. rNETs diagnosed or suspected before resection have a significantly higher complete resection rate compared to those treated as polyps and later diagnosed[18]. A retrospective analysis showed that it was possible to suspect a NET by macroscopic appearance of

endoscopy in 96% of cases[19]. The diagnosis of rNETs could be possible just by routine endoscopy.

rNETs are typically small (≤ 10 mm in diameter), solitary lesions located 5-10 cm from the anal verge[1,2]. They usually appear as sessile lesions with a yellowish or whitish reflection and smooth, intact covering mucosa. Under narrow-band imaging, small round pits are typical features of rNETs, distinguishing them from starry-shaped pits in hyperplastic polyps (Figure 1A and B)[20]. These tumors are often described as hard and movable, and their consistency can be assessed using a biopsy forceps[1]. For those more significantly elevated, enlarged surface pit pattern may be found; however, the shape remains unchanged (Figure 1C and D). Larger lesions may exhibit surface irregularity with dilated microvessels (Figure 1E and F). Irregular surfaces usually show as a doughnut-shaped lesion with central depression, which can suggest a more aggressive clinical course[3]. Central depression, once thought to be risk factor for lymph node involvement, has not been confirmed as an independent risk factor, but may still be relevant for reducing the risk of incomplete resection[21,22]. Furthermore, dilated vessels around the lesion may be associated with tumor grade 2 and deep submucosal invasion (Figure 1E and F)[23].

Biopsy

Guidelines recommend taking a biopsy during initial endoscopy to confirm the diagnosis of rNETs[1]. However, evidence suggests that the prior biopsy may complicate complete endoscopic resection, presumably due to fibrosis and blurred tumor borders caused by inflammation and tissue repairing[19,24]. Biopsy should only be considered in doubtful cases with atypical features or in tumors > 20 mm, which should be referred for surgery[1]. The potential benefit of biopsy is to confirm histology before endoscopic resection, but given that most rectal subepithelial lesions (SELs) are NETs, and modified endoscopic mucosal resection (mEMR) is a safe and cost-effective procedure, biopsy may not be essential for lesions < 10 mm.

Endoscopic ultrasound

rNETs in endoscopic ultrasound (EUS) typically present as hypoechoic, homogeneous lesions originating from the submucosal layer[1]. EUS helps with predicting histology, estimating the size, evaluating the invasion depth and assessing possible lymph node metastasis in the perirectal area[8]. For histological prediction, it may have little significance for a detected rectal SEL due to the predominance of NETs in such lesions[25]. In a retrospective study for rectal SELs, the diagnostic accuracy of EUS in identifying rNETs was 89%[26]. While seemingly accurate, the prevalence of NETs was 79% in the cohort. Only a small portion of patients can benefit from the histological prediction. Furthermore, some rectal lesions may mimic the endoscopic appearance, even with similar EUS features, therefore it might be difficult for EUS to differentiate[27,28].

Regarding size estimation, a retrospective study including 120 rNETs cases reported no difference between endoscopy and EUS (r = 0.914/0.727, respectively)[29]. For depth estimation, it is well established on the high concordance in identifying the involvement of MP layer[30]. However, in lesions ≤ 10 mm, MP involvement is extremely rare[31]. There is a similar situation in assessing lymph node metastasis[32]. EUS does not have an adequate range to assess nodal involvement beyond the perirectal area[3]. Therefore, EUS may not be essential for rNETs < 10 mm[1,32]. Currently, EUS is generally recommend for lesions > 10 mm or those with atypical features, such as central depression[8,33].

METASTASIS

Over 80% of rNETs are < 10 mm and low-grade at diagnosis[8]. Although the risk of metastasis is low, rNETs ≤ 10 mm still carry a potential risk. In some cases, patients may even present with metastasis before the primary tumor is detected. Currently, no single parameter can precisely predict the presence of metastasis, so lymph node involvement and distant metastasis should be carefully evaluated using appropriate imaging modalities. A meta-analysis including 4575 rNET cases revealed 8% of patients with regional lymph node metastases and 4% with distant metastases[34]. The metastasis rate was higher than expected. It is important to note that most literature on lymph node involvement is based on radical resection studies with severe selection bias. Long-term surveillance with an endoscopically treated cohort is more likely to reflect the true metastatic rate of small rNETs.

Lymph node metastasis risk factors

Lymph node status is considered as a relevant prognostic factor for rNETs. Multiple factors have been linked to lymph node involvement. A previous meta-analysis identified tumor size > 1 cm, depth of invasion, venous invasion and central depression as factors of lymph node involvement, while lymphatic invasion was not[35].

Tumor size > 10 mm: This is the primary parameter for determining the risk for metastasis in rNETs[13,36]. In a population-based study from the United States, 20% of lymphatic metastases were found in 226 suspected cases out of 9000 rNETs < 10 mm, corresponding to 0.5% of all patients. In contrast, the metastasis rate was 8% for tumors 10-20 mm and 17% of those > 20 mm[37]. However, there are significant variations in metastasis rates across the published literature. The Niigatta Tumor Registry in Japan reported a metastasis rate of 10% for rNETs ≤ 10 mm[38].

Invasion of the MP: MP invasion significantly increases the risk of metastasis[39,40]. A meta-analysis found that MP invasion increased the risk of lateral pelvic lymph node metastasis with an odds ratio of 4.51[41].

Lymphovascular invasion: Lymphovascular invasion (LVI) is defined as the presence of tumor cells in blood vessels and/or lymphatic structures. Vascular invasion may have a stronger impact on lymph node metastasis than lymphatic

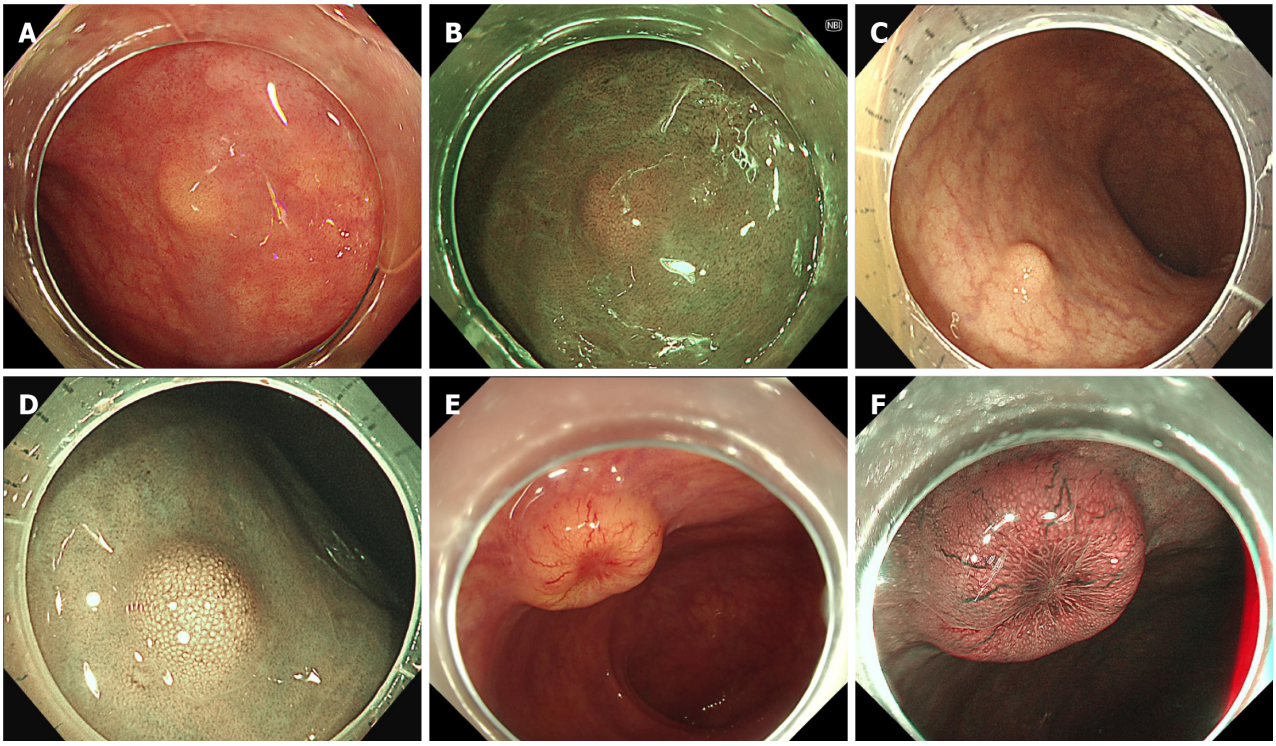

Figure 1 Endoscopic diagnosis of rectal neuroendocrine tumors. A and B: The rectal neuroendocrine tumor typically appears as a small, yellowish, and subepithelial tumor-like lesion without surface change under white light or narrow band imaging as shown in case 1; C and D: For lesions with more significant elevation, there may be enlarged surface pit openings, but the overall shape remains unchanged, as seen in case 2; E and F: As the lesion grows larger, central depression may develop, accompanied by dilated micro-vessels, as illustrated in case 3.

invasion has[21]. The overall prevalence of LVI in small rNETs ≤ 10 mm was 26% according to a meta-analysis[4]. However, the prognosis of endoscopically treated rNETs appears to be complex and not directly proportional to the presence of LVI. No recurrence was found in 109 cases with identified LVI during follow-up of 30-76 months[4]. Multiple confounding factors further influence the significance of LVI in metastasis. Evaluation of LVI is subject to interobserver variations[16,42]. Additionally, the detection rates for LVI vary with diagnostic modalities. Immunohistochemical staining significantly increased the detection rate of LVI (up to 36%) compared to hematoxylin and eosin sections (13%)[4,43].

Tumor grade (G2/G3): Higher tumor grades (G2/G3) are associated with aggressive behavior in rNETs. A recent meta-analysis identified tumor grade as a significant risk factor for lateral pelvic lymph node metastasis, with an odds ratio of 7.76[41]. A retrospective study of 601 cases found the incidence of lymph node was 5% in G1 rNETs compared with 44% in G2 tumors[44]. However, when adjusted for tumor size, the difference in lymph node metastasis only persisted in tumors measuring 10-20 mm. This suggests that tumor grade may have little influence on metastasis risk for rNETs < 10 mm[45].

These risk factors are closely related, and it would be interesting to determine which is the most reliable predictor. Tumor size is the easiest and most widely accepted factor to assess before treatment. Predictive scores that incorporate both tumor size and LVI have been shown to provide an accurate assessment of the risk of metastatic lymph node involvement[46,47]. However, some predictive models rely solely on tumor size as a useful risk factor[48,49].

Distant metastasis risk factors

For distant metastasis in rNETs, the liver is the most common site (58%) followed by bone (9%), mesentery/peritoneum (8%) and lungs (8%)[13]. As in lymph node metastasis, tumor size is the major parameter for the risk of developing distant metastases. The optimal cutoff for tumor size in predicting distant metastasis is 11.5 mm[13]. Besides tumor size, a study based on the SEER database found distant metastasis in rNETs was associated with tumor grade, and regional lymph node metastasis, while T stage was not a significant factor[50].

Imaging modalities to evaluate metastasis

Our understanding of metastasis may be an under-reported finding as magnetic resonance imaging (MRI) of the pelvis and rectum is not routinely mandated for small rNETs. The indolent behavior of rNETs may lead to delayed detection of metastasis[51]. However, improvements in imaging quality, with MRI and more recently gallium-68-somatostatin receptor-positron emission tomography/computed tomography (68Ga-SSR-PET/CT), have enhanced the characterization of suspicious lymph nodes and the identification of small nodal metastases[3].

CT: CT has limited value for detection and characterization of regional metastatic lymph nodes in rNET patients[13]. However, for distant metastasis, abdominopelvic CT is the imaging modality of choice, particularly for patients with tumor ≥ 10 mm or grade G2/G3[13]. Contrast-enhanced CT with acquisitions at the delayed arterial (30 seconds) and then the portal venous (70-90 seconds) phases are recommended, as some highly vascularized NETs are only visible at one of these phases[17].

MRI: For localized rectal tumors, MRI is the best imaging modality, allowing precise disease staging. It should be regarded as mandatory before treatment, even in the absence of specific risk factors[13]. Similar to rectal adenocarcinoma, MRI with diffusion-weighted imaging (DWI) is considered the most sensitive imaging method for detecting regional lymph node and pelvic structure involvement in more advanced tumors[13]. Ga-enhanced MRI with DWI is more sensitive than CT for detecting liver and bone metastases. If liver metastases are only detectable by MRI, it should then be used as the primary procedure for follow-up[17]. The European Neuroendocrine Tumor Society recommends MRI for all tumors ≥ 10 mm, all G2/G3 tumors and all cases with suspected lymph node or liver involvement prior to resection[8,13].

Somatostatin-receptor imaging: 68Ga-SSR-PET/CT can assess the primary and metastatic sites. However, it is not routinely recommended for evaluating small rNETs before treatment, as it is not clear whether somatostatin receptors are highly expressed in these tumors, even though most well-to-moderately differentiated NETs do express them. If there is concern of lymph node involvement on MRI, functional imaging should be considered[8]. There is no strong recommendation favoring one modality (*e.g.*, 68Ga-DOTA-PET/CT) over others (*e.g.* DOTATOC, DOTANOC, or DOTATATE)[17]. For PET/CT, it is important to understand the limitations, including its spatial resolution of about 5 mm and potential false positivity at sites of infection/inflammation. Imaging should be performed at an appropriate time after treatment with confirmed SSR expression, usually > 6 months[13]. Other lesions, such as leiomyomas with SSR expression, can also be a source of false positivity on PET/CT scans[52]. 68Ga-SSR-PET/CT is generally more sensitive than 18F-fluorodeoxyglucose-PET/CT[53]. Another promising somatostatin receptor imaging technique is 18F-AIF-NOTA-octreotide, which uses F-18 instead of Ga-68 for labeling. In a study of 26 patients with gastrointestinal NETs ≤ 10 mm, the patient-based sensitivity of 18F-AlF-octreotide PET/CT was 62%, compared to 38% for contrast-enhanced CT/MRI[54]. In rare cases, screening for distant metastasis in rNETs with PET/CT may help identify NETs in other location [55].

TREATMENT STRATEGY

There is ongoing debate regarding the management of rNETs. A key question is which tumors can be resected endoscopically, and which endoscopic technique should be used[8]. Unfortunately, due to the relatively low incidence of these tumors, most of current evidence comes from single-center and/or retrospective studies with inconsistent data. This inconsistency may stem from differences in endoscopic skills and training across centers, leading to a preference for one technique over another in specific situations. Meta-analyses have primarily included studies conducted in Asian countries, which may introduce bias due to regional variations in endoscopic expertise. Randomized clinical trials comparing the outcomes of specific techniques are scarce, and more studies are needed to support the existing evidence [13]. As a result, most guidelines do not strongly recommend specific techniques for endoscopic resection, or weakly recommend with low levels of evidence[40,56] (Table 1).

Benefit of histological complete resection

rNETs have metastatic potential, and resection offers the only curative option, reducing the risk of metastasis in most cases. Treatment should be carefully selected to ensure a histological complete (R0) resection[8]. R1 resection is defined when the tumor reaches the resection margin in the tissue sample[13]. Currently, there is no restriction for the extent of free margin; even a free margin < 1 mm is still considered R0[13]. However, measuring the vertical distance from the tumor border to the resection margin in the resected specimen may provide useful information about the adequacy of the resection margin[24]. Even with a 2-3-mm sampling interval thoroughly as in endoscopic submucosal dissection (ESD), an inadequate vertical margin distance still increases the risk of exposed tumor margins. However, there is no consensus on what constitutes an adequate margin. Theoretically, any endoscopic resection method that secures a longer vertical margin distance could achieve a more complete resection. This could potentially decrease surveillance burden, local recurrence, morbidity and mortality associated with rNET recurrence[24]. However, previous studies suggest that the vertical margin distance may be more related to invasion depth than to the endoscopic technique used[57]. Further studies are needed to validate the significance of vertical margin distance.

The slow progression of rNETs necessitates long-term follow-up, potentially up to 20 years. When properly treated, an R0 resection in grade 1 lesions ≤ 10 mm carries a low risk of recurrence and metastasis, allowing patients to be discharged from periodic follow-up[1,8]. Most incidentally diagnosed patients are relatively young and in good health, and they are likely to have only localized disease that can be cured with resection. Improper treatment can lead to a long-term burden for both the medical facilities and patients, increase the risk of metastasis, and result in repeated follow-up with radiological and endoscopic examinations, as well as the potential need for salvage therapy[1,3]. Therefore, it is crucial to balance the potential benefit of treatment against the risk of incomplete resection[8].

What not to do

Various endoscopic techniques have been attempted for the removal of rNETs, ranging from simple polypectomy to ESD

Table 1 Summary of resection techniques and recommendations for rectal neuroendocrine tumor less than 10 mm

Ref.	Endoscopic option	Strategy after R1 resection	Strategy after R0 resection with risk factors	General follow-up recommendations
French intergroup, 2020 [17]	EMRL/EMRC/ESD	Consider salvage resection	Surgical resection with lymphadenectomy	No follow-up required for rNETs that are G1, < 10 mm, T1 and R0 after the initial resection. For others, regular endoscopic examination and abdominal/pelvic MRI
JNETS, 2021[64]	Not specified	Surgery	Surgery for rNETs that are > 1 cm or G2; MP invasion; or suspected local LNM	Not specified
ESGE, 2022[56]	mEMR	Repeat endoscopy at 3-6 m. Salvage resection with confirmed residue disease in expert centers	Annual endoscopy as well as imaging modalities	No follow-up required for rNET that are < 10 mm, G1-G2, no MP invasion, and no LNM
ENETS, 2023[13]	mEMR/ESD/EFR	Watch and wait after discussion with patient if negative EUS, MRI and repeat biopsy. Salvage endoscopic resection or TAMIS	For rectal NET G1 L1 or V1 or G2/G3 ≤ 10 mm, 6 monthly abdominopelvic MRI and yearly sigmoidoscopy for at least 5 years. 68Ga-SSR-PET/CT initially and after 12 months	No follow-up for a rectal NET G1 L0 V0 ≤ 10 mm. After R1 resection without a second endoscopic resection, endoscopy and EUS or MRI 12 monthly for at least 5 years is recommended
Italian, 2024[33]	mEMR (EMRC preferred) or ESD	Watch and wait may be considered after patient consultation. Salvage resection with EMR > ESD > EFR or TAMIS	Not specified	Not specified
NCCN, 2025[122]	Not specified	Endoscopy at 6-12 m to assess for residue disease. For patients with residual disease, rectal MRI or EUS should be performed before TEM/ER	Not specified	No follow-up

R0 resection: Complete resection; R1 resection: Incomplete resection; EMRL: Endoscopic submucosal resection with a ligation device; EMRC: Cap-assisted endoscopic submucosal resection; ESD: Endoscopic submucosal dissection; rNET: Rectal neuroendocrine tumor; MRI: Magnetic resonance imaging; JNETS: Japanese Neuroendocrine Tumor Society; MP: Muscularis propria; LNM: Lymph node metastasis; ESGE: European Society of Gastrointestinal Endoscopy; mEMR: Modified endoscopic submucosal resection; EFR: Endoscopic full-thickness resection; EUS: Endoscopic ultrasound; TAMIS: Transanal minimally invasive surgery; NET: Neuroendocrine tumor; 68Ga-SSR-PET/CT: Gallium-68-somatostatin receptor-positron emission tomography/computed tomography; EMR: Endoscopic submucosal resection; NCCN: National Comprehensive Cancer Network; TEM: Transanal endoscopic microsurgery; ER: Endoscopic resection.

and endoscopic full-thickness resection (EFR). Cold biopsy often results in an unevaluable specimen, making it difficult to guarantee complete resection on histological analysis and increasing the risk of incomplete resection in subsequent treatment[1,31]. This is commonly used when the lesion is not recognized as an rNET and assumed to be a common polyp [13,16]. Although the optimal endoscopic resection method remains unclear, it is clear that when an rNET is suspected, advanced resection techniques should be preferred over standard polypectomy or conventional EMR due to the high rate of positive margins with the latter[17]. Polypectomy is ineffective for rNETs, as they are mostly submucosal. In one study, the complete resection rate by polypectomy was only 31%[58]. Similarly, conventional EMR achieves R0 resection in only 50% of cases for rNETs ≤ 10 mm[59]. Multiple meta-analyses have shown the low R0 resection rate in conventional EMR, which is the reason why conventional EMR is generally recommended only for lesions < 5 mm[60-62].

Principles for rNETs ≤ 10 mm

rNETs originate from the lower crypts and infiltrate the submucosal layer, exhibiting a subepithelial tumor-like growth pattern[24]. Therefore, any diagnosed or suspected rNETs should be treated as a submucosal malignancy. Scheduled resection should be arranged rather than surveillance. According to SEER data, a delay of > 6 months was associated with an increased risk on survival with a hazard ratio of 4.5[63].

Guidelines recommend that choosing resection technique of rNETs depends on tumor size, grade and presence of lymph node involvement[8]. However, tumor size is the only factor that can be accurately evaluated before resection. For rNETs < 10 mm, local resection is recommended[2]. Although there are slight variations, current guidelines generally suggest resection either by mEMR for lesions ≤ 10 mm or by ESD/transanal endoscopic microsurgery (TEM) for lesions up to 20 mm[40,56] (Table 1). Oncological surgical resections are not routinely recommended for small rNETs without adverse histological or endoscopic features[3].

The most important technical aspect in resecting rNETs is to obtain a negative vertical margin[64]. Specimen handling should be given particular caution to facilitate the evaluation of margin status. A common safe practice is to align the fresh sample on cardboard to reduce fixation shrinking artifacts, allowing pathologists to properly assess the margins

[13]. However, adherence to these practices is poor. According to a nationwide study in the Netherlands, resection margin was unsure or unknown in 48% of lesions. Tumor grade was unclassified in 50% of lesions, and only 33% and 13% of lesions were assessed for mitoses and Ki67 expression, respectively[65].

OPTIONS FOR ENDOSCOPIC RESECTION

mEMR techniques have been developed to improve the efficacy of conventional EMR. Some mEMR techniques enhance the resection depth by both a fluid cushion and submucosal stretching through suction, such as EMR with a ligation device (EMRL) and cap-assisted EMR (EMRC). Others do not include these steps, such as underwater EMR (EMRU) or circumferential incision EMR (CI-EMR).

mEMR with submucosal stretching

As mentioned earlier, mEMR with submucosal stretching combines submucosal injection and stretching to ensure adequate resection depth. EMRL is conducted using a ligation device attached to the endoscope. After submucosal injection with 3-5 mL normal saline, the lifted lesion is suctioned into the ligation device, allowing more submucosal tissue to be removed. An elastic band is then deployed, and the lesion is resected under the band using a snare[16]. In the EMRC procedure, a transparent cap with an inner groove is fitted to the scope. After submucosal injection with 3-5 mL normal saline, a crescent-shaped snare is looped along the inner groove, and the lesion is suctioned into the cap, grasped with the snare and resected[66]. These two mEMR techniques are the most commonly used methods. They provide undamaged round specimens with deeper and wider resection margins[24]. The key tip to obtain such specimens is to keep sustained suction to totally block the endoscopic view before releasing the rubber band or tightening the snare. The procedures are simple, have short procedure times and offer an excellent safety profile. Another advantage of EMRL or EMRC is that it requires less training. A Japanese retrospective study indicated EMRL performed by less-experienced endoscopists did not result in lower R0 resection[67]. Therefore, these techniques are recommended by guidelines for rNETs ≤ 10 mm (Table 1). There are also limitations for these methods. EMRL and EMRC rely on suction of submucosal tissue into the cap, and their performance dramatically compromises with significant submucosal fibrosis or larger lesions > 10 mm.

Several modifications of EMRL and EMRC have been proposed. Abe *et al*[68] used EUS to monitor the injection process, significantly improving the R0 resection rate. Li *et al*[69] performed EUS after deploying the rubber band to ensure completely ligation of the lesion. However, monitoring the injection process can be tricky, as it requires the simultaneous use of two devices. A linear EUS scope might be used instead of a regular endoscope. EUS after ligation may risk the rubber band becoming loose or falling off. In Li *et al*'s study[69], 12 of 48 lesions were considered as incomplete ligations requiring additional ligations, which seems less efficient when an 89% R0 resection rate was achieved in the control EMRL group. Similar to Li *et al*'s study[69], another study proposed routinely adding an extra band before snare resection in EMRL, but the additional benefit of this step remains debated[70]. Gao *et al*[71] suggested omitting the submucosal injection step in EMRC to aspirate more tissue and reduce device costs. They validated this method in a prospective trial, achieving a 97% R0 resection rate. However, the noninferior trial was designed to compare modified EMRC to ESD, not to standard EMRC with submucosal injection. Since mEMR relies on submucosal stretching after separating the tumor from underlying submucosal tissue with injection, it remains uncertain whether omitting injection compromises the vertical margin status.

Another form of mEMR with submucosal stretching is called strip biopsy or EMR using a dual-channel endoscope. Strip biopsy is performed with a dual-channel endoscope, usually without submucosal injection. The lesion is lifted with grasping forceps and then resected using a snare delivered through the other channel. There is limited data of strip biopsy, presumably less effective than ESD[72]. This technique is rarely used today due to the requirement for a multichannel endoscope. Lu *et al*[73] proposed using a prelooped snare on an attached transparent cap to substitute for the dual-channel endoscope. However, handling the snare can be tricky, and the efficacy of this method for achieving R0 resection remains to be validated.

mEMR without submucosal stretching

Several novel mEMR methods have been developed that omit the step of submucosal stretching. Many of them have been poorly evaluated for histological complete resection, with limited case numbers. A recent meta-analysis found that these techniques did not show superiority over convention EMR, unlike EMRL/EMRC[60].

The circumferential incision mEMR technique was first described as an option to facilitate *en bloc* resection for medium-sized mucosal lesions unsuitable for conventional EMR. It involves marking around the lesion, lifting the mucosal layer with injection, and then performing snare resection instead of dissection as in ESD. CI-EMR achieved an *en bloc* resection rate of 97% and a complete resection rate of 94%[74]. However, while this technique may improve lateral margin handling through mucosal circumferential incision, it does not enhance resection depth, as submucosal injection is the only measure to improve resection depth. A meta-analysis found that CI-EMR was less favorable than EMRL/EMRC in terms of positive vertical margin rates[62].

EMRU is inspired by the observation that the mucosa and submucosa separate from the MP when air is removed from the colorectal lumen and replaced with water. This reduces lumen stretching, thickens the submucosal layer, and facilitates resection with just a snare, allowing for the capture of a larger mucosal surface[16]. The main advantage of EMRU is that it requires no additional devices other than water immersion. However, there have been few studies with adequate case numbers and histological complete resection rate or resection depth for EMRU. Evidence from large sessile

colorectal polyps suggests that a thickened submucosal layer facilitates obtaining an adequate vertical margin[75]. However, it is unclear whether EMRU is as effective as mEMR with submucosal stretching. EMRU has only been compared to ESD, with an R0 resection rate of 86%[76]. Additionally, the narrowed visual field due to changes in the refractive index of light and the shrunken intestinal lumen during water immersion can make securing the lateral margin challenging.

ESD

Most rNETs extend into the submucosal layer and require resection at a deeper plane than mucosal lesions, ideally close to the MP. The adjustable dissection plane in ESD makes it a seemingly ideal technique for rNETs[57]. Guidelines recommend ESD as an optimal option for rNETs < 20 mm. However, it is technically difficult to maintain an adequate and steady resection depth during submucosal dissection, often resulting in positive vertical margins or perforation if losing control of dissection plane. ESD may also be less ideal for securing lateral margins in small lesions like rNET, as the fluid cushion may not last till the end of the procedure. Additionally, ESD requires a long learning curve to achieve proficiency. A subgroup analysis by Kitagawa *et al*[66] found that trainees achieved a lower histological complete resection rate with ESD (65%) compared to mEMR (88%), while experts showed no difference, indicating that ESD should be performed by experienced endoscopists for rNETs.

The comparison of R0 resection rates between ESD and mEMR is controversial. Retrospective data comparing EMRC to ESD showed that ESD achieved a 100% *en bloc* resection rate, but the histological complete resection rate was only 80% for rNETs ≤ 10 mm, which was inferior to the 92% rate in the EMRC group[77]. In a similar study comparing EMRL to ESD, the R0 resection rate was 91% for EMRL and 82% for ESD[66]. Multiple meta-analyses have failed to showed a significant difference between mEMR and ESD[78]. A network meta-analysis ranked EMRL as the best treatment over ESD, although there was no significant difference in R0 resection rates. However, ESD showed more positive vertical margin cases than EMRL showed[62]. Similarly, another meta-analysis of 14 studies involving 823 patients found that mEMR with suction was superior to ESD in terms of R0 resection, although this result was achieved by excluding outliers[79]. A recent nonrandomized prospective study involving 50 institutes in Japan found no difference in R0 resection rates between mEMR (95%) and ESD (95%) for colorectal NETs ≤ 10 mm[80]. Further evidence from randomized clinical trials is needed to clarify the efficacy of ESD compared to mEMR[81].

Although mEMR may be superior to ESD, there are situations where ESD is the only option. For lesions > 10 mm, ESD is often necessary, as most mEMR caps cannot accommodate such sizes. If there is significant fibrosis after extensive biopsy without lymph node involvement, ESD may also be preferred over mEMR[8]. Therefore, a proper strategy should be used to avoid noncurative resection margins. Endoscopic intermuscular dissection, an emerging therapeutic modality that has gained attention for its efficacy in reducing positive vertical margins, particularly in managing NETs[82,83]. Underwater endoscopic intermuscular dissection has also been reported to enhance procedural efficacy[83]. However, intermuscular dissection is also technically challenging, as it requires maintaining a dissection plane between circular and longitudinal muscle fibers. Clips and loop traction may help achieve adequate depth by expanding and stabilizing the view of submucosal space (Figure 2)[84,85]. However, a recent retrospective study found no significant difference in vertical margin distance or R0 resection rates between traction-assisted ESD and conventional ESD[57]. This is possibly due to the small number of 24 cases in the traction-assisted ESD group. The tunnel method may also facilitate intermuscular dissection[82].

EFR

When potential MP involvement is suspected, EFR should be utilized to ensure complete resection. Most EFR procedures are assisted by an over-the-scope clip (OTSC). The lesion is drawn into the cap of the endoscope by suction or grasping forceps, and OTSC is deployed over the lesion. A snare resection is performed above the clip, cutting through the entire bowel wall and enabling full-thickness resection[8]. A recent small study has reported a 100% R0 resection rate, with short intervention time and no major adverse events[86]. The short learning curve for OTSC makes it a user-friendly option for less-experienced endoscopists. However, these is a small chance of failing to capture the entire wall. Device malfunction, such as clip slippage, inadequate closure, and failed deployment, may occur, although they are uncommon [87]. Resection on the metal clip can also cause extensive thermal damage to the bowel wall and specimen, increasing the risk of indetermined margin status and postprocedural coagulation syndrome.

Traditional exposed EFR may also be performed. In other locations, such as the stomach, the defect produced by EFR is difficult to close due to compromised insufflation during the procedure[87]. In the rectum, however, the resection site is usually below the peritoneal reflection, and there is no free space if perforation occurs during the procedure. This allows the endoscopic view to be maintained, and closure of rectal wall defect may be easier (Figure 3). However, the risk of retroperitoneal infection remains, and closure with sufficient strength, such as using a detachable snare assisted clip closure, is recommended. Data are scarce on exposed EFR[88]. In small rNETs ≤ 10 mm, EFR is rarely needed, as ESD with intermuscular dissection should provide adequate resection depth to ensure clear margins.

STRATEGY AFTER INCOMPLETE RESECTION

Histological complete resection of an rNET with no risk factors for recurrence is considered curative. Incomplete resection can be categorized as R1, where there is microscopic involvement of the margins, or R2, where visible tumor remains after resection[8]. For rNETs at low risk of metastasis with an initial R1 endoscopic resection, salvage resection by ESD or TEM can be proposed, but this should be restricted to expert centers[17]. If metastasis is suspected, oncological surgical

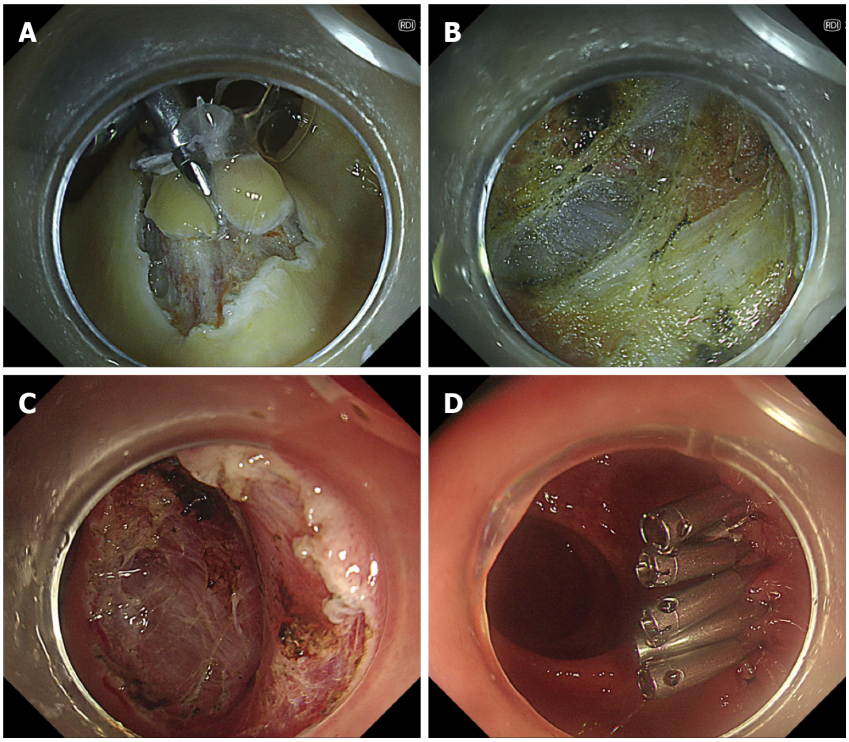

Figure 2 Endoscopic intermuscular dissection in a rectal neuroendocrine tumor. A: The lesion from case 2 (Figure 1C and D) was treated with intermuscular dissection. After circumferential incision, traction was applied with clips and a loop; B and C: During dissection, the circular muscle layer was carefully removed till the outer longitudinal muscle was fully exposed; D: Clips were used to close the mucosal defect.

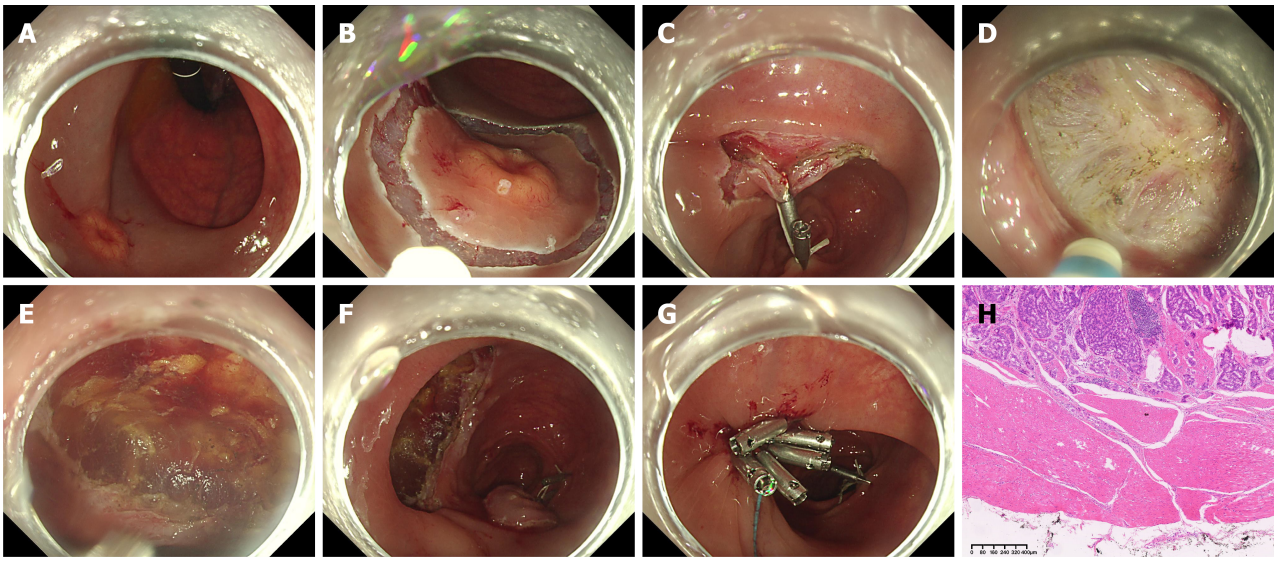

Figure 3 Endoscopic full-thickness dissection in a 15-mm rectal neuroendocrine tumor. A: The lesion from case 3 (Figure 1E and F) was treated with endoscopic full-thickness dissection. Preprocedural positron emission tomography/computed tomography ruled out metastasis, and endoscopic ultrasound confirmed the involvement of the muscularis propria (MP). The lesion showed poor lifting with submucosal injection, indicating involvement of MP; B and C: After circumferential incision, traction was applied with clips and a loop; D: During dissection, the circular muscle was attempted for removing. However, extensive fibrosis made it impossible to preserve the outer longitudinal muscle, likely due to tumor invasion into MP; E and F: The entire rectal muscular wall was removed; G: Clips with a detachable snare were used to close the defect; H: Histological analysis revealed a complete structure of MP and a negative vertical margin, classified as pT2Nx. The patient opted to follow-up instead of additional radical surgery.

resection should be considered. R1 resection is predominantly associated with endoscopic techniques[89]. It is crucial for endoscopists to properly recognized the lesion as an rNET and avoid routine biopsy[18,19]. Lesion characteristics, such as central depression and tumor size, may also play a role in R1 resection[22,90].

Detection of remnant tumor

The presence of remnant tumor after initial R1 resection varies significantly, ranging from 17% to 43%[13,91]. Many patients with R1 resection opt for follow-up rather than salvage resection, and only those with confirmed remnant tumors undergo additional treatment[1,13]. This may lead to biased patient selection in retrospective studies, with over-representation of cases with remnant tumors. In many studies addressing remnant tumors, a large number of cases were treated by biopsy or cold snaring rather than endoscopic resection techniques, sometimes accounting for up to 80% of cases[92]. For incidentally found lesion as small as 2-3 mm, complete resection may be achievable with biopsy alone[93]. However, for larger lesions, it is unlikely to achieve R0 resection with biopsy or cold snaring. Additionally, biopsied or cold snared specimens are rarely properly oriented, making margin status difficult to determine.

In cases where advanced techniques were used based on recommended treatment, the actual residual rate after additional treatment is < 20%. Therefore, adherence to guidelines is strongly recommended[40,94]. For lesions < 10 mm treated with endoscopic resection methods including EMR, the tumors with R1 resection are often resected at or close to the edge, which is technically an R1 resection by pathological standards. This does not necessarily mean that tumor tissue remains at the resection site, as the cautery effect may destroy residual tumor cells. However, the indolent nature of rNETs means that recurrence may take decades to manifest, as evidenced by a case report of recurrence 16 years after initial polypectomy[24]. The only independent factor related to residual disease appears to be the size of the lesion[92].

EUS has been recommended to assess the remaining submucosal tumors[17]. However, there is debate about whether EUS features can accurately predict residual disease[95]. A Korean retrospective study found that EUS had a similar area under the curve to simple visual detection (0.886 *vs* 0.870) for detecting remnant tumor[96]. A biopsy of the scar after close inspection may be useful, even if there is no visible evidence of remnant tumor on endoscopy, as residual disease may still be present.

Watch-and-wait strategy

Some patients may choose a watch-and-wait strategy, regardless of recommendations[1,97]. The significance of marginal status as a risk factor for recurrence remains uncertain[33,98]. One study of 436 patients with rNETs treated by ESD, with a median follow-up period of 61 months, found only one recurrence and one metastasis in 73 patients with R1 resection who opted for follow-up, compared to one recurrence and two metastases in 319 cases with R0 resection. There were no significant differences in survival between the two groups[94,99]. Similar results have been reported in multiple studies [22,94,100]. A meta-analysis comparing resection techniques for small rNETs found overall recurrence rates to be low (< 1%), with one local recurrence and one case of liver metastasis. However, the duration of follow-up was short[101]. Therefore, follow-up may be a feasible alternative to rigorous salvage therapy for patients who acknowledge the risk of possible recurrence and the need for long-term, potentially lifelong, follow-up[92,94]. When R1 resection occurs, the positive resection margins should be measured and discussed with pathologists to assess the risk of remnant tumor[102]. For grade 1 lesions ≤ 10 mm without LVI and no residual disease on scar biopsy, salvage procedure may not be necessary [1,8].

Endoscopic salvage therapy

Traditionally, rNETs with any risk factor for metastasis, including R1 resection, were considered for surgical resection with lymphadenectomy[17,94]. However, emerging evidence suggests that endoscopic procedures may be sufficient to achieve histological complete resection[103]. If there is evidence of residual disease in small tumors without lymph node involvement, local resection techniques such as TEM or ESD can be performed to achieve complete resection[8,92]. For patients who were not initially suspected of having an rNET and received nonrecommended endoscopic treatment (*e.g.*, biopsy or cold snare), salvage treatment should be recommended due to high risk of residual lesions[92,94]. Some endoscopists recommended systematic scar resection, regardless of whether residual tumor is detected, to allow patients to avoid long-term follow-up if no other high risk factors are present[8,92].

Salvage resection techniques (ESD/EFR *vs* EMR) have been reported as the only significant factor associated with curative resection. mEMR can be performed if the scar is not visible and the lesion elevates satisfactorily after injection. Choosing mEMR may reduce the complicate rates, technical difficulty and medical costs. However, it is unlikely that no scar presents if the previous attempt was endoscopic resection rather than biopsy[92]. Therefore, ESD or EFR are the only options in this situation. Salvage endoscopic procedures using ESD or EFR have shown an R0 resection rate of near 100% [92]. When performing salvage ESD, care must be taken to ensure adequate resection depth (Figure 4). The inner circular muscular layer should be completely removed, and if scar blurs the border of muscle fibers, dissection under the scar is recommended to ensure negative margins[104,105]. A traction device can also be used to provide sustained counter-traction during the procedure[106]. EFR has also been reported in salvage treatment for residual rNET lesions[107]. However, intentionally performing full-thickness resection may not be advisable when intermuscular dissection is likely to achieve adequate resection depth with a lower risk of adverse events.

Ju *et al*[108] proposed a type of polypectomy in salvage therapy of rNETs called wide hot snare polypectomy (WHSP). This technique involves placing a snare widely around the lesion to secure sufficient margins and then tightening it while pushing toward the lesion. They demonstrated a significantly higher R0 resection rate in the WHSP group (73%) compared to the ESD group (50%)[108]. However, this technique is more of a refinement of polypectomy rather than a novel procedure. The limitations of WHSP include the small size of the lesions (median 4 mm) and the fact that most previous treatments were biopsies (79%)[108].

Before considering salvage resection, endoscopic re-evaluation is essential to ensure complete removal of any residual rNET tumor[92]. Patients should undergo MRI evaluation of the scar area prior to second resection[8]. The primary benefit of salvage resection is to alleviate the burden of long-term follow-up[13,92]. However, it remains unclear whether

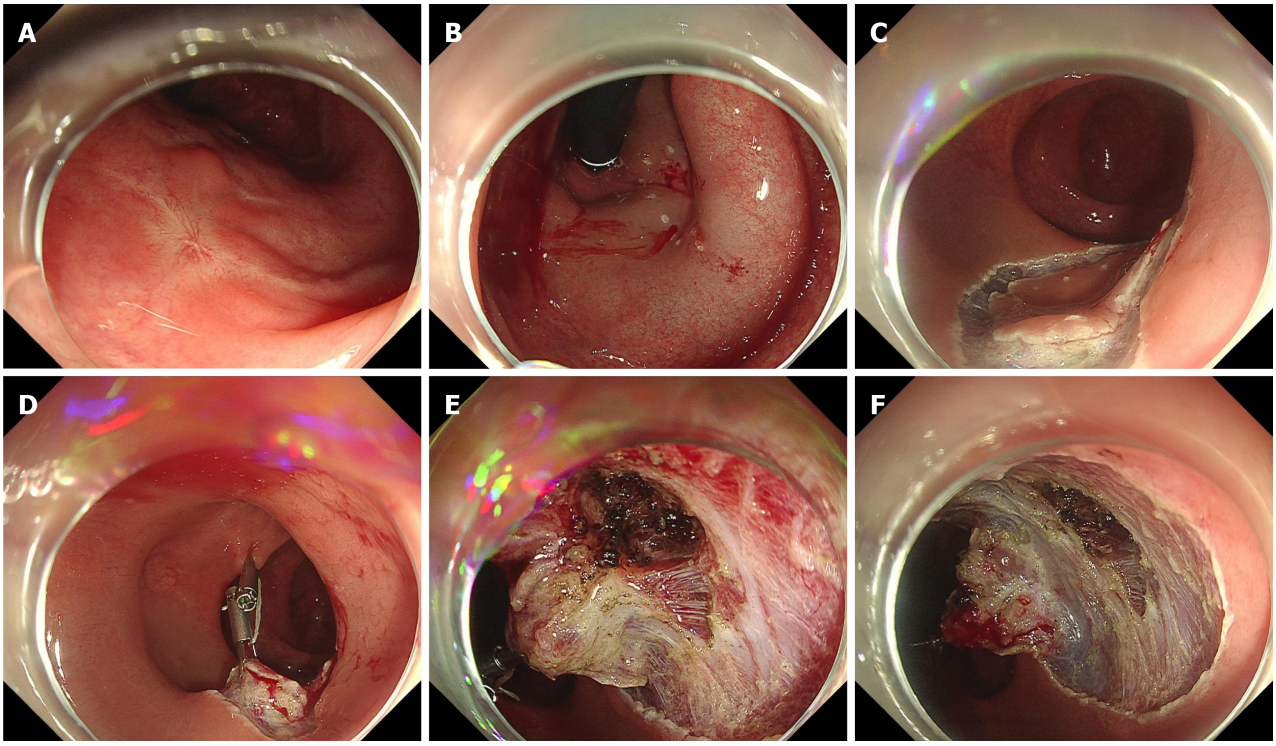

Figure 4 Endoscopic salvage resection in a scar after endoscopic resection of rectal neuroendocrine tumor. A and B: Previous polypectomy showed a positive margin on histology. The scar exhibited poor lifting with submucosal injection; C and D: After circumferential incision, traction was applied with clips and a loop; E and F: During dissection at the scar site, the circular muscle layer was carefully removed to perform intramuscular dissection. Histological analysis showed no residue tumor.

re-resection of R1-resected small rNETs affects long-term outcomes.

PROGNOSIS AND FOLLOW-UP

Prognosis

rNETs have the best prognosis among all gastrointestinal NETs, with 5-year survival rate ranging 74% to 98%, according to various registry analysis[109,110]. Even in cases with metastasis, up to 77% to 89% of patients survived the first 5 years [36,38]. For rNETs ≤ 10 mm with complete resection and no other risk factors, the prognosis is usually curative. However, there are limited studies on long-term outcome following endoscopic treatment[31,111]. It should not be assumed that a T1 primary lesion will always have no lymph node or distant metastasis[3,112]. There are multiple published cases of small, well-differentiated rNETs recurring with lymph node involvement or distant metastases after apparent complete removal *via* endoscopic treatment[113,114].

Individualized survival prediction has garnered significant interest. Theoretically, these nomograms and predictive tools could provide more precise survival estimates by incorporating more factors such as age, tumor size, grade and LVI [115]. However, these tools have limited efficacy and poor generalization ability. Although they perform significantly better than the World Health Organization grade and American Joint Committee on Cancer tumor-node-metastasis classification, their C-index is only 0.65-0.70 for predicting overall survival, likely due to the limited case numbers in the training and validation datasets[49,116,117]. Recently, a GATIS score was developed to predict individualized survival for rNET patients based on a cohort of 1183 patients from 17 hospitals. In addition to common factors like tumor grade, T staging, tumor size, and age, the GATIS score further includes the prognostic nutritional index as a key component. Given the slow progression of rNETs, prognostic nutritional index may be a useful prognostic factor, as it reflects nutritional status[118,119]. The GATIS score demonstrated higher predictive power than tumor-node-metastasis stage and World Health Organization grade, with a C-index of 0.812 for overall survival and 0.865 for progression-free survival in the validation set[118]. However, the median follow-up duration of 34 months was short[120]. These nomograms and tools require further validation before they can be widely used to guide clinical decision-making in rNET management [115,121].

Follow-up

Most current guidelines recommend that patients with histologically complete resected rNET ≤ 10 mm and no risk factors for metastasis require no additional follow-up[13,40,56] (Table 1). However, localized recurrence or metachronous lesions may still occur, albeit at a low rate. Since these patients are typically in their 50s to 60s, minimal follow-up with colonoscopy as average-risk people is still encouraged. While it is not cost-effective to routinely perform imaging

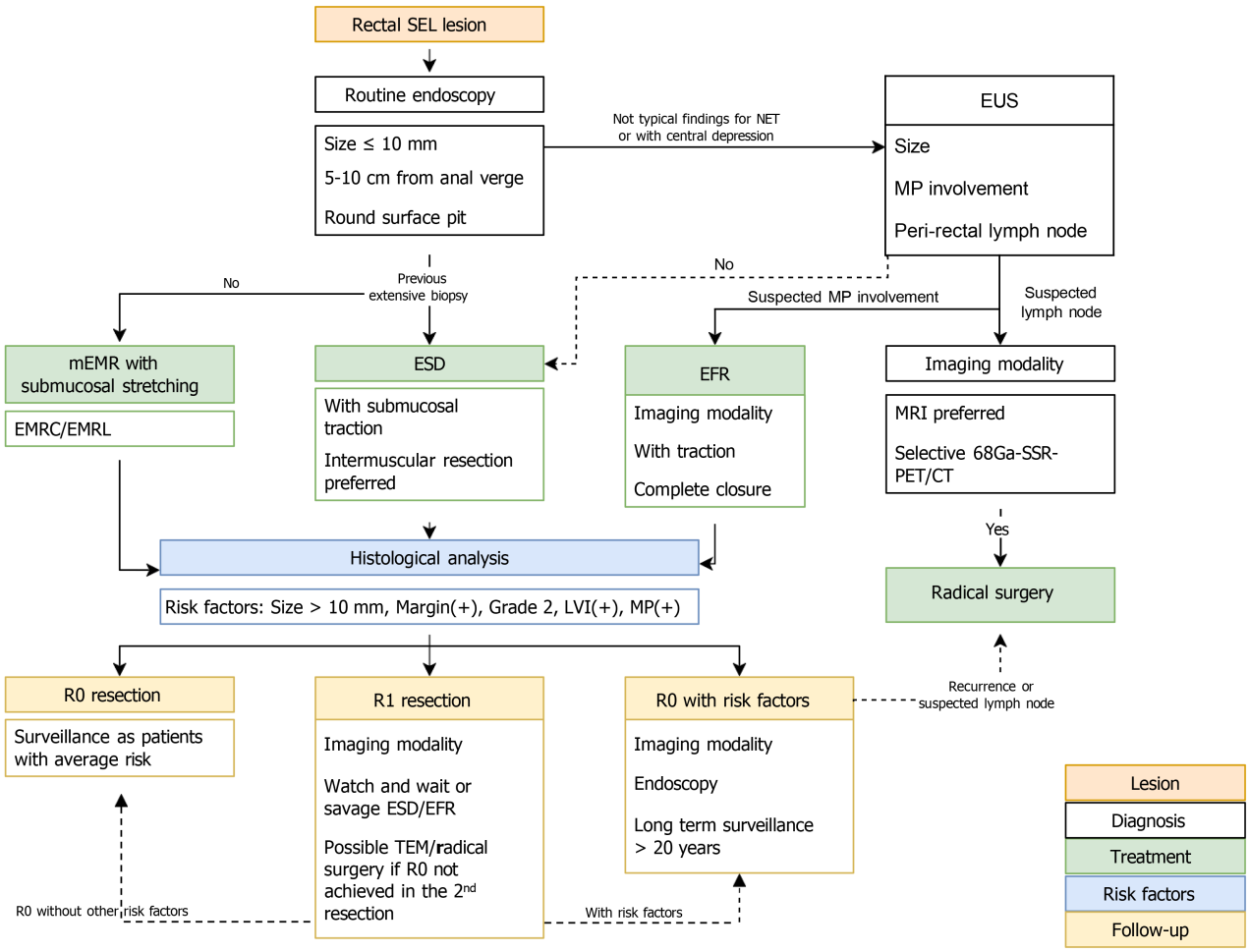

Figure 5 Proposed algorithm for the management of rectal neuroendocrine tumors. SEL: Subepithelial lesion; NET: Neuroendocrine tumor; EUS: Endoscopic ultrasound; MP: Muscularis propria; mEMR: Modified endoscopic submucosal resection; ESD: Endoscopic submucosal dissection; EFR: Endoscopic full-thickness resection; EMRC: Cap-assisted endoscopic submucosal resection; EMRL: Endoscopic submucosal resection with a ligation device; MRI: Magnetic resonance imaging; 68Ga-SSR-PET/CT: Gallium-68-somatostatin receptor-positron emission tomography/computed tomography; R0 resection: Complete resection; R1 resection: Incomplete resection; TEM: Transanal endoscopic microsurgery.

modalities such as MRI or PET/CT for surveillance, physicians should consider the possibility of recurrence based on the patient's history, if there is unknown lesion are detected incidentally.

For patients with R1 resection without additional treatment or R0 resection with risk factors (*e.g.*, tumor grade G2/G3, invasion of the MP, or LVI), the risk of metastatic spread is higher[8]. Immediate radical surgery is not absolutely necessary for these patients. However, there are reports of diffuse multiple rNETs remaining nonprogressive after 20 years of follow-up[112]. Metachronous metastatic recurrence may occur very late, and long-term follow-up is recommended for delayed recurrence (at least 20 years, potentially lifelong), starting from annual surveillance, although follow-up interval can be progressively lengthened[4,17,112]. This follow-up includes regular endoscopic examination and imaging. There have been limited studies on personalized follow-up stratified according to different risk factors; however, it could be a possible area to be explored.

Imaging, including abdominopelvic MRI with DWI, is recommended for rNETs with incomplete resection if a second endoscopic resection with R0 is not performed or if any of the aforementioned risk factors are present[13]. Most patients with NETs have prolonged survival, so radiation safety must be considered in their management. While imaging remains a cornerstone of follow-up, repeated CT-induced irradiation should be avoided, especially for patients with slowly or nonprogressive NETs. Nonionizing imaging techniques, such as MRI, should be considered as an alternative[17]. The role of functional imaging, particularly 68Ga-SSR-PET/CT, in follow-up remains unclear due to limited data[112]. According to European Neuroendocrine Tumor Society guideline, 68Ga-SSR-PET/CT is not recommended as a regularly performed modality during surveillance[13].

PROPOSED ALGORITHM FOR MANAGEMENT

As summarized in Figure 5, the initial evaluation of small rNET should thoroughly assess endoscopic features, including size, location, surface pit pattern and atypical changes including central depression. Imaging modalities, such as MRI-

DWI, should be used to rule out lymph node involvement and distant metastasis. The optimal technique for treating localized small NETs, as well as the follow-up strategy, remains uncertain. However, efforts should be made to avoid cold biopsy or polypectomy. mEMR with submucosal stretching, including EMRL/EMRC, should be prioritized. For R1-resected small tumors without risk factors, salvage resection may be considered to reduce the risk of late recurrence. Long-term follow-up will be necessary if patients decline additional treatment. For patients with R0 resection and risk factors, extended follow-up should be considered[13].

CONCLUSION

rNETs are no longer considered rare due to increased detection through colonoscopy screening. Endoscopists should familiarized themselves with the endoscopic features of rNETs. Advanced endoscopic resection techniques should be preferred over biopsy or cold snaring. Specimen obtained should be thoroughly evaluated for margin status and risk factors related to metastasis. Follow-up strategies should be carefully selected based on histological findings to ensure optimal patient outcomes. Developing novel techniques with more adequate vertical margin distance may further improved the long-term outcome of rNETs.

ACKNOWLEDGEMENTS

Thanks for the generous help from Janet Brandsma of University of Massachusetts Medical Center on manuscript preparation and language revision.

FOOTNOTES

Author contributions: Liu JN conceptualized the study, conducted the literature review and drafted the manuscript, created the artwork; Chen H and Fang N both supervised and made critical revisions, and all authors have read and approved the final manuscript. Chen H and Fang N equally contributed to the current manuscript as co-corresponding authors by providing instructive guidance and critical revisions.

Supported by Nanchang High-Level Scientific and Technological Innovation Talents 'Double Hundred Plan' Project, China, No. 2022-312.

Conflict-of-interest statement: All the authors report no relevant conflicts of interest for this article.

Country of origin: China

ORCID number: Nian Fang 0009-0006-9608-7404.

S-Editor: Wang JJ
L-Editor: A
P-Editor: Zhao S

REFERENCES

1 **Dąbkowski K**, Szczepkowski M, Kos-Kudła B, Starzynska T. Endoscopic management of rectal neuroendocrine tumours. How to avoid a mistake and what to do when one is made? *Endokrynol Pol* 2020; **71**: 343-349 [PMID: 32852049 DOI: 10.5603/EP.a2020.0045]
2 **Hrabe J**. Neuroendocrine Tumors of the Appendix, Colon, and Rectum. *Surg Oncol Clin N Am* 2020; **29**: 267-279 [PMID: 32151360 DOI: 10.1016/j.soc.2019.11.010]
3 **O'Neill S**, Haji A, Ryan S, Clement D, Sarras K, Hayee B, Mulholland N, Ramage JK, Srirajaskanthan R. Nodal metastases in small rectal neuroendocrine tumours. *Colorectal Dis* 2021; **23**: 3173-3179 [PMID: 34731512 DOI: 10.1111/codi.15978]
4 **Kang HS**, Kwon MJ, Kim TH, Han J, Ju YS. Lymphovascular invasion as a prognostic value in small rectal neuroendocrine tumor treated by local excision: A systematic review and meta-analysis. *Pathol Res Pract* 2019; **215**: 152642 [PMID: 31585816 DOI: 10.1016/j.prp.2019.152642]
5 **Dasari A**, Shen C, Halperin D, Zhao B, Zhou S, Xu Y, Shih T, Yao JC. Trends in the Incidence, Prevalence, and Survival Outcomes in Patients With Neuroendocrine Tumors in the United States. *JAMA Oncol* 2017; **3**: 1335-1342 [PMID: 28448665 DOI: 10.1001/jamaoncol.2017.0589]
6 **Basuroy R**, Haji A, Ramage JK, Quaglia A, Srirajaskanthan R. Review article: the investigation and management of rectal neuroendocrine tumours. *Aliment Pharmacol Ther* 2016; **44**: 332-345 [PMID: 27302838 DOI: 10.1111/apt.13697]

7 **Zhu Y**. Incidence trend of neuroendocrine tumors and disparities by sex and race/ethnicity in adults from the United States, 2000-2020. *Eur J Cancer Prev* 2024; **33**: 475-484 [PMID: 38375858 DOI: 10.1097/CEJ.0000000000000877]

8 **Frydman A**, Srirajaskanthan R. An Update on the Management of Rectal Neuroendocrine Neoplasms. *Curr Treat Options Oncol* 2024; **25**: 1461-1470 [PMID: 39476215 DOI: 10.1007/s11864-024-01267-4]

9 **Paciorek A**, Mulvey C, McKinley M, Zhang L, Cheng I, Moon F, Le BK, Shih BE, Whitman J, Bergsland E. Burdens of Gastroenteropancreatic Neuroendocrine Neoplasm by Diverse Race and Ethnicities- A Rigorous Structural Equation Modeling. *J Natl Compr Canc Netw* 2025; **23**: 27-32 [PMID: 39938473 DOI: 10.6004/jnccn.2024.7080]

10 **Jung YS**, Yun KE, Chang Y, Ryu S, Park JH, Kim HJ, Cho YK, Sohn CI, Jeon WK, Kim BI, Park DI. Risk factors associated with rectal neuroendocrine tumors: a cross-sectional study. *Cancer Epidemiol Biomarkers Prev* 2014; **23**: 1406-1413 [PMID: 24813818 DOI: 10.1158/1055-9965.EPI-14-0132]

11 **Pyo JH**, Hong SN, Min BH, Lee JH, Chang DK, Rhee PL, Kim JJ, Choi SK, Jung SH, Son HJ, Kim YH. Evaluation of the risk factors associated with rectal neuroendocrine tumors: a big data analytic study from a health screening center. *J Gastroenterol* 2016; **51**: 1112-1121 [PMID: 27025841 DOI: 10.1007/s00535-016-1198-9]

12 **Leoncini E**, Carioli G, La Vecchia C, Boccia S, Rindi G. Risk factors for neuroendocrine neoplasms: a systematic review and meta-analysis. *Ann Oncol* 2016; **27**: 68-81 [PMID: 26487581 DOI: 10.1093/annonc/mdv505]

13 **Rinke A**, Ambrosini V, Dromain C, Garcia-Carbonero R, Haji A, Koumarianou A, van Dijkum EN, O'Toole D, Rindi G, Scoazec JY, Ramage J. European Neuroendocrine Tumor Society (ENETS) 2023 guidance paper for colorectal neuroendocrine tumours. *J Neuroendocrinol* 2023; **35**: e13309 [PMID: 37345509 DOI: 10.1111/jne.13309]

14 **Sekiguchi M**, Kawamura T, Horiguchi G, Mizuguchi Y, Takamaru H, Toyoizumi H, Kato M, Kobayashi K, Sada M, Oda Y, Yokoyama A, Utsumi T, Tsuji Y, Ohki D, Takeuchi Y, Shichijo S, Ikematsu H, Matsuda K, Teramukai S, Kobayashi N, Matsuda T, Saito Y, Tanaka K. Colorectal Neuroendocrine Neoplasm Detection Rate During Colonoscopy: Results From Large-Scale Data of Colonoscopies in Japan. *Am J Gastroenterol* 2025; **120**: 473-477 [PMID: 39311566 DOI: 10.14309/ajg.0000000000003088]

15 **Abboud Y**, Pendyala N, Le A, Mittal A, Alsakarneh S, Jaber F, Hajifathalian K. The Incidence of Rectal Neuroendocrine Tumors Is Increasing in Younger Adults in the US, 2001-2020. *Cancers (Basel)* 2023; **15**: 5286 [PMID: 37958459 DOI: 10.3390/cancers15215286]

16 **Gallo C**, Rossi RE, Cavalcoli F, Barbaro F, Boškoski I, Invernizzi P, Massironi S. Rectal neuroendocrine tumors: Current advances in management, treatment, and surveillance. *World J Gastroenterol* 2022; **28**: 1123-1138 [PMID: 35431507 DOI: 10.3748/wjg.v28.i11.1123]

17 **de Mestier L**, Lepage C, Baudin E, Coriat R, Courbon F, Couvelard A, Do Cao C, Frampas E, Gaujoux S, Gincul R, Goudet P, Lombard-Bohas C, Poncet G, Smith D, Ruszniewski P, Lecomte T, Bouché O, Walter T, Cadiot G; Thésaurus National de Cancérologie Digestive (TNCD). Digestive Neuroendocrine Neoplasms (NEN): French Intergroup clinical practice guidelines for diagnosis, treatment and follow-up (SNFGE, GTE, RENATEN, TENPATH, FFCD, GERCOR, UNICANCER, SFCD, SFED, SFRO, SFR). *Dig Liver Dis* 2020; **52**: 473-492 [PMID: 32234416 DOI: 10.1016/j.dld.2020.02.011]

18 **Moon CM**, Huh KC, Jung SA, Park DI, Kim WH, Jung HM, Koh SJ, Kim JO, Jung Y, Kim KO, Kim JW, Yang DH, Shin JE, Shin SJ, Kim ES, Joo YE. Long-Term Clinical Outcomes of Rectal Neuroendocrine Tumors According to the Pathologic Status After Initial Endoscopic Resection: A KASID Multicenter Study. *Am J Gastroenterol* 2016; **111**: 1276-1285 [PMID: 27377520 DOI: 10.1038/ajg.2016.267]

19 **Lee SP**, Sung IK, Kim JH, Lee SY, Park HS, Shim CS. The effect of preceding biopsy on complete endoscopic resection in rectal carcinoid tumor. *J Korean Med Sci* 2014; **29**: 512-518 [PMID: 24753698 DOI: 10.3346/jkms.2014.29.4.512]

20 **Lin CK**, Chung CS, Huang WC. Rectal carcinoid tumour observed by magnifying colonoscopy with narrow band imaging. *Dig Liver Dis* 2014; **46**: e7 [PMID: 24411486 DOI: 10.1016/j.dld.2013.12.003]

21 **Hiyoshi Y**, Daitoku N, Mukai T, Nagasaki T, Yamaguchi T, Akiyoshi T, Yasue C, Chino A, Saito S, Takamatsu M, Fukunaga Y. Risk Factors for Lymph Node Metastasis of Rectal Neuroendocrine Tumor and Its Prognostic Impact: A Single-Center Retrospective Analysis of 195 Cases with Radical Resection. *Ann Surg Oncol* 2023; **30**: 3944-3953 [PMID: 36935432 DOI: 10.1245/s10434-023-13348-z]

22 **Zhuang X**, Zhang S, Chen G, Luo Z, Hu H, Huang W, Guo Y, Ouyang Y, Peng L, Qing Q, Chen H, Li B, Chen J, Wang X. Risk factors and clinical outcomes of incomplete endoscopic resection of small rectal neuroendocrine tumors in southern China: a 9-year data analysis. *Gastroenterol Rep (Oxf)* 2023; **11**: goac084 [PMID: 36632622 DOI: 10.1093/gastro/goac084]

23 **Zheng Y**, Hu Y, Li Y, Cui C, Wang X, Ji R. A new endoscopic tumor grading for rectal neuroendocrine tumors: Correlation of vascular pattern with histopathology. *Dig Liver Dis* 2025; **57**: 782-787 [PMID: 39690021 DOI: 10.1016/j.dld.2024.12.002]

24 **Lim HK**, Lee SJ, Baek DH, Park DY, Lee BE, Park EY, Park JW, Kim GH, Song GA. Resectability of Rectal Neuroendocrine Tumors Using Endoscopic Mucosal Resection with a Ligation Band Device and Endoscopic Submucosal Dissection. *Gastroenterol Res Pract* 2019; **2019**: 8425157 [PMID: 31687016 DOI: 10.1155/2019/8425157]

25 **Moon JS**. Endoscopic ultrasound-guided fine needle aspiration in submucosal lesion. *Clin Endosc* 2012; **45**: 117-123 [PMID: 22866250 DOI: 10.5946/ce.2012.45.2.117]

26 **Weng J**, Chen YF, Li SH, Lv YH, Chen RB, Xu GL, Lin SY, Bai KH. Endoscopic ultrasonography-related diagnostic accuracy and clinical significance on small rectal neuroendocrine neoplasms. *World J Gastroenterol* 2024; **30**: 774-778 [PMID: 38515953 DOI: 10.3748/wjg.v30.i7.774]

27 **Liu T**, Shi L, Tan Y. Primary rectal Hodgkin lymphoma mimicking neuroendocrine tumor successfully removed by endoscopic submucosal dissection. *Dig Endosc* 2024; **36**: 625 [PMID: 38558420 DOI: 10.1111/den.14790]

28 **Nishimura T**, Tanaka T, Ishimaru S, Arataki K, Shimamoto F. Benign Lymphoid Polyp of the Rectum Diagnosed and Treated With Endoscopic Submucosal Resection With a Ligation Device. *Cureus* 2024; **16**: e55921 [PMID: 38469365 DOI: 10.7759/cureus.55921]

29 **Park SB**, Kim DJ, Kim HW, Choi CW, Kang DH, Kim SJ, Nam HS. Is endoscopic ultrasonography essential for endoscopic resection of small rectal neuroendocrine tumors? *World J Gastroenterol* 2017; **23**: 2037-2043 [PMID: 28373770 DOI: 10.3748/wjg.v23.i11.2037]

30 **Ishii N**, Horiki N, Itoh T, Maruyama M, Matsuda M, Setoyama T, Suzuki S, Uchida S, Uemura M, Iizuka Y, Fukuda K, Suzuki K, Fujita Y. Endoscopic submucosal dissection and preoperative assessment with endoscopic ultrasonography for the treatment of rectal carcinoid tumors. *Surg Endosc* 2010; **24**: 1413-1419 [PMID: 20033710 DOI: 10.1007/s00464-009-0791-x]

31 **Ahmed M**. Gastrointestinal neuroendocrine tumors in 2020. *World J Gastrointest Oncol* 2020; **12**: 791-807 [PMID: 32879660 DOI: 10.4251/wjgo.v12.i8.791]

32 **Kim JH**, Moon W, Park SJ, Park MI, Kim SE, Ku KH, Lee GW, Choi YJ. Clinical impact of endoscopic ultrasonography for small rectal neuroendocrine tumors. *Turk J Gastroenterol* 2014; **25**: 657-660 [PMID: 25599777 DOI: 10.5152/tjg.2014.6647]

33 **Panzuto F**, Parodi MC, Esposito G, Massironi S, Fantin A, Cannizzaro R, Milione M, De Angelis CG, Annibale B. Endoscopic management of gastric, duodenal and rectal NETs: Position paper from the Italian Association for Neuroendocrine Tumors (Itanet), Italian Society of

Gastroenterology (SIGE), Italian Society of Digestive Endoscopy (SIED). *Dig Liver Dis* 2024; **56**: 589-600 [PMID: 38216439 DOI: 10.1016/j.dld.2023.12.015]

34 **McDermott FD**, Heeney A, Courtney D, Mohan H, Winter D. Rectal carcinoids: a systematic review. *Surg Endosc* 2014; **28**: 2020-2026 [PMID: 24584484 DOI: 10.1007/s00464-014-3430-0]

35 **Zhou X**, Xie H, Xie L, Li J, Fu W. Factors associated with lymph node metastasis in radically resected rectal carcinoids: a systematic review and meta-analysis. *J Gastrointest Surg* 2013; **17**: 1689-1697 [PMID: 23818123 DOI: 10.1007/s11605-013-2249-7]

36 **Wu X**, Peng C, Lin M, Li Z, Yang X, Liu J, Yang X, Zuo X. Risk of metastasis and survival in patients undergoing different treatment strategies with T1 colonic neuroendocrine tumors. *J Endocrinol Invest* 2024; **47**: 671-681 [PMID: 37653287 DOI: 10.1007/s40618-023-02185-2]

37 **Zhao B**, Hollandsworth HM, Lopez NE, Parry LA, Abbadessa B, Cosman BC, Ramamoorthy SL, Eisenstein S. Outcomes for a Large Cohort of Patients with Rectal Neuroendocrine Tumors: an Analysis of the National Cancer Database. *J Gastrointest Surg* 2021; **25**: 484-491 [PMID: 32016672 DOI: 10.1007/s11605-020-04525-6]

38 **Soga J**. Early-stage carcinoids of the gastrointestinal tract: an analysis of 1914 reported cases. *Cancer* 2005; **103**: 1587-1595 [PMID: 15742328 DOI: 10.1002/cncr.20939]

39 **Caplin M**, Sundin A, Nillson O, Baum RP, Klose KJ, Kelestimur F, Plöckinger U, Papotti M, Salazar R, Pascher A; Barcelona Consensus Conference participants. ENETS Consensus Guidelines for the management of patients with digestive neuroendocrine neoplasms: colorectal neuroendocrine neoplasms. *Neuroendocrinology* 2012; **95**: 88-97 [PMID: 22261972 DOI: 10.1159/000335594]

40 **Anthony LB**, Strosberg JR, Klimstra DS, Maples WJ, O'Dorisio TM, Warner RR, Wiseman GA, Benson AB 3rd, Pommier RF; North American Neuroendocrine Tumor Society (NANETS). The NANETS consensus guidelines for the diagnosis and management of gastrointestinal neuroendocrine tumors (nets): well-differentiated nets of the distal colon and rectum. *Pancreas* 2010; **39**: 767-774 [PMID: 20664474 DOI: 10.1097/MPA.0b013e3181ec1261]

41 **Chen Z**, Zhu D. Risk factors for lateral pelvic lymph node metastasis in patients with rectal neuroendocrine tumors: a systematic review and meta-analysis. *Front Oncol* 2025; **15**: 1500623 [PMID: 39959663 DOI: 10.3389/fonc.2025.1500623]

42 **de Mestier L**, Lorenzo D, Fine C, Cros J, Hentic O, Walter T, Panis Y, Couvelard A, Cadiot G, Ruszniewski P. Endoscopic, transanal, laparoscopic, and transabdominal management of rectal neuroendocrine tumors. *Best Pract Res Clin Endocrinol Metab* 2019; **33**: 101293 [PMID: 31326374 DOI: 10.1016/j.beem.2019.101293]

43 **Kwon MJ**, Kang HS, Soh JS, Lim H, Kim JH, Park CK, Park HR, Nam ES. Lymphovascular invasion in more than one-quarter of small rectal neuroendocrine tumors. *World J Gastroenterol* 2016; **22**: 9400-9410 [PMID: 27895428 DOI: 10.3748/wjg.v22.i42.9400]

44 **Li YW**, He YP, Liu FQ, Peng JJ, Cai SJ, Xu Y, Wang MH. Grade G2 Rectal Neuroendocrine Tumor Is Much More Invasive Compared With G1 Tumor. *Front Oncol* 2021; **11**: 646536 [PMID: 33777809 DOI: 10.3389/fonc.2021.646536]

45 **Zeng X**, Zhang R, Jiang W, Li C, Yu M, Liu W, Di M, Wu H, Sun Y, Xiong Z, Jiang C, Yu B, Zhou S, Li Y, Liao X, Xia L, Zhang W, Lin G, Tao K. Local Excision Versus Radical Resection for Grade 2 Rectal Neuroendocrine Tumors: A Multicenter Propensity Score-Matched Analysis. *Dis Colon Rectum* 2024; **67**: 911-919 [PMID: 38452369 DOI: 10.1097/DCR.0000000000003097]

46 **Ricci AD**, Pusceddu S, Panzuto F, Gelsomino F, Massironi S, De Angelis CG, Modica R, Ricco G, Torchio M, Rinzivillo M, Prinzi N, Rizzi F, Lamberti G, Campana D. Assessment of the Risk of Nodal Involvement in Rectal Neuroendocrine Neoplasms: The NOVARA Score, a Multicentre Retrospective Study. *J Clin Med* 2022; **11**: 713 [PMID: 35160165 DOI: 10.3390/jcm11030713]

47 **Chida K**, Watanabe J, Hirasawa K, Inayama Y, Misumi T, Kunisaki C, Endo I. A novel risk-scoring system for predicting lymph node metastasis of rectal neuroendocrine tumors. *Ann Gastroenterol Surg* 2020; **4**: 562-570 [PMID: 33005851 DOI: 10.1002/ags3.12355]

48 **Tie SJ**, Fan ML, Zhang JY, Yu J, Wu N, Su GQ, Xu Z, Huang WF. Clinical outcomes after endoscopic resection and the risk of lymph node metastasis in rectal neuroendocrine tumors: a single-center retrospective study. *Surg Endosc* 2024; **38**: 5178-5186 [PMID: 39043886 DOI: 10.1007/s00464-024-11088-z]

49 **Chen Q**, Chen J, Deng Y, Zhang Y, Huang Z, Zhao H, Cai J. Nomogram for the prediction of lymph node metastasis and survival outcomes in rectal neuroendocrine tumour patients undergoing resection. *J Gastrointest Oncol* 2022; **13**: 171-184 [PMID: 35284104 DOI: 10.21037/jgo-21-573]

50 **Li R**, Li X, Wang Y, Chang C, Lv W, Li X, Cao D. Risk factors for regional lymph node metastasis in rectal neuroendocrine tumors: a population-based study. *Front Med (Lausanne)* 2024; **11**: 1383047 [PMID: 39296902 DOI: 10.3389/fmed.2024.1383047]

51 **Kim SH**, Yang DH, Lee JS, Park S, Lee HS, Lee H, Park SH, Kim KJ, Ye BD, Byeon JS, Myung SJ, Yang SK, Kim JH, Kim CW, Kim J. Natural course of an untreated metastatic perirectal lymph node after the endoscopic resection of a rectal neuroendocrine tumor. *Intest Res* 2015; **13**: 175-179 [PMID: 25932004 DOI: 10.5217/ir.2015.13.2.175]

52 **Ponna NP**, Luong TV, Navalkissoor S. Small Bowel Leiomyoma Mimics Neuroendocrine Tumor on 68Ga-DOTATATE PET/CT. *Clin Nucl Med* 2025 [PMID: 39854675 DOI: 10.1097/RLU.0000000000005694]

53 **Bai L**, Xu J, Xu X, Zhang J, Liu X, Hu S, Chen J, Song S. The Application of 68Ga-Somatostatin Analog and 18F-FDG PET/CT for Bone Metastasis from Neuroendocrine Tumors. *Neuroendocrinology* 2024; **114**: 775-785 [PMID: 38824926 DOI: 10.1159/000539572]

54 **Hou G**, Cheng X, Yang Y, Zhao D, Wang G, Zhao H, Zheng R, Wang X, Chen X, Chi Y, Zhang J. Diagnostic performance and clinical impact of (18)F-AlF-NOTA-octreotide in a large cohort of patients with neuroendocrine neoplasms: A prospective single-center study. *Theranostics* 2024; **14**: 3213-3220 [PMID: 38855183 DOI: 10.7150/thno.96762]

55 **Teraishi F**, Shoji R, Fujiwara T. Rare case of rectal carcinoid with synchronous primary carcinoid tumors of the lung misdiagnosed as lung metastases. *JGH Open* 2024; **8**: e70003 [PMID: 39036414 DOI: 10.1002/jgh3.70003]

56 **Deprez PH**, Moons LMG, O'Toole D, Gincul R, Seicean A, Pimentel-Nunes P, Fernández-Esparrach G, Polkowski M, Vieth M, Borbath I, Moreels TG, Nieveen van Dijkum E, Blay JY, van Hooft JE. Endoscopic management of subepithelial lesions including neuroendocrine neoplasms: European Society of Gastrointestinal Endoscopy (ESGE) Guideline. *Endoscopy* 2022; **54**: 412-429 [PMID: 35180797 DOI: 10.1055/a-1751-5742]

57 **Hayasaka J**, Miura Y, Yamashita S, Matsui A, Kikuchi D, Takazawa Y, Hoteya S. Traction Devices May Not Affect the Vertical Margin Distance in the Endoscopic Submucosal Dissection of Rectal Neuroendocrine Tumors. *Cureus* 2024; **16**: e58976 [PMID: 38800345 DOI: 10.7759/cureus.58976]

58 **Son HJ**, Sohn DK, Hong CW, Han KS, Kim BC, Park JW, Choi HS, Chang HJ, Oh JH. Factors associated with complete local excision of small rectal carcinoid tumor. *Int J Colorectal Dis* 2013; **28**: 57-61 [PMID: 22821140 DOI: 10.1007/s00384-012-1538-z]

59 **Kim JS**, Kim YJ, Chung JW, Kim JH, Kim KO, Kwon KA, Park DK, An JS. Usefulness of endoscopic resection using the band ligation method for rectal neuroendocrine tumors. *Intest Res* 2016; **14**: 164-171 [PMID: 27175117 DOI: 10.5217/ir.2016.14.2.164]

60 **Zhang ST**, Chen Q, Zhang YM, Li QY, Gao YC, Meng WJ, Qiu LW, Zeng B. Comparative Efficacy and Acceptability of Endoscopic Methods for Rectal Neuroendocrine Neoplasms with Low Malignant Potential: A Network Meta-analysis. *Turk J Gastroenterol* 2024; **35**: 440-452 [PMID: 39128103 DOI: 10.5152/tjg.2024.23477]

61 **Zhou C**, Zhang F, We Y. Efficacy of endoscopic mucosal resection versus endoscopic submucosal dissection for rectal neuroendocrine tumors ≤10mm: a systematic review and meta-analysis. *Ann Saudi Med* 2023; **43**: 179-195 [PMID: 37270677 DOI: 10.5144/0256-4947.2023.179]

62 **Chen J**, Ye J, Zheng X, Chen J. Endoscopic treatments for rectal neuroendocrine tumors: a systematic review and network meta-analysis. *J Gastrointest Surg* 2024; **28**: 301-308 [PMID: 38445925 DOI: 10.1016/j.gassur.2023.12.016]

63 **Greenspun BC**, Metzger DA, Foshag A, Marshall TE, Pearson B, Zarnegar R, Fahey TJ 3rd, Finnerty BM. Impact of Delayed Surgery on Local Colorectal Neuroendocrine Tumors: Is Surveillance a Feasible Option? *Ann Surg Oncol* 2025 [PMID: 39888466 DOI: 10.1245/s10434-025-16944-3]

64 **Ito T**, Masui T, Komoto I, Doi R, Osamura RY, Sakurai A, Ikeda M, Takano K, Igarashi H, Shimatsu A, Nakamura K, Nakamoto Y, Hijioka S, Morita K, Ishikawa Y, Ohike N, Kasajima A, Kushima R, Kojima M, Sasano H, Hirano S, Mizuno N, Aoki T, Aoki T, Ohtsuka T, Okumura T, Kimura Y, Kudo A, Konishi T, Matsumoto I, Kobayashi N, Fujimori N, Honma Y, Morizane C, Uchino S, Horiuchi K, Yamasaki M, Matsubayashi J, Sato Y, Sekiguchi M, Abe S, Okusaka T, Kida M, Kimura W, Tanaka M, Majima Y, Jensen RT, Hirata K, Imamura M, Uemoto S. JNETS clinical practice guidelines for gastroenteropancreatic neuroendocrine neoplasms: diagnosis, treatment, and follow-up: a synopsis. *J Gastroenterol* 2021; **56**: 1033-1044 [PMID: 34586495 DOI: 10.1007/s00535-021-01827-7]

65 **Kuiper T**, van Oijen MGH, van Velthuysen MF, van Lelyveld N, van Leerdam ME, Vleggaar FD, Klümpen HJ. Endoscopically removed rectal NETs: a nationwide cohort study. *Int J Colorectal Dis* 2021; **36**: 535-541 [PMID: 33230657 DOI: 10.1007/s00384-020-03801-w]

66 **Kitagawa Y**, Suzuki T, Miyakawa A, Okimoto K, Matsumura T, Shiratori T, Ishigami H, Mine T, Takashiro H, Saito H, Kato N. Comparison of endoscopic submucosal dissection and modified endoscopic mucosal resection for rectal neuroendocrine tumors. *Sci Rep* 2025; **15**: 5424 [PMID: 39948094 DOI: 10.1038/s41598-024-82082-7]

67 **Matsuno K**, Miyamoto H, Kitada H, Yoshimatsu S, Tamura F, Sakurai K, Fukubayashi K, Shono T, Setoyama H, Matsuyama T, Suko S, Narita R, Honda M, Tateyama M, Naoe H, Morinaga J, Tanaka Y, Gushima R. Comparison of endoscopic submucosal resection with ligation and endoscopic submucosal dissection for small rectal neuroendocrine tumors: A multicenter retrospective study. *DEN Open* 2023; **3**: e163 [PMID: 36176350 DOI: 10.1002/deo2.163]

68 **Abe T**, Kakemura T, Fujinuma S, Maetani I. Successful outcomes of EMR-L with 3D-EUS for rectal carcinoids compared with historical controls. *World J Gastroenterol* 2008; **14**: 4054-4058 [PMID: 18609690 DOI: 10.3748/wjg.14.4054]

69 **Li D**, Xie J, Hong D, Liu G, Wang R, Jiang C, Ye Z, Xu B, Wang W. Efficacy and safety of ligation-assisted endoscopic submucosal resection combined with endoscopic ultrasonography for treatment of rectal neuroendocrine tumors. *Scand J Gastroenterol* 2022; **57**: 734-739 [PMID: 35108155 DOI: 10.1080/00365521.2022.2033828]

70 **Deng C**, Wu S, Xu F, Lv L, Zhou Z, He S. Double-band ligation-assisted endoscopic submucosal resection for type 1 gastric neuroendocrine tumor with type A gastritis. *Endoscopy* 2022; **54**: E724-E725 [PMID: 35272372 DOI: 10.1055/a-1759-2129]

71 **Gao X**, Huang S, Wang Y, Peng Q, Li W, Zou Y, Han Z, Cai J, Luo Y, Ye Y, Li A, Bai Y, Chen Y, Liu S, Li Y. Modified Cap-Assisted Endoscopic Mucosal Resection Versus Endoscopic Submucosal Dissection for the Treatment of Rectal Neuroendocrine Tumors ≤10 mm: A Randomized Noninferiority Trial. *Am J Gastroenterol* 2022; **117**: 1982-1989 [PMID: 36455222 DOI: 10.14309/ajg.0000000000001914]

72 **Lee HJ**, Kim SB, Shin CM, Seo AY, Lee DH, Kim N, Park YS, Yoon H. A comparison of endoscopic treatments in rectal carcinoid tumors. *Surg Endosc* 2016; **30**: 3491-3498 [PMID: 26514133 DOI: 10.1007/s00464-015-4637-4]

73 **Lu M**, Cui H, Qian M, Shen Y, Zhu J. Comparison of endoscopic resection therapies for rectal neuroendocrine tumors. *Minim Invasive Ther Allied Technol* 2024; **33**: 207-214 [PMID: 38701133 DOI: 10.1080/13645706.2024.2330580]

74 **Chen R**, Liu X, Sun S, Wang S, Ge N, Wang G, Guo J. Comparison of Endoscopic Mucosal Resection With Circumferential Incision and Endoscopic Submucosal Dissection for Rectal Carcinoid Tumor. *Surg Laparosc Endosc Percutan Tech* 2016; **26**: e56-e61 [PMID: 27213787 DOI: 10.1097/SLE.0000000000000266]

75 **Binmoeller KF**, Weilert F, Shah J, Bhat Y, Kane S. "Underwater" EMR without submucosal injection for large sessile colorectal polyps (with video). *Gastrointest Endosc* 2012; **75**: 1086-1091 [PMID: 22365184 DOI: 10.1016/j.gie.2011.12.022]

76 **Park SS**, Han KS, Kim B, Chang Kim B, Hong CW, Sohn DK, Chang HJ. Comparison of underwater endoscopic mucosal resection and endoscopic submucosal dissection of rectal neuroendocrine tumors (with videos). *Gastrointest Endosc* 2020; **91**: 1164-1171.e2 [PMID: 31904380 DOI: 10.1016/j.gie.2019.12.039]

77 **Park SB**, Kim HW, Kang DH, Choi CW, Kim SJ, Nam HS. Advantage of endoscopic mucosal resection with a cap for rectal neuroendocrine tumors. *World J Gastroenterol* 2015; **21**: 9387-9393 [PMID: 26309365 DOI: 10.3748/wjg.v21.i31.9387]

78 **Zhang HP**, Wu W, Yang S, Lin J. Endoscopic treatments for rectal neuroendocrine tumors smaller than 16 mm: a meta-analysis. *Scand J Gastroenterol* 2016; **51**: 1345-1353 [PMID: 27367942 DOI: 10.1080/00365521.2016.1200140]

79 **Pan J**, Zhang X, Shi Y, Pei Q. Endoscopic mucosal resection with suction vs. endoscopic submucosal dissection for small rectal neuroendocrine tumors: a meta-analysis. *Scand J Gastroenterol* 2018; **53**: 1139-1145 [PMID: 30193543 DOI: 10.1080/00365521.2018.1498120]

80 **Ito S**, Hotta K, Sekiguchi M, Takeuchi Y, Oka S, Yamamoto H, Shinmura K, Harada K, Uraoka T, Hisabe T, Sano Y, Kondo H, Horimatsu T, Kikuchi H, Kawamura T, Nagata S, Yamamoto K, Tajika M, Tsuji S, Kusaka T, Okuyama Y, Yoshida N, Moriyama T, Hasebe A, So S, Saito Y, Nakahira H, Ishikawa H, Matsuda T; C-NET STUDY Group. Short-term outcomes of endoscopic resection for colorectal neuroendocrine tumors: Japanese multicenter prospective C-NET STUDY. *Dig Endosc* 2024; **36**: 942-951 [PMID: 37986226 DOI: 10.1111/den.14728]

81 **Takada K**, Imai K, Yamada T, Ohata K, Kanesaka T, Nagami Y, Yamasaki Y, Kobara H, Inokuchi Y, Chino A, Yamaguchi S, Ikehara H, Kawamura T, Yabuuchi Y, Mizuguchi Y, Ikematsu H, Yokoi C, Hattori S, Ohno K, Yoshizawa Y, Fukuzawa M, Tsuji Y, Konishi J, Yamamura T, Osawa S, Oka S, Hikichi T, Togashi K, Hirasawa K, Uraoka T, Takeuchi Y, Chiba H, Komeda Y, Doyama H, Oba MS, Saito Y. Efficacy of endoscopic submucosal resection with a ligation device for small rectal neuroendocrine tumor: study protocol of a multicenter open-label randomized control trial (BANDIT trial). *BMC Gastroenterol* 2024; **24**: 69 [PMID: 38331727 DOI: 10.1186/s12876-024-03130-0]

82 **Sako T**, Morisawa T, Toyonaga T. Per Anal Endoscopic Myectomy Using a Double-Tunneling Technique for Rectal Neuroendocrine Neoplasm. *Clin Gastroenterol Hepatol* 2024; **22**: A19-A20 [PMID: 38191013 DOI: 10.1016/j.cgh.2023.12.031]

83 **Liao S**, Huang S, Yang G, Li B, Deng H, Tan Y, He G. Efficacy of underwater endoscopic intermuscular dissection in the management of a rectal neuroendocrine tumor. *Endoscopy* 2024; **56**: E524-E526 [PMID: 38889894 DOI: 10.1055/a-2333-9660]

84 **Liu J**, Fang N. Traction by dental floss loop for adequate submucosal dissection depth in a rectal neuroendocrine tumor. *Endoscopy* 2023; **55**:

E326-E327 [PMID: 36513110 DOI: 10.1055/a-1974-9297]
85 **Wallenhorst T**, Masgnaux LJ, Grimaldi J, Legros R, Rivory J, Jacques J, Pioche M. Obtaining a free vertical margin is challenging in endoscopic submucosal dissection of a rectal neuroendocrine tumor: use of adaptive traction to improve exposure in a child. *Endoscopy* 2023; **55**: E763-E764 [PMID: 37236253 DOI: 10.1055/a-2085-0449]
86 **Meier B**, Albrecht H, Wiedbrauck T, Schmidt A, Caca K. Full-thickness resection of neuroendocrine tumors in the rectum. *Endoscopy* 2020; **52**: 68-72 [PMID: 31614372 DOI: 10.1055/a-1008-9077]
87 **D'Souza LS**, Yang D, Diehl D. AGA Clinical Practice Update on Endoscopic Full-Thickness Resection for the Management of Gastrointestinal Subepithelial Lesions: Commentary. *Gastroenterology* 2024; **166**: 345-349 [PMID: 38108671 DOI: 10.1053/j.gastro.2023.11.016]
88 **Rushfeldt CF**, Nordbø M, Steigen SE, Dehli T, Gjessing P, Norderval S. Endoscopic full-thickness dissection (EFTD) in the rectum: a case series. *Tech Coloproctol* 2022; **26**: 187-193 [PMID: 34964075 DOI: 10.1007/s10151-021-02558-w]
89 **Fine C**, Roquin G, Terrebonne E, Lecomte T, Coriat R, Do Cao C, de Mestier L, Coffin E, Cadiot G, Nicolli P, Lepiliez V, Hautefeuille V, Ramos J, Girot P, Dominguez S, Céphise FV, Forestier J, Hervieu V, Pioche M, Walter T. Endoscopic management of 345 small rectal neuroendocrine tumours: A national study from the French group of endocrine tumours (GTE). *United European Gastroenterol J* 2019; **7**: 1102-1112 [PMID: 31662867 DOI: 10.1177/2050640619861883]
90 **Kim J**, Kim JH, Lee JY, Chun J, Im JP, Kim JS. Clinical outcomes of endoscopic mucosal resection for rectal neuroendocrine tumor. *BMC Gastroenterol* 2018; **18**: 77 [PMID: 29866049 DOI: 10.1186/s12876-018-0806-y]
91 **Chen WJ**, Wu N, Zhou JL, Lin GL, Qiu HZ. Full-thickness excision using transanal endoscopic microsurgery for treatment of rectal neuroendocrine tumors. *World J Gastroenterol* 2015; **21**: 9142-9149 [PMID: 26290641 DOI: 10.3748/wjg.v21.i30.9142]
92 **Cheminel L**, Lupu A, Wallenhorst T, Lepilliez V, Leblanc S, Albouys J, Abou Ali E, Barret M, Lorenzo D, De Mestier L, Burtin P, Girot P, Le Baleur Y, Gerard R, Yzet C, Tchirikhtchian K, Degand T, Culetto A, Lemmers A, Schaefer M, Chevaux JB, Zhong P, Hervieu V, Subtil F, Rivory J, Fine C, Jacques J, Walter T, Pioche M. Systematic Resection of the Visible Scar After Incomplete Endoscopic Resection of Rectal Neuroendocrine Tumors. *Am J Gastroenterol* 2024; **119**: 378-381 [PMID: 37734341 DOI: 10.14309/ajg.0000000000002516]
93 **Wang J**, Zhang X, Chen K, Liang Y, Liu Y, Jiang Z, He Y, Chen J, Liu J. Optimization of endoscopic treatment strategies for R0 resection of rectal neuroendocrine tumors smaller than 10 mm. *Clin Res Hepatol Gastroenterol* 2024; **48**: 102469 [PMID: 39332765 DOI: 10.1016/j.clinre.2024.102469]
94 **Wang L**, Qiu J, Zhang Y, Pan X. Do Rectal Neuroendocrine Tumors with Incomplete Endoscopic Resection for Positive Resection Margin Need Salvage Treatment? *Am J Gastroenterol* 2024; **119**: 1647-1648 [PMID: 38713143 DOI: 10.14309/ajg.0000000000002814]
95 **Pagano N**, Ricci C, Brighi N, Ingaldi C, Pugliese F, Santini D, Campana D, Mosconi C, Ambrosini V, Casadei R. Incidental diagnosis of very small rectal neuroendocrine neoplasms: when should endoscopic submucosal dissection be performed? A single ENETS centre experience. *Endocrine* 2019; **65**: 207-212 [PMID: 30919286 DOI: 10.1007/s12020-019-01907-y]
96 **Kim SJ**, Lee J, Kim GW, Kim SY. The role of endoscopic ultrasonography for diagnosis of residual rectal neuroendocrine tumor. *Surg Endosc* 2024; **38**: 4260-4267 [PMID: 38866946 DOI: 10.1007/s00464-024-10963-z]
97 **Cha JH**, Jung DH, Kim JH, Youn YH, Park H, Park JJ, Um YJ, Park SJ, Cheon JH, Kim TI, Kim WH, Lee HJ. Long-term outcomes according to additional treatments after endoscopic resection for rectal small neuroendocrine tumors. *Sci Rep* 2019; **9**: 4911 [PMID: 30894571 DOI: 10.1038/s41598-019-40668-6]
98 **Esposito G**, Dell'Unto E, Ligato I, Marasco M, Panzuto F. The meaning of R1 resection after endoscopic removal of gastric, duodenal and rectal neuroendocrine tumors. *Expert Rev Gastroenterol Hepatol* 2023; **17**: 785-793 [PMID: 37497604 DOI: 10.1080/17474124.2023.2242261]
99 **Sun D**, Ren Z, Xu E, Cai S, Qi Z, Chen Z, Liu J, Shi Q, Zhou P, Zhong Y. Long-term clinical outcomes of endoscopic submucosal dissection in rectal neuroendocrine tumors based on resection margin status: a real-world study. *Surg Endosc* 2023; **37**: 2644-2652 [PMID: 36380122 DOI: 10.1007/s00464-022-09710-z]
100 **Lee HJ**, Seo Y, Oh CK, Lee JM, Choi HH, Gweon TG, Lee SH, Cheung DY, Kim JI, Park SH, Lee HH. Assessing risk stratification in long-term outcomes of rectal neuroendocrine tumors following endoscopic resection: a multicenter retrospective study. *Scand J Gastroenterol* 2024; **59**: 868-874 [PMID: 38587111 DOI: 10.1080/00365521.2024.2340008]
101 **Yong JN**, Lim XC, Nistala KRY, Lim LKE, Lim GEH, Quek J, Tham HY, Wong NW, Tan KK, Chong CS. Endoscopic submucosal dissection versus endoscopic mucosal resection for rectal carcinoid tumor. A meta-analysis and meta-regression with single-arm analysis. *J Dig Dis* 2021; **22**: 562-571 [PMID: 34472210 DOI: 10.1111/1751-2980.13048]
102 **Ramage JK**, Valle JW, Nieveen van Dijkum EJM, Sundin A, Pascher A, Couvelard A, Kloeppel G; the ENETS 2016 Munich Advisory Board Participants; ENETS 2016 Munich Advisory Board Participants. Colorectal Neuroendocrine Neoplasms: Areas of Unmet Need. *Neuroendocrinology* 2019; **108**: 45-53 [PMID: 30219817 DOI: 10.1159/000493767]
103 **Park SS**, Kim BC, Lee DE, Han KS, Kim B, Hong CW, Sohn DK. Comparison of endoscopic submucosal dissection and transanal endoscopic microsurgery for T1 rectal neuroendocrine tumors: a propensity score-matched study. *Gastrointest Endosc* 2021; **94**: 408-415.e2 [PMID: 33600807 DOI: 10.1016/j.gie.2021.02.012]
104 **Kitagawa D**, Kanesaka T, Ishihara R. Salvage treatment after endoscopic submucosal dissection for a rectal neuroendocrine tumor: Premeditated peranal endoscopic myectomy. *Dig Endosc* 2024; **36**: 644-645 [PMID: 38514465 DOI: 10.1111/den.14791]
105 **Yao K**, Hotta K, Shimoda T, Imai K, Ito S, Takada K, Ono H. Peranal Endoscopic Myectomy for Salvage Resection of a Neuroendocrine Tumor in the Lower Rectum. *Am J Gastroenterol* 2025 [PMID: 39878446 DOI: 10.14309/ajg.0000000000003335]
106 **De Cristofaro E**, Rivory J, Masgnaux LJ, Wallenhorst T, Jacques J, Lafeuille P, Pioche M. Repeat endoscopic intermuscular dissection of the visible scar after noncurative endoscopic intermuscular dissection of a rectal neuroendocrine tumor. *Endoscopy* 2024; **56**: E205-E206 [PMID: 38428913 DOI: 10.1055/a-2261-7919]
107 **Azzolini F**, Cecinato P, Iori V, De Marco L, Sassatelli R. Endoscopic full-thickness resection for suspected residual rectal neuroendocrine tumor and closure of the defect with a new suturing system. *Endoscopy* 2015; **47** Suppl 1: E556-E557 [PMID: 26610082 DOI: 10.1055/s-0034-1393384]
108 **Ju Y**, Bong JW, Cheong C, Kang S, Min BW, Lee SI. Effective utilization of polypectomy in endoscopic salvage treatment of rectal neuroendocrine tumors: a retrospective cohort study. *Ann Surg Treat Res* 2024; **107**: 151-157 [PMID: 39282102 DOI: 10.4174/astr.2024.107.3.151]
109 **Poleé IN**, Hermans BCM, van der Zwan JM, Bouwense SAW, Dercksen MW, Eskens FALM, Havekes B, Hofland J, Kerkhofs TMA, Klümpen HJ, Latten-Jansen LM, Speel EM, Verburg FA, Walenkamp AME, Geurts SME, de Vos-Geelen J. Long-term survival in patients

with gastroenteropancreatic neuroendocrine neoplasms: A population-based study. *Eur J Cancer* 2022; **172**: 252-263 [PMID: 35803176 DOI: 10.1016/j.ejca.2022.06.003]

110 **Uhlig J**, Nie J, Gibson J, Cecchini M, Stein S, Lacy J, Kunz P, Kim HS. Epidemiology, treatment and outcomes of gastroenteropancreatic neuroendocrine neoplasms. *Sci Rep* 2024; **14**: 30536 [PMID: 39690170 DOI: 10.1038/s41598-024-81518-4]

111 **Sekiguchi M**, Sekine S, Sakamoto T, Otake Y, Nakajima T, Matsuda T, Taniguchi H, Kushima R, Ohe Y, Saito Y. Excellent prognosis following endoscopic resection of patients with rectal neuroendocrine tumors despite the frequent presence of lymphovascular invasion. *J Gastroenterol* 2015; **50**: 1184-1189 [PMID: 25936647 DOI: 10.1007/s00535-015-1079-7]

112 **Torres N**, El Moussaoui M, Basbous S, Fridman V, Borbath I, Deflandre J. Watch-an-wait strategy for multiple rectal neuroendocrine tumors with widespread invasion. *Acta Gastroenterol Belg* 2023; **86**: 563-565 [PMID: 38240551 DOI: 10.51821/86.4.10381]

113 **Li L**, Chen Z, Zhu D, Lv Q, Zhang T, Lai J. Primary small rectal neuroendocrine tumor with pelvic lateral lymph nodes metastasis: A case report and review of literature. *Int J Surg Case Rep* 2025; **127**: 110963 [PMID: 39889652 DOI: 10.1016/j.ijscr.2025.110963]

114 **Jo IH**, Lee KM, Kim DB, Lee JM. Low-grade Rectal Neuroendocrine Tumor Recurring as Multiple Hepatic Metastasis after Complete Endoscopic Removal: A Case Report. *Korean J Gastroenterol* 2020; **76**: 251-255 [PMID: 33234773 DOI: 10.4166/kjg.2020.096]

115 **Nassar M**, Baraka B, Talal AH. Innovative approaches in predicting outcomes for rectal neuroendocrine tumors. *World J Gastroenterol* 2025; **31**: 100517 [PMID: 39958439 DOI: 10.3748/wjg.v31.i6.100517]

116 **Xu R**, Zhou B, Hu P, Xue B, Gu D, Li X, Tang Q. Development and validation of prognostic nomograms for patients with colon neuroendocrine neoplasms. *World J Surg Oncol* 2021; **19**: 233 [PMID: 34364382 DOI: 10.1186/s12957-021-02338-8]

117 **Feng X**, Wei G, Wang W, Zhang Y, Zeng Y, Chen M, Chen Y, Chen J, Zhou Z, Li Y. Nomogram for individually predicting overall survival in rectal neuroendocrine tumours. *BMC Cancer* 2020; **20**: 865 [PMID: 32907602 DOI: 10.1186/s12885-020-07328-9]

118 **Zeng XY**, Zhong M, Lin GL, Li CG, Jiang WZ, Zhang W, Xia LJ, Di MJ, Wu HX, Liao XF, Sun YM, Yu MH, Tao KX, Li Y, Zhang R, Zhang P. GATIS score for predicting the prognosis of rectal neuroendocrine neoplasms: A Chinese multicenter study of 12-year experience. *World J Gastroenterol* 2024; **30**: 3403-3417 [PMID: 39091717 DOI: 10.3748/wjg.v30.i28.3403]

119 **Dell'Unto E**, Panzuto F, Esposito G. Rectal neuroendocrine tumors: Can we predict their behavior? *World J Gastroenterol* 2025; **31**: 101150 [PMID: 39926222 DOI: 10.3748/wjg.v31.i5.101150]

120 **Raj RPA**, Nashwan AJ. Enhancing prognostic accuracy in predicting rectal neuroendocrine neoplasms. *World J Gastroenterol* 2024; **30**: 4087-4089 [PMID: 39474400 DOI: 10.3748/wjg.v30.i37.4087]

121 **Feng YN**, Liu LH, Zhang HW. Evaluation of the GATIS score for predicting prognosis in rectal neuroendocrine neoplasms. *World J Gastroenterol* 2024; **30**: 4587-4590 [PMID: 39563742 DOI: 10.3748/wjg.v30.i42.4587]

122 **National Comprehensive Cancer Network**. NCCN Guidelines. [cited 10 January 2025]. Available from: https://www.nccn.org/guidelines/category_1

World Journal of Gastroenterology

Submit a Manuscript: https://www.f6publishing.com

World J Gastroenterol 2025 May 21; 31(19): 106406

DOI: 10.3748/wjg.v31.i19.106406

ISSN 1007-9327 (print) ISSN 2219-2840 (online)

MINIREVIEWS

Comparative study on the pathogenesis of Crohn's disease and ulcerative colitis

Qi-Hang Yang, Chuang-Nian Zhang

Specialty type: Gastroenterology and hepatology

Provenance and peer review: Unsolicited article; Externally peer reviewed.

Peer-review model: Single blind

Peer-review report's classification
Scientific Quality: Grade A, Grade B, Grade B
Novelty: Grade B, Grade B, Grade B
Creativity or Innovation: Grade B, Grade B, Grade C
Scientific Significance: Grade B, Grade B, Grade C

P-Reviewer: Batra K; El-Said NT

Received: February 26, 2025
Revised: March 25, 2025
Accepted: April 25, 2025
Published online: May 21, 2025
Processing time: 84 Days and 18 Hours

Qi-Hang Yang, Chinese Academy of Medical Science & Peking Union Medical College, Institute of Biomedical Engineering, Tianjin 300192, China

Qi-Hang Yang, University College London, Cancer Institute, London WC1E 6BT, United Kingdom

Chuang-Nian Zhang, Chinese Academy of Medical Science & Peking Union Medical College, State Key Laboratory of Advanced Medical Materials and Devices, Engineering Research Center of Pulmonary and Critical Care Medicine Technology and Device (Ministry of Education), Tianjin Key Laboratory of Biomaterial Research, Institute of Biomedical Engineering, Tianjin Institutes of Health Science, Tianjin 300192, China

Corresponding author: Chuang-Nian Zhang, Senior Researcher, Chinese Academy of Medical Science & Peking Union Medical College, State Key Laboratory of Advanced Medical Materials and Devices, Engineering Research Center of Pulmonary and Critical Care Medicine Technology and Device (Ministry of Education), Tianjin Key Laboratory of Biomaterial Research, Institute of Biomedical Engineering, Tianjin Institutes of Health Science, No. 236 Baidi Road, Nankai District, Tianjin 300192, China. cnzhang@mail.nankai.edu.cn

Abstract

Inflammatory bowel disease (IBD) is an incurable disease of the digestive system; however, the therapeutic methods for IBD remain limited. The pathogenesis of IBD was systematically discussed and compared in this paper, primarily comprising Crohn's disease and ulcerative colitis. This paper focused on six common aspects: (1) Dysregulated immune responses; (2) Gene function changes; (3) Intestinal microbes disorder and imbalance; (4) Microbial infections; (5) Associations between IBD and other inflammatory diseases; and (6) Other factors. In addition, the pathogenesis differences between these two forms of IBD were unraveled and clearly distinguished. These unique aspects of pathogenesis provide crucial insights for the precise treatment of both Crohn's disease and ulcerative colitis. This paper illustrates the root causes and beneficial factors of resistance to IBD, which provides novel insights on early prevention, development of new therapeutic agents, and treatment options of this disease.

Key Words: Inflammatory bowel disease; Crohn's disease; Ulcerative colitis; Pathogenesis; Immune responses; Gene function; Microbes

Core Tip: Six common and fourteen unique aspects of the pathogenesis of inflammatory bowel disease, primarily Crohn's disease and ulcerative colitis, illustrate the causes and beneficial factors of resistance to inflammatory bowel disease, providing critical insights for the targeted treatment of Crohn's disease and ulcerative colitis. Utilizing the main contents of this paper allows for the development of comprehensive interventions that reduce harmful influences, enhance protective factors and use an integrative approach to address the diseases for the benefit of the human being.

Citation: Yang QH, Zhang CN. Comparative study on the pathogenesis of Crohn's disease and ulcerative colitis. *World J Gastroenterol* 2025; 31(19): 106406
URL: https://www.wjgnet.com/1007-9327/full/v31/i19/106406.htm
DOI: https://dx.doi.org/10.3748/wjg.v31.i19.106406

INTRODUCTION

Inflammatory bowel disease (IBD) is a globally prevalent disease, with incidence rates continuing to rise in the 21st century[1]. It has become a public health challenge worldwide. IBD is a systemic disease affecting the gastrointestinal tract and also multiple organs and systems. Clinically, it is classified as one of the common, multiple and currently incurable digestive system disease, characterized by severe intestinal inflammation and mucosal destruction[2,3]. Intestinal inflammation can impair mucosal healing, leading to chronic inflammation of gastrointestinal tract, which is prone to chronic relapses[4,5]. Furthermore, IBD can not only affect many organs and systems such as eyes, mouth, skin, joints, liver, gallbladder and pancreas but also lead to complications such as internal and external infection of the digestive tract and tumor, significantly increasing the risk of cancer of gastrointestinal and other organs such as colorectal cancer, skin cancer, and cervical cancer[6,7].

The etiology of IBD is complex and multifactorial. The pathogenesis of IBD is an area of intense research and clinical interest. In the field of international biomedical applied basic research, the breakthrough and focus are also on the pathogenesis of IBD. Insight into the pathogenesis of IBD, which provides elucidation of IBD mechanisms, is also the cornerstone for clinical therapy. However, the exact pathogenesis and mechanisms have not been fully established, posing several challenges for both fundamental research and clinical treatment of IBD. These current challenges are as follows: (1) Existing therapeutic agents cannot completely cure this disease; (2) Choice of clinical treatment; (3) Resistance to anti-tumor necrosis factor (TNF) therapy; and (4) Targeted research of new IBD therapeutic agents.

Research on the pathogenesis is vital for identifying the root causes of IBD and provides significant insights into the patient's overall condition and potential pathways for curing the disease, primarily comprising Crohn's disease and ulcerative colitis. Moreover, it aids in discovering new therapeutic targets, which can enhance clinical diagnosis, treatment and even early prevention of IBD. This is particularly crucial for newly industrialized countries with traditionally low incidence rates such as those in Asia, Africa, and South America. Therefore, it is necessary to study the pathogenesis of IBD.

Therefore, this paper focused on six key aspects to analyze the root causes of the two most common forms of IBD, primarily comprising Crohn's disease and ulcerative colitis. The common pathogenesis of these two forms of IBD was systematically studied and discussed. Those were: (1) Dysregulated immune responses; (2) Gene function changes; (3) Intestinal microbes disorder and imbalance; (4) Microbial infections; (5) Associations between IBD and other inflammatory diseases; and (6) Other factors. It illustrated both the causes of IBD and factors contributing to resistance against the disease. Additionally, pathogenesis differences between these two forms of IBD were unraveled and clearly distinguished. These unique aspects of pathogenesis would provide crucial insights for the precise treatment of both Crohn's disease and ulcerative colitis.

COMMON PATHOGENESIS OF CROHN'S DISEASE AND ULCERATIVE COLITIS

The two most prevalent subtypes of IBD, Crohn's disease and ulcerative colitis, have common pathogenesis. Current research on the pathogenesis of IBD concentrates on six primary aspects: (1) Dysregulated immune responses; (2) Gene function changes; (3) Intestinal microbes disorder and imbalance; (4) Microbial infections; (5) Associations between IBD and other inflammatory diseases; and (6) Other factors (Figure 1). These factors collectively contribute to intestinal damage and inflammation, leading to the onset of IBD. This section also explores protective strategies for the intestines and resistance mechanisms against IBD. Moreover, corresponding treatment strategies and feasible treatment methods are proposed.

Dysregulated immune responses

The pathogenesis of the immune system function in IBD has identified key cytokines and their functions, cytokine regulation and influence, changes in inflammatory mediators, and the relationship between intestinal mucosal immunity and intestinal epithelial cells (Figure 2). Various feasible strategies for preventing and treating IBD have also been proposed. For instance, T cell-derived interleukin 22 (IL-22) binding protein (IL-22BP), IL-17F, and T helper 17 (Th17)

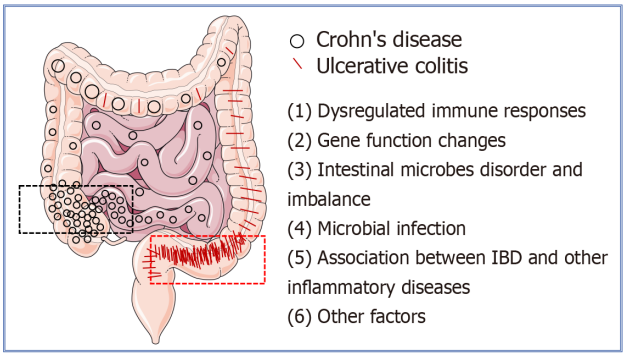

Figure 1 Study on the pathogenesis between Crohn's disease and ulcerative colitis. IBD: Inflammatory bowel disease.

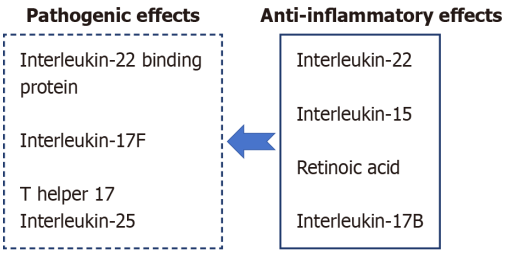

Figure 2 Key cytokines and their functions of immune system for the pathogenesis of inflammatory bowel disease.

have been identified as pathogenic[8,9]. However, IL-22, IL-17B, and IL-15 have anti-inflammatory effects.

IL-22BP is known to induce IBD, as evidenced by experiments in mice. In patients with IBD, high levels of IL-22BP are produced by $CD4^+$ T cells. While cytokine IL-22 exerts protective effects on tissues in the intestine, IL-22BP endogenously inhibits this effect of cytokine IL-22. During anti-TNF-α treatment, which is recognized as an effective IBD therapy, amounts of IL-22BP secreted by $CD4^+$ T cells are reduced. Despite the inhibition of IL-22BP, IL-22 is still expressed, thereby achieving the therapeutic objective for IBD[10].

Additionally, IL-17 family-related members play important roles in the pathogenesis of IBD. Both IL-17A and IL-17F contribute independently to IBD. IL-17A and IL-17F activate the nuclear factor kappa B (NK-kB) pathway to control bacterial and fungal infections. IL-17A and IL-17F in the intestines originate from T cells and some cellular subtypes, such as $CD4^+$ helper T cells, gamma delta T cells, alpha beta T cells, type 3 innate lymphoid cells (ILCs), natural killer T cells, and mucosal-associated invariant T cells[11]. IL-17A and TNF synergistically mediate signal to drive the expression of inflammatory genes in Crohn's disease immunopathogenetic mechanisms[12-14]. Inhibition of IL-17F promotes the production of microbiota-mediated regulatory T cells in the colon. Treatment with anti-IL-17F antibodies reduces the severity of colitis pathology. In ulcerative colitis, IL-17B and the IL-25, both members of the IL-17 family, exert opposite effects. Among them, IL-17B cytokines are protective and anti-inflammatory, whereas IL-25 is pathogenic[15]. Therefore, the development of new biological therapies selectively intervening or targeting IL-17s are also prospective strategies in IBD.

Furthermore, inflammation of Th17 cells has been linked to IBD[16]. Retinoic acid, a metabolite of intestinal vitamin A, promotes the differentiation of regulatory T cells and inhibits the differentiation of Th17 cells[9]. Cytokine IL-15, secreted by fibroblastic reticular cells in secondary lymphoid organs, maintains group 1 ILCs in Peyer's patches, thereby preventing immunopathological damage in the intestine[8]. Although ILCs accelerate virus clearance, they can cause severe intestinal inflammatory diseases, accompanied by symbiotic disorders and reduced intestinal barrier function.

The study of IBD's immune pathogenesis has led to the discovery of new treatment methods. During the episode period of IBD, some chemokines, chemokine receptors, and cell adhesion molecules are upregulated in IBD mucosa. Then circulating leukocytes migrate to the inflamed gut, regulated by cell adhesion molecules, chemokines, and chemokine receptors. Disrupting this migration can improve IBD therapy[17]. For instance, inhibiting or changing the migration of inflammatory leukocytes into the gut has shown therapeutic benefits[18].

Infliximab is a therapeutic antibody directed against TNF-α to treat IBD. Infliximab has a positive effect on intestinal mucosal gene expression in patients. Before infliximab therapy, most cell adhesion molecule genes are upregulated. However, most of these genes are significantly decreased after infliximab therapy. The gene response varies depending on whether the lesion is located in the colon or the ileum. In patients with colon IBD, chemokines C-C motif chemokine ligand 20 (CCL20) and C-X-C motif chemokine ligand (CXCL) 1 and 2 continue to increase, predisposing to IBD relapse. Meanwhile, in patients with ileum IBD, the expression of several genes increases before treatment such as mucosal vascular addressin cell adhesion molecule 1; thymus cell antigen 1; platelet endothelial cell adhesion molecule 1; CCL28; CXCL1, CXCL2, CXCL5, CXCL6, and CXCL11; and IL-8. However, cluster of differentiation 58 is decreased[17]. Genes in patients with IBD of the ileum are restored to control levels after infliximab therapy[18]. Other treatment methods are

used to reduce the immune response and control inflammation in the IBD, such as pro-inflammatory factor antagonists, anti-inflammatory factor mimics, cytokine inhibitors, and inhibition of inflammatory signal transduction.

The pathogenesis of immune responses to IBD offers new insight into pharmacological therapies, such as inhibiting inflammatory signaling. It also reveals that clinical parameters alone cannot sensitively stratify patients with IBD, highlighting the need for more accurate analytical methods. High-resolution analytical technologies for delivering precision agents and predicting responses to specific IBD therapies can facilitate more effective and personalized treatment[19]. Promising analytical methods include immune response profiling, germline genetics, *in vivo* real-time molecular endoscopy, gut micro-biome analysis, and tissue transcriptomics.

Gene function changes

Genetic research has made substantial progress in understanding the pathogenesis of IBD. Genome-wide studies have identified susceptibility gene loci, their functions, and interrelations between genes, opening new avenues for gene therapy for IBD. Genome-wide association studies have pinpointed hundreds of gene loci associated with IBD, contributing to both Crohn's disease and ulcerative colitis, as illustrated in Figure 3[20]. For instance, variations in genes linked to IBD pathogenesis include IL-23, the IL-23 receptor subunit (IL-23R), the p40 subunit of IL-23, IL-12, the p40 subunit encoding for IL-12 (IL12B), the IL12B variant, TNF superfamily member 15, the *RNASET2-FGFR1OP-CCR6*, Janus kinase 2, nucleotide-binding oligomerization domain 2 (*NOD2*), signal transducer and activator of transcription 3; the homeodomain-containing transcription factor NK2 transcription factor related, locus 3 (*NKX2-3*) gene regions[21]; the susceptibility genes regulating immune function PR domain zinc finger protein 1, *REL*, caspase-recruitment domain 9 (*CARD9*), *SMAD3*, *IL1R2*; immunity-related GTPase M (*IRGM*), autophagy related 16-like 1 (*ATG16L1*); IL-10 functional defects; Th17-IL23 pathway[22].

Encoding IL-23R is a genetic factor leading to Crohn's disease[23]. The *IL-23R* gene, located on chromosome *1p31*, encodes a subunit of the pro-inflammatory cytokine IL-23 receptor, which is a crucial peptide for the generation of Th17 cells. *Rs11209026* (c.1142G>A, p.Arg381Gln) is an uncommon coding variant that has a protective effect against Crohn's disease. IBD is associated with IL-23R regional abnormal signal transduction. At the same time, multiple independent signals are associated with IBD in the *IL-23R* gene region. Because of the polymorphism of IL-23R region, the effect on IBD is more complicated. Both the innate and adaptive immune systems contribute to IBD through the IL-23R region polymorphisms[24].

In addition, the homeodomain-containing transcription factor *NKX2-3* gene regions, involved in the homologous domain of lymphocyte development, differentiation and tissue, also affect Crohn's disease and ulcerative colitis pathogenesis. Susceptibility gene loci for IBD and that of mycobacterial infections are overlapped, suggesting shared human response pathways[25]. Functional variation of 45 specific genes affect IBD by high-resolution fine-mapping, including 18 associations (a single causal variant, > 95%) and 27 associations (a single variant, > 50%). These variants are as follows: Tissue-specific epigenetic marks, protein-coding changes, and transcription factor binding sites destruction[26].

Susceptibility genes for IBD vary among populations around the world, such as in Europe, America, Japan, South Korea, and China. For example, in Europe and the United States, common susceptibility genes include *ATG16L1*, *NOD2* defects, and *CARD9*. In Japan, common genes include *ATG16 L2-FCHSD2*, *SLC25A15-ELF1-WBP4*[27], Nudix Hydrolase 15 (*NUDT15*) *p.Arg139Cys*[28], *NUDT15 R139C*, and *NKX2-3* polymorphisms[29,30]. In South Korea, TNF superfamily member 15[22], IL-23R, *ATG16 L2*, *RNASET2-FGFR1OP-CCR6*[31], and *IRGM* are common, whereas in China, *CARD9* [32], *IL-10* gene variants[33], and *IL-17F* variants[34] are prevalent.

The concordance rates for Crohn's disease between monozygotic twins are 40%-50%[35]. Additionally, family inheritance proportions of IBD differ between Western and Asian countries. In Western countries, the proportion is significantly higher[36], with less than 20% for Western patients with IBD and less than 7% for Asian patients with IBD [37,38]. Gene interactions in IBD pathogenesis have paved the way for gene therapy, such as replacing defective genes and repairing sites in hematopoietic cells.

Intestinal microbes disorder and imbalance

IBD is associated with alterations in the composition of intestinal microbiota. The gut microbiota is indispensable for the pathogenesis of IBD, regulating the development and function of the immune system and playing both anti-inflammatory and pro-inflammatory roles. Changes in the intestinal microbes, including composition, abundance, richness, strain diversity, stability, gene variation, and function of gut microbiota, contribute to the onset of IBD[39]. In turn, oxidative and metabolic environment alterations in IBD shape the gut microbiota, leading to gut microbiota dysbiosis. The composition of intestinal microbiota in patients with IBD exhibits distinct characteristics.

The microbial composition in the intestines of patients with IBD is altered. Key bacterial species associated with IBD have been identified through species and strain-level profiles, bacterial growth rates, virulence factors, antibiotic resistance, and metabolic functions[40]. Moreover, the abundance of these gut microbiota changes significantly. For instance, the abundance of *Bacteroides* are increased in the intestinal microbiota of patients with IBD. *Bacteroides* are highly correlated with IBD[35]. In addition, *B. fragilis* and *B. vulgatus* are particularly elevated. Immunomodulatory molecules released by the outer membrane vesicles are produced by the gut microbe *B. fragilis*. In mouse experiments, these immunomodulatory molecules protect mice from experimentally induced colitis[35]. In patients with Crohn's disease, a deficiency in the *ATG16L1* and *NOD2* genes induces intestinal inflammation. Outer membrane vesicles mediate *ATG16L1* and *NOD2* genes to jointly protect humans from colitis. *ATG16L1* and *NOD2* genes cause transmission mechanism problems. The release of immunomodulatory molecules from the outer membrane vesicles require the combined action of *ATG16 L1* and *NOD2* genes for patients with IBD.

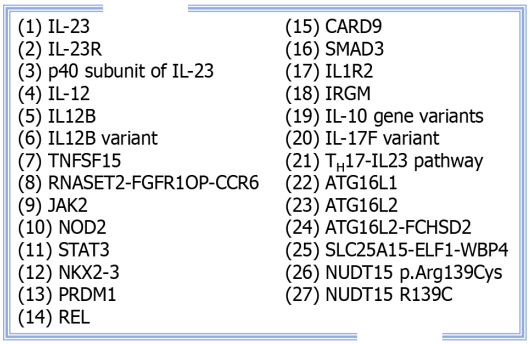

Figure 3 Gene function changes for the pathogenesis of inflammatory bowel disease. ATG16L1: Autophagy-related 16-like 1; CARD9: Caspase-recruitment domain 9; CCR6: CC-motif chemokine receptor 6; ELF1: Elongation factor 1; FCHSD2: FCH and double SH3 domains protein 2; FGFR1OP: Fibroblast growth factor receptor 1 oncogene partner; IL: Interleukin; IRGM: Immunity-related GTPase M; JAK2: Janus kinase 2; NKX2-3: NK2 transcription factor related, locus 3; NOD2: Nucleotide-binding oligomerization domain 2; NUDT15: Nudix hydrolase 15; PRDM1: PR domain zinc finger protein 1; SLC25A15: Solute carrier family 25 member 15; STAT3: Signal transducer and activator of transcription 3; TNFSF15: Tumor necrosis family superfamily member 15; WBP4: WW domain-binding protein 4.

In dendritic cells, outer membrane vesicles activate *ATG16L1* and *NOD2*-dependent noncanonical autophagy pathways. To protect against colitis, dendritic cells triggered by outer membrane vesicles can further induce regulatory T cells in the intestine, which helps protect against IBD. The gut microbiota regulates peripheral lymphoid volume expansion and maintenance by controlling the function of RALDH(+) dendritic cells[41]. During the early neonatal period, CD45(+)CD103(+)RALDH(+) cells in the intestine migrate to peripheral lymph nodes under the induction of symbiotic microorganisms, simultaneously inducing a substantial amount of retinoic acid locally. This mechanism promotes the differentiation of regulatory T cells and inhibits the differentiation of Th17 cells.

Additionally, the intestinal flora coordinates with the host to maintain intestinal immune homeostasis. Growth factors fibroblast growth factor 2 and IL-17 synergistically repair damage to the intestinal epithelium and maintain the immune homeostasis within the intestinal mucosal system. Growth factor fibroblast growth factor 2, which has a protective effect on the intestine, is secreted by intestinal regulatory T cells in response to an imbalance in the intestinal flora.

Enhancement of effector cell function or a decrease of regulatory cell function can lead to a dysregulated immune response to normal symbiotic bacteria[24]. Meanwhile, genetic predispositions influence the role of intestinal microflora and environmental factors within the gut[42]. In individuals with a high genetic predisposition, the immune response of the intestine to the control of symbiotic flora is dysregulated. This affects the intestinal microflora and environment, inducing changes in the colon. Intestinal homeostasis cells can promote inflammation, immune tolerance, and epithelial repair. The location of IBD within the intestine determines the composition of intestinal flora. For instance, the intestinal flora of patients with colonic type differs from those with ileal type in Crohn's disease, such as decreased alpha diversity [43]. Furthermore, certain microbial species are commonly affected in both Crohn's disease and ulcerative colitis. Four microbial species, including *Eggerthellaceae*, *Bacteroidaceae*, and *Lachnospiraceae*, are increased, while 16 microbial species, such as *Peptostreptococcaceae*, *Eubacteriaceae*, and *Streptomycetaceae*, are decreased[40].

Studying changes in the composition and function of gut microbiota in patients IBD not only advances our understanding of the disease's pathogenesis but also broadens the potential for future research directions. Therapeutic approaches could include promoting ecological agents to correct intestinal flora imbalance, such as IL-13[44]. From a nutritional and health perspective, interventions like yogurt consumption can help reduce inflammation by enhancing the integrity of the intestinal lining[45]. Improved intestinal integrity can prevent pro-inflammatory molecules produced by intestinal microorganisms from entering the blood[46]. Further treatments for IBD are likely to focus on microbiota-based interventions. Moreover, the development of probe technologies targeting specific intestinal microorganisms could enable accurate identification and differentiation of IBD subtypes. This approach could allow for the precise distinction between Crohn's disease and ulcerative colitis by targeting key bacterial species within the gut. Additionally, there is a need to develop immuno-regulatory therapeutic agents that can promote immune system activation and inhibit inflammatory response by bypassing cellular transport mechanisms, making them suitable for direct ingestion by patients with IBD. Furthermore, there is an urgent need to establish a comprehensive and sophisticated treatment system for IBD that utilizes one or more intestinal flora as bio-markers. Such a system could not only deliver therapeutic agents but also facilitate accurate diagnosis and simultaneous treatment of IBD.

Microbial infection

In the study of IBD, the pathogenesis with bacteria and fungi are limited. The enteric virome is an integral part of the gut microbiota ecosystem, yet its involvement in IBD pathogenesis has been largely overlooked. The enterovirus group, comprising various DNA and RNA viruses, remains relatively understudied. Common microorganisms implicated in IBD pathogenesis include bacteria, viruses, molds, and protozoa, some of which may also trigger allergic reactions (Table 1).

Microbial infections cause inflammation directly or indirectly by a damaged intestinal mucosal barrier, imbalance of microbial homeostasis, as well as altering immune system in IBD[47]. Microbial infections also lead to shifts in the composition of intestinal flora, intestinal disorders, and increased intestinal mucosal permeability, all of which signi-

Table 1 Microbial infection that affects inflammatory bowel disease

Items	Microbial infection	Ref.
1	Enterovirus B species of eukaryotic picornaviruses	[50]
2	Oral bacteria	[60-63]
3	Oropharyngeal bacteria	[64]
4	Candida albicans	[65]
5	Parasitic infection	[66]

ficantly elevate the risk of IBD. Moreover, there is mutual regulation and change between the intestinal microbiota and the genetic composition of the host, and between the microbiota composition and function and the neutrophil production and function under specific environmental factors, which are linked to the pathogenesis of IBD[48,49]. The eukaryotic viruses and viromes in colon resections are different between patients with IBD and non-IBD. Colon tissue viromes and enteric viruses affect intestinal homeostasis and shape the phenotype of IBD through divergent innate immunomodulation. The immune system detects disturbances in the enterovirus group, affecting the maintenance of normal intestinal homeostasis. For IBD, the enterovirus B species of eukaryotic picornaviruses increase in colon. Additionally, genetic variations contribute to altered virome sensing, resulting in the perturbation of colon tissue viromes and the onset of IBD [50].

Oral bacteria have been observed in the intestinal mucosa of patients IBD, where they become highly enriched and colonized during the disease. For example, bacteria in the oral cavity appear and accumulate in the intestinal tract of patients with IBD during periodontal disease. These oral bacteria enrich in the mucosal niche of IBD intestine, such as *Klebsiella spp.*, *Campylobacter concisus*, *Fusobacterium nucleatum*, and *Veillonella spp*[51-53]. In Crohn's disease, *Haemophilus parainfluenzae* and *F. nucleatum*, specific to the oral cavity, are significantly enriched in the intestinal mucosa[54]. Additionally, in the intestine of patients with IBD, the number of oral-associated species *Veillonella spp.* are enriched, which are nitrate reducers[55].

Intestinal epithelial permeability is increased due to impaired mucosal barrier in the patients with IBD. Oral microorganisms can not only interfere with intestinal barrier function, but also accumulate and colonize in the intestinal mucosa [56]. These microbial disturbances contribute to intestinal dysbiosis, which drives IBD pathogenesis. Moreover, the inflammatory environment within the intestine promotes the growth of oral-related bacteria and disrupts the symbiotic microbiota during IBD. During inflammation, concentrations of nitrate increase in the intestine. The *Enterobacteriaceae spp.* is increased rapidly[57-59].

The composition of oral bacterial microbiota changes significantly over time in patients with IBD. In pediatric Crohn's disease, *Rothia spp*. and *Capnocytophaga spp.* are enriched in the oral subgingival biofilm[60]. In patients with periodontitis, nitrate reductase-capable bacteria such as *Proteobacteria spp.* and *Veillonella spp.* are also increased[61]. In severe ulcerative colitis, the oral microbiota differs from that seen in Crohn's disease, with associations noted for *Campylobacter spp.*, *H. parainfluenzae*, *V. parvula*, and *V. dispar*[54,62].

A multistage model linking microbial and immune compartmental changes in the oral cavity and intestine has been used to assess the correlation between oral bacterial microbiota and IBD. This model suggests that oral disease-related bacteria trans-locate to the intestine, exacerbating IBD symptoms directly[63]. Additionally, oropharyngeal bacteria from the nasopharynx and mouth can migrate and colonize the stomach and intestines, leading to intestinal inflammation and malnutrition in children[64].

Non-bacterial microorganisms and viruses, including fungi like *Candida albicans*, are also present in the intestines of patients with IBD[65,66]. Additionally, parasitic infections can influence IBD by triggering beneficial changes in the gut microbiota, which in turn elicit specific parasite-associated immune responses that counteract intestinal inflammation [44]. Hence, harnessing viruses or viromes unique to IBD-affected colon tissue offer the potential for developing new therapeutic strategies, bio-markers, and early screening tools based on microbial markers linked to IBD pathogenesis. In addition, oral microbial signatures enriched in the intestinal mucosa or distinctive oral bacterial microbiota could help accurately distinguish between Crohn's disease and ulcerative colitis.

Association between IBD and other inflammatory diseases

The correlation between IBD and other inflammatory diseases helps to elucidate the underlying causes of IBD. These associations stem from factors such as genetic factors, common pathogenic triggers, or the consequences of other conditions or their treatments. Compared to individuals without IBD, patients with IBD have a higher susceptibility to autoimmune diseases. Patients with one immune-mediated disease have an increased incidence of developing several other immune-mediated diseases. Genome-wide studies have shown that chronic immune diseases tend to cluster in certain individuals. Consequently, the prevalence of multiple immune-mediated diseases is notably elevated in patients with IBD. Moreover, gene loci associated with IBD are also linked to other immune-mediated diseases, including ankylosing spondylitis and psoriasis[25].

The most frequently observed concurrent inflammatory diseases in patients with IBD are arthritis and asthma. Other extra-intestinal manifestations (EIMs) include ankylosing spondylitis, erythema nodosum, inflammatory eye disease, and periodontitis. Additionally, patients with IBD may present with peripheral arthritis, primary sclerosing cholangitis, pyoderma gangrenosum, uveitis, and oral ulcers[67-69]. The relationship between IBD activity and EIMs varies. Some

EIMs, such as uveitis and primary sclerosing cholangitis, occur independently of IBD activity, while others, including erythema nodosum and oral ulcers, are linked to IBD activity, suggesting shared pathogenic mechanisms[68,69].

IBD pathogenesis has been further explored by examining the correlation between IBD activity and EIMs[69,70]. However, the mechanisms behind most EIMs remain unclear. The pathogenesis of EIMs may arise from the following: (1) EIMs may represent independent inflammatory events triggered by genetic factors, microbial agents, or elevated inflammatory mediators and other factors[71]; and (2) EIMs may result from the extension of intestinal antigen-specific immune responses to non-intestinal sites, such as *via* microbial antigen cross-reactions and ectopic inflammation.

A large Canadian population-based study revealed that 63% of patients were diagnosed with chronic inflammatory diseases before the onset of IBD. These patients exhibited a significantly higher risk of inflammatory diseases such as bronchitis, psoriasis, and pericarditis. Patients with ulcerative colitis were found to have an increased risk of chronic kidney disease and multiple sclerosis[72]. Additionally, patients with IBD face an increased risk of concurrent mental health conditions, including depression and anxiety. The potential mechanisms linking IBD to psychiatric conditions include elevated pro-inflammatory cytokines, gut dysbiosis, altered vagal nerve signaling, and changes in brain morphology and function[73].

Other factors

In addition to the previously discussed factors, alterations in colonic epithelial cell diversity contribute to IBD. Single colonic epithelial cellular subtypes have been identified, including progenitor cells, colonocytes, and goblet cells in the crypts. The positional re-modelling of goblet cells plays a key role in IBD pathogenesis. Goblet cells, which express the anti-protease molecule WAP four-disulfide core domain protein 2, not only inhibit bacterial growth but also prevent invasion by commensal bacteria and mucosal inflammation[74]. Additionally, absorptive cells located at the top of the crypts, which are responsible for sensing pH, are dysregulated in IBD. These cells express the proton channel otopetrin 2 and the satiety peptide uroguanylin. Furthermore, elevated levels of transforming growth factor beta 1 and nitric oxide have been detected in the saliva of both patients with Crohn's disease and ulcerative colitis[75,76].

Many other non-pathological factors associated with the development of human society are closely linked to IBD. These factors include changes in the natural environment, economic development, living conditions, dietary structure, lifestyle changes, disease exposure factors, population size, increased immune-related diseases, and improved diagnostic capabilities[77]. In terms of diet, excessive consumption of high-fat and sugary foods, coupled with unhealthy lifestyle habits such as lack of exercise, smoking, antibiotic overuse, and an obsession with hygiene, have been identified as contributors to IBD[1,78]. The pursuit of excessive cleanliness has led to a reduction in exposure to intestinal worms, which are thought to play a role in host immune system training. As a result, the intestinal immune systems of some individuals may become overly sensitive, predisposing them to IBD. Additionally, the incidence of IBD has been shown to be positively correlated with population density. As the population increases, the number of patients also increases. The greater the population density, the higher the incidence of IBD[79].

Epidemiological studies comparing patients with IBD and healthy controls have identified several protective factors that may lower the risk of developing Crohn's disease and ulcerative colitis. These factors include breastfeeding > 12 months, consumption of tea, vegetables, fruits, plant fiber intake, physical exercise, and pet ownership (specifically dogs) for Crohn's disease[38]. Similarly, protective factors for ulcerative colitis include breastfeeding > 12 months, consumption of tea, hot water bath, consumption of coffee, intake of vitamins C and D, and use of flush toilets during childhood[80,81]. These factors are essential not only for maintaining physical health but also for fostering mental well-being. Thus, prevention strategies for IBD should promote both a healthy lifestyle and a positive psychological construction.

PATHOGENESIS DIFFERENCES BETWEEN CROHN'S DISEASE AND ULCERATIVE COLITIS

While Crohn's disease and ulcerative colitis share some commonalities, they also exhibit significant distinctions in their pathogenesis. These two major subtypes of IBD have their own unique pathological characteristics, and the specific mechanisms contributing to the development of each have been discussed in detail. Through a comparative analysis of the pathogenesis of Crohn's disease and ulcerative colitis, the specific immune mechanisms, genetic abnormalities, and intestinal microbiota alterations that underpin these conditions have been identified, allowing a clear distinction between these two. Clinically, the pathogenesis of Crohn's disease and ulcerative colitis differ markedly, with each condition possessing its own distinctive features. Moreover, gut microbiota profiles differ significantly between patients with Crohn's disease and those with ulcerative colitis. Each condition is associated with a unique microbial environment and distinct gut microbiota characteristics. These unique aspects of pathogenesis provide crucial insights for the precise treatment of both Crohn's disease and ulcerative colitis.

The unique pathogenesis of Crohn's disease

The unique pathogenesis for Crohn's disease is manifested in the following aspects: (1) The disease is driven primarily by interferon gamma and IL-12, as observed in both patients and mouse models; (2) It is caused by defects in the innate immune system. The pathogenesis of Crohn's disease is associated with genes encoding *NOD2*, *ATG16L1*, and *IRGM*. These genes play critical roles in the innate immune system and the intracellular processing of bacterial components. In addition, *NOD2* gene is mutated in patients with Crohn's disease. The ability of *NOD2* sense bacterial peptidoglycan, activate NK-kB, and mitogen-activated protein kinase pathways are decreased. Deficiencies in *NOD2* or *ATG16L1* contribute to Crohn's disease susceptibility, with the functional impact being assessed through altered function of *ATG16L1* and *IRGM* polymorphisms[24,35]; (3) Mutations in genes encoding Toll-like receptor 4, *NOD1*, and *NOD2*

contribute to the inflammation in Crohn's disease, which are innate immune recognition receptors. Therapeutically, inflammatory cytokines TNF and IL-12/23 are effective in the treatment of the disease; (4) It is strongly linked to specific immune cells; (5) The gene encoding leucine-rich repeat kinase 2 (LRRK2) has been identified as a major susceptibility gene for Crohn's disease by genome-wide association studies[82,83]. LRRK2 acts as a negative regulator of the transcription factor nuclear factor of activated T cells and plays a critical role in modulating disease severity. LRRK2 protein regulates the transport and secretion of lysozyme in lysosomes, inhibits intestinal inflammation, and regulates intestinal immune homeostasis in murine cells. LRRK2 deficiency shows increased susceptibility to colitis in experimental mice [84]; (6) Salivary inflammatory markers such as IL-6, IL-1β, and TNF are elevated for Crohn's disease[85]; (7) The diversity of pathogenic species, as well as pro-inflammatory flora, is notably elevated in patients with Crohn's disease. This includes members of the *Enterobacteriaceae* family, such as *Escherichia spp.* and *Shigella spp.*, which are associated with colon ulceration and bloody diarrhea. Additionally, gut microbiota alterations reveal increased levels of *Enterobacteriaceae*, *Streptococcaceae*, and *Erysipelotrichaceae* in these patients; (8) The diversity and abundance of beneficial gut microbes are markedly reduced. For instance, *Clostridia*, known to counteract inflammation through interactions with pathogenic intestinal bacteria associated with IBD, are diminished[44]. *Faecalibacterium prausnitzii*, also referred to as *Clostridium prausnitzii*, which has anti-inflammatory properties, shows reduced levels in patients with Crohn's disease[86,87]. This butyrate-producing bacterium is especially depleted in the ileum during disease onset. Similarly, the strain diversity of *Roseburia intestinalis*, which converts acetate to butyrate, is also decreased. *Bifidobacterium longum*, which provides resistance against *Shigella*-induced enteric infections, is likewise reduced. Other microbial species, including *Actinomycetaceae*, *Bifidobacteriaceae*, *Atopobiaceae*, *Prevotellaceae*, and *Firmicutes_noname*, show decreased numbers in Crohn's disease; and (9) The microbial environment within the gut of Crohn's disease patients undergoes significant alterations. The inflammatory conditions promote increased sugar degradation and quinone biosynthesis, while fermentation pathways are diminished[40].

The unique pathogenesis of ulcerative colitis

Compared to Crohn's disease, ulcerative colitis exhibits distinct pathogenic characteristics, which are outlined as follows: (1) It is driven by natural killer T cells, which produces IL-13, as observed in both IBD patients and mouse models[24]; (2) It is caused by mutations in the coding genes of Toll-like receptor 4 and *NOD1*. These innate immune recognition receptor proteins play a role in detecting microorganisms. The inflammatory cytokine TNF are effective in the treatment of ulcerative colitis; (3) It is associated with gut mucosa. The correlation between ulcerative colitis and gut mucosa is stronger[19,26]; (4) Certain microbial species like *B. uniformis* and *Bifidobacterium bifidum* are associated specifically with ulcerative colitis. Increased gut microbiome includes *Bifidobacteriaceae* and *Acidaminococcaceae*. Conversely, reduced microbial species include *Propionibacteriaceae* and *Nectriaceae*; and (5) The microbial environment in ulcerative colitis displays increase lactate production pathways, while butyrate and acetate production pathways are diminished, which exacerbates inflammation in the intestinal environment[40].

In conclusion, the differentiation in pathogenesis between Crohn's disease and ulcerative colitis, along with the identification of highly specific markers, enables precise early diagnosis, screening, and treatment. Such distinctions offer significant potential for personalized treatment strategies for Crohn's disease and ulcerative colitis. Furthermore, the unique microbial characteristics associated with each disease subtype facilitate their accurate classification, providing a foundation for targeted treatment and advancing precision agents for IBD.

CONCLUSION

The incidence and prevalence of IBD continue to rise globally; however, effective treatment options for this disease remain limited. IBD is led by a combination of dysregulated immune responses, gene alterations, imbalances in intestinal microbiota, microbial infections, associations with other inflammatory diseases, and shifts in social and environmental factors. These immune, genetic, and environmental factors are intertwined and act synergistically, often triggering and amplifying one another in the progression of IBD. Changes in genetic, immune, and intestinal microbial factors also contribute to shaping the distinct IBD phenotype. Unique aspects of pathogenesis provide crucial insights for the precise treatment of both Crohn's disease and ulcerative colitis. Despite significant challenges in understanding the pathogenesis of IBD, research has yielded substantial insights, offering potential solutions for patients. Continued scientific efforts and exploration have shed light on the fundamental mechanisms underlying IBD, which is crucial for developing effective prevention and treatment strategies. Utilizing these main contents allow for the development of comprehensive interventions that reduce harmful influences, enhance protective factors and use an integrative approach to address the diseases for the benefit of human being.

FOOTNOTES

Author contributions: Yang QH and Zhang CN made substantial contributions to the article; Yang QH performed the literature research and drafted the manuscript; Zhang CN provided critical input on the intellectual content, and reviewed and revised this manuscript; All authors have approved the final version of the manuscript.

Supported by Tianjin Municipal Science and Technology Commission Grant, No. 24ZXRKSY00010; and Program for Innovative Research Team in Peking Union Medical College, CAMS Initiative for Innovative Medicine, No. 2023-I2M-2-008.

Conflict-of-interest statement: The authors have no conflicts of interest to declare.

Country of origin: China

ORCID number: Chuang-Nian Zhang 0000-0002-1639-4900.

S-Editor: Wang JJ
L-Editor: Filipodia
P-Editor: Wang WB

REFERENCES

1 **Ng SC**, Shi HY, Hamidi N, Underwood FE, Tang W, Benchimol EI, Panaccione R, Ghosh S, Wu JCY, Chan FKL, Sung JJY, Kaplan GG. Worldwide incidence and prevalence of inflammatory bowel disease in the 21st century: a systematic review of population-based studies. *Lancet* 2017; **390**: 2769-2778 [PMID: 29050646 DOI: 10.1016/S0140-6736(17)32448-0]

2 **Kaplan GG**. The global burden of IBD: from 2015 to 2025. *Nat Rev Gastroenterol Hepatol* 2015; **12**: 720-727 [PMID: 26323879 DOI: 10.1038/nrgastro.2015.150]

3 **Xavier RJ**, Podolsky DK. Unravelling the pathogenesis of inflammatory bowel disease. *Nature* 2007; **448**: 427-434 [PMID: 17653185 DOI: 10.1038/nature06005]

4 **Gilliland A**, Chan JJ, De Wolfe TJ, Yang H, Vallance BA. Pathobionts in Inflammatory Bowel Disease: Origins, Underlying Mechanisms, and Implications for Clinical Care. *Gastroenterology* 2024; **166**: 44-58 [PMID: 37734419 DOI: 10.1053/j.gastro.2023.09.019]

5 **Sanmarco LM**, Chao CC, Wang YC, Kenison JE, Li Z, Rone JM, Rejano-Gordillo CM, Polonio CM, Gutierrez-Vazquez C, Piester G, Plasencia A, Li L, Giovannoni F, Lee HG, Faust Akl C, Wheeler MA, Mascanfroni I, Jaronen M, Alsuwailm M, Hewson P, Yeste A, Andersen BM, Franks DG, Huang CJ, Ekwudo M, Tjon EC, Rothhammer V, Takenaka M, de Lima KA, Linnerbauer M, Guo L, Covacu R, Queva H, Fonseca-Castro PH, Bladi MA, Cox LM, Hodgetts KJ, Hahn ME, Mildner A, Korzenik J, Hauser R, Snapper SB, Quintana FJ. Identification of environmental factors that promote intestinal inflammation. *Nature* 2022; **611**: 801-809 [PMID: 36266581 DOI: 10.1038/s41586-022-05308-6]

6 **Rogler G**, Singh A, Kavanaugh A, Rubin DT. Extraintestinal Manifestations of Inflammatory Bowel Disease: Current Concepts, Treatment, and Implications for Disease Management. *Gastroenterology* 2021; **161**: 1118-1132 [PMID: 34358489 DOI: 10.1053/j.gastro.2021.07.042]

7 **Nadeem MS**, Kumar V, Al-Abbasi FA, Kamal MA, Anwar F. Risk of colorectal cancer in inflammatory bowel diseases. *Semin Cancer Biol* 2020; **64**: 51-60 [PMID: 31112753 DOI: 10.1016/j.semcancer.2019.05.001]

8 **Gil-Cruz C**, Perez-Shibayama C, Onder L, Chai Q, Cupovic J, Cheng HW, Novkovic M, Lang PA, Geuking MB, McCoy KD, Abe S, Cui G, Ikuta K, Scandella E, Ludewig B. Fibroblastic reticular cells regulate intestinal inflammation *via* IL-15-mediated control of group 1 ILCs. *Nat Immunol* 2016; **17**: 1388-1396 [PMID: 27798617 DOI: 10.1038/ni.3566]

9 **Kitamoto S**, Nagao-Kitamoto H, Jiao Y, Gillilland MG 3rd, Hayashi A, Imai J, Sugihara K, Miyoshi M, Brazil JC, Kuffa P, Hill BD, Rizvi SM, Wen F, Bishu S, Inohara N, Eaton KA, Nusrat A, Lei YL, Giannobile WV, Kamada N. The Intermucosal Connection between the Mouth and Gut in Commensal Pathobiont-Driven Colitis. *Cell* 2020; **182**: 447-462.e14 [PMID: 32758418 DOI: 10.1016/j.cell.2020.05.048]

10 **Pelczar P**, Witkowski M, Perez LG, Kempski J, Hammel AG, Brockmann L, Kleinschmidt D, Wende S, Haueis C, Bedke T, Witkowski M, Krasemann S, Steurer S, Booth CJ, Busch P, König A, Rauch U, Benten D, Izbicki JR, Rösch T, Lohse AW, Strowig T, Gagliani N, Flavell RA, Huber S. A pathogenic role for T cell-derived IL-22BP in inflammatory bowel disease. *Science* 2016; **354**: 358-362 [PMID: 27846573 DOI: 10.1126/science.aah5903]

11 **Navarro-Compán V**, Puig L, Vidal S, Ramírez J, Llamas-Velasco M, Fernández-Carballido C, Almodóvar R, Pinto JA, Galíndez-Aguirregoikoa E, Zarco P, Joven B, Gratacós J, Juanola X, Blanco R, Arias-Santiago S, Sanz Sanz J, Queiro R, Cañete JD. The paradigm of IL-23-independent production of IL-17F and IL-17A and their role in chronic inflammatory diseases. *Front Immunol* 2023; **14**: 1191782 [PMID: 37600764 DOI: 10.3389/fimmu.2023.1191782]

12 **Schmitt H**, Neurath MF, Atreya R. Role of the IL23/IL17 Pathway in Crohn's Disease. *Front Immunol* 2021; **12**: 622934 [PMID: 33859636 DOI: 10.3389/fimmu.2021.622934]

13 **Fauny M**, Moulin D, D'Amico F, Netter P, Petitpain N, Arnone D, Jouzeau JY, Loeuille D, Peyrin-Biroulet L. Paradoxical gastrointestinal effects of interleukin-17 blockers. *Ann Rheum Dis* 2020; **79**: 1132-1138 [PMID: 32719044 DOI: 10.1136/annrheumdis-2020-217927]

14 **Frieder J**, Kivelevitch D, Menter A. Secukinumab: a review of the anti-IL-17A biologic for the treatment of psoriasis. *Ther Adv Chronic Dis* 2018; **9**: 5-21 [PMID: 29344327 DOI: 10.1177/2040622317738910]

15 **Reynolds JM**, Lee YH, Shi Y, Wang X, Angkasekwinai P, Nallaparaju KC, Flaherty S, Chang SH, Watarai H, Dong C. Interleukin-17B Antagonizes Interleukin-25-Mediated Mucosal Inflammation. *Immunity* 2015; **42**: 692-703 [PMID: 25888259 DOI: 10.1016/j.immuni.2015.03.008]

16 **Dutzan N**, Kajikawa T, Abusleme L, Greenwell-Wild T, Zuazo CE, Ikeuchi T, Brenchley L, Abe T, Hurabielle C, Martin D, Morell RJ, Freeman AF, Lazarevic V, Trinchieri G, Diaz PI, Holland SM, Belkaid Y, Hajishengallis G, Moutsopoulos NM. A dysbiotic microbiome triggers T(H)17 cells to mediate oral mucosal immunopathology in mice and humans. *Sci Transl Med* 2018; **10**: eaat0797 [PMID: 30333238 DOI: 10.1126/scitranslmed.aat0797]

17 **Arijs I**, De Hertogh G, Machiels K, Van Steen K, Lemaire K, Schraenen A, Van Lommel L, Quintens R, Van Assche G, Vermeire S, Schuit F, Rutgeerts P. Mucosal gene expression of cell adhesion molecules, chemokines, and chemokine receptors in patients with inflammatory bowel disease before and after infliximab treatment. *Am J Gastroenterol* 2011; **106**: 748-761 [PMID: 21326222 DOI: 10.1038/ajg.2011.27]

18 **Triantafillidis JK**, Zografos CG, Konstadoulakis MM, Papalois AE. Combination treatment of inflammatory bowel disease: Present status and future perspectives. *World J Gastroenterol* 2024; **30**: 2068-2080 [PMID: 38681984 DOI: 10.3748/wjg.v30.i15.2068]

19 **Digby-Bell JL**, Atreya R, Monteleone G, Powell N. Interrogating host immunity to predict treatment response in inflammatory bowel disease. *Nat Rev Gastroenterol Hepatol* 2020; **17**: 9-20 [PMID: 31767987 DOI: 10.1038/s41575-019-0228-5]

20 **Sazonovs A**, Stevens CR, Venkataraman GR, Yuan K, Avila B, Abreu MT, Ahmad T, Allez M, Ananthakrishnan AN, Atzmon G, Baras A, Barrett JC, Barzilai N, Beaugerie L, Beecham A, Bernstein CN, Bitton A, Bokemeyer B, Chan A, Chung D, Cleynen I, Cosnes J, Cutler DJ, Daly A, Damas OM, Datta LW, Dawany N, Devoto M, Dodge S, Ellinghaus E, Fachal L, Farkkila M, Faubion W, Ferreira M, Franchimont D, Gabriel SB, Ge T, Georges M, Gettler K, Giri M, Glaser B, Goerg S, Goyette P, Graham D, Hämäläinen E, Haritunians T, Heap GA, Hiltunen M, Hoeppner M, Horowitz JE, Irving P, Iyer V, Jalas C, Kelsen J, Khalili H, Kirschner BS, Kontula K, Koskela JT, Kugathasan S, Kupcinskas J, Lamb CA, Laudes M, Lévesque C, Levine AP, Lewis JD, Liefferinckx C, Loescher BS, Louis E, Mansfield J, May S, McCauley JL, Mengesha E, Mni M, Moayyedi P, Moran CJ, Newberry RD, O'Charoen S, Okou DT, Oldenburg B, Ostrer H, Palotie A, Paquette J, Pekow J, Peter I, Pierik MJ, Ponsioen CY, Pontikos N, Prescott N, Pulver AE, Rahmouni S, Rice DL, Saavalainen P, Sands B, Sartor RB, Schiff ER, Schreiber S, Schumm LP, Segal AW, Seksik P, Shawky R, Sheikh SZ, Silverberg MS, Simmons A, Skeiceviciene J, Sokol H, Solomonson M, Somineni H, Sun D, Targan S, Turner D, Uhlig HH, van der Meulen AE, Vermeire S, Verstockt S, Voskuil MD, Winter HS, Young J; Belgium IBD Consortium; Cedars-Sinai IBD; International IBD Genetics Consortium; NIDDK IBD Genetics Consortium; NIHR IBD BioResource; Regeneron Genetics Center; SHARE Consortium; SPARC IBD Network; UK IBD Genetics Consortium, Duerr RH, Franke A, Brant SR, Cho J, Weersma RK, Parkes M, Xavier RJ, Rivas MA, Rioux JD, McGovern DPB, Huang H, Anderson CA, Daly MJ. Large-scale sequencing identifies multiple genes and rare variants associated with Crohn's disease susceptibility. *Nat Genet* 2022; **54**: 1275-1283 [PMID: 36038634 DOI: 10.1038/s41588-022-01156-2]

21 **Zhang YZ**, Li YY. Inflammatory bowel disease: pathogenesis. *World J Gastroenterol* 2014; **20**: 91-99 [PMID: 24415861 DOI: 10.3748/wjg.v20.i1.91]

22 **Yang SK**, Hong M, Zhao W, Jung Y, Baek J, Tayebi N, Kim KM, Ye BD, Kim KJ, Park SH, Lee I, Lee EJ, Kim WH, Cheon JH, Kim YH, Jang BI, Kim HS, Choi JH, Koo JS, Lee JH, Jung SA, Lee YJ, Jang JY, Shin HD, Kang D, Youn HS, Liu J, Song K. Genome-wide association study of Crohn's disease in Koreans revealed three new susceptibility loci and common attributes of genetic susceptibility across ethnic populations. *Gut* 2014; **63**: 80-87 [PMID: 23850713 DOI: 10.1136/gutjnl-2013-305193]

23 **Duerr RH**, Taylor KD, Brant SR, Rioux JD, Silverberg MS, Daly MJ, Steinhart AH, Abraham C, Regueiro M, Griffiths A, Dassopoulos T, Bitton A, Yang H, Targan S, Datta LW, Kistner EO, Schumm LP, Lee AT, Gregersen PK, Barmada MM, Rotter JI, Nicolae DL, Cho JH. A genome-wide association study identifies IL23R as an inflammatory bowel disease gene. *Science* 2006; **314**: 1461-1463 [PMID: 17068223 DOI: 10.1126/science.1135245]

24 **Bouma G**, Strober W. The immunological and genetic basis of inflammatory bowel disease. *Nat Rev Immunol* 2003; **3**: 521-533 [PMID: 12876555 DOI: 10.1038/nri1132]

25 **Jostins L**, Ripke S, Weersma RK, Duerr RH, McGovern DP, Hui KY, Lee JC, Schumm LP, Sharma Y, Anderson CA, Essers J, Mitrovic M, Ning K, Cleynen I, Theatre E, Spain SL, Raychaudhuri S, Goyette P, Wei Z, Abraham C, Achkar JP, Ahmad T, Amininejad L, Ananthakrishnan AN, Andersen V, Andrews JM, Baidoo L, Balschun T, Bampton PA, Bitton A, Boucher G, Brand S, Büning C, Cohain A, Cichon S, D'Amato M, De Jong D, Devaney KL, Dubinsky M, Edwards C, Ellinghaus D, Ferguson LR, Franchimont D, Fransen K, Gearry R, Georges M, Gieger C, Glas J, Haritunians T, Hart A, Hawkey C, Hedl M, Hu X, Karlsen TH, Kupcinskas L, Kugathasan S, Latiano A, Laukens D, Lawrance IC, Lees CW, Louis E, Mahy G, Mansfield J, Morgan AR, Mowat C, Newman W, Palmieri O, Ponsioen CY, Potocnik U, Prescott NJ, Regueiro M, Rotter JI, Russell RK, Sanderson JD, Sans M, Satsangi J, Schreiber S, Simms LA, Sventoraityte J, Targan SR, Taylor KD, Tremelling M, Verspaget HW, De Vos M, Wijmenga C, Wilson DC, Winkelmann J, Xavier RJ, Zeissig S, Zhang B, Zhang CK, Zhao H; International IBD Genetics Consortium (IIBDGC), Silverberg MS, Annese V, Hakonarson H, Brant SR, Radford-Smith G, Mathew CG, Rioux JD, Schadt EE, Daly MJ, Franke A, Parkes M, Vermeire S, Barrett JC, Cho JH. Host-microbe interactions have shaped the genetic architecture of inflammatory bowel disease. *Nature* 2012; **491**: 119-124 [PMID: 23128233 DOI: 10.1038/nature11582]

26 **Huang H**, Fang M, Jostins L, Umićević Mirkov M, Boucher G, Anderson CA, Andersen V, Cleynen I, Cortes A, Crins F, D'Amato M, Deffontaine V, Dmitrieva J, Docampo E, Elansary M, Farh KK, Franke A, Gori AS, Goyette P, Halfvarson J, Haritunians T, Knight J, Lawrance IC, Lees CW, Louis E, Mariman R, Meuwissen T, Mni M, Momozawa Y, Parkes M, Spain SL, Théâtre E, Trynka G, Satsangi J, van Sommeren S, Vermeire S, Xavier RJ; International Inflammatory Bowel Disease Genetics Consortium, Weersma RK, Duerr RH, Mathew CG, Rioux JD, McGovern DPB, Cho JH, Georges M, Daly MJ, Barrett JC. Fine-mapping inflammatory bowel disease loci to single-variant resolution. *Nature* 2017; **547**: 173-178 [PMID: 28658209 DOI: 10.1038/nature22969]

27 **Fuyuno Y**, Yamazaki K, Takahashi A, Esaki M, Kawaguchi T, Takazoe M, Matsumoto T, Matsui T, Tanaka H, Motoya S, Suzuki Y, Kiyohara Y, Kitazono T, Kubo M. Genetic characteristics of inflammatory bowel disease in a Japanese population. *J Gastroenterol* 2016; **51**: 672-681 [PMID: 26511940 DOI: 10.1007/s00535-015-1135-3]

28 **Sato T**, Takagawa T, Kakuta Y, Nishio A, Kawai M, Kamikozuru K, Yokoyama Y, Kita Y, Miyazaki T, Iimuro M, Hida N, Hori K, Ikeuchi H, Nakamura S. NUDT15, FTO, and RUNX1 genetic variants and thiopurine intolerance among Japanese patients with inflammatory bowel diseases. *Intest Res* 2017; **15**: 328-337 [PMID: 28670229 DOI: 10.5217/ir.2017.15.3.328]

29 **Arimura Y**, Isshiki H, Onodera K, Nagaishi K, Yamashita K, Sonoda T, Matsumoto T, Takahashi A, Takazoe M, Yamazaki K, Kubo M, Fujimiya M, Imai K, Shinomura Y. Characteristics of Japanese inflammatory bowel disease susceptibility loci. *J Gastroenterol* 2014; **49**: 1217-1230 [PMID: 23942620 DOI: 10.1007/s00535-013-0866-2]

30 **Kakuta Y**, Naito T, Onodera M, Kuroha M, Kimura T, Shiga H, Endo K, Negoro K, Kinouchi Y, Shimosegawa T. NUDT15 R139C causes thiopurine-induced early severe hair loss and leukopenia in Japanese patients with IBD. *Pharmacogenomics J* 2016; **16**: 280-285 [PMID: 26076924 DOI: 10.1038/tpj.2015.43]

31 **Moon CM**, Shin DJ, Kim SW, Son NH, Park A, Park B, Jung ES, Kim ES, Hong SP, Kim TI, Kim WH, Cheon JH. Associations between genetic variants in the IRGM gene and inflammatory bowel diseases in the Korean population. *Inflamm Bowel Dis* 2013; **19**: 106-114 [PMID: 22508677 DOI: 10.1002/ibd.22972]

32 **Shi D**, Zhong Z, Wang M, Cai L, Fu D, Peng Y, Guo L, Mao H, Yu X, Li M. Identification of susceptibility locus shared by IgA nephropathy and inflammatory bowel disease in a Chinese Han population. *J Hum Genet* 2020; **65**: 241-249 [PMID: 31857673 DOI: 10.1038/s10038-019-0699-9]

33 **Cai J**, Zhang Z. An Analysis of IL-10/IL-10R Genetic Factors Related to Risk of Colon Cancer and Inflammatory Bowel Disease in a Han Chinese Population. *Clin Lab* 2016; **62**: 1147-1154 [PMID: 27468578 DOI: 10.7754/clin.lab.2015.151120]

34 **Zhang X**, Yu P, Wang Y, Jiang W, Shen F, Wang Y, Tu H, Yang X, Shi R, Zhang H. Genetic polymorphisms of interleukin 17A and

interleukin 17F and their association with inflammatory bowel disease in a Chinese Han population. *Inflamm Res* 2013; **62**: 743-750 [PMID: 23652560 DOI: 10.1007/s00011-013-0629-9]

35 **Chu H**, Khosravi A, Kusumawardhani IP, Kwon AH, Vasconcelos AC, Cunha LD, Mayer AE, Shen Y, Wu WL, Kambal A, Targan SR, Xavier RJ, Ernst PB, Green DR, McGovern DP, Virgin HW, Mazmanian SK. Gene-microbiota interactions contribute to the pathogenesis of inflammatory bowel disease. *Science* 2016; **352**: 1116-1120 [PMID: 27230380 DOI: 10.1126/science.aad9948]

36 **Thia KT**, Loftus EV Jr, Sandborn WJ, Yang SK. An update on the epidemiology of inflammatory bowel disease in Asia. *Am J Gastroenterol* 2008; **103**: 3167-3182 [PMID: 19086963 DOI: 10.1111/j.1572-0241.2008.02158.x]

37 **Yang SK**, Yun S, Kim JH, Park JY, Kim HY, Kim YH, Chang DK, Kim JS, Song IS, Park JB, Park ER, Kim KJ, Moon G, Yang SH. Epidemiology of inflammatory bowel disease in the Songpa-Kangdong district, Seoul, Korea, 1986-2005: a KASID study. *Inflamm Bowel Dis* 2008; **14**: 542-549 [PMID: 17941073 DOI: 10.1002/ibd.20310]

38 **Gearry RB**, Richardson AK, Frampton CM, Dodgshun AJ, Barclay ML. Population-based cases control study of inflammatory bowel disease risk factors. *J Gastroenterol Hepatol* 2010; **25**: 325-333 [PMID: 20074146 DOI: 10.1111/j.1440-1746.2009.06140.x]

39 **Ni J**, Wu GD, Albenberg L, Tomov VT. Gut microbiota and IBD: causation or correlation? *Nat Rev Gastroenterol Hepatol* 2017; **14**: 573-584 [PMID: 28743984 DOI: 10.1038/nrgastro.2017.88]

40 **Vich Vila A**, Imhann F, Collij V, Jankipersadsing SA, Gurry T, Mujagic Z, Kurilshikov A, Bonder MJ, Jiang X, Tigchelaar EF, Dekens J, Peters V, Voskuil MD, Visschedijk MC, van Dullemen HM, Keszthelyi D, Swertz MA, Franke L, Alberts R, Festen EAM, Dijkstra G, Masclee AAM, Hofker MH, Xavier RJ, Alm EJ, Fu J, Wijmenga C, Jonkers DMAE, Zhernakova A, Weersma RK. Gut microbiota composition and functional changes in inflammatory bowel disease and irritable bowel syndrome. *Sci Transl Med* 2018; **10**: eaap8914 [PMID: 30567928 DOI: 10.1126/scitranslmed.aap8914]

41 **Zhang Z**, Li J, Zheng W, Zhao G, Zhang H, Wang X, Guo Y, Qin C, Shi Y. Peripheral Lymphoid Volume Expansion and Maintenance Are Controlled by Gut Microbiota *via* RALDH+ Dendritic Cells. *Immunity* 2016; **44**: 330-342 [PMID: 26885858 DOI: 10.1016/j.immuni.2016.01.004]

42 **Khor B**, Gardet A, Xavier RJ. Genetics and pathogenesis of inflammatory bowel disease. *Nature* 2011; **474**: 307-317 [PMID: 21677747 DOI: 10.1038/nature10209]

43 **Imhann F**, Vich Vila A, Bonder MJ, Fu J, Gevers D, Visschedijk MC, Spekhorst LM, Alberts R, Franke L, van Dullemen HM, Ter Steege RWF, Huttenhower C, Dijkstra G, Xavier RJ, Festen EAM, Wijmenga C, Zhernakova A, Weersma RK. Interplay of host genetics and gut microbiota underlying the onset and clinical presentation of inflammatory bowel disease. *Gut* 2018; **67**: 108-119 [PMID: 27802154 DOI: 10.1136/gutjnl-2016-312135]

44 **Ramanan D**, Bowcutt R, Lee SC, Tang MS, Kurtz ZD, Ding Y, Honda K, Gause WC, Blaser MJ, Bonneau RA, Lim YA, Loke P, Cadwell K. Helminth infection promotes colonization resistance *via* type 2 immunity. *Science* 2016; **352**: 608-612 [PMID: 27080105 DOI: 10.1126/science.aaf3229]

45 **Pei R**, DiMarco DM, Putt KK, Martin DA, Gu Q, Chitchumroonchokchai C, White HM, Scarlett CO, Bruno RS, Bolling BW. Low-fat yogurt consumption reduces biomarkers of chronic inflammation and inhibits markers of endotoxin exposure in healthy premenopausal women: a randomised controlled trial. *Br J Nutr* 2017; **118**: 1043-1051 [PMID: 29179781 DOI: 10.1017/S0007114517003038]

46 **Pei R**, DiMarco DM, Putt KK, Martin DA, Chitchumroonchokchai C, Bruno RS, Bolling BW. Premeal Low-Fat Yogurt Consumption Reduces Postprandial Inflammation and Markers of Endotoxin Exposure in Healthy Premenopausal Women in a Randomized Controlled Trial. *J Nutr* 2018; **148**: 910-916 [PMID: 29767743 DOI: 10.1093/jn/nxy046]

47 **Quaglio AEV**, Grillo TG, De Oliveira ECS, Di Stasi LC, Sassaki LY. Gut microbiota, inflammatory bowel disease and colorectal cancer. *World J Gastroenterol* 2022; **28**: 4053-4060 [PMID: 36157114 DOI: 10.3748/wjg.v28.i30.4053]

48 **Danne C**, Skerniskyte J, Marteyn B, Sokol H. Neutrophils: from IBD to the gut microbiota. *Nat Rev Gastroenterol Hepatol* 2024; **21**: 184-197 [PMID: 38110547 DOI: 10.1038/s41575-023-00871-3]

49 **Larabi A**, Barnich N, Nguyen HTT. New insights into the interplay between autophagy, gut microbiota and inflammatory responses in IBD. *Autophagy* 2020; **16**: 38-51 [PMID: 31286804 DOI: 10.1080/15548627.2019.1635384]

50 **Adiliaghdam F**, Amatullah H, Digumarthi S, Saunders TL, Rahman RU, Wong LP, Sadreyev R, Droit L, Paquette J, Goyette P, Rioux JD, Hodin R, Mihindukulasuriya KA, Handley SA, Jeffrey KL. Human enteric viruses autonomously shape inflammatory bowel disease phenotype through divergent innate immunomodulation. *Sci Immunol* 2022; **7**: eabn6660 [PMID: 35394816 DOI: 10.1126/sciimmunol.abn6660]

51 **Xun Z**, Zhang Q, Xu T, Chen N, Chen F. Dysbiosis and Ecotypes of the Salivary Microbiome Associated With Inflammatory Bowel Diseases and the Assistance in Diagnosis of Diseases Using Oral Bacterial Profiles. *Front Microbiol* 2018; **9**: 1136 [PMID: 29899737 DOI: 10.3389/fmicb.2018.01136]

52 **Strauss J**, Kaplan GG, Beck PL, Rioux K, Panaccione R, Devinney R, Lynch T, Allen-Vercoe E. Invasive potential of gut mucosa-derived Fusobacterium nucleatum positively correlates with IBD status of the host. *Inflamm Bowel Dis* 2011; **17**: 1971-1978 [PMID: 21830275 DOI: 10.1002/ibd.21606]

53 **Man SM**, Zhang L, Day AS, Leach ST, Lemberg DA, Mitchell H. Campylobacter concisus and other Campylobacter species in children with newly diagnosed Crohn's disease. *Inflamm Bowel Dis* 2010; **16**: 1008-1016 [PMID: 19885905 DOI: 10.1002/ibd.21157]

54 **Gevers D**, Kugathasan S, Denson LA, Vázquez-Baeza Y, Van Treuren W, Ren B, Schwager E, Knights D, Song SJ, Yassour M, Morgan XC, Kostic AD, Luo C, González A, McDonald D, Haberman Y, Walters T, Baker S, Rosh J, Stephens M, Heyman M, Markowitz J, Baldassano R, Griffiths A, Sylvester F, Mack D, Kim S, Crandall W, Hyams J, Huttenhower C, Knight R, Xavier RJ. The treatment-naive microbiome in new-onset Crohn's disease. *Cell Host Microbe* 2014; **15**: 382-392 [PMID: 24629344 DOI: 10.1016/j.chom.2014.02.005]

55 **Hyde ER**, Andrade F, Vaksman Z, Parthasarathy K, Jiang H, Parthasarathy DK, Torregrossa AC, Tribble G, Kaplan HB, Petrosino JF, Bryan NS. Metagenomic analysis of nitrate-reducing bacteria in the oral cavity: implications for nitric oxide homeostasis. *PLoS One* 2014; **9**: e88645 [PMID: 24670812 DOI: 10.1371/journal.pone.0088645]

56 **Dinakaran V**, Mandape SN, Shuba K, Pratap S, Sakhare SS, Tabatabai MA, Smoot DT, Farmer-Dixon CM, Kesavalu LN, Adunyah SE, Southerland JH, Gangula PR. Identification of Specific Oral and Gut Pathogens in Full Thickness Colon of Colitis Patients: Implications for Colon Motility. *Front Microbiol* 2018; **9**: 3220 [PMID: 30666239 DOI: 10.3389/fmicb.2018.03220]

57 **Winter SE**, Winter MG, Xavier MN, Thiennimitr P, Poon V, Keestra AM, Laughlin RC, Gomez G, Wu J, Lawhon SD, Popova IE, Parikh SJ, Adams LG, Tsolis RM, Stewart VJ, Bäumler AJ. Host-derived nitrate boosts growth of E. coli in the inflamed gut. *Science* 2013; **339**: 708-711 [PMID: 23393266 DOI: 10.1126/science.1232467]

58 **Avdagić N**, Zaćiragić A, Babić N, Hukić M, Seremet M, Lepara O, Nakaš-Ićindić E. Nitric oxide as a potential biomarker in inflammatory bowel disease. *Bosn J Basic Med Sci* 2013; **13**: 5-9 [PMID: 23448603 DOI: 10.17305/bjbms.2013.2402]

59 **Topcu Ali O**, Akalin FA, Sahbazoglu KB, Yamalik N, Kilinc K, Karabulut E, Tözüm TF. Nitrite and nitrate levels of gingival crevicular fluid and saliva in subjects with gingivitis and chronic periodontitis. *J Oral Maxillofac Res* 2014; **5**: e5 [PMID: 25089177 DOI: 10.5037/jomr.2014.5205]

60 **Kelsen J**, Bittinger K, Pauly-Hubbard H, Posivak L, Grunberg S, Baldassano R, Lewis JD, Wu GD, Bushman FD. Alterations of the Subgingival Microbiota in Pediatric Crohn's Disease Studied Longitudinally in Discovery and Validation Cohorts. *Inflamm Bowel Dis* 2015; **21**: 2797-2805 [PMID: 26288001 DOI: 10.1097/MIB.0000000000000557]

61 **Nassar M**, Tabib Y, Capucha T, Mizraji G, Nir T, Pevsner-Fischer M, Zilberman-Schapira G, Heyman O, Nussbaum G, Bercovier H, Wilensky A, Elinav E, Burstyn-Cohen T, Hovav AH. GAS6 is a key homeostatic immunological regulator of host-commensal interactions in the oral mucosa. *Proc Natl Acad Sci U S A* 2017; **114**: E337-E346 [PMID: 28049839 DOI: 10.1073/pnas.1614926114]

62 **Schirmer M**, Denson L, Vlamakis H, Franzosa EA, Thomas S, Gotman NM, Rufo P, Baker SS, Sauer C, Markowitz J, Pfefferkorn M, Oliva-Hemker M, Rosh J, Otley A, Boyle B, Mack D, Baldassano R, Keljo D, LeLeiko N, Heyman M, Griffiths A, Patel AS, Noe J, Kugathasan S, Walters T, Huttenhower C, Hyams J, Xavier RJ. Compositional and Temporal Changes in the Gut Microbiome of Pediatric Ulcerative Colitis Patients Are Linked to Disease Course. *Cell Host Microbe* 2018; **24**: 600-610.e4 [PMID: 30308161 DOI: 10.1016/j.chom.2018.09.009]

63 **Read E**, Curtis MA, Neves JF. The role of oral bacteria in inflammatory bowel disease. *Nat Rev Gastroenterol Hepatol* 2021; **18**: 731-742 [PMID: 34400822 DOI: 10.1038/s41575-021-00488-4]

64 **Vonaesch P**, Morien E, Andrianonimiadana L, Sanke H, Mbecko JR, Huus KE, Naharimanananirina T, Gondje BP, Nigatoloum SN, Vondo SS, Kaleb Kandou JE, Randremanana R, Rakotondrainipiana M, Mazel F, Djorie SG, Gody JC, Finlay BB, Rubbo PA, Wegener Parfrey L, Collard JM, Sansonetti PJ; Afribiota Investigators. Stunted childhood growth is associated with decompartmentalization of the gastrointestinal tract and overgrowth of oropharyngeal taxa. *Proc Natl Acad Sci U S A* 2018; **115**: E8489-E8498 [PMID: 30126990 DOI: 10.1073/pnas.1806573115]

65 **Sokol H**, Leducq V, Aschard H, Pham HP, Jegou S, Landman C, Cohen D, Liguori G, Bourrier A, Nion-Larmurier I, Cosnes J, Seksik P, Langella P, Skurnik D, Richard ML, Beaugerie L. Fungal microbiota dysbiosis in IBD. *Gut* 2017; **66**: 1039-1048 [PMID: 26843508 DOI: 10.1136/gutjnl-2015-310746]

66 **Peters BA**, Wu J, Hayes RB, Ahn J. The oral fungal mycobiome: characteristics and relation to periodontitis in a pilot study. *BMC Microbiol* 2017; **17**: 157 [PMID: 28701186 DOI: 10.1186/s12866-017-1064-9]

67 **Cardile S**, Romano C. Current issues in pediatric inflammatory bowel disease-associated arthropathies. *World J Gastroenterol* 2014; **20**: 45-52 [PMID: 24415857 DOI: 10.3748/wjg.v20.i1.45]

68 **Jang HJ**, Kang B, Choe BH. The difference in extraintestinal manifestations of inflammatory bowel disease for children and adults. *Transl Pediatr* 2019; **8**: 4-15 [PMID: 30881893 DOI: 10.21037/tp.2019.01.06]

69 **Harbord M**, Annese V, Vavricka SR, Allez M, Barreiro-de Acosta M, Boberg KM, Burisch J, De Vos M, De Vries AM, Dick AD, Juillerat P, Karlsen TH, Koutroubakis I, Lakatos PL, Orchard T, Papay P, Raine T, Reinshagen M, Thaci D, Tilg H, Carbonnel F; European Crohn's and Colitis Organisation. The First European Evidence-based Consensus on Extra-intestinal Manifestations in Inflammatory Bowel Disease. *J Crohns Colitis* 2016; **10**: 239-254 [PMID: 26614685 DOI: 10.1093/ecco-jcc/jjv213]

70 **Garber A**, Regueiro M. Extraintestinal Manifestations of Inflammatory Bowel Disease: Epidemiology, Etiopathogenesis, and Management. *Curr Gastroenterol Rep* 2019; **21**: 31 [PMID: 31098819 DOI: 10.1007/s11894-019-0698-1]

71 **Greuter T**, Vavricka SR. Extraintestinal manifestations in inflammatory bowel disease - epidemiology, genetics, and pathogenesis. *Expert Rev Gastroenterol Hepatol* 2019; **13**: 307-317 [PMID: 30791773 DOI: 10.1080/17474124.2019.1574569]

72 **Halling ML**, Kjeldsen J, Knudsen T, Nielsen J, Hansen LK. Patients with inflammatory bowel disease have increased risk of autoimmune and inflammatory diseases. *World J Gastroenterol* 2017; **23**: 6137-6146 [PMID: 28970729 DOI: 10.3748/wjg.v23.i33.6137]

73 **Bisgaard TH**, Allin KH, Keefer L, Ananthakrishnan AN, Jess T. Depression and anxiety in inflammatory bowel disease: epidemiology, mechanisms and treatment. *Nat Rev Gastroenterol Hepatol* 2022; **19**: 717-726 [PMID: 35732730 DOI: 10.1038/s41575-022-00634-6]

74 **Parikh K**, Antanaviciute A, Fawkner-Corbett D, Jagielowicz M, Aulicino A, Lagerholm C, Davis S, Kinchen J, Chen HH, Alham NK, Ashley N, Johnson E, Hublitz P, Bao L, Lukomska J, Andev RS, Björklund E, Kessler BM, Fischer R, Goldin R, Koohy H, Simmons A. Colonic epithelial cell diversity in health and inflammatory bowel disease. *Nature* 2019; **567**: 49-55 [PMID: 30814735 DOI: 10.1038/s41586-019-0992-y]

75 **Rezaie A**, Ghorbani F, Eshghtork A, Zamani MJ, Dehghan G, Taghavi B, Nikfar S, Mohammadirad A, Daryani NE, Abdollahi M. Alterations in salivary antioxidants, nitric oxide, and transforming growth factor-beta 1 in relation to disease activity in Crohn's disease patients. *Ann N Y Acad Sci* 2006; **1091**: 110-122 [PMID: 17341608 DOI: 10.1196/annals.1378.060]

76 **Rezaie A**, Khalaj S, Shabihkhani M, Nikfar S, Zamani MJ, Mohammadirad A, Daryani NE, Abdollahi M. Study on the correlations among disease activity index and salivary transforming growth factor-beta 1 and nitric oxide in ulcerative colitis patients. *Ann N Y Acad Sci* 2007; **1095**: 305-314 [PMID: 17404043 DOI: 10.1196/annals.1397.034]

77 **Hodson R**. Inflammatory bowel disease. *Nature* 2016; **540**: S97 [PMID: 28002398 DOI: 10.1038/540S97a]

78 **Dutta AK**, Chacko A. Influence of environmental factors on the onset and course of inflammatory bowel disease. *World J Gastroenterol* 2016; **22**: 1088-1100 [PMID: 26811649 DOI: 10.3748/wjg.v22.i3.1088]

79 **Kaplan GG**, Ng SC. Understanding and Preventing the Global Increase of Inflammatory Bowel Disease. *Gastroenterology* 2017; **152**: 313-321.e2 [PMID: 27793607 DOI: 10.1053/j.gastro.2016.10.020]

80 **Christensen C**, Knudsen A, Arnesen EK, Hatlebakk JG, Sletten IS, Fadnes LT. Diet, Food, and Nutritional Exposures and Inflammatory Bowel Disease or Progression of Disease: an Umbrella Review. *Adv Nutr* 2024; **15**: 100219 [PMID: 38599319 DOI: 10.1016/j.advnut.2024.100219]

81 **Sakamoto N**, Kono S, Wakai K, Fukuda Y, Satomi M, Shimoyama T, Inaba Y, Miyake Y, Sasaki S, Okamoto K, Kobashi G, Washio M, Yokoyama T, Date C, Tanaka H; Epidemiology Group of the Research Committee on Inflammatory Bowel Disease in Japan. Dietary risk factors for inflammatory bowel disease: a multicenter case-control study in Japan. *Inflamm Bowel Dis* 2005; **11**: 154-163 [PMID: 15677909 DOI: 10.1097/00054725-200502000-00009]

82 **Liu Z**, Lee J, Krummey S, Lu W, Cai H, Lenardo MJ. The kinase LRRK2 is a regulator of the transcription factor NFAT that modulates the severity of inflammatory bowel disease. *Nat Immunol* 2011; **12**: 1063-1070 [PMID: 21983832 DOI: 10.1038/ni.2113]

83 **Liu Z**, Lenardo MJ. The role of LRRK2 in inflammatory bowel disease. *Cell Res* 2012; **22**: 1092-1094 [PMID: 22430149 DOI: 10.1038/cr.2012.42]

84 **Zhang Q**, Pan Y, Yan R, Zeng B, Wang H, Zhang X, Li W, Wei H, Liu Z. Commensal bacteria direct selective cargo sorting to promote symbiosis. *Nat Immunol* 2015; **16**: 918-926 [PMID: 26237551 DOI: 10.1038/ni.3233]

85 **Szczeklik K**, Owczarek D, Pytko-Polończyk J, Kęsek B, Mach TH. Proinflammatory cytokines in the saliva of patients with active and non-active Crohn's disease. *Pol Arch Med Wewn* 2012; **122**: 200-208 [PMID: 22538761 DOI: 10.20452/pamw.1256]

86 **Heinken A**, Khan MT, Paglia G, Rodionov DA, Harmsen HJ, Thiele I. Functional metabolic map of Faecalibacterium prausnitzii, a beneficial human gut microbe. *J Bacteriol* 2014; **196**: 3289-3302 [PMID: 25002542 DOI: 10.1128/JB.01780-14]

87 **Lopez-Siles M**, Duncan SH, Garcia-Gil LJ, Martinez-Medina M. Faecalibacterium prausnitzii: from microbiology to diagnostics and prognostics. *ISME J* 2017; **11**: 841-852 [PMID: 28045459 DOI: 10.1038/ismej.2016.176]

World Journal of Gastroenterology

Submit a Manuscript: https://www.f6publishing.com

World J Gastroenterol 2025 May 21; 31(19): 101913

DOI: 10.3748/wjg.v31.i19.101913

ISSN 1007-9327 (print) ISSN 2219-2840 (online)

ORIGINAL ARTICLE

Retrospective Study

Direct comparison of simultaneous and sequential endoscopic metallic bilateral stenting in malignant hilar biliary obstruction

Thomas Guilmoteau, Olivier Rouquette, Anthony Buisson, Sébastien Cambier, Armand Abergel, Laurent Poincloux

Specialty type: Gastroenterology and hepatology

Provenance and peer review: Unsolicited article; Externally peer reviewed.

Peer-review model: Single blind

Peer-review report's classification

Scientific Quality: Grade A, Grade B, Grade B

Novelty: Grade A, Grade A, Grade B

Creativity or Innovation: Grade A, Grade B, Grade B

Scientific Significance: Grade B, Grade B, Grade B

P-Reviewer: Guan F; Liu LJ; Xu HJ

Received: September 30, 2024

Revised: March 18, 2025

Accepted: April 17, 2025

Published online: May 21, 2025

Processing time: 232 Days and 11.1 Hours

Thomas Guilmoteau, Olivier Rouquette, Laurent Poincloux, Digestive Endoscopy Unit, Estaing University Hospital, Clermont-Ferrand 63000, Auvergne-Rhône-Alpes, France

Anthony Buisson, Department of Gastroenterology, Estaing University Hospital, Clermont-Ferrand 63000, Auvergne-Rhône-Alpes, France

Sébastien Cambier, Biostatistics Unit, Department of Clinical Research and Innovation, Clermont-Ferrand University Hospital, Clermont-Ferrand 63000, Auvergne-Rhône-Alpes, France

Armand Abergel, Department of Hepatology and Gastroenterology, Estaing University Hospital, Clermont-Ferrand 63000, Auvergne-Rhône-Alpes, France

Corresponding author: Thomas Guilmoteau, MD, Digestive Endoscopy Unit, Estaing University Hospital, 1 Place Lucie Et Raymond Aubrac, Clermont-Ferrand 63000, Auvergne-Rhône-Alpes, France. tguilmoteau@chu-clermontferrand.fr

Abstract

BACKGROUND

Endoscopic bilateral biliary drainage is a first line palliative treatment for unresectable malignant hilar biliary obstruction (MHBO) but remains technically challenging. The emergence of self-expandable metallic stents carried by an ultra-thin (6 Fr or smaller) delivery system now permits simultaneous bilateral stent placement. To date, only a few studies have compared this new method with conventional sequential bilateral stenting.

AIM

To evaluate a possible superiority of simultaneous "side by side" (SBS) biliary drainage in unresectable MHBO.

METHODS

We identified 135 patients who benefited from bilateral drainage using uncovered self-expandable metallic stents between 2010 and 2023. Among them, 62 benefited from simultaneous SBS bilateral drainage between 2017 and 2023, and 73 benefited from sequential bilateral drainage [38 using "stent in stent" (SIS) technique and 35 using SBS technique between 2010 and 2017].

RESULTS
Technical success was significantly increased in simultaneous drainage compared with sequential drainage (94% *vs* 75%, $P = 0.008$). However, simultaneous SBS drainage and sequential SIS drainage had a similar technical success (94% *vs* 95%). We observed no differences regarding clinical success, procedure duration and recurrent biliary obstruction rate. Stent patency was shorter in the SIS group compared with the simultaneous group (103 days *vs* 144 days). Early adverse events were more frequent in the sequential group (31% *vs* 21%, $P = 0.205$), with no differences regarding SIS or SBS technique. Technical failure was associated with a higher rate of infectious fatal adverse events (9.5% *vs* 1.7%, $P = 0.02$). Reintervention after recurrent biliary obstruction seems to be more successful after using SBS rather than SIS techniques (83% *vs* 75%, $P = 0.53$).

CONCLUSION
Simultaneous SBS metallic stent placement using an ultra-thin delivery system was technically easier and as efficient as sequential bilateral stenting in unresectable MHBO to achieve bilateral drainage. The SIS procedure remains a good option in unresectable MHBO.

Key Words: Malignant hilar biliary obstruction; Endoscopic retrograde cholangiopancreatography; Self expandable metallic stent; Simultaneous drainage; Side by side; Stent in stent

Core Tip: This retrospective study focused on the different drainage techniques using endoscopic retrograde cholangiopancreatography for malignant hilar biliary obstruction. It highlighted the benefits of parallel drainage, particularly when performed simultaneously using ultra-thin delivery devices. This resulted in a clear advantage in terms of technical success and reduced the risk of complications associated with technical failure, which was more frequently observed in the case of sequential drainage, especially in a "side by side" fashion.

Citation: Guilmoteau T, Rouquette O, Buisson A, Cambier S, Abergel A, Poincloux L. Direct comparison of simultaneous and sequential endoscopic metallic bilateral stenting in malignant hilar biliary obstruction. *World J Gastroenterol* 2025; 31(19): 101913
URL: https://www.wjgnet.com/1007-9327/full/v31/i19/101913.htm
DOI: https://dx.doi.org/10.3748/wjg.v31.i19.101913

INTRODUCTION

Management of malignant hilar biliary obstruction (MHBO) remains a challenging situation. Most obstructions are unresectable due to the patient's general condition or local/metastatic tumor extent[1]. The latest guidelines recommend endoscopic biliary drainage as a first-line option, using preferentially uncovered metallic stents over plastic stents[2-6]. Bilateral drainage must be preferred to unilateral drainage in high-grade malignant hilar stricture because it provides a longer stent patency, with a lower reintervention rate for recurrent biliary obstruction (RBO) and similar clinical outcomes and adverse events (AEs)[7-10]. Drainage of at least 50% of total functional liver volume must be obtained[11].

Bilateral drainage can be performed using either "side by side" (SBS) or "stent in stent" (SIS) techniques, with no difference regarding technical and clinical success, stent patency, and survival[12,13]. Nevertheless, bilateral biliary drainage using metallic stents is still a technical challenge and includes many failed procedures even for a trained operator. Emergence of a new ultra-thin (6 Fr or smaller) delivery system enables simultaneous SBS metallic stent deployment. To date, there are few reports regarding the simultaneous bilateral biliary stenting with this new device. Only a small case series from Inoue *et al*[14] reported a higher technical success and a shorter procedure time for simultaneous drainage compared with sequential SBS procedure[14-16]. In this study, we aimed to compare simultaneous SBS *vs* sequential (SBS or SIS) bilateral biliary drainage in a large monocentric retrospective series.

MATERIALS AND METHODS

We investigated all patients who underwent bilateral biliary metallic stenting during endoscopic retrograde cholangiopancreatography (ERCP) for MHBO in Clermont-Ferrand University Hospital between January 1, 2010 and January 1, 2023. Conventional sequential SBS placement was performed at our institution between 2010 and 2017. Since 2017, simultaneous SBS placement has been performed on patients with unresectable MHBOs requiring bilateral drainage. The patient cohort was divided into those who underwent sequential SBS or SIS placement between 2010 and 2017 (sequential group) and those who underwent simultaneous SBS placement between 2017 and 2023 (simultaneous group). The two groups were compared retrospectively. Exclusion criteria included patients with no jaundice, resectable obstructions, minors, pregnancy, or patients concerned with limited judicial protection.

MHBO is confirmed after histological or cytological analysis [endoscopic ultrasound (EUS)-fine needle aspiration or fine needle biopsy, ERCP bile duct brushing, single-operator cholangioscopy system biopsy (SpyGlass®, Boston Scientific Corporation, United States) or percutaneous biopsy] when possible. Due to the mild diagnosis rentability of cytological brushing and the difficulties to obtain direct endoscopic biopsies in cholangiocarcinoma, histological/cytological proof was not systematically achieved. Thus, diagnosis was sometimes confirmed by a multidisciplinary team regarding medical history and biological and imaging findings. Unresectable status was assessed according to general medical condition and locoregional or metastatic extent after a medicosurgical multidisciplinary approach. The study was approved by our local Ethics Committee (IRB00013412, "CHU de Clermont Ferrand IRB #1", IRB number 2023-CF003) with compliance to the French policy of individual data protection and was performed in accordance with the principles of the Declaration of Helsinki.

Data collection

We retrospectively collected clinical data from patient charts including: Demographic information; type of procedure; type of stent and delivery-system catheter used; date of procedure; tumor type and biliary extent according to Bismuth and Corlette classification; procedure duration (in minutes); postoperative chemotherapy status; total bilirubin rate (μmol/L) at day 0 and day 7; early AE related to the procedure (day 0-day 7); late stent-related complications (RBO, *i.e.* stent patency and/or dysfunction); type and success of reintervention after RBO; and time until death or last follow-up.

Procedures

All patients underwent sectional cross imaging (CT or magnetic resonance imagery) to evaluate hepatic volumetry and biliary extension of the MHBO and to assess surgical resectability. All procedures were performed by two ERCP-trained operators (> 2000 biliary stenting each) in an interventional endoscopy room equipped with fluoroscopy ad patients in dorsal decubitus position under general anesthesia after orotracheal intubation. Antibiotic prophylaxis was administered at the discretion of the anesthesiologist following the Société Française d'Anesthésie et de Réanimation recommendations [17]. Rectal nonsteroidal anti-inflammatory drugs (100 mg diclofenac or indomethacin) were administered based on the operator's discretion. All procedures were performed using carbon dioxide insufflation with a 4.2 mm working channel duodenoscope (TJF-160® and TJF-190®, Olympus Medical Systems Corp., Tokyo, Japan). All patients underwent complete biliary sphincterotomy when deep biliary catheterization (either transpapillary or using the "double guidewire technique") was achieved or large fistulotomy if transpapillary catheterization was unsuccessful. In some cases, sphincterotomies had been previously performed.

Sequential SBS technique

Once deep biliary catheterization was achieved, multiple guidewires (0.035 inch straight or angle tip hydrophilic guidewire, JagWire® or DreamWire®, Boston Scientific Co., United States) were inserted whenever possible in both left and right hepatic ducts. Contrast agent was injected selectively only after a guidewire was passed through the hilar stricture. Following the insertion of the guidewires into the main left and right intrahepatic bile ducts, both strictures were dilated using 6-mm or 8-mm diameter dilation balloons (Hurricane®, Boston Scientific Co., United States) followed by bilateral self-expandable metallic stent (SEMS) placement (sequential SBS or SIS technique and simultaneous technique). After dilation of both strictures, the first SEMS (10 mm diameter, 8 cm, 10 cm, or 12 cm length, 8 Fr delivery shaft catheter, uncovered Wallflex Biliary RX Stent®, Boston Scientific Co., United States) was placed, usually in the left biliary duct because of a more challenging stent placement due to the sharp angulation between the left and main bile ducts compared with right bile duct. The second SEMS was inserted and placed alongside the first SEMS over the other guidewire and then deployed parallel to the first SEMS.

Sequential SIS technique

We used a Y-shaped stent with a wide wire mesh design (either M-Hilar Bonastent®, Mi-Tech, South Korea, or Y-Type Niti-S Stent®, Taewoong Medical, South Korea) to perform the SIS technique (or "through the mesh"). These stents have a thin delivery catheter of 7 Fr allowing to cross the wide wire mesh and an 8 mm diameter once they are deployed. For this technique, a bilateral guidewire catheterization is not mandatory. After deployment of the first stent across the hilar stricture, the guidewire left across the primary stent was carefully withdrawn, without pulling it back completely, and was then inserted into the undrained contralateral hepatic duct through the central wide mesh of the primary stent. Another uncovered SEMS was then introduced over the guidewire and deployed in the contralateral hepatic duct (Figure 1).

Simultaneous SBS technique

For this technique, we used SEMS with an ultra-thin delivery system that allowed simultaneous SBS bilateral hilar stenting achievement with a 4.2 mm working channel duodenoscope. First, a laser-cut SEMS aixstent® (Leufen Medical GmbH, Berlin, Germany) was carried by a 5 Fr delivery system from 2017 to 2020, and then the Niti-S M-Type® (TaeWoong Medical, Seoul, Korea) was carried by a 6 Fr delivery system from 2020 to 2023. Due to the ultra-thin delivery system, we had to use a 0.025-inch guidewire (either straight VisiGlide®, Olympus, Japan, or angle tip JagWire® Revolution, Boston Scientific Co., United States) when selective insertion of the guidewire into the intrahepatic duct was difficult to achieve bilateral main left and right bile duct catheterization. Biliary strictures were dilated using a 4-mm, 6-mm, or 8-mm balloon dilation (Hurricane® RX, Boston Scientific Co., United States), followed by simultaneous insertion of two SEMS delivery system devices and pushed over each guidewire. Then, the two SEMS were simultaneously deployed across the hilar stenosis in an SBS configuration. This procedure required the assistance of two endoscopy

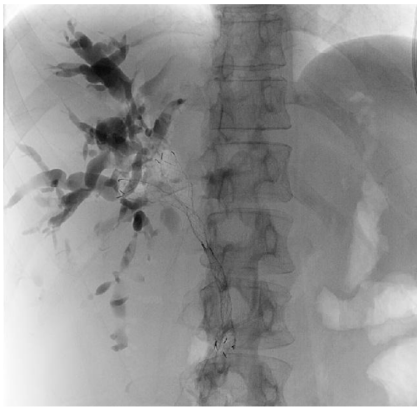

Figure 1 Sequential stent in stent bilateral drainage on X-ray view.

nurses. All SEMS had an 8 mm diameter, with a varying length from 10-12 cm according to the length of the stricture and the need for all SEMS to be positioned above the duodenal papilla. Furthermore, alignment of the distal stent ends was attempted. Nevertheless, if needed, a third distal stent could be inserted in the distal tip of one of the initial SEMS to achieve duodenal lumen expansion (Figure 2, Video 1).

Outcomes and definitions

The primary outcome for this study was to determine the technical success rate for each procedure (sequential or simultaneous bilateral stenting). Secondary outcomes included clinical success, procedure duration (in minutes), early AE rate and stent-related AE rate, RBO rate, and time to RBO (or stent patency, in days). Technical success was defined by the accurate positioning of two metallic stents across the left and right hilar strictures (SBS in simultaneous group, SBS or SIS in sequential group). Clinical success was defined by a decrease of at least 50% of total bilirubin (in μmol/L) at day 7 compared with day 0. AEs were classified as early AE when they occurred in the intraprocedural time or within 1 week after procedure and were graded according to the new AE Gastrointestinal Endoscopy (AGREE) classification[18]. Stent dysfunction was defined as RBO.

Statistical analysis

Study data were collected and managed using REDCap electronic data capture tools hosted at the University Hospital of Clermont-Ferrand, France. Statistical analysis was performed using STATA 15 (Stata Corp LLC, TX, United States). Categorical variables were expressed as *n* (%). Continuous variables were expressed as mean or median and interquartile range. Group differences were evaluated using Fisher's or χ^2 tests for categorical variables. For continuous variables, group differences were evaluated using Wilcoxon's, Mann-Whitney's, or Kruskal-Wallis tests. Survival time was determined using the Kaplan-Meier method. Univariate and multivariate analyses were evaluated using the logistic regression model. Significance was defined as $P < 0.05$.

RESULTS

Patient characteristics

We identified 146 patients who benefited from bilateral drainage for MHBO between 2010 and 2023. Among them, 135 patients were included: 62 were treated with simultaneous bilateral drainage (between 2017 and 2023); and 73 were treated with sequential bilateral drainage (38 had SBS bilateral stent placement and 35 had SIS bilateral stent placement between 2010 and 2017). The flowchart of the study is presented in Figure 3. Patient characteristics were retrospectively collected and included age, sex, tumor type, Bismuth and Corlette classification of biliary extent, bilirubin rate at day 0, postoperative chemotherapy treatment status, and survival time. Results are presented in Table 1 and we observed no significant differences between the two groups.

Technical success

Technical success was achieved in 94% of patients in the simultaneous group and in 77% of patients in the sequential group ($P = 0.008$). In the sequential group, technical success was more often achieved for the SIS technique (95%) than with the SBS technique (57%) ($P = 0.001$). A total of 58 patients underwent technical success in the simultaneous group: 21 using aixstent BDH® device (Leufen Medical GmbH, Berlin, Germany) and 37 using Niti-S M-Type® device (TaeWoong Medical, Seoul, Korea). We did not observe any significant difference in technical success between patients who had aixstent BDH or Niti-S stent implantation. Technical failure tended to be associated with a higher risk of death (hazard ratio: 1.35, $P = 0.22$). Baseline bilirubin rate did not appear to impact technical success. In the univariate and multivariate analysis, technical success was less frequent for Bismuth and Corlette IV type and metastatic hilar obstruction (Table 2). Patient outcomes are presented in Table 3.

Table 1 Patient characteristics at baseline

Characteristics	Sequential group, overall	Sequential group, side by side	Sequential group, stent in stent	Simultaneous group	*P* value
Number of patients	73	35	38	62	
Male	41 (56)	21 (51)	20 (49)	35 (56)	0.82
Age, years, median	71	71	71	68	0.59
Tumor type					0.32
Cholangiocarcinoma	34 (47)	19 (54)	15 (39)	38 (61)	
Hilar metastasis	34 (47)	14 (40)	20 (53)	21 (34)	
Hepatocarcinoma	5 (6)	2 (6)	3 (8)	3 (5)	
Bismuth and Corlette classification					0.053
II	1 (1)	0 (0)	1 (2)	8 (12)	
IIIa	17 (23)	11 (31)	6 (16)	9 (15)	
IIIb	5 (7)	2 (6)	3 (8)	9 (15)	
IV	50 (69)	22 (63)	28 (74)	36 (58)	
Bilirubin rate, day 0, µmol/L, median (IQR)	224 (158-340)	238 (162-342)	220 (150-338)	225 (132-334)	0.80
Postoperative chemotherapy	25 (36)	14 (42)	11 (30)	31 (53)	0.095
Survival time, days, median (IQR)	61 (39-78)	69 (43-128)	43 (27-65)	67 (56-105)	0.24

Data are presented as *n* (%). IQR: Interquartile range.

Table 2 Univariate and multivariate analyses for technical success

Variables	Univariate analysis, OR	Univariate analysis, 95%CI	Univariate analysis, *P* value	Multivariate analysis, OR	Multivariate analysis, 95%CI	Multivariate analysis, *P* value
Baseline bilirubin rate	0.98	0.63-1.52	0.931	0.90	0.51-1.57	0.703
Bismuth and Corlette type IV	0.50	0.17-1.45	0.202	0.23	0.42-1.22	0.085
Hilar metastasis	0.45	0.17-1.19	0.106	0.27	0.06-1.10	0.068

OR: Odds ratio; CI: Confidence interval.

Clinical success

Clinical success was observed in 75% of patients in the simultaneous group and in 72% of patients in the sequential group. In the sequential group, there was no significant difference concerning clinical success between the SBS and SIS techniques (76% and 69%, respectively, $P = 0.823$).

Procedure duration

Median procedure duration was 80 min in the sequential group and 72 min in the simultaneous group ($P = 0.92$), with no difference between sequential SBS and SIS techniques (75 and 80 minutes, respectively, $P = 0.75$).

Early AEs related to the procedure

Overall, an early AE was observed in 31% of patients in the sequential group and 21% in the simultaneous group, with no significant difference ($P = 0.205$). Complication rates were similar between the SBS and SIS techniques in sequential group (34% and 29%, respectively, $P = 0.39$). Early AEs included 13 pancreatitis (no patient required intensive care unit admission or endoscopic/surgical intervention), 16 cholangitis (2 patients admitted in intensive care unit, 4 died), 6 hemorrhagic complications (due to sphincterotomy or iatrogenic duodenal ulcer, all medically managed), and 1 duodenal perforation occurred (in SBS sequential group, surgically managed). Cholangitis had a trend to be more frequently observed in the sequential group (16% *vs* 6%, $P = 0.07$), with no differences between the SBS or SIS techniques (17% and 16% respectively, $P = 0.19$). Early AE rates are represented in Figure 4A.

Table 3 Patient outcomes

Patient outcomes	Sequential group, overall	Sequential group, side by side	Sequential group, stent in stent	Simultaneous group	*P* value
Technical success	56 (77)			58 (94)	0.008
	56 (77)	20 (57)	36 (95)	58 (94)	0.001
Clinical success (*n* = 101)	33 (72)	13 (76)	20 (69)	41 (75)	0.82
Procedure duration, minutes, median (IQR)	80 (60-90)	75 (35-93)	80 (60-90)	72 (58-99)	0.75
Early adverse event					
Overall	23 (31)	12 (34)	11 (29)	12 (21)	0.39
Pancreatitis	8 (11)	4 (11)	4 (11)	5 (8)	0.81
Cholangitis	12 (16)	6 (17)	6 (16)	4 (6)	0.19
Hemorrhage	2 (3)	1 (3)	1 (3)	4 (6)	0.66
Duodenal perforation	1 (1)	1 (3)	0 (0)	0 (0)	0.26
Recurrent biliary obstruction	9 (18)	1 (5)	8 (20)	13 (22)	0.049
Time to RBO, days, mean	112	182[1]	103	144	
Reintervention after RBO	9 (100)	1 (100)	8 (100)	11 (85)	0.49
Successful reintervention	7 (78)	1 (100)	6 (75)	9 (82)	1

[1]*n* = 1. Data are presented as *n* (%). RBO: Recurrent biliary obstruction; IQR: Interquartile range.

Most of the AEs were graded AGREE II (64% of overall AEs). We observed three fatal complications (AGREE V) in the sequential group and 1 fatal complication in the simultaneous group; both were infectious complications due to cholangitis. Technical and clinical failures were associated with a higher rate of AGREE V complications (9.5% and 7.4% respectively, $P = 0.02$). Patients with technical success had a lower risk of infectious complications [odds ratio (OR) = 0.25, 0.08-0.78, $P = 0.016$], and technical failure was associated with an increased risk of fatal sepsis (AGREE V, OR = 5.89, 0.78-44.4, $P = 0.085$). We did not report any procedure-related death except for patients who suffered cholangitis with multivisceral failure due to septic shock (4 patients, 3% of overall patients). Distribution of AE severity is detailed in Figure 4B.

RBO

Among patients with technical success, RBO was observed in 13 patients in the simultaneous group and 9 patients in the sequential group (22% and 18%, respectively). In the sequential group, RBO occurred in 1 patient (5%) in the SBS group and in 8 patients (20%) in the SIS group ($P = 0.049$). Mean time to RBO was 144 and 112 days in the simultaneous and sequential groups, respectively. Only 1 patient experienced RBO in the sequential SBS group after 182 days. Mean time to RBO in the sequential SIS group was 103 days. Using the Kaplan-Meier method among the patients with technical success, the risk of RBO was not different between the simultaneous and sequential groups ($P = 0.39$) (Figure 4C). After RBO, all patients underwent endoscopic reintervention, except 2 patients in the simultaneous group (15%, $P = 0.49$) who were not compatible with general anesthesia. Technical and clinical success were obtained in 82%, 75%, and 100% of cases in the simultaneous, sequential SIS, and SBS groups, respectively. Reintervention seemed to be more efficient when SBS bilateral drainage (either simultaneous or sequential) was performed compared with the SIS technique (83% *vs* 75%, $P = 0.53$).

Overall survival

We observed a median survival time of 67 days in the simultaneous group *vs* 61 days in the sequential group (69 days in the SBS group and 43 days in the SIS group). No significant difference was observed between groups ($P = 0.24$).

DISCUSSION

Complete biliary drainage in cases of unresectable MHBO frequently requires bilateral metallic drainage, a technically challenging endoscopic procedure. The emergence of SEMS associated to an ultra-thin delivery system such as aixstent® BDH (Leufen Medical GmbH, Berlin, Germany) carried by a 5 Fr delivery system and Niti-S M-Type® (TaeWoong Medical, Seoul, Korea) carried by a 6 Fr delivery system has been a true revolution in our practice by highly increasing technical success without impacting clinical outcomes or RBO rate compared with sequential stenting. Our study showed that simultaneous bilateral biliary drainage using a 6 Fr or 5 Fr delivery system was superior to sequential drainage when

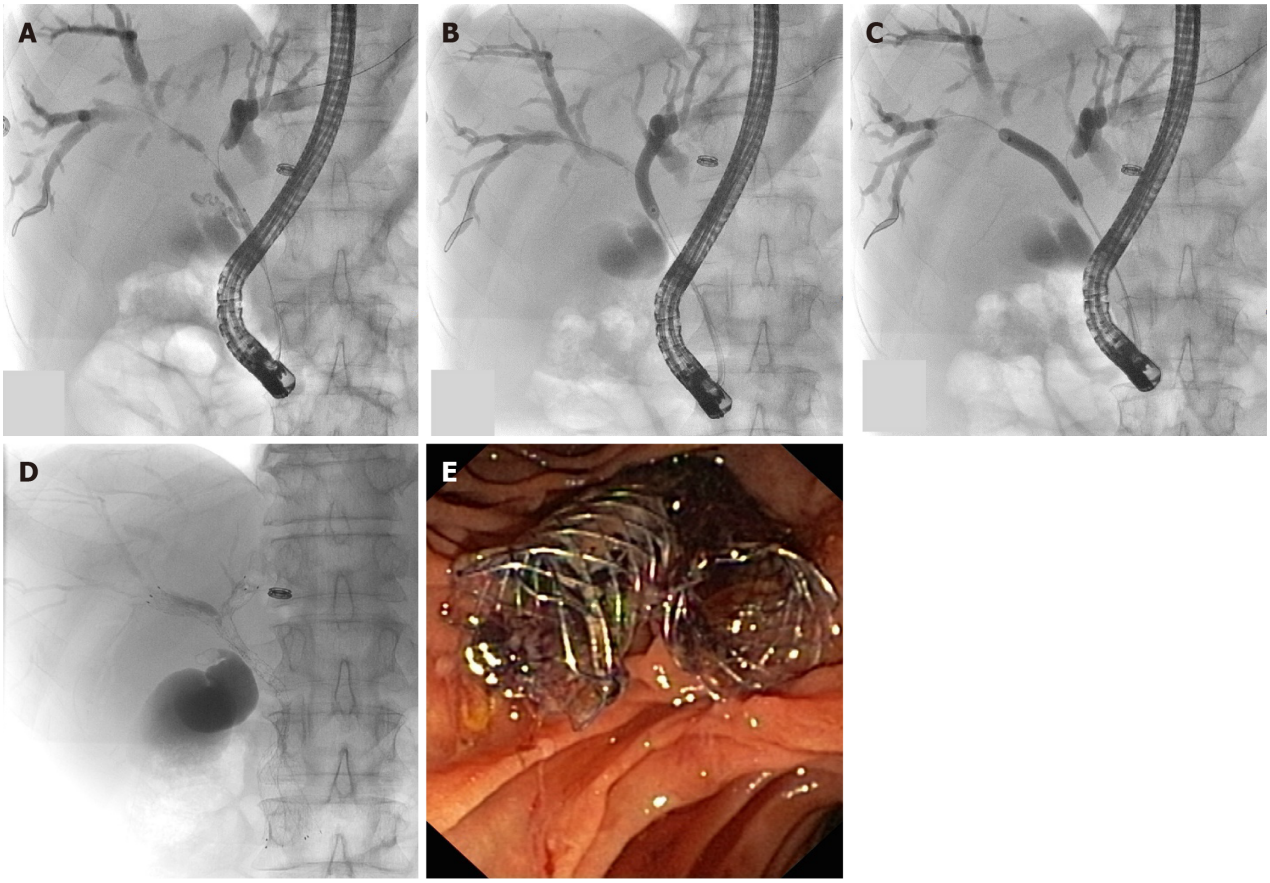

Figure 2 Sequential side by side bilateral drainage on X-ray and endoscopic view. A: Placement of guidewires across the strictures; B: Dilation of left stricture; C: Dilation of right stricture; D: Simultaneous placement of two metallic biliary stents; E: Endoscopic view after drainage with two biliary self-expandable metallic stent well distinct in the duodenal lumen.

an SBS approach is chosen. Technical success was achieved in 94% of cases, a success rate that is similar with previous studies that evaluated feasibility of simultaneous SBS drainage, with a technical success ranging from 71% to 100%[14-16, 19]. Our results concerning technical success of sequential SBS drainage are comparable with Inoue *et al*[14] (71% of technical success, P = 0.045). We also observed a high technical success rate of 95% for the SIS procedure and was comparable with previously existing literature (approximately 100%). Interestingly, we observed a higher rate of technical failure for patients who suffered hilar metastatic obstruction and for type IV of Bismuth and Corlette strictures. Baseline bilirubin rate did not appear to interfere with technical success or failure. A high technical success is important because it is closely related to the risk of post-procedure AE, particularly cholangitis, even though contrast agent injection in the non-catheterized liver segments was carefully avoided, whatever technique we used.

We reported a lower rate of early AE in the simultaneous group compared with the sequential group (21% *vs* 31%, P = 0.205). Cholangitis was observed more in the sequential group, with no difference between the SBS or SIS technique (Figure 4D). The higher rate of cholangitis in the sequential SBS group might be explained by the higher rate of technical failure. Concerning the sequential SIS group, the higher rate of cholangitis might be explained by the unilateral balloon dilatation of the bile duct before bilateral stenting or the difficulty of accurate positioning of the proximal tip of the crossing stent due to the frictional forces at the crossing point of the two stents. Recent meta-analysis evaluating SIS and SBS bilateral drainage found no differences in terms of AE between the two techniques (risk difference: -0.09, P = 0.07) [20], despite the fact that some authors suggest a higher rate of cholangitis with SBS techniques due to higher incidence of portal vein occlusion or obstruction of one of the two stents[21]. Use of thinner stents of 8 mm in simultaneous and sequential SIS groups probably contributed to lower the portal vein occlusion rate.

Technical failure was associated with a significantly higher rate of fatal cholangitis (OR 5.89, 0.78-44.4, P = 0.085), reminding us of the absolute necessity of adequate drainage of all opacified biliary areas, using if necessary in case of ERCP failure, alternative techniques such as percutaneous transhepatic biliary drainage (PTBD) or EUS-guided biliary drainage (EUS-BD). Furthermore, Vienne *et al*[11] proved that drainage of an atrophic biliary area is useless and improved cholangitis, supporting the necessity for hepatic volumetry assessment prior to ERCP to reduce post-procedural cholangitis. Kongkam *et al*[22] compared the association of ERCP + EUS-BD over PTBD for unresectable MHBO and showed a high technical success rate with a similar clinical success rate and a significantly lower RBO rate at 3 months and 6 months. Vanella *et al*[23] confirmed superiority of EUS-BD over PTBD after failed ERCP and proposed EUS-BD as a first option after failure of retrograde stenting. Those results are supported by the latest 2022 European Society of Gastrointestinal Endoscopy (ESGE) recommendations, which now suggest hepaticogastrostomy using EUS-BD after ERCP or PTBD failure[24].

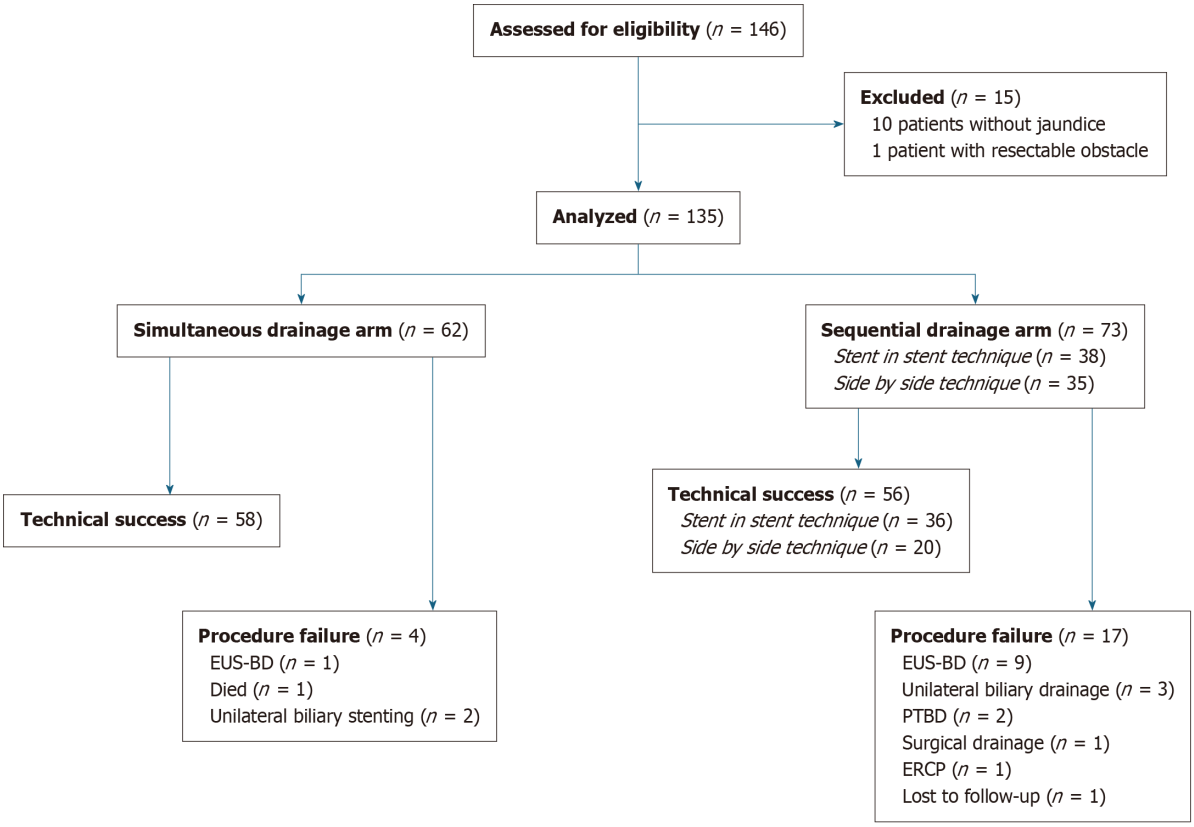

Figure 3 Flow diagram of the participants analyzed. EUS-BD: Endoscopic ultrasound-guided biliary drainage; PTBD: Percutaneous transhepatic biliary drainage; ERCP: Endoscopic retrograde cholangiopancreatography.

We expected a shorter procedure time in the simultaneous group since Inoue *et al*[14] and Kawakubo *et al*[15] proved that simultaneous drainage shortens procedure time compared with sequential procedure (22 min and 25 min for simultaneous bilateral stenting in their study, respectively). In our study, the median procedure time was not different between the simultaneous and sequential procedures (80 min *vs* 72 min, $P = 0.92$). It was close to the simultaneous procedure time found by Chennat *et al*[19] and Law and Baron[15] (64 min and 75 min, respectively). We suffered from a lack of data concerning procedure duration. This is explained by the possibility for a same patient to benefit from both diagnostic EUS and therapeutic ERCP in the same procedure time. We excluded from procedure duration analysis all patient who benefited from the two procedures at the same time to not interfere with data of ERCP alone. Procedure time could sometimes include anesthetic induction and/or orotracheal extubation, which probably increased procedure time in our study.

Clinical success was defined in our study as a decrease of at least 50% of the bilirubin rate at day 7. Recent ESGE recommendations suggest that clinical success should be defined as a decrease of 50%-75% bilirubin rate after 2-4 weeks. We observed a similar clinical success rate (72% to 75%, $P = 0.82$) between the sequential and simultaneous group, a result that might be better with a different definition of clinical success, such as recommended by the ESGE[24]. Due to retrospective collection of data in our study, missing data would have been too important with such definition. Paik *et al*[25] reported a clinical success rate of 69%-97% after using a metallic stent, and these results are comparable to our findings. Those results support the fact that despite the use of less wide stents in the simultaneous group (8 mm *vs* 10 mm diameter), we did not observe a decrease of clinical success or stent patency.

We observed a shorter median survival time compared with other studies (61 days in the sequential group and 67 days in the simultaneous group in our study), especially in the sequential SIS group (43 days). In comparison, median survival time ranged from 146 days to 381 days in a meta-analysis by Chen *et al*[26] (five studies comparing SIS and SBS, 250 patients). This survival does not seem to be influenced by the stenting technique used but is rather a reflection of the severity of the underlying pathology, particularly in the SIS group where a slightly higher proportion of patients present with metastatic disease and have less access to postoperative chemotherapy.

That observation might also explain the lower RBO rate we observed in our study knowing that the usual RBO rate ranges from 18% to 53% in the studies that compared SIS and SBS, with a median stent patency of 118 days to 262 days, respectively[26]. Mean time to RBO was 144 days in the simultaneous group and 103 days in the SIS group. A difference that might be explained by the large cell mesh design of the stents used in the SIS technique, favoring tumor ingrowth[26,27]. Reintervention after RBO seems to be more successful with SBS stenting (sequential and simultaneous combined) than with SIS stenting (83% *vs* 75%, $P = 0.53$). This non-significant difference might be explained by the easier access to both distal tip of the stents with SBS drainage rather than with SIS techniques (two end-tip stents in the duodenal lumen with SBS technique *vs* one with SIS technique).

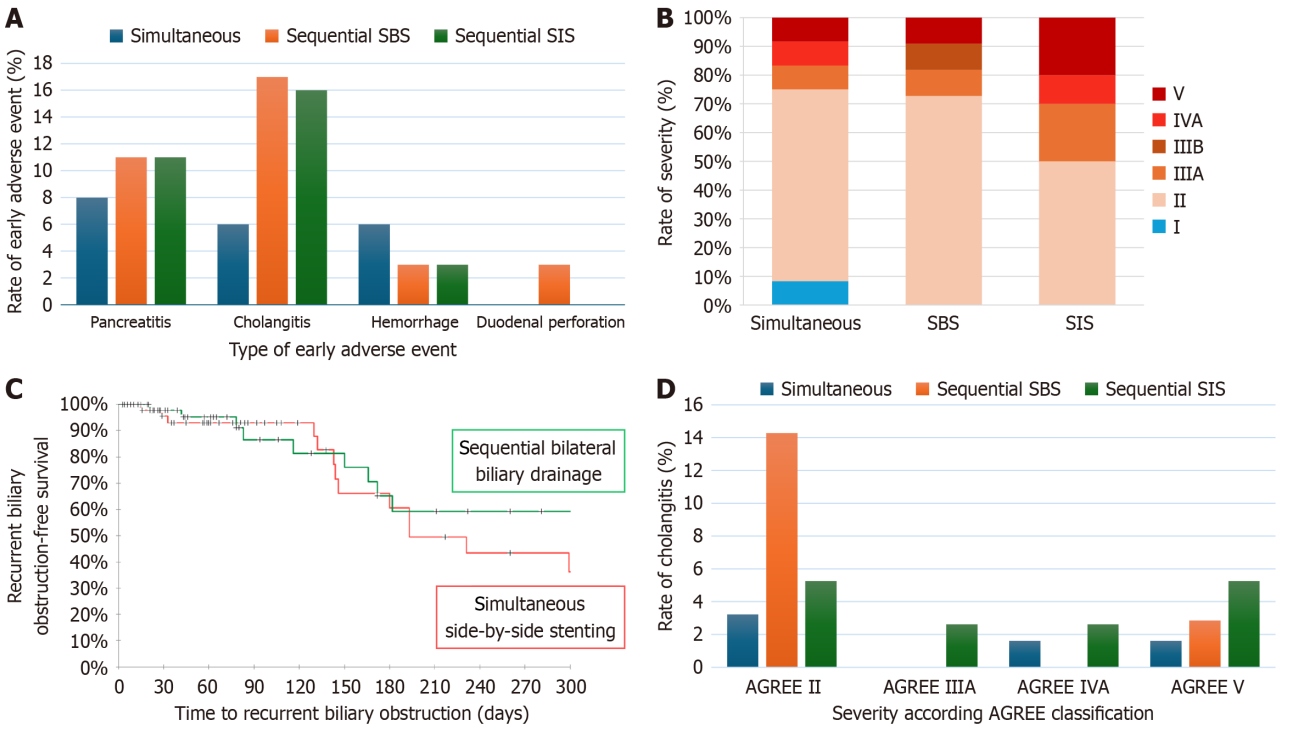

Figure 4 Adverse event and recurrent biliary obstruction outcomes. A: Rate of early adverse events among groups; B: Repartition of severity according the Adverse Event Gastrointestinal Endoscopy classification among patients who suffered from an adverse event; C: Kaplan-Meier curves compared recurrent biliary obstruction-free survival between simultaneous and sequential groups; D: Repartition of severity according to the Adverse Event Gastrointestinal Endoscopy classification among patients with cholangitis. AGREE: Adverse Event Gastrointestinal Endoscopy; SBS: Side by side; SIS: Stent in stent.

To date, this study was the largest concerning comparison of simultaneous and sequential bilateral biliary drainage. Patients were recruited over a large period of 13 years, and procedures were realized all along by only two trained operators. Most reinterventions for RBO proceeded in our tertiary center. The limits of this study were the single center retrospective design, with missing data affecting clinical success and procedure duration. It is important to note that the only study that compared simultaneous and sequential bilateral biliary drainage was also a retrospective monocentric study, with a smaller cohort of 34 patients[16]. Furthermore, due to a large recruitment period, technical success of the sequential technique might have been negatively impacted (procedures performed from 2010 to 2017 in comparison with the simultaneous technique performed from 2017 and 2023).

CONCLUSION

Endoscopic simultaneous bilateral metallic stenting using new SEMS with an ultra-thin (5 Fr or 6 Fr) delivery system is technically easier and as efficient as sequential bilateral stenting in unresectable MHBO to achieve bilateral drainage and can be useful to avoid the risk of a failed second stent placement. However, we reported a similar technical and clinical success in simultaneous SBS and sequential SIS groups with a higher rate of infectious complications in the sequential group even after successful SIS placement. Technical failure was significantly associated with fatal infectious complications. The RBO rate was similar in simultaneous and sequential SIS groups but with a shorter stent patency in the SIS group. We failed to show a difference in terms of procedure duration between the two techniques. Both simultaneous SBS and sequential SIS are valuable options for palliative endoscopic drainage in MHBO. However, the technical requirements are high and need to be completed by trained endoscopists. Further prospective multicentric trials are needed to investigate the place of simultaneous SBS technique as a first-line treatment in unresectable MHBO compared with the SIS technique.

ACKNOWLEDGEMENTS

We dedicate this work to the memory of Professor Laurent Poincloux.

FOOTNOTES

Author contributions: Guilmoteau T, Rouquette O, and Poincloux L conceived and designed the analysis; Guilmoteau T collected the data; Cambier S and Buisson A contributed data or analysis tools; Guilmoteau T and Poincloux L performed the analysis; Guilmoteau T, Rouquette O, Buisson A, Cambier S, Abergel A, and Poincloux L contributed to interpretation and final approval of the manuscript.

Institutional review board statement: The study was approved by local Ethics Committee (IRB00013412, "CHU de Clermont Ferrand IRB #1", IRB number 2023-CF003) with compliance to the French policy of individual data protection and was performed in accordance with the principles of the Declaration of Helsinki.

Informed consent statement: Informed consent was waived because of the retrospective nature of the study, and the analysis used anonymous clinical data.

Conflict-of-interest statement: All authors report no relevant conflicts of interest for this article.

Data sharing statement: No additional data are available.

Country of origin: France

ORCID number: Thomas Guilmoteau 0000-0003-0058-9276; Armand Abergel 0000-0001-7480-1052.

S-Editor: Wei YF
L-Editor: Filipodia
P-Editor: Wang WB

REFERENCES

1 **Jarnagin WR**, Fong Y, DeMatteo RP, Gonen M, Burke EC, Bodniewicz BS J, Youssef BA M, Klimstra D, Blumgart LH. Staging, resectability, and outcome in 225 patients with hilar cholangiocarcinoma. *Ann Surg* 2001; **234**: 507-17; discussion 517 [PMID: 11573044 DOI: 10.1097/00000658-200110000-00010]

2 **Dumonceau JM**, Tringali A, Papanikolaou IS, Blero D, Mangiavillano B, Schmidt A, Vanbiervliet G, Costamagna G, Devière J, García-Cano J, Gyökeres T, Hassan C, Prat F, Siersema PD, van Hooft JE. Endoscopic biliary stenting: indications, choice of stents, and results: European Society of Gastrointestinal Endoscopy (ESGE) Clinical Guideline - Updated October 2017. *Endoscopy* 2018; **50**: 910-930 [PMID: 30086596 DOI: 10.1055/a-0659-9864]

3 **Rerknimitr R**, Angsuwatcharakon P, Ratanachu-ek T, Khor CJ, Ponnudurai R, Moon JH, Seo DW, Pantongrag-Brown L, Sangchan A, Pisespongsa P, Akaraviputh T, Reddy ND, Maydeo A, Itoi T, Pausawasdi N, Punamiya S, Attasaranya S, Devereaux B, Ramchandani M, Goh KL; Asia-Pacific Working Group on Hepatobiliary Cancers. Asia-Pacific consensus recommendations for endoscopic and interventional management of hilar cholangiocarcinoma. *J Gastroenterol Hepatol* 2013; **28**: 593-607 [PMID: 23350673 DOI: 10.1111/jgh.12128]

4 **Xia MX**, Pan YL, Cai XB, Wu J, Gao DJ, Ye X, Wang TT, Hu B. Comparison of endoscopic bilateral metal stent drainage with plastic stents in the palliation of unresectable hilar biliary malignant strictures: Large multicenter study. *Dig Endosc* 2021; **33**: 179-189 [PMID: 32249460 DOI: 10.1111/den.13680]

5 **Sangchan A**, Kongkasame W, Pugkhem A, Jenwitheesuk K, Mairiang P. Efficacy of metal and plastic stents in unresectable complex hilar cholangiocarcinoma: a randomized controlled trial. *Gastrointest Endosc* 2012; **76**: 93-99 [PMID: 22595446 DOI: 10.1016/j.gie.2012.02.048]

6 **Mukai T**, Yasuda I, Nakashima M, Doi S, Iwashita T, Iwata K, Kato T, Tomita E, Moriwaki H. Metallic stents are more efficacious than plastic stents in unresectable malignant hilar biliary strictures: a randomized controlled trial. *J Hepatobiliary Pancreat Sci* 2013; **20**: 214-222 [PMID: 22415652 DOI: 10.1007/s00534-012-0508-8]

7 **Naitoh I**, Ohara H, Nakazawa T, Ando T, Hayashi K, Okumura F, Okayama Y, Sano H, Kitajima Y, Hirai M, Ban T, Miyabe K, Ueno K, Yamashita H, Joh T. Unilateral versus bilateral endoscopic metal stenting for malignant hilar biliary obstruction. *J Gastroenterol Hepatol* 2009; **24**: 552-557 [PMID: 19220678 DOI: 10.1111/j.1440-1746.2008.05750.x]

8 **Lee TH**, Kim TH, Moon JH, Lee SH, Choi HJ, Hwangbo Y, Hyun JJ, Choi JH, Jeong S, Kim JH, Park DH, Han JH, Park SH. Bilateral versus unilateral placement of metal stents for inoperable high-grade malignant hilar biliary strictures: a multicenter, prospective, randomized study (with video). *Gastrointest Endosc* 2017; **86**: 817-827 [PMID: 28479493 DOI: 10.1016/j.gie.2017.04.037]

9 **Aghaie Meybodi M**, Shakoor D, Nanavati J, Ichkhanian Y, Vosoughi K, Brewer Gutierrez OI, Kalloo AN, Singh V, Kumbhari V, Ngamruengphong S, Khashab MA. Unilateral versus bilateral endoscopic stenting in patients with unresectable malignant hilar obstruction: a systematic review and meta-analysis. *Endosc Int Open* 2020; **8**: E281-E290 [PMID: 32118102 DOI: 10.1055/a-1067-4326]

10 **Yang F**, Wang XM, Xia FF, Han XQ. Endoscopic metal stenting for malignant hilar biliary obstruction: an update meta-analysis of unilateral versus bilateral stenting. *Wideochir Inne Tech Maloinwazyjne* 2021; **16**: 472-481 [PMID: 34691298 DOI: 10.5114/wiitm.2021.104196]

11 **Vienne A**, Hobeika E, Gouya H, Lapidus N, Fritsch J, Choury AD, Chryssostalis A, Gaudric M, Pelletier G, Buffet C, Chaussade S, Prat F. Prediction of drainage effectiveness during endoscopic stenting of malignant hilar strictures: the role of liver volume assessment. *Gastrointest Endosc* 2010; **72**: 728-735 [PMID: 20883850 DOI: 10.1016/j.gie.2010.06.040]

12 **Lee TH**, Moon JH, Choi JH, Lee SH, Lee YN, Paik WH, Jang DK, Cho BW, Yang JK, Hwangbo Y, Park SH. Prospective comparison of

endoscopic bilateral stent-in-stent versus stent-by-stent deployment for inoperable advanced malignant hilar biliary stricture. *Gastrointest Endosc* 2019; **90**: 222-230 [PMID: 30905729 DOI: 10.1016/j.gie.2019.03.011]

13 **Naitoh I**, Inoue T. Optimal endoscopic drainage strategy for unresectable malignant hilar biliary obstruction. *Clin Endosc* 2023; **56**: 135-142 [PMID: 36600654 DOI: 10.5946/ce.2022.150]

14 **Inoue T**, Ishii N, Kobayashi Y, Kitano R, Sakamoto K, Ohashi T, Nakade Y, Sumida Y, Ito K, Nakao H, Yoneda M. Simultaneous Versus Sequential Side-by-Side Bilateral Metal Stent Placement for Malignant Hilar Biliary Obstructions. *Dig Dis Sci* 2017; **62**: 2542-2549 [PMID: 28766242 DOI: 10.1007/s10620-017-4691-y]

15 **Law R**, Baron TH. Bilateral metal stents for hilar biliary obstruction using a 6Fr delivery system: outcomes following bilateral and side-by-side stent deployment. *Dig Dis Sci* 2013; **58**: 2667-2672 [PMID: 23625287 DOI: 10.1007/s10620-013-2671-4]

16 **Kawakubo K**, Kawakami H, Kuwatani M, Kudo T, Abe Y, Kawahata S, Kubo K, Kubota Y, Sakamoto N. Single-step simultaneous side-by-side placement of a self-expandable metallic stent with a 6-Fr delivery system for unresectable malignant hilar biliary obstruction: a feasibility study. *J Hepatobiliary Pancreat Sci* 2015; **22**: 151-155 [PMID: 25345586 DOI: 10.1002/jhbp.173]

17 **Martin C**, Auboyer C, Boisson M, Dupont H, Gauzit R, Kitzis M, Leone M, Lepape A, Mimoz O, Montravers P, Pourriat JL; Steering committee of the French Society of Anaesthesia and Intensive Care Medicine (SFAR) responsible for the establishment of the guidelines. Antibioprophylaxis in surgery and interventional medicine (adult patients). Update 2017. *Anaesth Crit Care Pain Med* 2019; **38**: 549-562 [PMID: 30836191 DOI: 10.1016/j.accpm.2019.02.017]

18 **Nass KJ**, Zwager LW, van der Vlugt M, Dekker E, Bossuyt PMM, Ravindran S, Thomas-Gibson S, Fockens P. Novel classification for adverse events in GI endoscopy: the AGREE classification. *Gastrointest Endosc* 2022; **95**: 1078-1085.e8 [PMID: 34890695 DOI: 10.1016/j.gie.2021.11.038]

19 **Chennat J**, Waxman I. Initial performance profile of a new 6F self-expanding metal stent for palliation of malignant hilar biliary obstruction. *Gastrointest Endosc* 2010; **72**: 632-636 [PMID: 20579991 DOI: 10.1016/j.gie.2010.04.037]

20 **de Souza GMV**, Ribeiro IB, Funari MP, de Moura DTH, Scatimburgo MVCV, de Freitas Júnior JR, Sánchez-Luna SA, Baracat R, de Moura ETH, Bernardo WM, de Moura EGH. Endoscopic retrograde cholangiopancreatography drainage for palliation of malignant hilar biliary obstruction - stent-in-stent or side-by-side? A systematic review and meta-analysis. *World J Hepatol* 2021; **13**: 595-610 [PMID: 34131473 DOI: 10.4254/wjh.v13.i5.595]

21 **Naitoh I**, Hayashi K, Nakazawa T, Okumura F, Miyabe K, Shimizu S, Yoshida M, Yamashita H, Ohara H, Joh T. Side-by-side versus stent-in-stent deployment in bilateral endoscopic metal stenting for malignant hilar biliary obstruction. *Dig Dis Sci* 2012; **57**: 3279-3285 [PMID: 22732832 DOI: 10.1007/s10620-012-2270-9]

22 **Kongkam P**, Orprayoon T, Boonmee C, Sodarat P, Seabmuangsai O, Wachiramatharuch C, Auan-Klin Y, Pham KC, Tasneem AA, Kerr SJ, Romano R, Jangsirikul S, Ridtitid W, Angsuwatcharakon P, Ratanachu-Ek T, Rerknimitr R. ERCP plus endoscopic ultrasound-guided biliary drainage versus percutaneous transhepatic biliary drainage for malignant hilar biliary obstruction: a multicenter observational open-label study. *Endoscopy* 2021; **53**: 55-62 [PMID: 32515005 DOI: 10.1055/a-1195-8197]

23 **Vanella G**, Bronswijk M, Maleux G, van Malenstein H, Laleman W, Van der Merwe S. EUS-guided intrahepatic biliary drainage: a large retrospective series and subgroup comparison between percutaneous drainage in hilar stenoses or postsurgical anatomy. *Endosc Int Open* 2020; **8**: E1782-E1794 [PMID: 33269311 DOI: 10.1055/a-1264-7511]

24 **van der Merwe SW**, van Wanrooij RLJ, Bronswijk M, Everett S, Lakhtakia S, Rimbas M, Hucl T, Kunda R, Badaoui A, Law R, Arcidiacono PG, Larghi A, Giovannini M, Khashab MA, Binmoeller KF, Barthet M, Perez-Miranda M, van Hooft JE. Therapeutic endoscopic ultrasound: European Society of Gastrointestinal Endoscopy (ESGE) Guideline. *Endoscopy* 2022; **54**: 185-205 [PMID: 34937098 DOI: 10.1055/a-1717-1391]

25 **Paik WH**, Park YS, Hwang JH, Lee SH, Yoon CJ, Kang SG, Lee JK, Ryu JK, Kim YT, Yoon YB. Palliative treatment with self-expandable metallic stents in patients with advanced type III or IV hilar cholangiocarcinoma: a percutaneous versus endoscopic approach. *Gastrointest Endosc* 2009; **69**: 55-62 [PMID: 18657806 DOI: 10.1016/j.gie.2008.04.005]

26 **Chen L**, Gao GM, Li DL, Chen ZK. Side-by-side versus stent-in-stent bilateral stenting for malignant hilar biliary obstruction: a meta-analysis. *Wideochir Inne Tech Maloinwazyjne* 2022; **17**: 279-288 [PMID: 35707334 DOI: 10.5114/wiitm.2021.112477]

27 **Heo JY**, Lee HS, Son JH, Lee SH, Bang S. Clinical Outcomes of Bilateral Stent-in-Stent Placement Using Self-Expandable Metallic Stent for High-Grade Malignant Hilar Biliary Obstruction. *Yonsei Med J* 2018; **59**: 827-833 [PMID: 30091315 DOI: 10.3349/ymj.2018.59.7.827]

World Journal of Gastroenterology

Submit a Manuscript: https://www.f6publishing.com

World J Gastroenterol 2025 May 21; 31(19): 104563

DOI: 10.3748/wjg.v31.i19.104563

ISSN 1007-9327 (print) ISSN 2219-2840 (online)

ORIGINAL ARTICLE

Retrospective Study

Development and validation of a radiomics-based prediction model for variceal bleeding in patients with Budd-Chiari syndrome-related gastroesophageal varices

Ze-Dong Wang, Hui-Jie Nan, Su-Xin Li, Lu-Hao Li, Zhao-Chen Liu, Hua-Hu Guo, Lin Li, Sheng-Yan Liu, Hai Li, Yan-Liang Bai, Xiao-Wei Dang

Specialty type: Gastroenterology and hepatology

Provenance and peer review: Unsolicited article; Externally peer reviewed.

Peer-review model: Single blind

Peer-review report's classification

Scientific Quality: Grade A, Grade A, Grade A, Grade A

Novelty: Grade A, Grade A, Grade B, Grade B

Creativity or Innovation: Grade A, Grade A, Grade A, Grade B

Scientific Significance: Grade A, Grade A, Grade A, Grade A

P-Reviewer: Meng QY; Montasser IF

Received: December 28, 2024

Revised: March 24, 2025

Accepted: April 27, 2025

Published online: May 21, 2025

Processing time: 147 Days and 23.4 Hours

Ze-Dong Wang, Su-Xin Li, Lu-Hao Li, Zhao-Chen Liu, Hua-Hu Guo, Lin Li, Sheng-Yan Liu, Xiao-Wei Dang, Department of Hepatopancreatobiliary Surgery, The First Affiliated Hospital of Zhengzhou University, Zhengzhou 450052, Henan Province, China

Ze-Dong Wang, Su-Xin Li, Lu-Hao Li, Zhao-Chen Liu, Hua-Hu Guo, Lin Li, Sheng-Yan Liu, Xiao-Wei Dang, Key Laboratory of Precision Diagnosis and Treatment in General Surgical (Hepatobiliary and Pancreatic) Diseases of Health Commission of Henan Province, The First Affiliated Hospital of Zhengzhou University, Zhengzhou 450052, Henan Province, China

Ze-Dong Wang, Su-Xin Li, Lu-Hao Li, Zhao-Chen Liu, Hua-Hu Guo, Lin Li, Sheng-Yan Liu, Xiao-Wei Dang, Henan Province Engineering Research Center of Minimally Invasive Diagnosis and Treatment of Hepatobiliary and Pancreatic Diseases, The First Affiliated Hospital of Zhengzhou University, Zhengzhou 450052, Henan Province, China

Ze-Dong Wang, Su-Xin Li, Lu-Hao Li, Zhao-Chen Liu, Hua-Hu Guo, Lin Li, Sheng-Yan Liu, Xiao-Wei Dang, Budd-Chiari Syndrome Diagnosis and Treatment Center of Henan Province, The First Affiliated Hospital of Zhengzhou University, Zhengzhou 450052, Henan Province, China

Hui-Jie Nan, Yan-Liang Bai, Department of Hematology, Zhengzhou University People's Hospital and Henan Provincial People's Hospital, Zhengzhou 450003, Henan Province, China

Hai Li, Department of Hepatopancreatobiliary Surgery, Zhengzhou University People's Hospital and Henan Provincial People's Hospital, Zhengzhou 450003, Henan Province, China

Co-first authors: Ze-Dong Wang and Hui-Jie Nan.

Co-corresponding authors: Yan-Liang Bai and Xiao-Wei Dang.

Corresponding author: Xiao-Wei Dang, PhD, Chief Physician, Professor, Department of Hepatopancreatobiliary Surgery, The First Affiliated Hospital of Zhengzhou University, No. 1 Jianshe East Road, Erqi District, Zhengzhou 450052, Henan Province, China.
dangxw1001@zzu.edu.cn

Abstract

BACKGROUND

Budd-Chiari syndrome (BCS) is caused by obstruction of the hepatic veins or suprahepatic inferior vena cava, leading to portal hypertension and the development of gastroesophageal varices (GEVs), which are associated with an increased risk of bleeding. Existing risk models for variceal bleeding in cirrhotic patients have limited applicability to BCS due to differences in pathophysiology. Radiomics, as a noninvasive technique, holds promise as a tool for more accurate prediction of bleeding risk in BCS-related GEVs.

AIM

To develop and validate a personalized risk model for predicting variceal bleeding in BCS patients with GEVs.

METHODS

We retrospectively analyzed clinical data from 444 BCS patients with GEVs in two centers. Radiomic features were extracted from portal venous phase computed tomography (CT) scans. A training cohort of 334 patients was used to develop the model, with 110 patients serving as an external validation cohort. LASSO Cox regression was used to select radiomic features for constructing a radiomics score (Radscore). Univariate and multivariate Cox regression identified independent clinical predictors. A combined radiomics + clinical (R + C) model was developed using stepwise regression. Model performance was assessed using the area under the receiver operating characteristic curve (AUC), calibration plots, and decision curve analysis (DCA), with external validation to evaluate generalizability.

RESULTS

The Radscore comprised four hepatic and six splenic CT features, which predicted the risk of variceal bleeding. Multivariate analysis identified invasive treatment to relieve hepatic venous outflow obstruction, anticoagulant therapy, and hemoglobin levels as independent clinical predictors. The R + C model achieved C-indices of 0.906 (training) and 0.859 (validation), outperforming the radiomics and clinical models alone (AUC: training 0.936 *vs* 0.845 *vs* 0.823; validation 0.876 *vs* 0.712 *vs* 0.713). DCA showed higher clinical net benefit across the thresholds. The model stratified patients into low-, medium- and high-risk groups with significant differences in bleeding rates ($P < 0.001$). An online tool is available at https://bcsvh.shinyapps.io/BCS_Variceal_Bleeding_Risk_Tool/.

CONCLUSION

We developed and validated a novel radiomics-based model that noninvasively and conveniently predicted risk of variceal bleeding in BCS patients with GEVs, aiding early identification and management of high-risk patients.

Key Words: Budd-Chiari syndrome; Gastroesophageal varices; Variceal bleeding; Radiomics; Prognostic model

Core Tip: This study develops a personalized, noninvasive predictive model for variceal bleeding risk in Budd-Chiari syndrome (BCS) patients with gastroesophageal varices. By combining radiomic features from computed tomography imaging with clinical data, the model demonstrated superior predictive performance over traditional approaches, offering a promising tool for early risk assessment and improving patient management in BCS.

Citation: Wang ZD, Nan HJ, Li SX, Li LH, Liu ZC, Guo HH, Li L, Liu SY, Li H, Bai YL, Dang XW. Development and validation of a radiomics-based prediction model for variceal bleeding in patients with Budd-Chiari syndrome-related gastroesophageal varices. *World J Gastroenterol* 2025; 31(19): 104563

URL: https://www.wjgnet.com/1007-9327/full/v31/i19/104563.htm

DOI: https://dx.doi.org/10.3748/wjg.v31.i19.104563

INTRODUCTION

Budd-Chiari syndrome (BCS) is a complex hepatic vascular disorder characterized by the obstruction of the hepatic veins and/or the suprahepatic inferior vena cava, leading to impaired hepatic blood outflow. This obstruction can result in posthepatic portal hypertension, subsequently causing gastroesophageal varices (GEVs)[1-3]. Rupture and bleeding of GEVs are fatal complications associated with high mortality rates linked to portal hypertension. Approximately 50%-60% of patients with liver cirrhosis develop GEVs, with 10%-15% experiencing variceal bleeding annually[4,5]. Therefore, early and accurate prediction of variceal bleeding risk is crucial for timely intervention and improving patient prognosis.

Currently, risk assessment models for variceal bleeding in cirrhotic patients are well established, with endoscopic examination and clinical scoring systems widely utilized. However, the pathophysiological mechanisms of BCS differ from those of cirrhosis, leading to distinct risks and characteristics of GEVs. Existing predictive models have limited applicability in BCS patients[6]. Endoscopy, as an invasive procedure, may cause discomfort and potential complications, especially in patients with severely impaired liver function[7].

Radiomics, an emerging technology, transforms medical imaging into high-dimensional quantitative features, including shape, intensity and texture. This technique can capture complex patterns in imaging data that are difficult for the human eye to discern, providing a more comprehensive risk assessment for portal hypertension and its complications [8-10]. The application of radiomics holds promise for offering more accurate bleeding risk predictions in BCS patients, addressing the limitations of traditional endoscopic evaluations.

The aim of this multicenter study was to develop and validate a radiomics-based predictive model for noninvasive assessment of variceal hemorrhage risk in patients with GEVs associated with BCS, with the aim of providing reliable tools for enhancing clinical decision-making and optimizing patient outcomes.

MATERIALS AND METHODS

Ethical approval and patient selection

This retrospective study was conducted at two tertiary hospitals in Zhengzhou, China: Zhengzhou University First Affiliated Hospital and Zhengzhou University People's Hospital. The study adhered to the ethical principles outlined in the Declaration of Helsinki and was approved by the Ethics Committee of the First Affiliated Hospital of Zhengzhou University (Approval No. 2021-KY-1137-002). As a retrospective observational study, the requirement for informed consent was waived. To ensure confidentiality, all private patient information was deidentified before analysis.

The study included patients diagnosed with BCS complicated by GEVs, with data collected from Zhengzhou University First Affiliated Hospital between January 1, 2016 and December 31, 2021, and Zhengzhou University People's Hospital between January 1, 2016 and December 31, 2022. The diagnosis of BCS was based on criteria from the Chinese Society of Hospital Medicine for Budd-Chiari Syndrome and Liver Vascular Diseases and the European Study Group on Vascular Diseases of the Liver. Imaging modalities such as ultrasound, computed tomography (CT) venography, magnetic resonance venography and digital subtraction angiography were used to confirm the presence of vascular outflow obstruction. Enhanced CT imaging was utilized by two experienced radiologists to confirm the diagnosis of GEVs and generate imaging reports.

Participants were included if they met the following criteria: (1) Definitive diagnosis of BCS based on imaging evidence of venous outflow obstruction; and (2) First-time diagnosis of GEVs based on three-phase enhanced CT imaging. Patients were excluded if they met any of the following criteria: (1) Previous variceal treatment; (2) Presence of malignant tumors; (3) Other liver diseases such as viral, alcoholic or autoimmune hepatitis; (4) Incomplete or poor-quality imaging or clinical data; (5) In-hospital death or concurrent severe organ dysfunction; (6) Transjugular intrahepatic portosystemic shunt (TIPS) for massive ascites; or (7) Prophylactic treatment for GEVs during follow-up. The inclusion and exclusion process is summarized in Figure 1.

Image preprocessing and feature extraction

Each patient underwent a standardized GE 64-row spiral CT examination. Patients were instructed to fast for 6-8 hours before scanning, and an iodine allergy test was conducted. For patients without iodine allergy, 800-1000 mL of warm water was consumed 5 minutes before scanning to ensure adequate gastric filling. Scanning parameters included a tube voltage of 120 kVp, tube current of 290-650 mA and scan thickness of 5.0 mm. Contrast-enhanced scans were performed using iodixanol (300 mgI/mL) as the contrast agent, with a weight-adjusted dose administered at 2.5-3.5 mL/s. Images were acquired during the arterial (approximately 30 seconds postinjection) and venous (60-70 seconds postinjection) phases and reconstructed on the AW4.4 workstation with a slice thickness of 0.63 mm.

To avoid any variations in scanning accuracy and three-dimensional (3D) reconstruction between centers, all imaging examinations at both hospitals were performed using identical GE 64-row spiral CT scanners, strictly standardized acquisition protocols and the same 3D reconstruction software. This uniformity ensures that any potential differences attributable to device or software variability are effectively minimized, thereby providing consistent imaging data processing and reliable radiomics feature extraction.

Two regions of interest (ROIs) were manually delineated at the hepatic (Figure 2A) and splenic (Figure 2B) hilum levels using 3D Slicer (version 5.6.1). Two experienced radiologists (each with > 7 years of experience) independently segmented the ROIs, ensuring that they captured relevant anatomical structures while excluding major blood vessels, artefacts, and focal hepatic lesions. Any inconsistencies were resolved through discussion with a senior radiologist (> 15 years of experience). To validate segmentation consistency, the ROIs were independently redrawn by two experienced radiologists (Reader 1 and Reader 2), and the intraclass correlation coefficient (ICC) values above 0.75 confirmed high reproducibility.

Radiomic features were extracted from the delineated ROIs using PyRadiomics (version 3.1.0). Preprocessing steps included Z-score normalization to standardize feature distributions, grayscale discretization into 25 bins, and symmetrical gray-level co-occurrence matrix (GLCM) enforcement to improve texture feature reproducibility. Voxel resampling was not applied due to consistent voxel spacing across datasets. A total of 851 radiomic features were extracted for each ROI, spanning seven categories: shape (14), first-order intensity (162), and second-order texture features, including gray-level co-occurrence matrix (216), gray-level run length matrix (144), gray-level size zone matrix

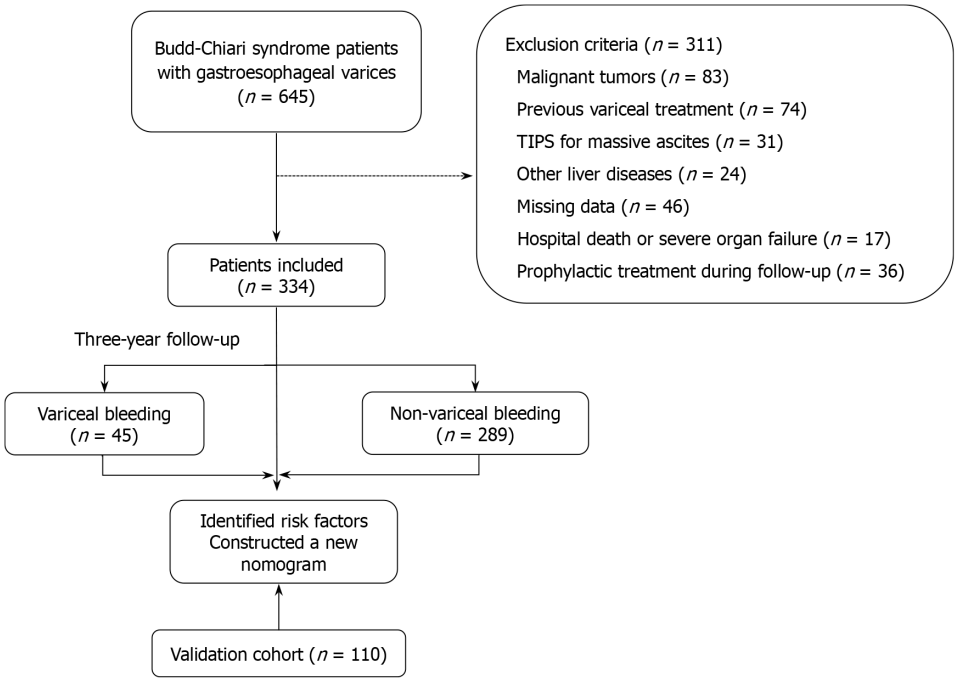

Figure 1 Study flow chart. TIPS: Transjugular intrahepatic portosystemic shunt.

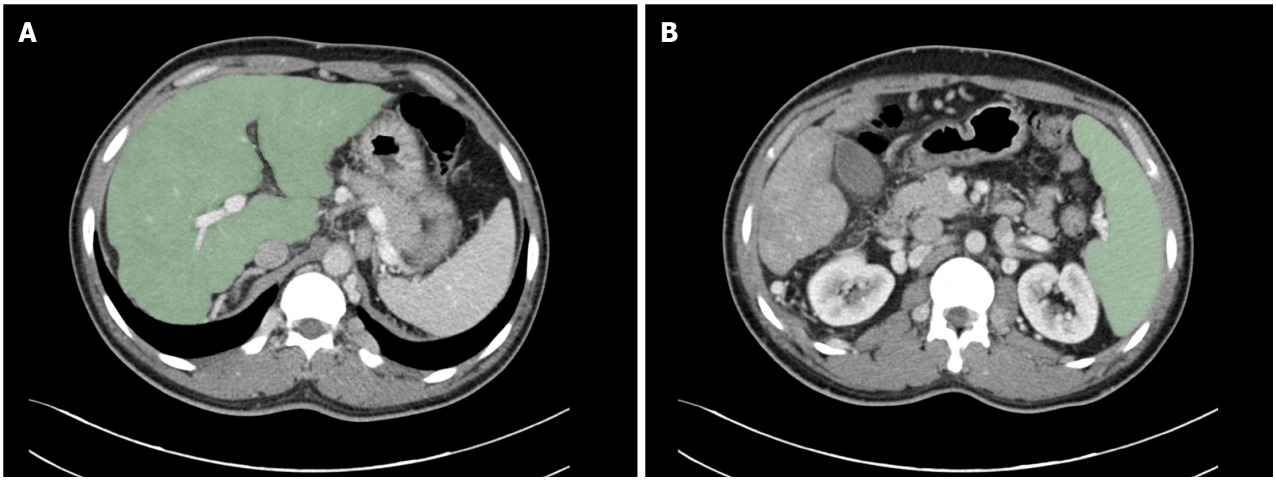

Figure 2 Regions of interest for the liver and spleen. A: Region of interest (ROI) for the liver delineated at the hepatic hilum; B: ROI for the spleen delineated at the splenic hilum.

(144), gray-level dependence matrix (126), and neighbouring gray tone difference matrix (45). In total, 1702 features (851 per ROI) were extracted for subsequent analysis.

Clinical and radiomics data

The clinical data included key demographic, laboratory and imaging parameters relevant to bleeding risk and BCS severity. Imaging parameters derived from contrast-enhanced CT scans included measurements reflecting vascular obstruction and splenic and portal hemodynamics. These parameters were selected based on their clinical relevance and ease of measurement, ensuring consistency and reproducibility across retrospective datasets.

Extracted radiomic features underwent preprocessing to ensure consistency and comparability across datasets. Features were standardized using *Z*-score normalization, and feature selection was performed to identify the most predictive radiomic variables for model development. The selected features were integrated with clinical data to develop predictive models for bleeding risk.

Follow-up and outcomes

The follow-up period was set at 3 years (or until the occurrence of a bleeding event, whichever occurred first). The primary endpoint of the study was the initial occurrence of esophagogastric variceal bleeding, which was confirmed through clinical diagnosis. This diagnosis was based on pertinent clinical manifestations of upper gastrointestinal

bleeding, such as hematemesis and/or melena, that necessitated treatment *via* endoscopic therapy, interventional procedures, or surgery. Patients with upper gastrointestinal bleeding caused by ulcers, gastric diseases related to portal hypertension, or other nonvariceal factors were excluded.

Statistical analysis

The statistical analysis was conducted using SPSS 26, R 4.2.3, and X-tile. Normally distributed quantitative data are presented as mean ± SD, and group comparisons were performed using *t* tests, while non-normally distributed data were expressed as M (Q1, Q3) and compared using Mann-Whitney *U* tests. Numerical data were reported as frequencies (percentages) and analyzed using χ^2 tests or Fisher's exact test. Independent risk factors for bleeding were identified through univariate and multivariate Cox regression analyses. LASSO Cox regression was applied for radiomic feature selection, thereby reducing the dimensionality of the data. The penalty parameter (λ) was optimized *via* 10-fold cross-validation based on the minimum deviance criterion. The proportional hazards assumption was validated using a multivariate Cox model. The receiver operating characteristic (ROC) curve for the predictive model was visualized using the rms package and deployed as a web tool on shinyapp.io *via* DynNom. Model discrimination was evaluated using the C index and its 95% confidence interval (95%CI), while calibration was assessed using a calibration curve generated with the rms package. Clinical efficacy was evaluated through decision curve analysis (DCA) using the ggDCA package. The optimal risk score cut-off for hierarchical risk classification was determined using X-tile. Kaplan-Meier survival analysis was performed, with significance set at $P < 0.05$.

RESULTS

Patient demographics and baseline characteristics (bleeding vs nonbleeding groups)

A total of 444 BCS patients with GEVs were included in this study. The mean age of the cohort was 51.5 ± 10.9 years (range 21-85 years), and 58.9% were male. During the follow-up period, 61 patients (13.7%) experienced their first variceal bleeding event. Patients were classified into the bleeding group (n = 61) and the nonbleeding group (n = 383). A comparison of baseline characteristics between the two groups is presented in Table 1.

Patients in the bleeding group had significantly lower platelet counts, albumin levels and sodium levels but higher creatinine, aspartate aminotransferase (AST), Child-Pugh grade, albumin-bilirubin score, and Model for End-stage Liver Disease score (all $P < 0.05$). In contrast, fewer patients in the bleeding group had undergone invasive treatment to relieve hepatic venous outflow obstruction compared to the nonbleeding group ($P < 0.001$), suggesting a potential protective effect of this intervention (Table 1).

Comparison of the training and validation cohorts

To develop and validate the risk prediction model, patients from the First Affiliated Hospital of Zhengzhou University (n = 334) were designated as the training cohort, whereas those from Zhengzhou University People's Hospital (n = 110) constituted the validation cohort. There were no significant differences (all $P > 0.05$) in baseline demographics, clinical parameters or imaging findings between these two cohorts (Table 2). Such comparability ensures a robust basis for subsequent model development and external validation.

Radiomics feature selection and clinical correlation analysis

A total of 1702 radiomic features were extracted per patient, with 851 features from each ROI. To ensure data stability, reliability was assessed by computing the ICC for a randomly selected subset of 30 patients. Features with ICC > 0.75 were retained, resulting in 1333 reliable radiomic features for subsequent analysis. Feature selection was performed using LASSO Cox regression with 10-fold cross-validation to optimize the penalty parameter (λ), which identified 10 nonzero radiomic features for constructing the Radscore (Figure 3). These features included nine wavelet-transformed texture features and one GLCM-derived feature, reflecting their relevance in capturing multi-scale texture patterns and texture coarseness (Supplementary Table 1). Univariate Cox regression analysis of clinical variables revealed significant associations with sex, portal vein thrombosis, invasive treatment to relieve hepatic venous outflow obstruction, use of anticoagulant medication, ascites, spleen thickness, red blood cell count, hemoglobin level, platelet count, serum sodium level, creatinine level, AST level, alkaline phosphatase level, albumin level, direct bilirubin level, prothrombin time, BCS type, and Child-Turcotte-Pugh class. Multivariate Cox regression further identified three independent risk factors for GEV bleeding in BCS patients. Invasive treatment to relieve hepatic venous outflow obstruction, use of anticoagulant medication and hemoglobin levels (Table 3). These variables were used to construct a clinical-only risk prediction model (C model), which demonstrated significant predictive performance.

Development and validation of a prognostic model for GEV bleeding

To construct a comprehensive risk prediction model, the radiomics-based Radscore was integrated with significant clinical variables identified through multivariate Cox regression analysis. The final model revealed that the following were independent risk factors for bleeding in patients with BCS. Invasive treatment to relieve hepatic venous outflow obstruction [hazard ratio (HR) = 0.089, 95%CI = 0.044-0.181, $P < 0.001$), use of anticoagulants (HR = 10.653, 95%CI = 3.102-36.582, $P < 0.001$), gender (HR = 2.332, 95%CI = 1.057-5.144, $P = 0.036$), platelet count (HR = 0.992, 95%CI = 0.984-0.999, $P = 0.035$), and Radscore (HR = 1.545, 95%CI = 1.236-1.932, $P < 0.001$). These variables were incorporated into a nomogram for individualized prediction (Figure 4). The predictive accuracy of the radiomics + clinical (R + C) model was assessed

Table 1 Baseline characteristics of Budd-Chiari syndrome patients with gastroesophageal varices stratified by variceal bleeding status

Variables	Bleeding group (*n* = 61)	Non-bleeding group (*n* = 383)	*P* value
Age (years)	52.1 ± 11.2	51.4 ± 10.8	0.640
Sex (male)	50 (82)	209 (54.6)	< 0.001
Diabetes	3 (4.9)	29 (7.6)	0.633
Ascites	33 (54.1)	144 (37.6)	0.015
Hepatic encephalopathy	2 (3.3)	11(2.9)	1.000
IVC or HV thrombosis	9 (14.8)	79 (20.6)	0.285
Portal vein thrombosis	7 (11.5)	16 (4.2)	0.038
Spleen thickness (mm)	46 (39, 58)	45 (39, 49)	0.041
Portal vein diameter (mm)	12.7 (10.0, 14.5)	12.7 (10.0, 15.0)	0.994
BCS type			0.042
HV type	19 (31.1)	67 (17.5)	
Mixed type	35 (57.4)	269 (70.2)	
IVC type	7 (11.5)	47 (12.3)	
Child-Pugh grade			< 0.001
A	26 (42.6)	256 (66.8)	
B	21 (34.4)	121 (31.6)	
C	14 (23)	6 (1.6)	
ALBI, median (IQR)	-2.07 (-2.57, -1.28)	-2.38 (-2.75, -1.97)	< 0.001
MELD, median (IQR)	8.22 (4.07, 13.00)	4.15 (1.72, 7.19)	< 0.001
Use of anticoagulant medication	56 (91.8)	310 (80.9)	0.038
Invasive treatment to relieve hepatic venous outflow obstruction	27 (44.3)	344 (89.8)	< 0.001
White blood cell (× 10^9/L)	3.8 (2.9, 5.0)	3.4 (2.7, 4.5)	0.271
Red blood cell (× 10^{12}/L)	3.7 (2.8, 4.4)	4.0 (3.6, 4.4)	0.016
Hemoglobin (g/L)	115 (77.5, 134.0)	124 (109, 138)	0.005
Platelet (× 10^9/L)	71 (48.5, 98)	90 (67, 126)	< 0.001
Sodium (mmol/L)	140 (137.5, 142.0)	142 (140, 143.9)	< 0.001
Creatinine (μmol/L)	62 (48.5, 76.5)	55 (46, 65)	0.007
Alanine aminotransferase (U/L)	23 (19, 39.5)	21 (17, 27)	0.019
Aspartate aminotransferase (U/L)	32 (23.5, 50)	27 (23, 34)	0.001
Gamma-glutamyl transferase (U/L)	74 (41, 151)	60.6 (36.5, 111)	0.065
Alkaline phosphatase (U/L)	106 (80.6, 142)	90 (72, 117)	0.006
Total protein (g/L)	61.1 (54.1, 66.9)	63.2 (58.7, 67.8)	0.018
Albumin (g/L)	33.2 (28.7, 39.8)	38.3 (34, 42)	< 0.001
Total bilirubin (μmol/L)	26.5 (14.8, 60.2)	21 (14.1, 31.5)	0.015
Prothrombin time (s)	16.3 (14.7, 18.5)	14.6 (13.7, 16.0)	< 0.001

BCS: Budd-Chiari syndrome; IVC: Inferior vena cava; HV: Hepatic veins; ALBI: Albumin-bilirubin; MELD: Model for end-stage liver disease.

using the C-index, which achieved values of 0.906 in the training set and 0.859 in the validation set, indicating excellent discrimination. The R + C model demonstrated better predictive performance compared to the clinical-only model (C model) and the radiomics-only model (Radscore; Table 4). ROC curves were generated to assess model discrimination over a 3-year follow-up period. The results showed that the R + C model achieved superior discrimination compared to the individual Radscore and C model, as reflected by its larger AUC in both the training and validation datasets (Figure 5). Calibration curves confirmed a strong alignment between predicted and observed outcomes (Figure 6), while

Table 2 Comparison of patient characteristics between the training and validation cohorts

Variables	Training cohort (*n* = 334)	Validation cohort (*n* = 110)	*P* value
Age (years)	51.4 ± 11.1	51.9 ± 10.3	0.663
Sex (male)	193 (57.8)	66 (60)	0.683
Diabetes	26 (7.8)	6 (5.5)	0.412
Ascites	131 (39.2)	46 (41.8)	0.630
Hepatic encephalopathy	10 (3)	3 (2.7)	1
IVC or HV thrombosis	60 (18)	28 (25.5)	0.087
Portal vein thrombosis	20 (6)	3 (2.7)	0.181
Spleen thickness (mm)	45 (39, 49)	43 (38, 51)	0.700
Portal vein diameter (mm)	12.7 (10.2, 14.6)	12.7 (10, 15)	0.763
BCS type			0.389
HV type	69 (20.6)	17 (15.5)	
Mixed type	227 (68)	77 (70)	
IVC type	38 (11.4)	16 (14.5)	
Child-Pugh grade			0.683
A	210 (62.9)	72 (65.4)	
B	110 (32.9)	32 (29.1)	
C	14 (4.2)	6 (5.5)	
ALBI, median (IQR)	-2.34 (-2.74, -1.89)	-2.31 (-2.64, -1.85)	0.494
MELD, median (IQR)	4.74 (2.18, 8.00)	4.14 (1.60, 7.34)	0.252
Use of anticoagulant medication	271 (81.1)	73 (66.4)	0.001
Invasive treatment to relieve hepatic venous outflow obstruction	276 (82.6)	95 (86.4)	0.360
White blood cell (× 10^9/L)	3.4 (2.7, 4.4)	3.7 (2.7, 5.0)	0.107
Red blood cell (× 10^{12}/L)	4.0 (3.5, 4.4)	4 (3.6, 4.6)	0.145
Hemoglobin (g/L)	122 (105, 136)	124 (106, 140.3)	0.358
Platelet (× 10^9/L)	86 (65, 118.3)	91 (67, 141)	0.434
Sodium (mmol/L)	142 (140, 143.5)	142 (140, 143.3)	0.677
Creatinine (μmol/L)	56 (47, 67)	55 (44, 65.3)	0.251
Alanine aminotransferase (U/L)	22 (17, 27.2)	19.7 (15.6, 29.1)	0.126
Aspartate aminotransferase (U/L)	28 (23, 35)	27.3 (21.7, 34.5)	0.357
Gamma-glutamyl transferase (U/L)	61 (35.8, 117)	64.2 (45.0, 111.6)	0.272
Alkaline phosphatase (U/L)	92 (72, 121.3)	96.4 (79, 127.3)	0.273
Total protein (g/L)	63.2 (58.5, 67.7)	62.6 (57.6, 67.6)	0.526
Albumin (g/L)	38 (33.3, 41.8)	37.7 (33.3, 41.3)	0.672
Total bilirubin (μmol/L)	21 (13.9, 33.4)	22.8 (15.1, 35.4)	0.536
Prothrombin time (s)	14.8 (13.8, 16.4)	14.6 (13.2, 16.1)	0.064

BCS: Budd-Chiari syndrome; IVC: Inferior vena cava; HV: Hepatic veins; ALBI: Albumin-bilirubin; MELD: Model for end-stage liver disease.

DCA demonstrated the superior net clinical benefit of the R + C model across a wide range of threshold probabilities (Figure 7).

Clinical performance and risk stratification

According to the R + C model, the risk analysis was performed for individuals diagnosed with BCS complicated by GEVs. The relevant equation was as follows: Risk assessment = 0.847 Sex - 0.008 platelet count - 2.417 invasive treatment to

Table 3 Univariate and multivariate analyses of factors associated with gastroesophageal variceal bleeding in patients with Budd-Chiari syndrome and gastroesophageal varices

Variables	Univariate cox regression		Multivariate cox regression	
	HR (95%CI)	*P* value	HR (95%CI)	*P* value
Age	0.994 (0.968-1.020)	0.646		
Sex	3.621 (1.686-7.777)	0.001		
Hepatic encephalopathy	0.712 (0.098-5.166)	0.737		
Diabetes	0.535 (0.130-2.209)	0.388		
Portal vein thrombosis	3.329 (1.486-7.460)	0.003		
IVC or HV thrombosis	0.696 (0.295-1.645)	0.409		
Invasive treatment to relieve hepatic venous outflow obstruction	0.127 (0.070-0.230)	< 0.001	0.123 (0.048-0.318)	<0.001
Use of anticoagulant medication	3.408 (1.056-10.994)	0.040	8.905 (2.296-34.534)	0.002
Ascites	1.798 (1.001-3.229)	0.050		
Portal vein diameter (mm)	1.003 (0.915-1.099)	0.953		
Spleen thickness (mm)	1.041 (1.015-1.068)	0.002		
White blood cell ($\times 10^9$/L)	1.071 (0.946-1.221)	0.271		
Red blood cell ($\times 10^{12}$/L)	0.563 (0.388-0.818)	0.003		
Hemoglobin (g/L)	0.976 (0.965-0.986)	< 0.001	0.974 (0.955-0.994)	0.012
Platelet ($\times 10^9$/L)	0.988 (0.979-0.997)	0.006		
Sodium (mmol/L)	0.828 (0.773-0.887)	< 0.001		
Creatinine (μmol/L)	1.025 (1.014-1.037)	< 0.001		
Aspartate aminotransferase (U/L)	1.009 (1.001-1.017)	0.020		
Gamma-glutamyl transferase (U/L)	1.000 (0.998-1.002)	0.864		
Alkaline phosphatase (U/L)	1.004 (1.002-1.007)	0.002		
Albumin	0.899 (0.861-0.939)	< 0.001		
Direct bilirubin	1.012 (1.007-1.016)	< 0.001		
Prothrombin time	1.080 (1.047-1.113)	< 0.001		
BCS type		0.081		
Mixed type *vs* HV type	0.501 (0.265-0.945)	0.033		
IVC type *vs* HV type	0.450 (0.149-1.355)	0.156		
Child		< 0.001		
B *vs* A	1.408 (0.706-2.808)	0.311		
C *vs* A	14.353 (6.881-29.937)	< 0.001		

HR: Hazard ratio; 95%CI: 95% confidence interval; BCS: Budd-Chiari syndrome; IVC: Inferior vena cava; HV: Hepatic veins; ALBI: Albumin-bilirubin; MELD: Model for end-stage liver disease.

relieve hepatic venous outflow obstruction + 2.366 use of anticoagulant medication + 0.435 Radscore. The specific threshold was identified through X-tile, and all participants were classified into low-, moderate- or high-risk categories according to their likelihood of bleeding (low risk: < 0.57; medium risk: 0.57-1.11; high risk: > 1.11). In the training set, the cumulative occurrence rates of variceal hemorrhage were 2.2%, 14.7% and 85.3% for the low-, moderate- and high-risk groups, respectively (log-rank test, $P < 0.001$; Figure 8A). Within the validation group, the cumulative incidence rates were 3.9%, 17.4% and 90% for each group (log-rank test, $P < 0.001$; Figure 8B), which suggests that the model effectively differentiated the risk of variceal bleeding in patients with BCS complicated by GEVs.

Table 4 C-indices of various models

Variables	Training cohort			Validation cohort		
	C-index (95%CI)	AIC	*P* value	C-index (95%CI)	AIC	*P* value
R + C model	0.906 (0.864-0.947)	407.267	-	0.859 (0.761-0.958)	112.684	-
R model	0.825 (0.761-0.889)	474.138	0.006	0.706 (0.566-0.846)	142.004	0.015
C model	0.802 (0.724-0.879)	442.580	0.003	0.699 (0.539-0.859)	136.163	0.035
MELD	0.721 (0.646-0.796)	481.666	< 0.001	0.635 (0.485-0.786)	147.129	0.002
ALBI	0.667 (0.581-0.753)	490.816	< 0.001	0.634 (0.491-0.776)	147.705	0.004

R + C: Radiomic + clinical model; R: Radiomic model; C: Clinical model; MELD: Model for end-stage liver disease; ALBI: Albumin-bilirubin; 95%CI: 95% confidence Interval; AIC: Akaike information criterion.

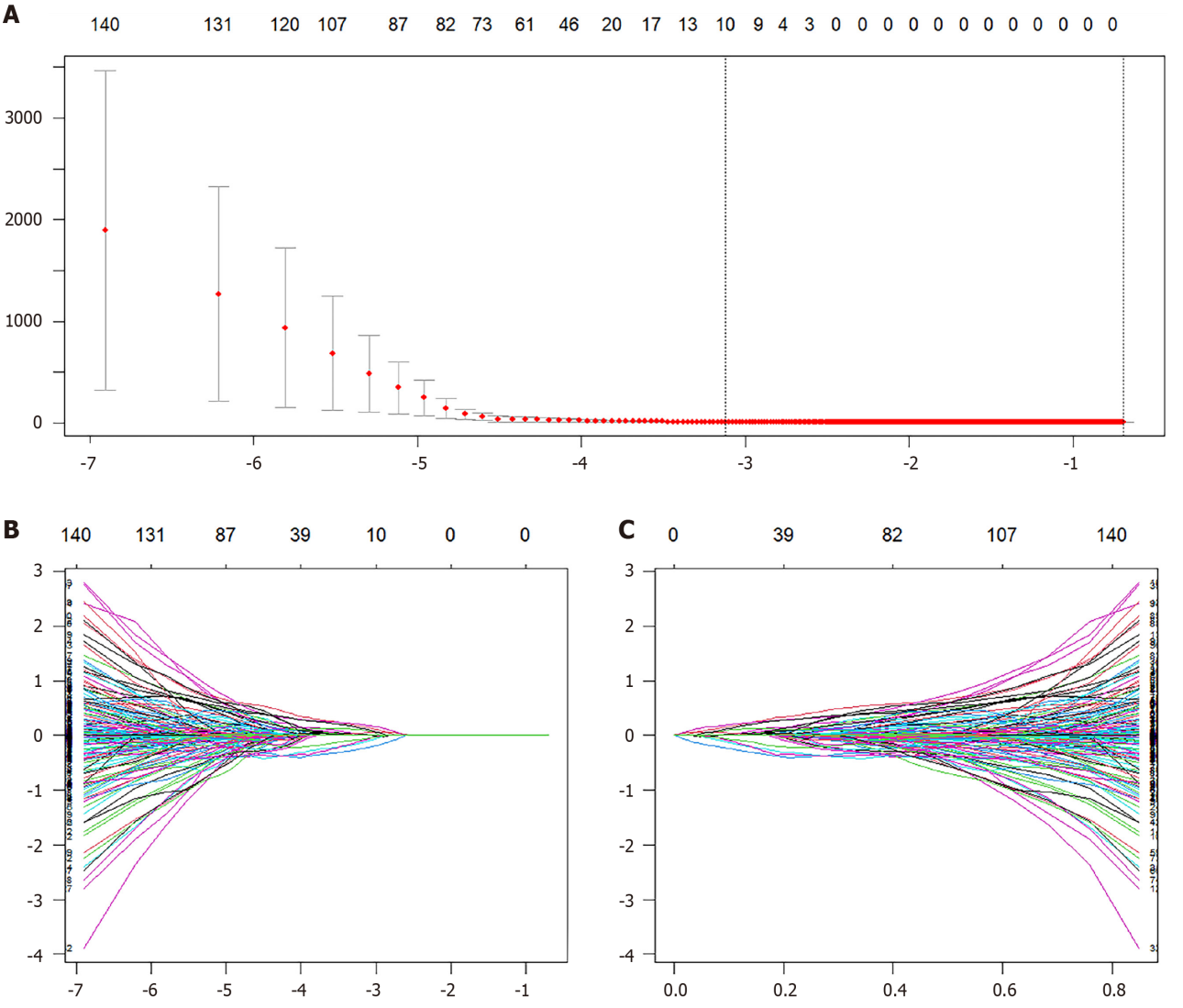

Figure 3 The LASSO-regularized Cox regression for radiomics feature selection is illustrated. Ten-fold cross-validation was used to determine the optimal model parameter (*λ*). A: Relationship between the partial likelihood deviance and log(*λ*), which aided in selecting the optimal *λ* value; B: Coefficient profiles of all candidate features as a function of log(*λ*), with each colored line representing a different feature; C: Trajectories of the feature coefficients relative to the fraction of deviance explained.

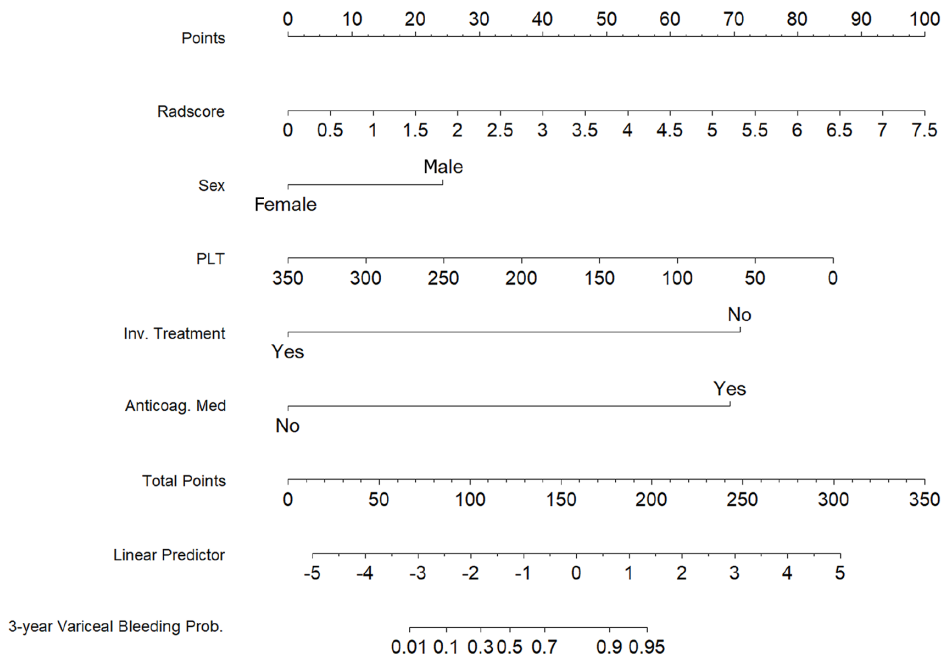

Figure 4 Nomogram for predicting the probability of variceal hemorrhage in patients with gastroesophageal varices associated with Budd-Chiari syndrome. PLT: Platelet count; Inv.Treatment: Invasive treatment to relieve hepatic venous outflow obstruction; Anticoag.med: Use of anticoagulant medication.

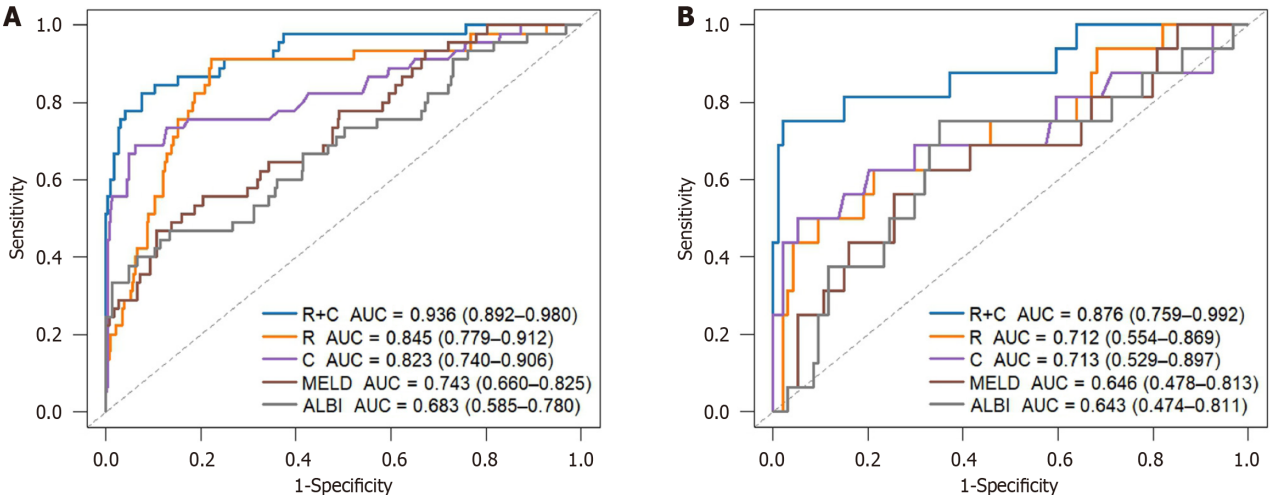

Figure 5 Receiver operating characteristic curves of the nomogram. A: Receiver operating characteristic (ROC) curve in the training cohort; B: ROC curve in the validation cohort. R + C: Radiomic + clinical model; R: Radiomic model; C: Clinical model; MELD: Model for end-stage liver disease; ALBI: Albumin-bilirubin; AUC: The area under the receiver operating characteristic curves.

DISCUSSION

This study successfully developed and validated a noninvasive risk prediction model (R + C model) by integrating radiomics features with clinical characteristics to evaluate the risk of first variceal bleeding in BCS patients with GEVs. The model incorporated Radscore and key clinical predictors, such as invasive treatments to alleviate hepatic venous outflow obstruction, anticoagulation use, sex, and platelet count, significantly enhancing the accuracy of bleeding risk prediction. This model provides an effective tool for the management and treatment of BCS patients.

Radiomics technology, as a novel imaging analysis method, has been extensively applied in the oncology field[11-14]. It has also shown substantial potential in diagnosing and predicting outcomes in non-oncological liver diseases, such as liver fibrosis and portal hypertension syndrome[4,15-18]. For example, Luo *et al*[15] successfully predicted the risk of bleeding in cirrhotic patients by constructing liver and spleen radiomics models. Zhang *et al*[4] explored the risk of variceal bleeding in hepatitis-B-related cirrhotic patients within 1 year. Due to the distinct pathophysiological characteristics of BCS, which mainly manifest as hepatic venous outflow obstruction, the risk of variceal bleeding and treatment response in BCS patients differ significantly from those in cirrhotic patients[19,20]. China, being the country with the

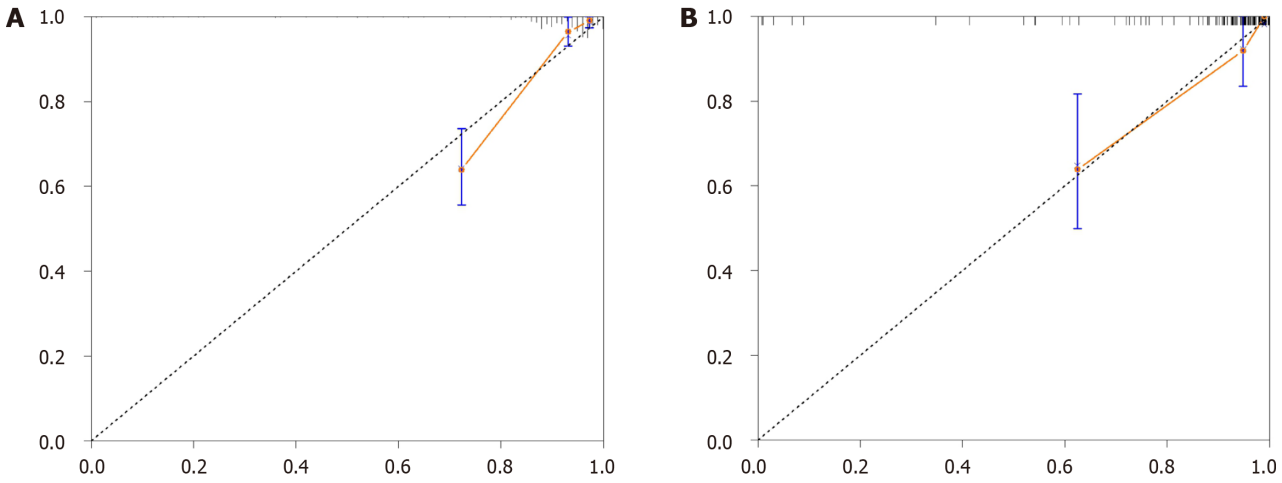

Figure 6 Calibration curves of the radiomic and clinical model. A: Calibration curve in the training cohort; B: Calibration curve in the validation cohort.

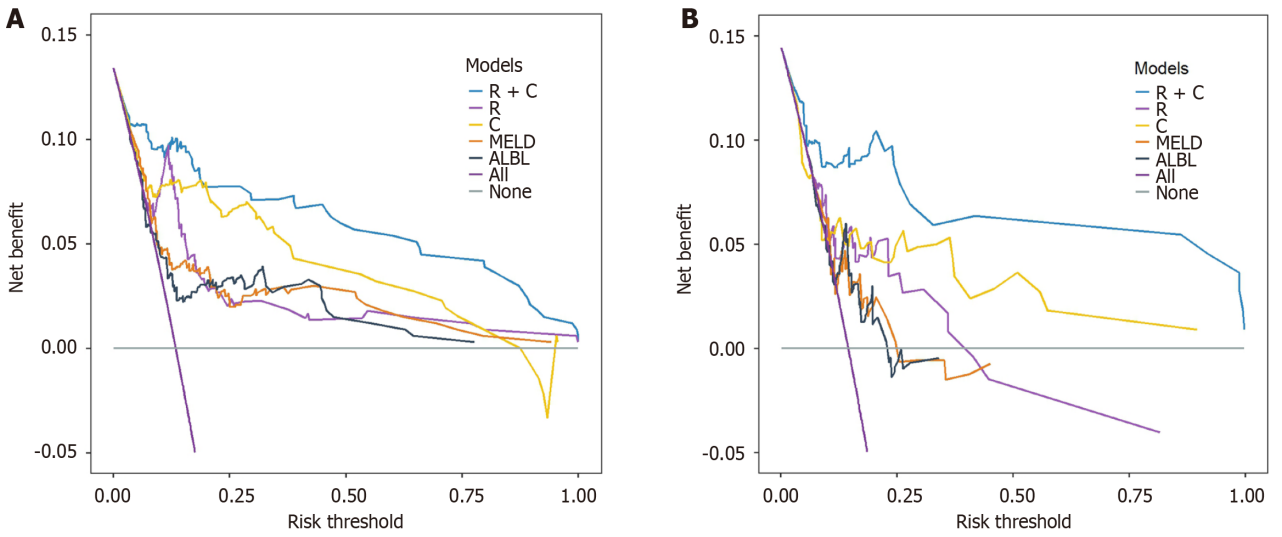

Figure 7 Decision curve analysis of the nomogram. A: Decision curve analysis (DCA) in the training cohort; B: DCA in the validation cohort. R + C: Radiomic + clinical model; R: Radiomic model; C: Clinical model; MELD: Model for end-stage liver disease; ALBI: Albumin-bilirubin.

highest number of diagnosed BCS cases globally, still lacks a comprehensive risk prediction model for variceal bleeding in BCS patients[21,22]. This study innovatively combined liver and spleen radiomics features with clinical factors, significantly improving the predictive ability for variceal bleeding risk in BCS patients. It enables the development of more precise treatment strategies based on individual risk levels, thereby optimizing personalized management and significantly improving patient outcomes.

In this study, we found that invasive treatments and anticoagulation therapy are independent risk factors for variceal bleeding in BCS patients with GEVs. Invasive treatments, such as TIPS and angioplasty, effectively reduce the risk of variceal bleeding by relieving hepatic venous outflow obstruction and lowering portal pressure[3]. However, invasive procedures themselves carry a risk of treatment-related bleeding events (*e.g.*, procedural site bleeding or abdominal hemorrhage), which are typically observed within 24-48 hours post-procedure. Although this type of bleeding is distinct from variceal bleeding, as it is more closely associated with procedural trauma and the intensity of pre-procedural anticoagulation therapy, it highlights the complex interplay between invasive treatments and anticoagulation management in BCS patients. For example, Rautou *et al*[23] reported that in BCS patients undergoing TIPS or other invasive treatments, excessive pre-procedural anticoagulation significantly increased the risk of procedural bleeding events, underscoring the need for balanced anticoagulation protocols. Similarly, our study identified anticoagulation therapy as an independent risk factor for variceal bleeding, which may reflect the broader challenge of managing anticoagulation intensity and timing in BCS patients with GEVs. These findings emphasize the importance of tailoring anticoagulation therapy to individual patient needs, especially in the context of invasive treatments, to minimize both treatment-related and variceal bleeding risks.

Although invasive treatments are beneficial in reducing portal pressure and the long-term risk of variceal bleeding, inappropriate anticoagulation therapy [*e.g.*, excessive dosage, improper timing, or insufficient international normalized ratio (INR) monitoring] may exacerbate the risk of variceal bleeding[24]. In BCS patients with GEVs, this risk may be

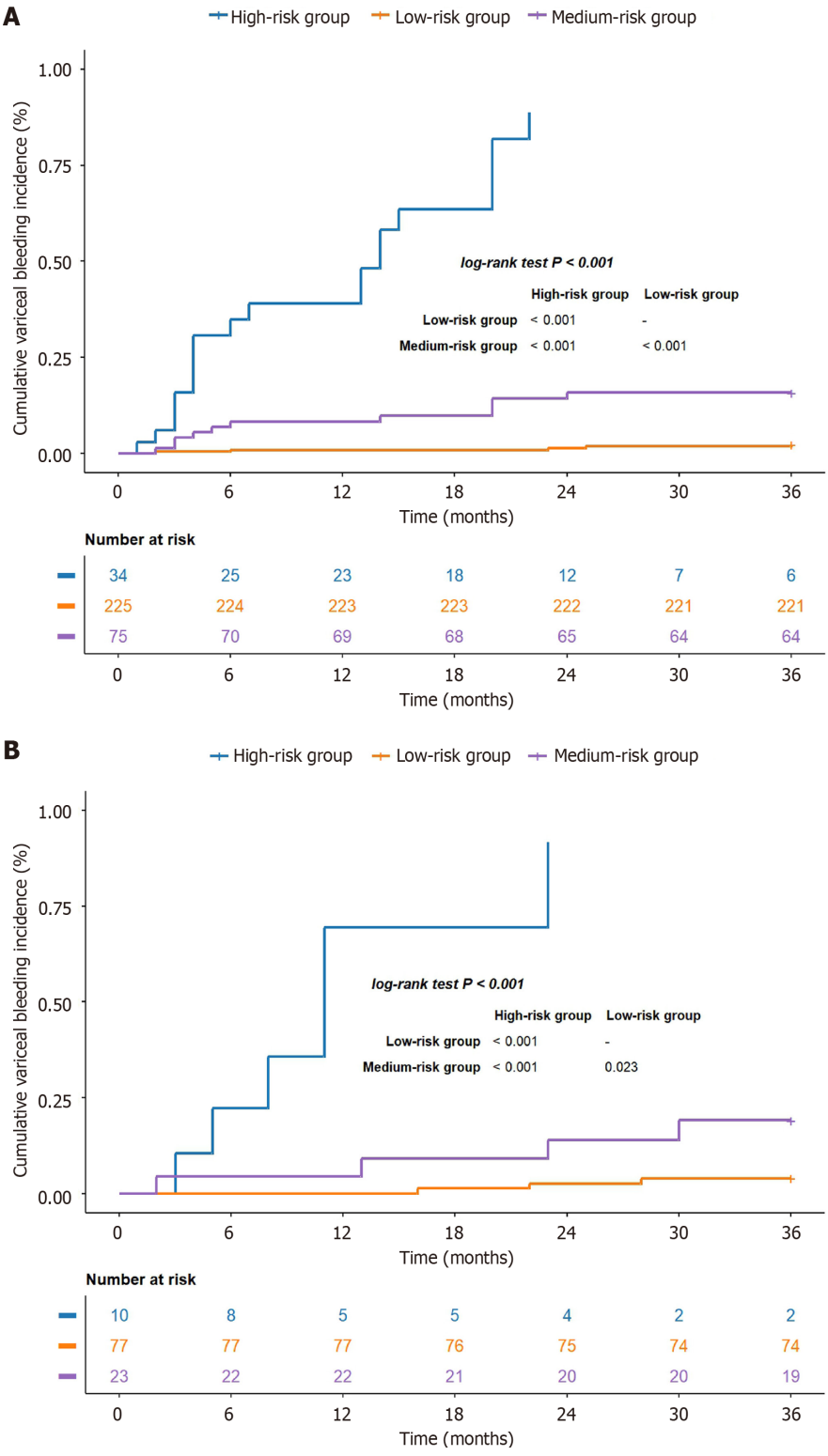

Figure 8 Cumulative risk curves stratified by the risk score. A: Cumulative risk curve in the training cohort; B: Cumulative risk curve in the validation cohort.

further amplified due to existing portal hypertension and variceal fragility. Our findings suggest that careful evaluation and optimization of anticoagulation protocols are critical for balancing the risks and benefits of therapy. Specifically, for patients undergoing invasive treatments, it is necessary to comprehensively evaluate the intensity and timing of anticoagulation therapy before, during and after the procedure. Strict adherence to anticoagulation protocols, including individualized dosing and careful INR monitoring, can mitigate the risk of variceal bleeding while preventing treatment-related bleeding events. Additionally, future research should focus on developing evidence-based guidelines to further refine anticoagulation management strategies in BCS patients.

Our study identified male sex as a significant risk factor for variceal bleeding, in contrast to previous studies that reported a higher incidence of portal-hypertension-related complications in female patients[25,26]. This discrepancy may be attributed to differences in patient characteristics, study design or clinical management strategies. In our cohort, male patients demonstrated a higher mean spleen thickness (46.36 mm *vs* 42.99 mm) and portal vein diameter (12.98 mm *vs* 12.00 mm) compared to females; both of which are recognized markers of severe portal hypertension. These findings may indirectly contribute to the observed increased bleeding risk in male patients. Additionally, it is possible that male patients were less adherent to anticoagulation protocols or presented with more advanced disease at the time of diagnosis, as suggested by prior studies in similar populations[27]. Hormonal differences, such as the vascular protective effects of estrogen in females, might also play a role in reducing bleeding risk in female patients. However, these hypotheses could not be directly evaluated in the present study due to the retrospective design and require further investigation in larger, prospective cohorts. Understanding these sex-based variations is essential for tailoring individualized management strategies in BCS patients with GEVs.

Platelet count also plays a crucial role in assessing bleeding risk. BCS patients often develop splenomegaly, resulting in thrombocytopenia, which indicates increased portal hypertension severity and a higher risk of variceal bleeding[28,29]. Our findings confirmed that low platelet count is significantly associated with bleeding risk, thereby improving the model's predictive capability and offering clinicians a more comprehensive assessment tool.

In terms of diagnostic methods, this study used portal venous phase contrast-enhanced CT, which not only facilitates the diagnosis of BCS but also effectively evaluates GEVs, providing a comprehensive assessment of patients[30,31]. Compared with traditional endoscopy, enhanced CT offers noninvasive, highly sensitive and simultaneous evaluation of hepatic and splenic hemodynamics[32-34]. This imaging technology serves as a reliable alternative for patients unsuitable for endoscopy, reducing discomfort and potential complications during examinations and providing crucial pathophysiological information for clinical decision-making.

The risk stratification system based on the R + C model divided patients into low-, medium-, and high-risk groups, with a significant difference in variceal bleeding incidence between the groups. The bleeding incidence in the high-risk group was significantly higher than that in the medium- and low-risk groups. This risk stratification system offers valuable guidance for the clinical management of BCS patients with GEVs.

In this study, the bleeding rate in the high-risk group reached 85.3%, indicating a high risk of variceal rupture and bleeding. For these patients, we recommend active preventive interventions, such as endoscopic treatment (*e.g.*, endoscopic variceal ligation or sclerotherapy)[35]. Additionally, if high-risk patients experience recurrent hepatic venous outflow obstruction or other portal-hypertension-related complications (*e.g.*, symptoms of portal hypertension not effectively controlled by medication or endoscopic therapy), TIPS treatment should be considered under certain circumstances even if the standard indications for TIPS have not yet been met[36]. TIPS can improve hepatic venous outflow and reduce portal pressure, thereby decreasing the risk of variceal bleeding. It is a safe and effective treatment option[37]. Therefore, for high-risk patients, a comprehensive assessment of their condition and potential benefits should be conducted, and TIPS intervention should be actively considered when necessary to prevent bleeding events.

For medium-risk patients, the bleeding rate was 14.7%, comparable to the annual bleeding rate reported in cirrhotic patients with GEVs (10%-15%)[4,5]. Therefore, we recommend that medium-risk patients be managed according to standard preventive strategies outlined in existing guidelines, including the use of nonselective beta-blockers (*e.g.*, propranolol) to reduce portal pressure and regular endoscopic surveillance to monitor variceal progression. For patients with high-risk features of variceal bleeding (*e.g.*, severe varices or red wale marks) or significantly elevated portal pressure (hepatic venous pressure gradient > 12 mmHg), enhanced endoscopic therapy and medication management are recommended to further reduce bleeding risk, along with close monitoring of disease progression. If conventional treatment is ineffective or the condition continues to worsen, early TIPS intervention should be considered to further reduce the risk of bleeding[7].

For low-risk patients, the incidence of variceal bleeding was only 2.2%, indicating a low overall bleeding risk. For these patients, we recommend regular follow-up and monitoring of hepatic venous outflow patency, with timely adjustment of management strategies if significant changes in imaging parameters or hemodynamic indicators are observed[38]. The use of nonselective beta-blockers (*e.g.*, propranolol) in low-risk patients should be approached cautiously, especially in cases of hemodynamic instability or poor liver function reserve, where a thorough evaluation of potential adverse effects and benefits is necessary to avoid unnecessary interventions and treatments[39].

This study developed and validated a noninvasive risk prediction model integrating radiomics and clinical characteristics, demonstrating excellent predictive performance and clinical utility. However, several limitations need to be addressed. First, as a retrospective study, potential selection bias and the limited sample size may affect the generalization of the findings. While BCS in western populations is often driven by thrombophilic states (*e.g.*, factor V Leiden mutation), BCS in China predominantly arises from membranous obstruction of the inferior vena cava or short-segment hepatic vein stenosis. Consequently, our institutional protocol favors endovascular interventions (*e.g.*, angioplasty or TIPS), followed by bridging low-molecular-weight heparin and long-term warfarin therapy, rather than routine thrombophilia workup or first-line use of direct oral anticoagulants[2]. Therefore, larger multicenter or prospective studies - including settings where thrombophilia-driven BCS prevails - are needed to validate the stability and applicability of our model across diverse etiological and therapeutic contexts. Second, the use of single-level ROIs for the liver and spleen may not fully capture the heterogeneity of the entire organ. Although these specific levels are clinically relevant for assessing portal and splenic hemodynamics, volumetric ROIs or multislice approaches should be considered to better characterize tissue variability. Finally, greater automation and standardization of radiomics feature extraction would enhance the clinical feasibility of the model. Global validation in broader populations remains critical to confirm the robustness and facilitate wider adoption of this approach.

CONCLUSION

This study was the first to combine radiomics and clinical characteristics to develop a noninvasive model capable of predicting variceal bleeding risk in BCS patients with GEVs. The model demonstrated excellent predictive performance in clinical applications and provides robust support for individualized patient management and treatment strategies.

ACKNOWLEDGMENTS

We would like to thank our colleagues in the Department of Hepatopancreatobiliary Surgery and the Department of Hematology at Zhengzhou University People's Hospital, as well as those in the Department of Hepatopancreatobiliary Surgery at The First Affiliated Hospital of Zhengzhou University for their valuable contributions.

FOOTNOTES

Author contributions: Wang ZD and Nan HJ contributed equally to this work as co-first authors; they were responsible for designing the study, collecting and analyzing data, and writing the manuscript; Dang XW and Bai YL contributed equally by guiding the overall content and ensuring the scientific rigor of the article as co-corresponding authors; Dang XW is designated as the primary corresponding author for journal communications; Li SX, Li LH, Liu ZC, Guo HH, Li L, Liu SY and Li H provided technical support; all authors have read and approve the final manuscript.

Supported by Natural Science Foundation of Henan Province, China, No. 232300420232; and Henan Provincial Key Research and Development Project, No. 231111313500.

Institutional review board statement: The study was reviewed and approved by the Ethics Committee of the First Affiliated Hospital of Zhengzhou University (No. 2021-KY-1137-002).

Informed consent statement: As a retrospective observational study, the requirement for informed consent was waived. To ensure confidentiality, all private patient information was deidentified before analysis.

Conflict-of-interest statement: The authors declare that the research was conducted in the absence of any commercial or financial relationships.

Data sharing statement: The data supporting the findings of this study are included in the article and its supplementary materials. Further inquiries can be directed to the corresponding authors.

Country of origin: China

ORCID number: Lu-Hao Li 0000-0001-6676-3914; Yan-Liang Bai 0000-0003-2422-7720; Xiao-Wei Dang 0000-0001-7940-6385.

S-Editor: Lin C
L-Editor: A
P-Editor: Zhao S

REFERENCES

1 **Borsani O**, Pietra D, Rumi E. Primary Budd-Chiari Syndrome. *N Engl J Med* 2023; **389**: 769 [PMID: 37611130 DOI: 10.1056/NEJMc2305391]

2 **Budd-Chiari Syndrome and Hepatic Vascular Diseases Professional Committee of Chinese Research Hospital Association**. [Chinese multidisciplinary collaborative expert consensus for the diagnosis and treatment of Budd-Chiari syndrome (2021 version)]. *Zhonghua Wai Ke Za Zhi* 2022; **60**: 329-336 [PMID: 35272423 DOI: 10.3760/cma.j.cn112139-20211224-00619]

3 **Shukla A**, Shreshtha A, Mukund A, Bihari C, Eapen CE, Han G, Deshmukh H, Cua IHY, Lesmana CRA, Al Meshtab M, Kage M, Chaiteeraki R, Treeprasertsuk S, Giri S, Punamiya S, Paradis V, Qi X, Sugawara Y, Abbas Z, Sarin SK. Budd-Chiari syndrome: consensus guidance of the Asian Pacific Association for the study of the liver (APASL). *Hepatol Int* 2021; **15**: 531-567 [PMID: 34240318 DOI: 10.1007/s12072-021-10189-4]

4 **Zhang Q**, Niu S, Yang L, Zhu B, Shi K, Zhang X, Zhang Y, Bi Y, Mu Y, Wang X. A novel prognostic model for predicting the risk of first variceal hemorrhage in patients with HBV-related cirrhosis. *Front Cell Infect Microbiol* 2023; **13**: 1062172 [PMID: 36733609 DOI: 10.3389/fcimb.2023.1062172]

5 **Chen J**, Luo S, Tang F, Han M, Zheng J, Deng M, Luo G. Development and validation of a practical prognostic nomogram for evaluating

inpatient mortality of cirrhotic patients with acute variceal hemorrhage. *Ann Hepatol* 2023; **28**: 101086 [PMID: 36889674 DOI: 10.1016/j.aohep.2023.101086]

6 **Zhou PL**, Wu G, Han XW, Yan L, Zhang WG. Budd-Chiari syndrome with upper gastrointestinal hemorrhage: Characteristic and long-term outcomes of endovascular treatment. *Vascular* 2017; **25**: 642-648 [PMID: 28610476 DOI: 10.1177/1708538117710087]

7 **Gralnek IM**, Camus Duboc M, Garcia-Pagan JC, Fuccio L, Karstensen JG, Hucl T, Jovanovic I, Awadie H, Hernandez-Gea V, Tantau M, Ebigbo A, Ibrahim M, Vlachogiannakos J, Burgmans MC, Rosasco R, Triantafyllou K. Endoscopic diagnosis and management of esophagogastric variceal hemorrhage: European Society of Gastrointestinal Endoscopy (ESGE) Guideline. *Endoscopy* 2022; **54**: 1094-1120 [PMID: 36174643 DOI: 10.1055/a-1939-4887]

8 **Whybra P**, Zwanenburg A, Andrearczyk V, Schaer R, Apte AP, Ayotte A, Baheti B, Bakas S, Bettinelli A, Boellaard R, Boldrini L, Buvat I, Cook GJR, Dietsche F, Dinapoli N, Gabryś HS, Goh V, Guckenberger M, Hatt M, Hosseinzadeh M, Iyer A, Lenkowicz J, Loutfi MAL, Löck S, Marturano F, Morin O, Nioche C, Orlhac F, Pati S, Rahmim A, Rezaeijo SM, Rookyard CG, Salmanpour MR, Schindele A, Shiri I, Spezi E, Tanadini-Lang S, Tixier F, Upadhaya T, Valentini V, van Griethuysen JJM, Yousefirizi F, Zaidi H, Müller H, Vallières M, Depeursinge A. The Image Biomarker Standardization Initiative: Standardized Convolutional Filters for Reproducible Radiomics and Enhanced Clinical Insights. *Radiology* 2024; **310**: e231319 [PMID: 38319168 DOI: 10.1148/radiol.231319]

9 **Zwanenburg A**, Vallières M, Abdalah MA, Aerts HJWL, Andrearczyk V, Apte A, Ashrafinia S, Bakas S, Beukinga RJ, Boellaard R, Bogowicz M, Boldrini L, Buvat I, Cook GJR, Davatzikos C, Depeursinge A, Desseroit MC, Dinapoli N, Dinh CV, Echegaray S, El Naqa I, Fedorov AY, Gatta R, Gillies RJ, Goh V, Götz M, Guckenberger M, Ha SM, Hatt M, Isensee F, Lambin P, Leger S, Leijenaar RTH, Lenkowicz J, Lippert F, Losnegård A, Maier-Hein KH, Morin O, Müller H, Napel S, Nioche C, Orlhac F, Pati S, Pfaehler EAG, Rahmim A, Rao AUK, Scherer J, Siddique MM, Sijtsema NM, Socarras Fernandez J, Spezi E, Steenbakkers RJHM, Tanadini-Lang S, Thorwarth D, Troost EGC, Upadhaya T, Valentini V, van Dijk LV, van Griethuysen J, van Velden FHP, Whybra P, Richter C, Löck S. The Image Biomarker Standardization Initiative: Standardized Quantitative Radiomics for High-Throughput Image-based Phenotyping. *Radiology* 2020; **295**: 328-338 [PMID: 32154773 DOI: 10.1148/radiol.2020191145]

10 **Guiot J**, Vaidyanathan A, Deprez L, Zerka F, Danthine D, Frix AN, Lambin P, Bottari F, Tsoutzidis N, Miraglio B, Walsh S, Vos W, Hustinx R, Ferreira M, Lovinfosse P, Leijenaar RTH. A review in radiomics: Making personalized medicine a reality *via* routine imaging. *Med Res Rev* 2022; **42**: 426-440 [PMID: 34309893 DOI: 10.1002/med.21846]

11 **Mayerhoefer ME**, Materka A, Langs G, Häggström I, Szczypiński P, Gibbs P, Cook G. Introduction to Radiomics. *J Nucl Med* 2020; **61**: 488-495 [PMID: 32060219 DOI: 10.2967/jnumed.118.222893]

12 **Bera K**, Braman N, Gupta A, Velcheti V, Madabhushi A. Predicting cancer outcomes with radiomics and artificial intelligence in radiology. *Nat Rev Clin Oncol* 2022; **19**: 132-146 [PMID: 34663898 DOI: 10.1038/s41571-021-00560-7]

13 **Harding-Theobald E**, Louissaint J, Maraj B, Cuaresma E, Townsend W, Mendiratta-Lala M, Singal AG, Su GL, Lok AS, Parikh ND. Systematic review: radiomics for the diagnosis and prognosis of hepatocellular carcinoma. *Aliment Pharmacol Ther* 2021; **54**: 890-901 [PMID: 34390014 DOI: 10.1111/apt.16563]

14 **Liu Z**, Wang S, Dong D, Wei J, Fang C, Zhou X, Sun K, Li L, Li B, Wang M, Tian J. The Applications of Radiomics in Precision Diagnosis and Treatment of Oncology: Opportunities and Challenges. *Theranostics* 2019; **9**: 1303-1322 [PMID: 30867832 DOI: 10.7150/thno.30309]

15 **Luo R**, Gao J, Gan W, Xie WB. Clinical-radiomics nomogram for predicting esophagogastric variceal bleeding risk noninvasively in patients with cirrhosis. *World J Gastroenterol* 2023; **29**: 1076-1089 [PMID: 36844133 DOI: 10.3748/wjg.v29.i6.1076]

16 **Yang JQ**, Zeng R, Cao JM, Wu CQ, Chen TW, Li R, Zhang XM, Ou J, Li HJ, Mu QW. Predicting gastro-oesophageal variceal bleeding in hepatitis B-related cirrhosis by CT radiomics signature. *Clin Radiol* 2019; **74**: 976.e1-976.e9 [PMID: 31604574 DOI: 10.1016/j.crad.2019.08.028]

17 **Lin Y**, Li L, Yu D, Liu Z, Zhang S, Wang Q, Li Y, Cheng B, Qiao J, Gao Y. A novel radiomics-platelet nomogram for the prediction of gastroesophageal varices needing treatment in cirrhotic patients. *Hepatol Int* 2021; **15**: 995-1005 [PMID: 34115257 DOI: 10.1007/s12072-021-10208-4]

18 **Meng D**, Wei Y, Feng X, Kang B, Wang X, Qi J, Zhao X, Zhu Q. CT-Based Radiomics Score Can Accurately Predict Esophageal Variceal Rebleeding in Cirrhotic Patients. *Front Med (Lausanne)* 2021; **8**: 745931 [PMID: 34805214 DOI: 10.3389/fmed.2021.745931]

19 **Turon F**, Casu S, Hernández-Gea V, Garcia-Pagán JC. Variceal and other portal hypertension related bleeding. *Best Pract Res Clin Gastroenterol* 2013; **27**: 649-664 [PMID: 24160925 DOI: 10.1016/j.bpg.2013.08.004]

20 **Diaz-Soto MP**, Garcia-Tsao G. Management of varices and variceal hemorrhage in liver cirrhosis: a recent update. *Therap Adv Gastroenterol* 2022; **15**: 17562848221101712 [PMID: 35757384 DOI: 10.1177/17562848221101712]

21 **Wang Z**, Wang Z, Zhang Z, Li J, Pan Z, Liu A, Lu J, Guo J, Zu M, Xu H. Establishment and validation of a prediction model for the first recurrence of Budd-Chiari syndrome after endovascular treatment: a large sample size, single-center retrospective study. *Hepatol Int* 2023; **17**: 159-169 [PMID: 36567373 DOI: 10.1007/s12072-022-10464-y]

22 **Cheng D**, Xu H, Lu ZJ, Hua R, Qiu H, Du H, Xu X, Zhang J. Clinical features and etiology of Budd-Chiari syndrome in Chinese patients: a single-center study. *J Gastroenterol Hepatol* 2013; **28**: 1061-1067 [PMID: 23425079 DOI: 10.1111/jgh.12140]

23 **Rautou PE**, Douarin L, Denninger MH, Escolano S, Lebrec D, Moreau R, Vidaud M, Itzykson R, Moucari R, Bezeaud A, Valla D, Plessier A. Bleeding in patients with Budd-Chiari syndrome. *J Hepatol* 2011; **54**: 56-63 [PMID: 20889223 DOI: 10.1016/j.jhep.2010.06.019]

24 **Sharma A**, Goel A, Moses V, Keshava SN, Zachariah UG, Elias E, Eapen CE. Anticoagulating Budd-Chiari syndrome patients presenting with variceal bleed: A retrospective study. *J Gastroenterol Hepatol* 2020; **35**: 1397-1403 [PMID: 31900982 DOI: 10.1111/jgh.14971]

25 **Bizzaro D**, Becchetti C, Trapani S, Lavezzo B, Zanetto A, D'Arcangelo F, Merli M, Lapenna L, Invernizzi F, Taliani G, Burra P; AISF Special Interest Group on Gender in Hepatology. Influence of sex in alcohol-related liver disease: Pre-clinical and clinical settings. *United European Gastroenterol J* 2023; **11**: 218-227 [PMID: 36866682 DOI: 10.1002/ueg2.12370]

26 **Neong SF**, Billington EO, Congly SE. Sexual Dysfunction and Sex Hormone Abnormalities in Patients With Cirrhosis: Review of Pathogenesis and Management. *Hepatology* 2019; **69**: 2683-2695 [PMID: 30468515 DOI: 10.1002/hep.30359]

27 **Rauch U**. Gender differences in anticoagulation and antithrombotic therapy. *Handb Exp Pharmacol* 2012; 523-542 [PMID: 23027465 DOI: 10.1007/978-3-642-30726-3_23]

28 **Mendizabal M**, Cançado GGL, Albillos A. Evolving portal hypertension through Baveno VII recommendations. *Ann Hepatol* 2024; **29**: 101180 [PMID: 37984701 DOI: 10.1016/j.aohep.2023.101180]

29 **Brusilovskaya K**, Hofer BS, Simbrunner B, Eichelberger B, Lee S, Bauer DJM, Mandorfer M, Schwabl P, Panzer S, Reiberger T, Gremmel T. Platelet Function Decreases with Increasing Severity of Liver Cirrhosis and Portal Hypertension-A Prospective Study. *Thromb Haemost* 2023; **123**: 1140-1150 [PMID: 37517407 DOI: 10.1055/s-0043-1771187]

30 **Darwish Murad S**, Plessier A, Hernandez-Guerra M, Fabris F, Eapen CE, Bahr MJ, Trebicka J, Morard I, Lasser L, Heller J, Hadengue A, Langlet P, Miranda H, Primignani M, Elias E, Leebeek FW, Rosendaal FR, Garcia-Pagan JC, Valla DC, Janssen HL; EN-Vie (European Network for Vascular Disorders of the Liver). Etiology, management, and outcome of the Budd-Chiari syndrome. *Ann Intern Med* 2009; **151**: 167-175 [PMID: 19652186 DOI: 10.7326/0003-4819-151-3-200908040-00004]

31 **Porrello G**, Mamone G, Miraglia R. Budd-Chiari Syndrome Imaging Diagnosis: State of the Art and Future Perspectives. *Diagnostics (Basel)* 2023; **13** [PMID: 37443650 DOI: 10.3390/diagnostics13132256]

32 **Kim SH**, Kim YJ, Lee JM, Choi KD, Chung YJ, Han JK, Lee JY, Lee MW, Han CJ, Choi JI, Shin KS, Choi BI. Esophageal varices in patients with cirrhosis: multidetector CT esophagography--comparison with endoscopy. *Radiology* 2007; **242**: 759-768 [PMID: 17229872 DOI: 10.1148/radiol.2423050784]

33 **Salahshour F**, Mehrabinejad MM, Rashidi Shahpasandi MH, Salahshour M, Shahsavari N, Nassiri Toosi M, Ayoobi Yazdi N. Esophageal variceal hemorrhage: the role of MDCT characteristics in predicting the presence of varices and bleeding risk. *Abdom Radiol (NY)* 2020; **45**: 2305-2314 [PMID: 32447415 DOI: 10.1007/s00261-020-02585-5]

34 **Calame P**, Ronot M, Bouveresse S, Cervoni JP, Vilgrain V, Delabrousse É. Predictive value of CT for first esophageal variceal bleeding in patients with cirrhosis: Value of para-umbilical vein patency. *Eur J Radiol* 2017; **87**: 45-52 [PMID: 28065374 DOI: 10.1016/j.ejrad.2016.12.006]

35 **Vashishtha C**, Sarin SK. Bleeding Complications of Portal Hypertension. *Clin Liver Dis* 2024; **28**: 483-501 [PMID: 38945639 DOI: 10.1016/j.cld.2024.03.006]

36 **Inchingolo R**, Posa A, Mariappan M, Tibana TK, Nunes TF, Spiliopoulos S, Brountzos E. Transjugular intrahepatic portosystemic shunt for Budd-Chiari syndrome: A comprehensive review. *World J Gastroenterol* 2020; **26**: 5060-5073 [PMID: 32982109 DOI: 10.3748/wjg.v26.i34.5060]

37 **Vizzutti F**, Schepis F, Arena U, Fanelli F, Gitto S, Aspite S, Turco L, Dragoni G, Laffi G, Marra F. Transjugular intrahepatic portosystemic shunt (TIPS): current indications and strategies to improve the outcomes. *Intern Emerg Med* 2020; **15**: 37-48 [PMID: 31919780 DOI: 10.1007/s11739-019-02252-8]

38 **Kaplan DE**, Ripoll C, Thiele M, Fortune BE, Simonetto DA, Garcia-Tsao G, Bosch J. AASLD Practice Guidance on risk stratification and management of portal hypertension and varices in cirrhosis. *Hepatology* 2024; **79**: 1180-1211 [PMID: 37870298 DOI: 10.1097/HEP.0000000000000647]

39 **Turco L**, Reiberger T, Vitale G, La Mura V. Carvedilol as the new non-selective beta-blocker of choice in patients with cirrhosis and portal hypertension. *Liver Int* 2023; **43**: 1183-1194 [PMID: 36897563 DOI: 10.1111/liv.15559]

World Journal of Gastroenterology

Submit a Manuscript: https://www.f6publishing.com

World J Gastroenterol 2025 May 21; 31(19): 104897

DOI: 10.3748/wjg.v31.i19.104897

ISSN 1007-9327 (print) ISSN 2219-2840 (online)

ORIGINAL ARTICLE

Retrospective Study

Application of deep learning models in the pathological classification and staging of esophageal cancer: A focus on Wave-Vision Transformer

Wei Wei, Xiao-Lei Zhang, Hong-Zhen Wang, Lin-Lin Wang, Jing-Li Wen, Xin Han, Qian Liu

Specialty type: Gastroenterology and hepatology

Provenance and peer review: Unsolicited article; Externally peer reviewed.

Peer-review model: Single blind

Peer-review report's classification

Scientific Quality: Grade A, Grade B, Grade B, Grade B, Grade B

Novelty: Grade A, Grade A, Grade B, Grade B, Grade B

Creativity or Innovation: Grade A, Grade A, Grade B, Grade B, Grade B

Scientific Significance: Grade A, Grade B, Grade B, Grade B, Grade B

P-Reviewer: Ding D; Wang Z; Zhang W

Received: January 5, 2025

Revised: March 12, 2025

Accepted: April 27, 2025

Published online: May 21, 2025

Processing time: 135 Days and 20.6 Hours

Wei Wei, Xiao-Lei Zhang, Hong-Zhen Wang, Jing-Li Wen, Xin Han, Qian Liu, Department of Oncology, Dongying People's Hospital, Dongying 257091, Shandong Province, China

Lin-Lin Wang, Department of Pathology, Dongying People's Hospital, Dongying 257091, Shandong Province, China

Corresponding author: Wei Wei, PhD, Department of Oncology, Dongying People's Hospital, No. 317 Dongcheng South Road, Dongying District, Dongying 257091, Shandong Province, China. ww19810122@163.com

Abstract

BACKGROUND

Esophageal cancer is the sixth most common cancer worldwide, with a high mortality rate. Early prognosis of esophageal abnormalities can improve patient survival rates. The progression of esophageal cancer follows a sequence from esophagitis to non-dysplastic Barrett's esophagus, dysplastic Barrett's esophagus, and eventually esophageal adenocarcinoma (EAC). This study explored the application of deep learning technology in the precise diagnosis of pathological classification and staging of EAC to enhance diagnostic accuracy and efficiency.

AIM

To explore the application of deep learning models, particularly Wave-Vision Transformer (Wave-ViT), in the pathological classification and staging of esophageal cancer to enhance diagnostic accuracy and efficiency.

METHODS

We applied several deep learning models, including multi-layer perceptron, residual network, transformer, and Wave-ViT, to a dataset of clinically validated esophageal pathology images. The models were trained to identify pathological features and assist in the classification and staging of different stages of esophageal cancer. The models were compared based on accuracy, computational complexity, and efficiency.

RESULTS

The Wave-ViT model demonstrated the highest accuracy at 88.97%, surpassing the transformer (87.65%), residual network (85.44%), and multi-layer perceptron

(81.17%). Additionally, Wave-ViT exhibited low computational complexity with significantly reduced parameter size, making it highly efficient for real-time clinical applications.

CONCLUSION

Deep learning technology, particularly the Frequency-Domain Transformer model, shows promise in improving the precision of pathological classification and staging of EAC. The application of the Frequency-Domain Transformer model enhances the automation of the diagnostic process and may support early detection and treatment of EAC. Future research may further explore the potential of this model in broader medical image analysis applications, particularly in the field of precision medicine.

Key Words: Esophageal cancer; Deep learning; Wave-Vision Transformer; Pathological classification; Staging; Early detection

Core Tip: This study demonstrates the application of deep learning models, particularly Wave-Vision Transformer, for the pathological classification and staging of esophageal cancer. Wave-Vision Transformer outperformed other models such as transformer, residual network, and multi-layer perceptron, achieving the highest accuracy of 88.97% with low computational complexity. This innovative approach shows promise for improving early detection and personalized treatment strategies for esophageal cancer, potentially enhancing clinical outcomes in real-time applications.

Citation: Wei W, Zhang XL, Wang HZ, Wang LL, Wen JL, Han X, Liu Q. Application of deep learning models in the pathological classification and staging of esophageal cancer: A focus on Wave-Vision Transformer. *World J Gastroenterol* 2025; 31(19): 104897
URL: https://www.wjgnet.com/1007-9327/full/v31/i19/104897.htm
DOI: https://dx.doi.org/10.3748/wjg.v31.i19.104897

INTRODUCTION

Esophageal cancer is the sixth most common cancer globally and is associated with a high mortality rate. Its progression typically begins with esophagitis, advancing to Barrett's esophagus and eventually developing into esophageal adenocarcinoma (EAC)[1,2]. Although current medical techniques, such as endoscopy and pathological examination, enable the diagnosis of esophageal cancer to some extent, the complexity of staging and the subtle differences in pathological features present significant limitations in the accuracy and efficiency of traditional diagnostic methods[3,4]. Therefore, developing a precision diagnostic method based on modern technology, particularly for the rapid and accurate pathological classification and staging of early-stage esophageal cancer, is essential for improving patient survival and treatment outcomes[5,6].

In recent years, with the rapid development of artificial intelligence (AI), particularly deep learning technology, the application of image analysis in medical imaging and pathological analysis has grown significantly[7,8]. Deep learning algorithms, through automated feature learning and extraction, surpass traditional manual feature extraction methods, providing a more comprehensive and in-depth capacity for pathological information mining[9]. This technology demonstrates considerable potential in cancer pathology analysis, markedly enhancing diagnostic accuracy and efficiency [10,11]. The progression of esophageal cancer involves several distinct pathological stages, including esophagitis, Barrett's esophagus, and EAC. Early diagnosis of these stages is crucial for effective prevention and treatment[12,13]. However, existing pathological analysis methods struggle to differentiate these pathological types at early stages, resulting in missed or delayed diagnoses for many patients[14]. Thus, leveraging modern technology - especially deep learning - to improve the precision of pathological classification and staging diagnosis in esophageal cancer has become an urgent scientific challenge.

In the field of medical imaging analysis, deep learning models have become essential tools for disease diagnosis due to their powerful feature extraction capabilities and high-precision classification performance[15,16]. Esophageal cancer, a highly heterogeneous malignant tumor, requires early diagnosis to improve patient survival rates. However, traditional imaging analysis methods rely on manual feature extraction and shallow machine learning models, which struggle to capture the subtle differences in lesion areas. This challenge is particularly evident in complex medical images where early-stage lesions may exhibit hidden features, increasing the risk of misdiagnosis or missed diagnosis. In recent years, deep learning techniques - especially convolutional neural networks (CNNs)[17,18] and Vision Transformers (ViTs)[19] - have significantly advanced medical image analysis. These models can automatically learn multi-level features within images, enabling more accurate identification of lesion areas. However, traditional CNN models face limitations in capturing long-range dependencies, while ViT models, despite overcoming this issue through self-attention mechanisms, suffer from high computational complexity and limited ability to capture fine-grained local details.

Against this background, the Wave-ViT model[20] emerges as an innovative approach that integrates wavelet transform with transformer architecture, offering distinct advantages. Wavelet transform effectively captures multi-scale image features, which is particularly beneficial in medical imaging where lesions can exhibit different morphological and

textural characteristics at varying scales. By incorporating wavelet transform into the ViT framework, Wave-ViT retains the transformer's strengths in global feature extraction while enhancing sensitivity to local details, enabling a more comprehensive analysis of complex medical images. Additionally, Wave-ViT reduces computational complexity, improving efficiency and making it more suitable for large-scale medical imaging data analysis.

Wave-ViT's advantages are especially evident in esophageal cancer diagnosis. Early-stage esophageal lesions, such as Barrett's esophagus or mild dysplasia, often present as subtle mucosal changes in medical images. The multi-scale feature extraction capability of Wave-ViT allows for the precise identification of these early signals[21]. Moreover, the high computational efficiency of Wave-ViT enables rapid processing of endoscopic or computed tomography images, providing real-time diagnostic support for clinicians. Consequently, using Wave-ViT for esophageal cancer diagnosis not only enhances diagnostic accuracy and robustness but also offers an efficient and reliable tool for clinical applications, potentially advancing early screening and precision treatment of esophageal cancer.

In this context, this project introduces a deep learning-based approach that integrates advanced algorithms, including multi-layer perceptron (MLP), residual network (ResNet), transformer, and Wave-ViT, to automate the analysis and identification of pathological features in esophageal cancer images. These models combine self-attention mechanisms with frequency domain feature extraction, effectively capturing complex structures and lesion areas within pathological images. In particular, the Wave-ViT employs wavelet transform to extract high- and low-frequency information from images, significantly enhancing the model's sensitivity and diagnostic accuracy for esophageal cancer lesions. The inclusion of frequency domain information not only improves the model's ability to capture both local and global image features but also enables differentiation of subtle variations across pathological stages, thereby increasing diagnostic precision and stability.

Additionally, this study conducts experimental validation using open datasets such as Hyper Kvasir, which includes a large volume of high-quality esophageal pathology images labeled by professional endoscopists, covering various pathological stages such as esophagitis and Barrett's esophagus. Through the training and optimization of deep learning models, the study fully exploits the key pathological features within these images to construct an accurate diagnostic model for the classification and staging of esophageal cancer. This model not only aids clinicians in achieving faster and more accurate diagnoses but also provides novel technological support for the early detection and personalized treatment of esophageal cancer. In summary, this project addresses the clinical needs for esophageal cancer diagnosis and leverages advances in deep learning technology. By incorporating deep learning and frequency domain analysis, it aims to enhance the accuracy and efficiency of pathological classification and staging for esophageal cancer. This research holds significant scientific value and has the potential to contribute to improved early diagnostic capabilities and treatment outcomes for esophageal cancer in clinical applications[22].

MATERIALS AND METHODS

Sources and collection of clinical imaging data for different pathological stages of esophageal cancer

This study aims to collect clinical imaging data from various pathological stages of esophageal cancer to enable a detailed performance comparison of four representative deep learning models in the precise diagnosis of esophageal cancer. This data serves as a strong foundation for supporting early detection and treatment of the disease. The primary source of data is the Hyper Kvasir dataset[23], which was collected using endoscopy equipment from the Vestre Viken Health Trust (VV) in Norway. VV comprises four hospitals that provide healthcare services to approximately 470000 people. One of these hospitals, Bærum Hospital, houses a large gastroenterology department that has contributed training data and will continue to expand the dataset in the future. The dataset used in this study was obtained through the following steps: (1) Endoscopic examination: A research team conducted routine endoscopic examinations in hospitals, covering various parts of the gastrointestinal tract, including the esophagus, stomach, and colon. High-resolution endoscopy was used to capture images and videos, ensuring high-quality data collection; (2) Image and video recording: During the examinations, endoscopic operators recorded videos and captured multiple static images, documenting both normal and diseased tissues. Clinicians also took additional images of regions of interest based on real-time observations, providing a foundation for subsequent data annotation; and (3) Data storage: The collected images and videos were stored in the Picsara image documentation database, an extension of the hospital's electronic medical records system used for managing medical images. Additionally, these images have been meticulously annotated by one or more medical experts from VV and the Cancer Registry of Norway (CRN). Through cancer research, the CRN contributes new insights into cancer and operates under the Oslo University Hospital Trust as an independent entity within the South-Eastern Norway Regional Health Authority. CRN manages the national cancer screening program, with the objective of detecting cancer or precancerous lesions early to prevent cancer-related mortality.

Additionally, the Hyper Kvasir dataset consists of images annotated and validated by experienced endoscopists, covering various categories, including anatomical landmarks, pathological findings, and endoscopic procedures within the gastrointestinal tract. Each category contains hundreds of images. For this study, we utilized a subset of this dataset, which includes images categorized as esophagitis types A and B-D, short-segment Barrett's esophagus, and Barrett's esophagus, with representative images shown in Figure 1. As part of the dataset preprocessing, the research team performed data cleaning before publication, removing low-quality or blurry images to ensure high dataset quality. These images have varying resolutions, ranging from 720 × 576 to 1920 × 1072 pixels, and are organized into separate folders named according to their contents. This study primarily focuses on the reflux esophagitis and Barrett's esophagus subsets of the dataset.

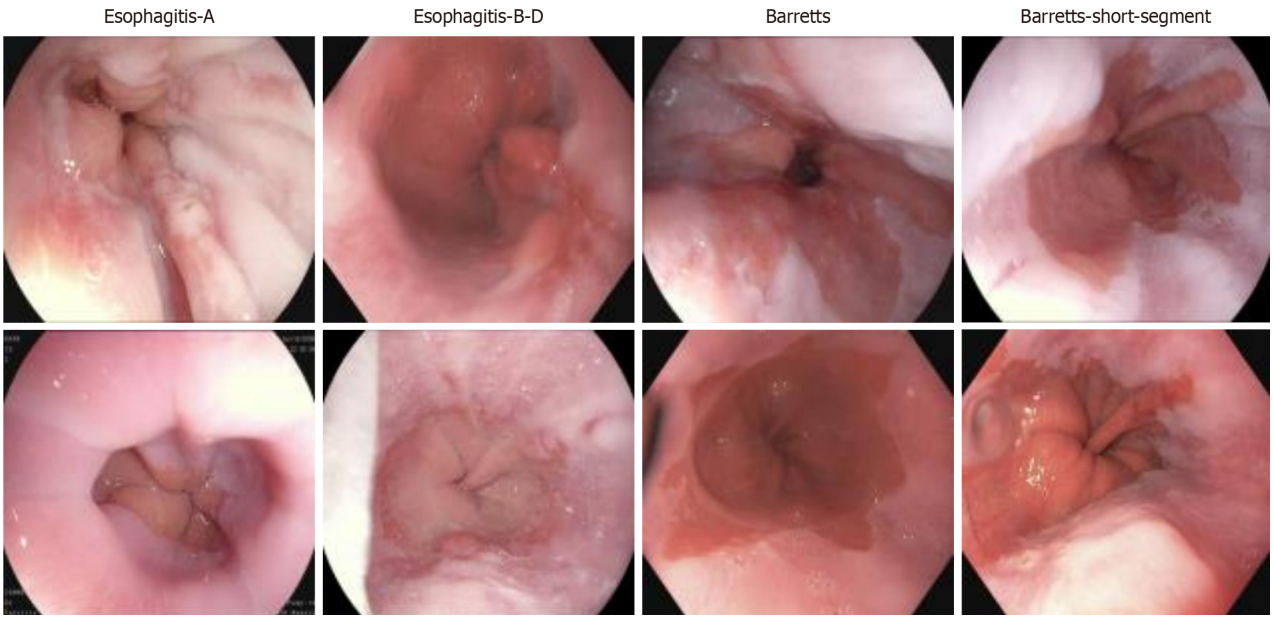

Figure 1 Display of different types of esophageal diseases. From left to right are esophagitis type A, esophagitis types B-D, short-segment Barrett's esophagus, and Barrett's esophagus, with the severity of esophageal conditions increasing sequentially. By visualizing these results, the study enhances the understanding of esophageal inflammation and Barrett's esophagus progression, providing insights into the gradual deterioration of esophageal tissue as the disease advances[23].

Quality control and preprocessing of the esophageal cancer dataset

The original dataset contains images of varying resolutions, which can reduce the efficiency of model training. Images with different resolutions require varying amounts of computational resources and processing time, leading to inconsistent processing speeds and significantly impacting training efficiency. Additionally, these variations in resolution can reduce the model's generalization ability. The model needs to learn features from images of different resolutions, which increases training complexity and may cause performance inconsistencies across images, ultimately lowering the model's generalizability. Furthermore, high-resolution images consume substantial memory, especially when dealing with large datasets, which can lead to memory overflow and affect the stability of the training process.

To address these issues, this study standardizes the resolution of all imaging data to 256 × 256 pixels during the preprocessing stage. This approach strikes a balance between retaining essential image information and improving computational efficiency. The selection of 256 × 256 pixels is based on the following considerations: First, this resolution preserves sufficient image detail to meet the model's feature extraction requirements. Lower resolutions could result in the loss of critical details, thereby reducing model accuracy. Second, this resolution ensures computational efficiency, avoiding excessive processing costs associated with high-resolution images. While higher resolutions may capture additional information, the associated increase in computational costs and training time would likely outweigh any performance gains. Thus, a resolution of 256 × 256 pixels achieves an optimal balance between resource consumption and information retention, enhancing model training efficiency and performance and ultimately improving the model's predictive accuracy and stability[24].

Selection and adaptation of early-stage esophageal cancer classification models

This study aims to develop an early-stage classification model for esophageal cancer and to evaluate the adaptability of various models. To this end, we selected four deep learning models that perform well in image recognition and sequential data processing: The MLP, ResNet, transformer, and Wave-ViT. Each model has unique strengths in architecture and application scenarios. By selecting these models, we aim to investigate the suitability and performance of different architectures in the early diagnosis of esophageal cancer, ultimately choosing or integrating the optimal model to achieve the best classification performance and adaptability. The following provides a detailed explanation of the main differences among the four models and the reasons for their selection.

MLP: The MLP is a basic feedforward neural network consisting of multiple fully connected layers. It learns data features through simple linear transformations and nonlinear activation functions. The MLP is advantageous for its simple structure, making it easy to understand and implement. However, its capacity to learn high-dimensional data and complex features is limited, especially in image processing, where extensive feature engineering is required to achieve satisfactory results. In this study, MLP is selected as a baseline model to facilitate comparison with the performance improvements achieved by more complex models.

ResNet: ResNet is a CNN that addresses the vanishing gradient problem in deep network training by introducing residual blocks, enabling the training of deeper networks with improved performance. ResNet uses skip connections, which add the input directly to the output of subsequent layers, facilitating easier gradient backpropagation. ResNet has

achieved remarkable success in image recognition due to its strong feature extraction capabilities, making it a key candidate for this study. ResNet was chosen for its advantages in handling image data, particularly in early-stage esophageal cancer diagnosis, where extracting complex image features may be necessary[25,26].

Transformer model: Originally developed for natural language processing (NLP), the transformer model is built around a core self-attention mechanism. This self-attention mechanism captures long-range dependencies within the data, enabling the transformer model to effectively process sequential information. In recent years, the transformer has also been applied successfully to image recognition. In this study, the transformer model is selected to explore its potential in handling early-stage esophageal cancer imaging data and other sequential feature data, such as time-series clinical indicators. Its powerful capacity for modeling long-range dependencies may be beneficial for capturing patterns related to disease progression[27,28].

Wave-ViT: Wave-ViT is a variant of the transformer model applied to frequency domain data. It first transforms the input data into the frequency domain and then uses the transformer model to learn frequency-domain features. This approach effectively captures frequency information, which may be more advantageous than spatial information in certain applications. Wave-ViT was selected to explore its potential benefits in processing early-stage esophageal cancer imaging data. If early esophageal cancer lesions exhibit more pronounced differences in frequency domain features, Wave-ViT may be more effective than traditional spatial domain transformer models[29,30].

In summary, the selection of these four models aims to comprehensively evaluate the performance of different architectures in early-stage esophageal cancer diagnosis. Through comparative analysis, the goal is to select or integrate the optimal model to construct an early-stage esophageal cancer classification model with high accuracy and strong adaptability. The model's adaptability will be assessed based on its generalization ability across different datasets and robustness to variations in data distribution. Additionally, since ResNet, the transformer model, and Wave-ViT all share a U-shaped network framework (Supplementary Figure 1), the following analysis will focus on the key differences among these three models.

MLP-based esophageal cancer pathological recognition model

The MLP is a feedforward artificial neural network consisting of multiple layers of fully connected neurons, each employing a nonlinear activation function[31]. MLP is capable of distinguishing non-linearly separable data, making it widely applicable across various domains such as image recognition and NLP. The strength of MLP lies in its ability to learn and represent complex input-output relationships, making it a powerful machine learning model. MLP is typically trained using the backpropagation algorithm, enabling it to learn and optimize based on input data and corresponding output labels. Its structure includes an input layer, hidden layers, and an output layer. The input layer receives data, the hidden layers perform feature extraction and transformation, and the output layer generates predictions. Connections between neurons carry weights and biases, which are adjusted during training to minimize the loss of function. In sum, MLP is a robust machine learning model capable of learning and representing complex relationships, making it a widely used approach in various fields.

To fully leverage the potential of MLP, Tolstikhin *et al*[32] developed an upgraded model called the MLP-mixer, a purely MLP-based architecture. The MLP-mixer comprises two types of layers: One type of MLP operates independently on each image patch, mixing features at each location, while the other type applies MLP across patches, mixing spatial information. The application of the MLP-mixer model on the dataset in this study is illustrated in Figure 2.

ResNet-based esophageal cancer pathological recognition model

ResNet is a deep CNN designed to address the issues of vanishing gradients and network degradation in deep neural network training by introducing "residual blocks". This innovation allows for the training of deeper networks with improved performance[25].

The core concept of ResNet is to shift the learning objective of each layer to focus on the residual between the input and output (*i.e.*, output minus input). This is achieved by adding a "skip connection" in each layer, which directly adds the input to the layer's output. With this design, gradients can propagate more easily back to earlier layers, even as the network depth increases, thus mitigating the vanishing gradient problem. The significance of ResNet lies in its ability to overcome training limitations in deep neural networks, enabling the training of deeper networks. Such deeper networks can learn more complex features, enhancing the model's representational capacity and accuracy[33].

ResNet has achieved significant success in computer vision tasks such as image classification, object detection, and image segmentation and has become the foundational architecture for many subsequent deep learning models. Its outstanding performance in the ILSVRC 2015 competition further validated its effectiveness, making it a primary choice for evaluating the most suitable model for the early-stage classification of esophageal cancer in this study. To adapt ResNet for this specific application, we modified the network's decoder structure from its original design for image classification to better suit esophageal cancer classification needs. The bottleneck block, a key component of ResNet's residual module, is shown in Figure 3.

Transformer-based esophageal cancer pathological recognition model

The transformer model is a deep learning architecture based on attention mechanisms, revolutionizing NLP and other sequential data processing fields. Unlike traditional sequential models that rely on recurrent neural networks or CNN, the transformer eliminates the need for recurrence. Instead, it processes all elements of the input sequence in parallel through a self-attention mechanism, significantly enhancing computational efficiency and its ability to handle long

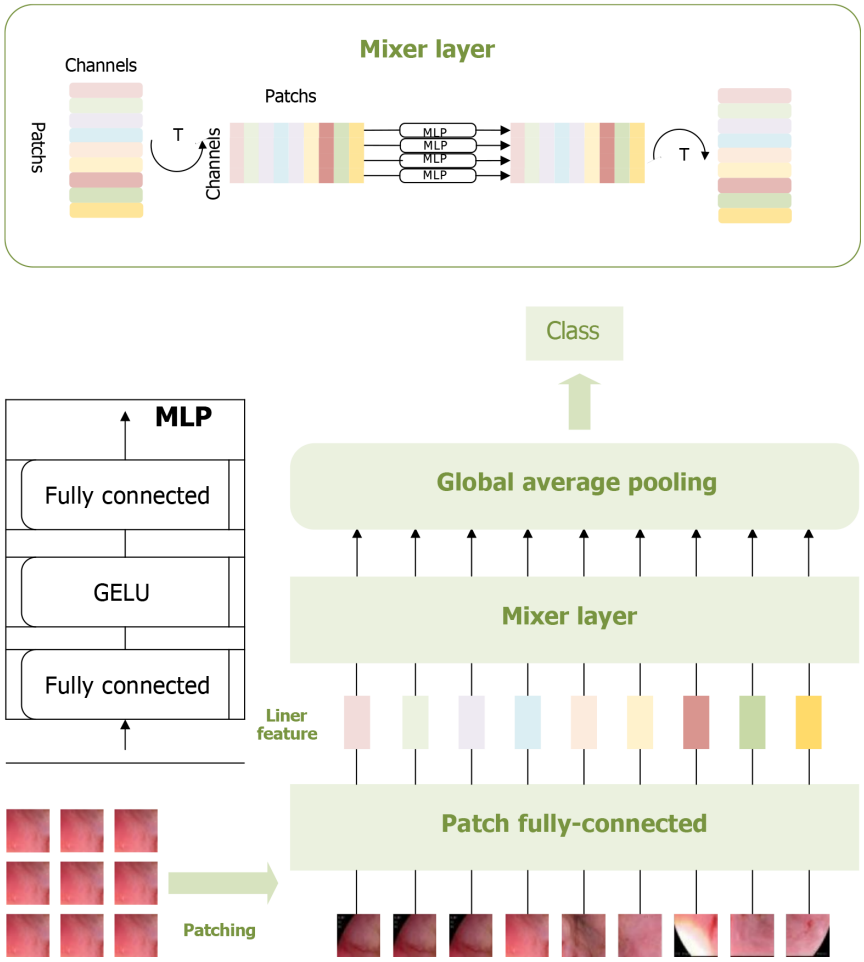

Figure 2 Multi-layer perceptron-based pathological recognition model for esophageal cancer. This figure visualizes the patching, feature extraction, and classification process of esophageal adenocarcinoma images using the multi-layer perceptron-based model. These three operations constitute the core components of this model. Visualizing these processes provides valuable insights into the multi-layer perceptron model's recognition performance, facilitating a comprehensive analysis of its effectiveness[23]. MLP: Multi-layer perceptron.

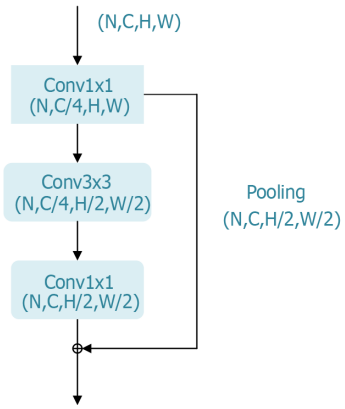

Figure 3 Bottleneck block of the residual network residual module. The bottleneck block in residual network's residual module is a key architectural component in deep convolutional neural networks and holds significant research value. This design effectively reduces the number of parameters and computational complexity, enabling networks to be deepened to hundreds of layers without encountering vanishing or exploding gradient issues. Consequently, this enhancement significantly improves the performance of deep learning models in image classification and other tasks.

sequences.

In this study, we adapted the basic transformer model proposed by Chen *et al*[34] to develop a classification model for esophageal cancer. The overall network architecture is shown in Supplementary Figure 1, with the transformer module illustrated in Figure 4. This transformer module overcomes the limitations of traditional sequential models by addressing the inefficiencies of recurrent neural networks in processing long sequences and mitigating the vanishing gradient

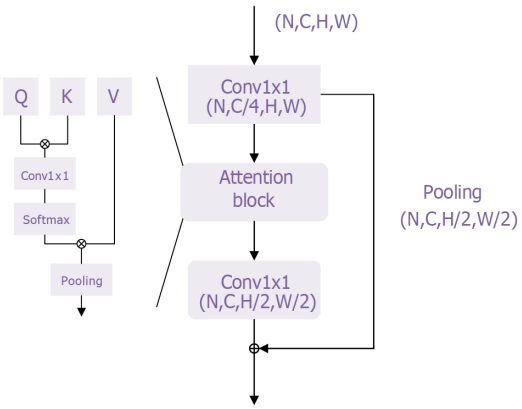

Figure 4 Transformer module of the transformer model. This figure provides an intuitive visualization of the core structure and functionality of the transformer architecture. The self-attention mechanism and multi-head attention mechanism effectively capture and process relationships among different features in the input data. This structure enhances the model's ability to comprehend contextual information while enabling parallel processing, which improves computational efficiency. By presenting a visual representation, researchers and clinicians can better understand how the transformer model functions in esophageal adenocarcinoma classification, increasing confidence in the model's reliability. Furthermore, this figure supports the study's findings by offering clear structural explanations and visual validations, demonstrating the effectiveness and robustness of the transformer model in tackling complex medical problems. This further underscores its potential for clinical applications.

problem, enabling the model to handle longer sequences effectively. Additionally, its self-attention mechanism enhances the model's representational power by better capturing contextual information and long-range dependencies, thereby improving both expressiveness and accuracy.

Wave-ViT-based esophageal cancer pathological recognition model

To further improve model performance, it is crucial to minimize information loss, particularly regarding high-frequency components such as texture details within the target. Yao *et al*[20] addressed this by modifying the transformer structure based on wavelet transforms, enabling the model to extract more frequency domain information and thereby enhance its performance. The wavelets module of the Wave-ViT model is shown in Figure 5.

The wavelets module performs reversible downsampling through wavelet transform, aiming to retain original image details for self-attention learning while reducing computational costs. Wavelet transform is a fundamental time-frequency analysis method that decomposes the input signal into different frequency sub-bands to address aliasing issues. Specifically, discrete wavelet transfor achieves reversible downsampling by transforming 2D data into four discrete wavelet sub-bands. Here, the low-frequency component reflects the coarse-grained structure of the primary object, while the high-frequency component retains fine-grained texture details[35]. In this way, different levels of image detail are preserved in lower-resolution sub-bands without information loss. Additionally, inverse discrete wavelet transform can be used to reconstruct the original image in the wavelet ViTs. This information-preserving transform enables the design of an efficient transformer block with lossless and reversible downsampling, facilitating self-attention learning on multi-scale feature maps.

Evaluation metrics and calculation methods for model validation

In deep learning research and application, evaluating model performance is crucial. This study selects three commonly used evaluation metrics: Accuracy, computational complexity, and efficiency. Accuracy measures the proportion of correct predictions out of all predictions. It reflects the overall classification performance of the model, with values closer to 1 indicating stronger predictive capability. However, in cases where class imbalance exists, accuracy alone can be misleading. Therefore, it is necessary to incorporate additional metrics such as precision, recall, and F1-score for a comprehensive assessment of the model's performance. The formulas for these metrics are as follows: (1) Where: True positives represents the number of actual positive cases correctly classified as positive. True negatives represents the number of actual negative cases correctly classified as negative. False positives represents the number of actual negative cases incorrectly classified as positive. False negatives represents the number of actual positive cases incorrectly classified as negative; (2) Computational complexity evaluates the computational resources required for training or inference. This metric is critical for understanding how computational demand scales with increasing input data size. A lower computational complexity implies better scalability and faster processing, making the model more suitable for practical applications. The formula for computational complexity is as follows: Where: N represents the input data size. d denotes the depth or dimensionality of the model; and (3) Efficiency measures the number of correct predictions per unit of time. In real-world applications, optimizing computation time and resource usage is essential. A highly efficient model can make more predictions within a shorter time, improving responsiveness, especially in real-time decision-making scenarios. Maintaining high efficiency enhances user experience and overall system performance.

To summarize, accuracy, computational complexity, and efficiency are three key evaluation metrics for deep learning models. Accuracy provides a direct understanding of the model's predictive performance, while computational complexity and efficiency assess the model's resource utilization and scalability. A comprehensive evaluation using these metrics guides model improvement and optimization, ensuring a balance between performance and practical usability in

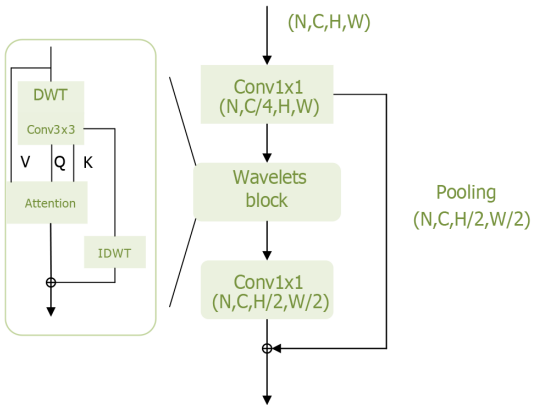

Figure 5 Wavelets module of the Wave-Vision Transformer model. This figure visually illustrates the Wavelets module's structure and functionality within the Wave-Vision Transformer model. The module is designed to leverage wavelet transform for multi-scale feature extraction while preserving information integrity. By integrating wavelet transform with self-attention mechanisms, Wave-Vision Transformer achieves lossless downsampling, effectively retaining high-frequency information such as textures and edges, which enhances the model's sensitivity to fine details. DWT: Discrete wavelet transform.

real-world applications.

Statistical analysis

In this study, various software tools and statistical methods were used to construct predictive models evaluating surgical outcomes and postoperative recovery. The programming and data processing were primarily conducted in Jupyter Notebook using Python. Data processing and visualization were performed with the Python libraries pandas and Matplotlib, while visualization plots were created with Visio. Statistical methods included data normalization, calculation of model accuracy, sensitivity, and specificity, as well as model performance assessment through loss function curves. In the data processing phase, imaging data was first normalized to eliminate differences in scale between various features. Additionally, all images were resized to a consistent resolution, facilitating subsequent model training.

During the model evaluation phase, we calculated accuracy, sensitivity, and specificity to assess the model's performance in practical applications. Accuracy reflects the model's overall predictive capability, sensitivity measures its ability to identify positive cases, and specificity evaluates its ability to recognize negative samples. Calculating these metrics provides a comprehensive understanding of the model's performance, ensuring its effectiveness in clinical applications.

During model training, we employed the cross-entropy loss function as the primary evaluation criterion. The cross-entropy loss is highly effective for classification tasks, as it quantifies the discrepancy between the model's predicted probability distribution and the actual labels, thereby enhancing classification accuracy. To optimize the learning process, we selected the Adam optimizer, which combines the advantages of momentum optimization and adaptive learning rate adjustments. This optimization method enables faster convergence and effectively handles sparse gradient problems.

Additionally, the batch size was set as a crucial parameter for efficient data processing. A well-chosen batch size improves training efficiency while balancing memory usage. The learning rate is another key hyperparameter that controls the step size of weight updates, directly influencing both convergence speed and final model performance. Through extensive experimentation, we determined an optimal initial learning rate to ensure stable training.

The entire training process was conducted in a high-performance computing environment, utilizing the NVIDIA RTX 3090 GPU. This GPU offers powerful parallel computing capabilities and efficient memory management, significantly accelerating deep learning model training and supporting the achievement of high-quality experimental results. These hardware settings and parameter configurations collectively enhanced the training efficiency and performance of the model, ensuring the smooth execution of deep learning tasks.

Additionally, we used the loss function value curve to further evaluate model performance. The loss function curve is a vital tool for assessing training effectiveness, diagnosing model issues, and guiding improvements. By analyzing the shape, trend, and differences in loss values between the training and validation sets, we gain insights into the model's learning process and can identify the optimal-performing model. For data visualization, we used the matplotlib library to display arrays, illustrating spatial features of samples and model performance. This visualization approach aids in understanding data distribution and clearly reflects the model's performance under varying conditions, providing valuable insights for future research and clinical applications. Through the integration of these statistical methods and visualization techniques, we comprehensively validate the model's effectiveness, ensuring its reliability in practical use.

RESULTS

Quantitative analysis of four different deep learning models

In this study, the collected esophageal disease imaging data was first normalized. The data was then divided into training, testing, and validation sets based on the quantity of images in each category. Details of the specific data split are

provided in Table 1. To further analyze the performance of each deep learning model, we conducted a statistical evaluation using quantitative metrics. Table 2 presents a comparison of the performance metrics for the four deep learning models - MLP, ResNet, transformer, and Wave-ViT - on the image recognition task. By examining these metrics, we gain a deeper understanding of each model's efficiency, complexity, and performance, allowing us to draw important conclusions regarding their relative strengths and suitability for this task.

The significance of each metric in the table is as follows: (1) Accuracy (%): The model's accuracy on the image recognition task is expressed as a percentage. Higher accuracy indicates better model performance; (2) Input size (MB): The size of the input image in megabytes (MB), which reflects the memory space required for the model to process image data; (3) Params (MB): The number of model parameters in megabytes (MB). The parameter count indicates model complexity; generally, more parameters imply a more complex model with higher computational demand; (4) Madd (G): The number of multiply-accumulate (Madd) operations in billions (G). Madd is a common computational operation in deep learning models, and its count indicates the model's computational complexity; and (5) Flops (G): The number of floating-point operations (flops) in billions (G). Floating-point operations include addition, subtraction, multiplication, and division, and the flops count serves as an essential indicator of the model's computational complexity.

First, we observe that the input size for all four models is 3.15 MB, indicating that they process image data of the same scale, which facilitates a direct comparison of model performance. In terms of accuracy, Wave-ViT performs the best (88.97%), followed by transformer (87.65%), ResNet (85.44%), and MLP (81.17%). This suggests that the transformer and Wave-ViT models exhibit higher accuracy in image recognition tasks compared to the traditional MLP and ResNet models. This performance improvement may stem from the architectural advantages of the transformer and Wave-ViT models; for instance, the self-attention mechanism in the transformer model allows it to better capture long-range dependencies between image features, while Wave-ViT combines the strengths of convolutional and transformer architectures, effectively extracting both local and global features. In this study, the Wave-ViT model demonstrated superior diagnostic accuracy, achieving an accuracy of 0.8897, surpassing the transformer model (0.8765). This improvement highlights Wave-ViT's effectiveness in esophageal cancer diagnosis. Compared to previous deep learning approaches for esophageal cancer diagnosis, Wave-ViT outperforms CNN models, which typically achieve accuracy scores between 0.75 and 0.85[36]. This suggests that Wave-ViT significantly surpasses traditional CNN architectures in image recognition accuracy. Moreover, in comparison to traditional machine learning methods, such as support vector machines, which typically achieve accuracy scores ranging from 0.70 to 0.80[37], both Wave-ViT and transformer models demonstrate significantly improved early detection capabilities for esophageal cancer, providing a more reliable tool for clinical diagnosis. This comparative analysis highlights Wave-ViT's potential in processing esophageal cancer imaging data, as it effectively captures and identifies lesion features.

However, high accuracy does not necessarily equate to high efficiency. Let us analyze model complexity and computational load. The ResNet model has a significantly larger parameter count than the other three models (45.20 MB *vs* 1.10 MB, 1.45 MB, 1.29 MB), indicating that ResNet is the most complex model. Correspondingly, ResNet's Madd (71.21 G) and flops (35.63 G) are also substantially higher than those of the other models. This suggests that while ResNet achieves relatively high accuracy, it also incurs a considerable computational cost.

In contrast, the transformer and Wave-ViT models have relatively low parameter counts and computational loads, comparable to or even lower than those of the MLP model. Wave-ViT has the lowest Madd and flops (1.04 G and 1.12 G), indicating that it achieves the highest computational efficiency while maintaining high accuracy. The transformer model also demonstrates relatively low computational demands, which can be attributed to its parallel processing capability. Although the MLP model has the fewest parameters and lowest computational load, it also has the lowest accuracy, suggesting that while simple models offer high computational efficiency, their limited representational capacity makes it challenging to capture complex features within images.

In summary, the data in Table 2 indicates that transformer-based models, particularly Wave-ViT, demonstrate a favorable balance of performance and efficiency in image recognition tasks. These models achieve a better trade-off between accuracy and computational efficiency, suggesting a promising direction for the development of deep learning models. Future research could explore further improvements to these models to achieve an optimal balance among accuracy, efficiency, and resource consumption.

Analysis of the four models based on loss function variation

To further identify the optimal model, this study analyzes the variation in loss function values during training. The four models - MLP, ResNet, transformer, and Wave-ViT - show significant differences in their training performance, as reflected in the stability and final values of their loss functions, which follow a trend of progressive improvement and reduction, as shown in Figure 6. These differences stem from their unique network architectures and training strategies. The following analysis, based on Figure 6, will detail the distinctions among these models in terms of loss function stability and final loss values.

MLP is a basic deep learning model composed of multiple fully connected layers. During training, the loss function for MLP often exhibits significant fluctuations, especially in the early stages. This is due to the longer gradient propagation paths in MLP, which make it prone to gradient vanishing or explosion issues, resulting in unstable parameter updates and pronounced oscillations in the loss function. Furthermore, the MLP's limited representational capacity makes it challenging to effectively learn complex data features, leading to slower loss convergence and a relatively high final loss value. Its loss function curve typically shows a jagged pattern with slow convergence and is prone to get trapped in local minima.

ResNet mitigates the gradient vanishing problem in deep neural networks by introducing skip connections, allowing gradients to bypass certain layers during backpropagation. This design makes the model easier to train and enables the training of deeper networks. During training, ResNet's loss function shows greater stability than MLP, with significantly

Table 1 Distribution of samples across the dataset

	Esophagitis A	Esophagitis B-D	Barretts-short-segment	Barretts
Tarin set	320	208	42	32
Test set	42	26	6	5
Val set	41	26	5	4
Total	403	260	53	41

Table 2 Performance metrics of four deep learning models

Model name	Accuracy (%)	Input size (MB)	Params (MB)	Madd (G)	Flops (G)
MLP	81.17	3.15	1.10	1.57	0.95
ResNet	85.44	3.15	45.20	71.21	35.63
Transfomer	87.65	3.15	1.45	2.17	1.57
Wave-ViT	88.97	3.15	1.29	1.04	1.12

MLP: Multi-layer perceptron; ResNet: Residual network; Wave-ViT: Wave-Vision Transformer.

reduced fluctuations. This is due to the skip connections, which improve gradient propagation and stabilize parameter updates. Additionally, ResNet's convolutional layers effectively capture local features in image data and, through stacking multiple convolutional layers, learn higher-level feature representations, enhancing the model's expressive power. As a result, ResNet achieves lower final loss values and faster convergence than MLP. Its loss function curve is relatively smooth, converges more quickly, and is more likely to approach the global minimum.

The core of the transformer model is the self-attention mechanism, which captures relationships between any two elements in the input sequence, effectively learning long-range dependencies. Unlike MLP and ResNet, the transformer model processes all elements in the input sequence in parallel, resulting in faster training and the ability to handle longer sequences. During training, the transformer model's loss function exhibits even greater stability than that of ResNet, with smaller fluctuations. This stability arises from the self-attention mechanism's capacity to capture contextual information, leading to more stable parameter updates and better learning of global data features. Additionally, the transformer model's strong representational ability enables it to learn more complex feature representations, resulting in lower loss values and faster convergence than ResNet. Its loss function curve is exceptionally smooth, converges very quickly, and typically achieves very low loss values.

Wave-ViT is a model that applies the transformer architecture in the frequency domain. It first transforms input data into the frequency domain and then utilizes the transformer model for feature extraction in this domain. This approach effectively captures frequency information in the data and leverages the transformer model's parallel processing capability to enhance computational efficiency. During training, the loss function of Wave-ViT is even more stable than that of the transformer model, with minimal fluctuations. This is because frequency domain representation can effectively reduce noise and highlight essential features in the data, resulting in more stable parameter updates. Additionally, Wave-ViT excels in capturing global data features and effectively learns frequency-based information, leading to lower loss values and faster convergence than the transformer model. Its loss function curve is exceptionally smooth, with rapid convergence to very low loss values, and is less prone to getting trapped in local minima.

In summary, from the perspective of loss function variation, these four models exhibit a clear progression in stability and final loss values: MLP shows the most volatile loss function with large fluctuations and a high final loss value; ResNet is relatively stable with smaller fluctuations and a lower final loss value than MLP; the transformer model is even more stable, with minimal fluctuations and a lower final loss value than ResNet; and Wave-ViT demonstrates the highest stability, with minimal fluctuations and the lowest final loss value. This difference primarily stems from the unique architecture and training strategies of each model. MLP lacks effective mechanisms to address the vanishing gradient problem; ResNet alleviates this issue through skip connections; the transformer captures long-range dependencies through its self-attention mechanism; and Wave-ViT combines the benefits of frequency domain representation and the transformer model, further enhancing model stability and representational capacity. This increased stability directly translates into better generalization and robustness, with Wave-ViT often showing optimal performance on the test set. Naturally, actual outcomes may be influenced by factors such as datasets and hyperparameters, but the overall trend follows this pattern.

Comparison and analysis of model modules based on feature map visualization

Visualizing the feature maps of each module in each model allows us to understand the internal mechanisms by which the models identify esophageal diseases. This is especially useful for examining the differences in feature extraction and semantic understanding across models. Figure 7 shows the results of visualizing different models for the identification of

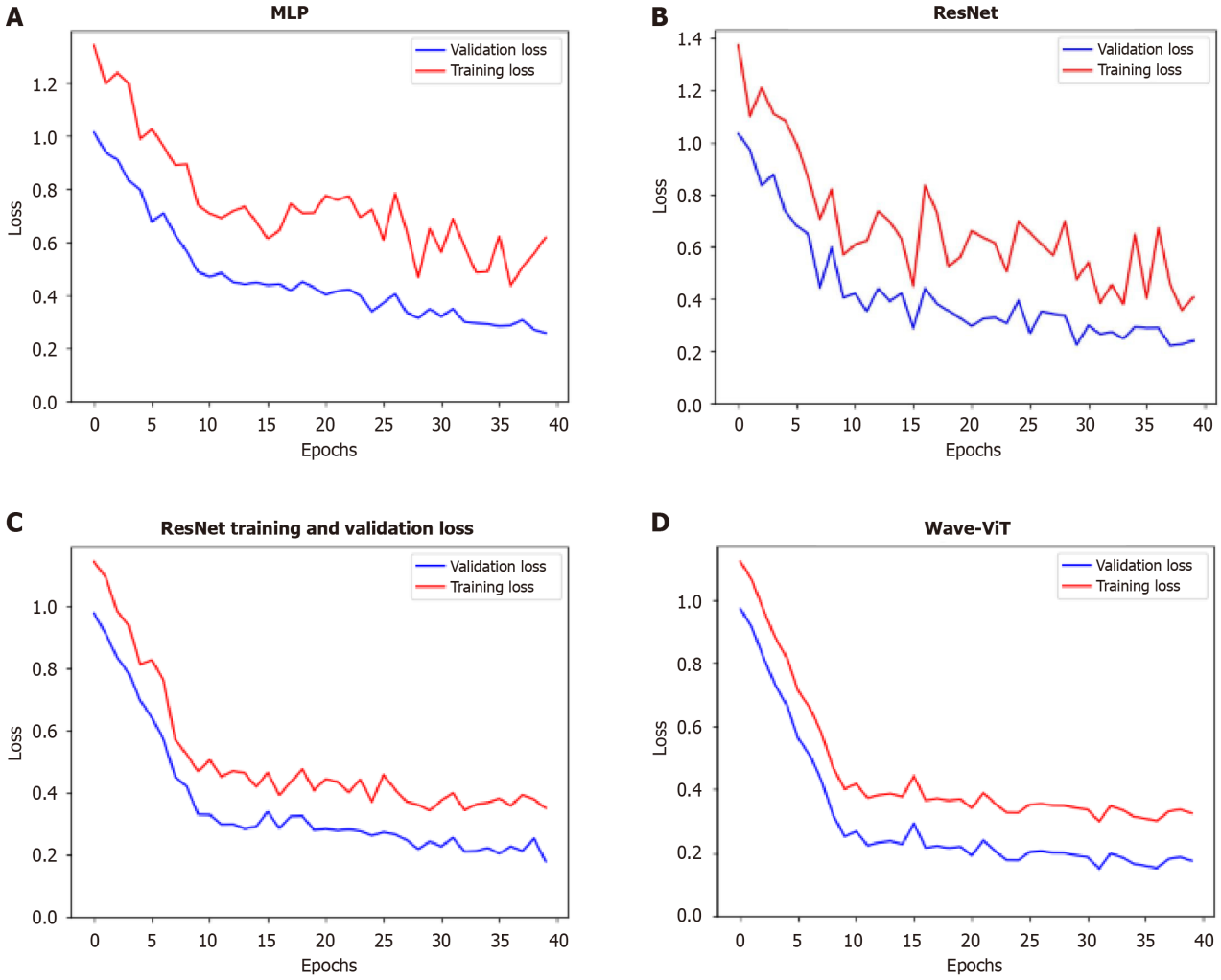

Figure 6 Variation of loss function and validation accuracy during model training. A-D: The changes in loss function values during training for the multi-layer perceptron, residual network, transformer, and Wave-Vision Transformer (Wave-ViT) models, respectively, on the training and validation sets. This visualization illustrates the convergence behavior, generalization ability, and risk of overfitting for each model. By comparing loss function curves, we can assess training stability and efficiency. In this study, if Wave-ViT exhibits faster convergence and lower validation loss, this directly supports its superiority in esophageal cancer diagnosis. This would indicate that Wave-ViT can more effectively learn complex features in medical images while avoiding overfitting, providing strong evidence for its practical application. MLP: Multi-layer perceptron; ResNet: Residual network; Wave-ViT: Wave-Vision Transformer.

a particular case of esophagitis. This paper analyzes the differences in feature maps extracted by modules across four levels in ResNet, the transformer model, and Wave-ViT, with a focus on how Wave-ViT leverages frequency domain information to enhance its focus on disease regions in the esophagus.

By observing the intermediate feature maps extracted by each model, this study conducted a detailed analysis of the correlation between the model's focus areas and pathological features[38]. ResNet primarily captures local details, such as the texture of the esophageal wall and the distribution of blood vessels. As the network depth increases, the model gradually learns higher-level features, such as the integrity of the esophageal mucosa and the shape and size of inflamed areas. However, ResNet mainly focuses on local spatial information within the image and has limited sensitivity to global information and different frequency components. The transformer model, on the other hand, captures relationships between different regions of the esophagus, such as the connection between inflamed areas and surrounding tissue. Due to its global perspective enabled by the self-attention mechanism, the transformer model is more effective than ResNet in identifying disease regions. Wave-ViT has the advantage of simultaneously capturing both local details and global contextual information in diseased regions. The wavelet transform highlights high-frequency details in diseased areas, such as irregular edges and abnormal textures. Additionally, the wavelet block extracts information at different scales from feature maps of various frequency components: High-frequency components highlight details within diseased areas, while low-frequency components capture global contextual information. As a result, the Wave-ViT model demonstrates a higher degree of focus on disease regions and achieves more precise localization of these areas.

In summary, the ResNet visualization results may indicate attention to the entire esophageal region but show a lower degree of focus on disease areas compared to the other two models. All three models' shallow feature maps display local texture information, while deeper feature maps reveal more abstract regional features. However, both ResNet and transformer models lack emphasis on specific frequency domain information. Wave-ViT, in contrast, captures more frequency domain information, allowing it to extract richer semantic information from the esophagus, which explains

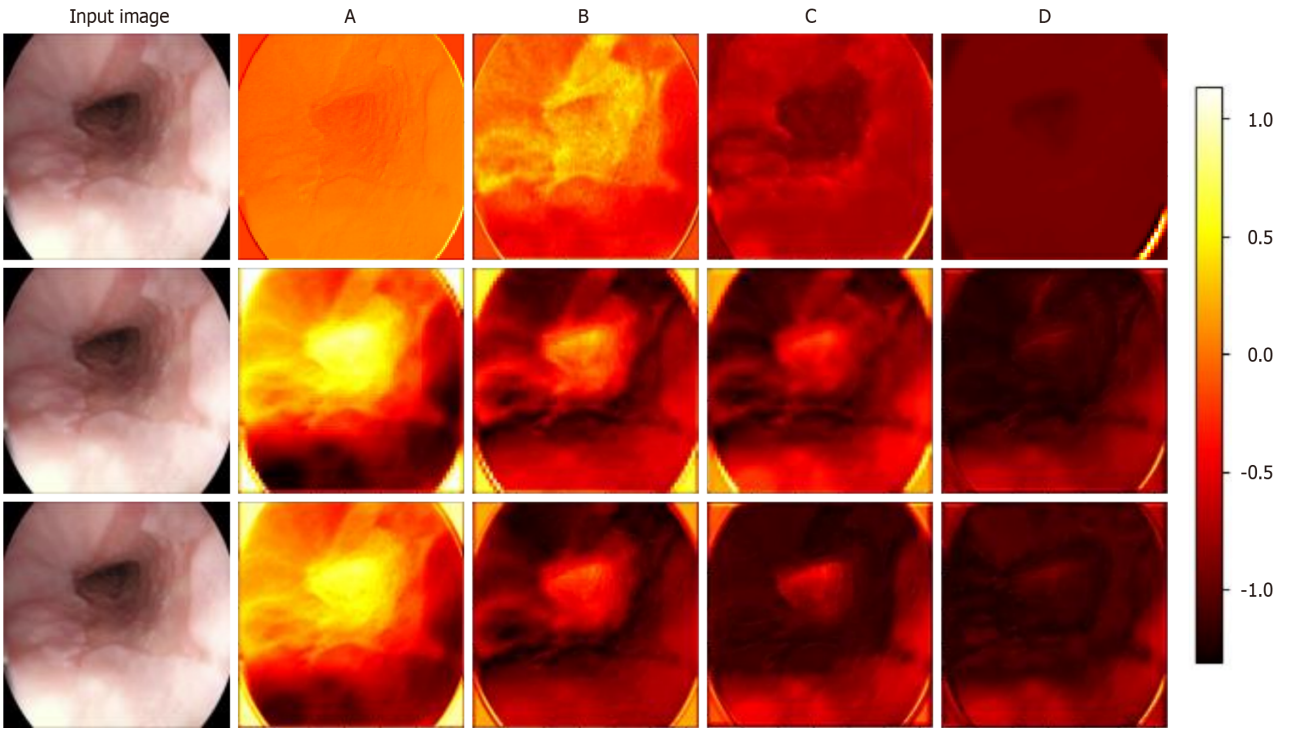

Figure 7 Visualization of feature extraction from different layers in the prognostic model. The first to third rows correspond to the feature maps extracted by the bottleneck block in residual network, the transformer block in the transformer model, and the wavelet block in Wave-Vision Transformer (Wave-ViT), respectively. A-D: The feature maps extracted by the four different levels of modules illustrated in Supplementary Figure 1. This visualization provides an intuitive comparison of the feature extraction capabilities of the three models. The contrast in feature maps clearly reveals Wave-ViT's advantage in multi-scale feature extraction, particularly in its balance between detail and global information. These results support Wave-ViT's superiority in medical imaging analysis, particularly in esophageal cancer diagnosis, where it more accurately detects early-stage lesions and complex pathological features. This visualization validates Wave-ViT's architectural design and provides critical insights for further model optimization[23].

why Wave-ViT demonstrates a higher focus on esophageal disease regions.

To further analyze how the wavelet block in Wave-ViT extracts frequency domain features, this study visualizes the first wavelet block's feature extraction process, as shown in Figure 8. The wavelet block employs a fundamental time-frequency analysis method, decomposing the input signal into different frequency sub-bands - namely, low-frequency components (top-left in Figure 8) and high-frequency components (top-right, bottom-left, and bottom-right in Figure 8) - to address aliasing issues. Specifically, the low-frequency component reflects the coarse-grained structure of basic objects, while the high-frequency components retain fine-grained texture details. In this way, various levels of image detail are captured in the extracted feature maps without information loss.

The Wave-ViT model incorporates wavelet transform to leverage frequency domain decomposition, significantly improving the detection of EAC lesions. Wavelet transform allows the model to conduct multi-scale analysis in the frequency domain, enabling effective feature extraction across different frequency bands[39]. Specifically, the model first applies wavelet transform to decompose EAC images (*e.g.*, biopsy tissue slides or medical scans) into low-frequency and high-frequency components: Low-frequency components retain global structural information. High-frequency components capture fine-grained texture features, such as cell morphology and pathological changes. This multi-scale feature extraction enables Wave-ViT to distinguish subtle differences between healthy and cancerous tissues. In EAC, where lesion features can be extremely subtle, capturing high-frequency information is particularly critical. By integrating self-attention mechanisms, Wave-ViT can dynamically focus on the most representative regions in medical images, further enhancing sensitivity to key lesions. For example, when detecting specific cellular structures in adenocarcinoma, the model prioritizes regions with prominent high-frequency features, improving detection accuracy and reliability.

Overall, Wave-ViT integrates frequency domain decomposition with deep learning, advancing early diagnosis and precise recognition of EAC, and supporting clinical decision-making[40]. This frequency domain mechanism enables Wave-ViT to simultaneously analyze local details and global context, capturing EAC's pathological characteristics more comprehensively. High-frequency information helps identify subtle anomalies in early-stage lesions, while low-frequency information assists in assessing lesion extent and severity. Experimental results further confirm that Wave-ViT precisely localizes lesion areas and achieves higher classification accuracy on EAC datasets. This advancement provides critical support for early detection and treatment planning. This translation effectively conveys the training process, performance comparison, feature visualization, and clinical implications of Wave-ViT while integrating relevant references from the manuscript.

From the quantitative and visualization results, it is evident that none of the four models achieved optimal accuracy, and each exhibited different errors. When applying MLP, CNNs, transformers, and Wave-ViT for EAC classification, various sources of error may significantly impact model performance and clinical interpretability.

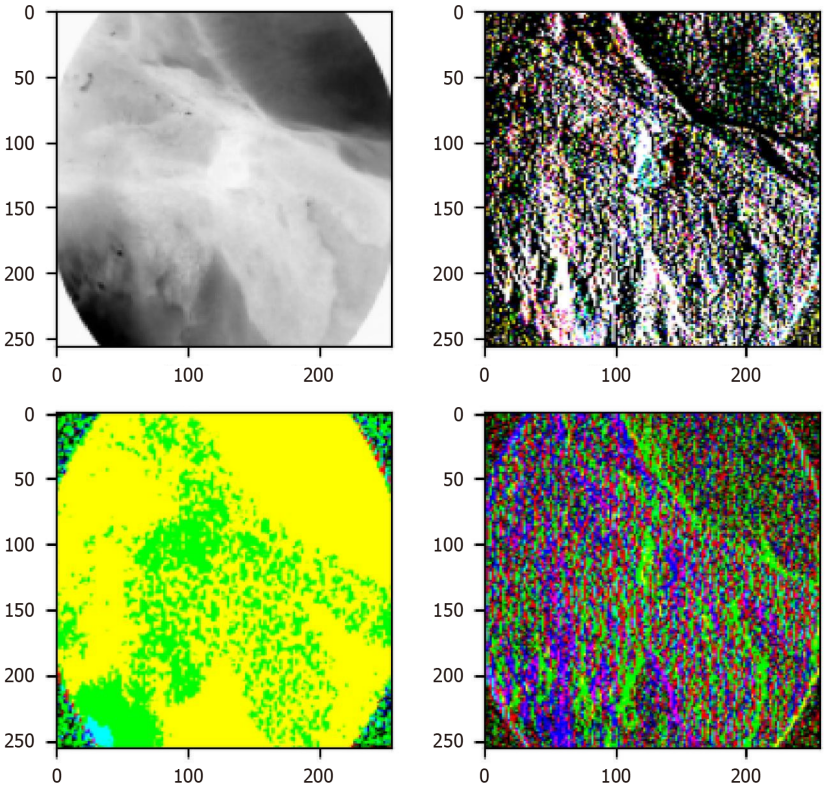

Figure 8 Visualization of wavelet block extracting different frequency domain features. The top left image represents the low-frequency sub-band, while the other images depict high-frequency sub-bands. After processing the different sub-band images, they can be combined into a single image through the inverse wavelet transform, allowing for the extraction of additional information. After processing different sub-bands and applying the inverse wavelet transform, these components can be recombined into a single image, thereby extracting richer information. This demonstrates how wavelet transform decomposes an original image into low- and high-frequency sub-bands, where the low-frequency sub-band preserves the primary structure and global information, while the high-frequency sub-bands capture fine details and edge features. By processing and reconstructing these sub-bands, the multi-scale feature representation of the image is enhanced without losing critical information. This process significantly improves the model's ability to detect subtle pathological changes, which is crucial for esophageal cancer diagnosis. Particularly in early-stage esophageal cancer, small and hidden morphological differences among subtypes can be better captured. Therefore, the figure not only validates the effectiveness of wavelet transform in feature extraction but also provides strong technical support for the study. The findings demonstrate that the Wave-Vision Transformer model, by integrating multi-scale feature fusion, substantially enhances the accuracy and robustness of esophageal cancer diagnosis [23].

MLP: Limited feature engineering, overfitting, and nonlinear constraints may prevent the model from effectively capturing the complexity of clinical data, reducing diagnostic accuracy and generalizability.

CNN: CNN models may be affected by data bias, image quality variations, and overfitting, leading to missed or misdiagnosed high-risk patients, which increases psychological burdens on patients.

Transformer: While transformers have strong feature extraction capabilities, their reliance on large datasets makes them vulnerable to performance degradation due to insufficient training samples. Additionally, high computational complexity in inference may limit real-time decision-making.

Wave-ViT: Although Wave-ViT excels in multi-scale feature extraction, improper utilization of multi-scale information may lead to performance degradation or overfitting. These potential sources of error could lead to the omission of critical pathological features, undermining model interpretability and credibility, thereby affecting clinical decision-making and treatment strategies. In clinical practice, physicians must carefully assess these models' limitations to make comprehensive patient evaluations and deliver more effective treatments. To further reduce these errors, future research will focus on optimizing multiple aspects of esophageal cancer prediction models.

Expanding the dataset: Enhancing generalization and performance by collecting diverse, multi-center data covering various patient demographics (age, gender, ethnicity) and pathological subtypes of esophageal cancer. This diversity will improve rare lesion detection and ensure better adaptability across different clinical scenarios.

Optimizing models for different esophageal cancer types: Specialized testing and optimization of models for adenocarcinoma and squamous cell carcinoma are crucial due to their distinct pathogenesis, pathological characteristics, and clinical manifestations. Optimizing models for specific subtypes can improve classification accuracy, while exploring subtype-specific feature selection and preprocessing techniques can further enhance performance.

Integrating AI models into clinical workflows: Embedding deep learning models into clinical decision support systems can facilitate real-time diagnostic suggestions following patient examinations. Future studies should also prioritize model interpretability and transparency to help physicians understand model decisions, thereby increasing trust and adoption in clinical settings. By expanding datasets, optimizing models for specific cancer subtypes, and integrating AI technology into clinical workflows, this research aims to improve the accuracy and precision of esophageal cancer detection and treatment.

Evaluating model generalization using 5-fold cross-validation

To assess the generalization ability of the Wave-ViT model, we conducted a 5-fold cross-validation. The dataset was evenly split into five subsets, where one subset was used for validation while the remaining four were used for training in each iteration. This process was repeated five times, and the final accuracy was calculated as the average of all experiments. The results demonstrated that the Wave-ViT model performed consistently across all subsets, achieving an average accuracy of 89%, confirming its robustness under different data distributions. Moreover, a comparison of the loss curves between training and validation sets indicated no significant overfitting, further validating its strong generalization ability. This evaluation method ensures that the Wave-ViT model effectively mitigates data bias, demonstrating strong potential for real-world applications in esophageal cancer diagnosis. Future research will continue to expand the dataset by incorporating more EAC samples to further enhance model generalizability.

DISCUSSION

This study demonstrates significant research value and clinical potential by applying deep learning technology to the pathological classification and staging of esophageal cancer. As the sixth most common cancer worldwide, esophageal cancer is characterized by a high mortality rate and complex pathological features, making early diagnosis and staging crucial for improving patient survival rates[41,42]. However, traditional diagnostic methods often rely on the manual judgment of pathology experts, which is not only time-consuming and labor-intensive but also prone to human error, leading to misdiagnoses or missed diagnoses[43]. Therefore, enhancing diagnostic accuracy and efficiency for esophageal cancer, particularly through automated diagnostic tools in early pathological classification and staging, has become a pressing issue in the medical field.

In this context, deep learning serves as an automated and intelligent image analysis tool, providing a new solution for processing pathological images. The use of ResNet, MLP, transformer model, and Wave-ViT in this project significantly enhances the diagnostic accuracy of esophageal cancer pathological images. Among these, the Wave-ViT represents an innovative aspect of this study, combining the advantages of self-attention mechanisms and frequency domain information extraction. This model not only captures complex features in pathological images but also precisely identifies high-frequency and low-frequency characteristics through wavelet transform. As a result, the model demonstrates outstanding performance in classifying pathological stages from esophagitis to esophageal cancer, exhibiting higher accuracy and efficiency compared to traditional methods, particularly in the staging diagnosis of complex pathological structures.

In the application of deep learning models, the authenticity and validity of the dataset directly influence the model's generalization ability and reliability. This study utilized clinical real-world data from two types of esophagitis and two types of Barrett's esophagus, encompassing a diverse range of pathological classification and staging scenarios, which enhances the practical applicability of the model. In contrast, some existing studies often rely on publicly available datasets or relatively homogeneous pathological types, making it difficult to cover the variable pathological features encountered in clinical practice. Moreover, the quality of the data and the consistency of annotations largely determine the model's diagnostic accuracy and generalizability. We strictly controlled data balance during model training and validation to ensure that the model could accurately identify different types of lesions. In comparison, other studies may struggle to achieve the same level of recognition performance due to limitations in their datasets. The dataset construction strategy employed in this research not only improves the model's adaptability but also provides a solid foundation for clinical implementation.

Through a detailed evaluation of the performance of each model, this study found that the Wave-ViT excels in both accuracy and efficiency. In the tasks of pathological classification and staging of esophageal cancer, Wave-ViT achieved an accuracy of 88.97%, significantly higher than that of the transformer (87.65%), ResNet (85.44%), and MLP (81.17%). Furthermore, Wave-ViT exhibits low computational complexity, with key metrics such as parameter count, Madd, and flops maintained at appropriate levels, indicating its suitability for real-time analysis in practical applications. In contrast, existing studies often report deep learning models that require high computational resources and parameter counts, making them less feasible for implementation in resource-limited clinical settings. This research demonstrates the advantage of Wave-ViT in maintaining high accuracy while reducing computational complexity, laying the groundwork for its widespread application in pathological diagnosis. One of the key aspects to highlight is that the Wave-ViT model, by integrating wavelet transform with the transformer architecture, has demonstrated exceptional performance in medical image analysis. Its multi-scale feature extraction capability enables more accurate detection of subtle early-stage esophageal cancer lesions, such as Barrett's esophagus or mild dysplasia, thereby significantly enhancing early detection sensitivity. Additionally, Wave-ViT effectively differentiates between esophageal cancer subtypes, including esophageal squamous cell carcinoma and EAC, providing clinicians with more precise pathological classification information to support personalized treatment planning. For example, based on the model's high-precision diagnostic outputs, phy-

sicians can implement early interventions, choosing targeted therapies or chemo-radiotherapy strategies tailored to the specific esophageal cancer subtype, ultimately improving treatment outcomes and patient survival rates. Furthermore, the high computational efficiency of Wave-ViT allows for the rapid processing of large-scale medical imaging data, offering real-time support for clinical decision-making, thereby advancing the field of precision medicine. Thus, Wave-ViT's advantages extend beyond technical performance to tangible clinical value, providing a powerful tool for early esophageal cancer screening and personalized treatment.

In this study, we propose a step-by-step clinical workflow to integrate Wave-ViT as an auxiliary screening tool into the endoscopic examination process to improve early diagnosis efficiency and accuracy for EAC. Specifically, this model is designed to automatically analyze images from real-time endoscopic video streams and utilize frequency-domain decomposition techniques (*e.g.*, wavelet transform) to extract high-frequency details (such as irregular edges and abnormal textures) and low-frequency global information (such as lesion size and its relationship with surrounding tissues). When a suspicious lesion is detected, the model automatically highlights the region in real time, prompting endoscopists to focus on potentially malignant areas, thereby reducing the risk of missed or misdiagnoses. This real-time assistance not only enhances endoscopic examination efficiency but also provides clinicians with a more comprehensive understanding of lesions, supporting more accurate clinical decision-making. Additionally, we explored the potential complementary role of Wave-ViT in pathological biopsy analysis. Traditional biopsy-based histopathology relies heavily on subjective assessment by pathologists, whereas Wave-ViT can provide objective, quantitative lesion characterization, including lesion size, shape, texture features, and contrast with surrounding tissues. For instance, the model can generate probability heatmaps of malignancy likelihood and combine frequency-domain feature analysis to offer multi-scale lesion descriptions. These quantitative insights, when combined with microscopic pathological observations, can significantly enhance diagnostic accuracy and consistency. This is particularly valuable for early-stage EAC diagnosis, where the model's heightened sensitivity to microscopic lesions can compensate for sampling bias and the limited field of view in biopsies. Notably, Wave-ViT exhibits significant advantages for clinical applications.

Multi-scale feature extraction for complex lesion detection

Its frequency-domain decomposition enables superior lesion detection in complex backgrounds, effectively distinguishing early-stage esophageal cancer from normal tissues.

Real-time & automated screening for large-scale clinical use

The model's efficiency and automation make it well-suited for high-throughput screening scenarios, significantly reducing the workload of endoscopists.

Enhanced integration with pathological biopsy for precision medicine

By combining Wave-ViT analysis with histopathology, the model enables more accurate and personalized EAC diagnoses. Future research should focus on optimizing the model's generalization ability and conducting multi-center clinical trials to validate its clinical applicability.

This study focuses on the classification and staging of different pathological types of esophageal cancer, particularly the precise identification and analysis of the progression from esophagitis to Barrett's esophagus and EAC. Traditional pathological classification methods often face challenges in accurately identifying precancerous lesions, especially in distinguishing atypical hyperplasia from typical hyperplasia in Barrett's esophagus[44,45]. However, deep learning models can automatically extract deep features from images, significantly enhancing the accuracy and consistency of classification. The Wave-ViT model employed in this study effectively extracts frequency domain information, enabling it to accurately differentiate between various pathological types, thus providing a more reliable tool for early cancer screening. Compared to models in other studies, the model presented here demonstrates not only greater efficiency in recognizing pathological features but also excellent adaptability in maintaining stability during staging.

We also performed a subgroup analysis of the two primary histological subtypes of esophageal cancer: Esophageal squamous cell carcinoma: Predominantly associated with smoking, alcohol consumption, and malnutrition. More prevalent in Asian and African populations. Pathologically characterized by dysplastic changes in squamous epithelial cells, progressing to invasive carcinoma. Treatment options: Surgery and chemo-radiotherapy remain the mainstay. Molecular characteristics: Frequently involves TP53, CDKN2A mutations, and Wnt/β-catenin pathway alterations[46]. EAC: More common in Western populations, strongly linked to gastroesophageal reflux disease, obesity, and Barrett's esophagus. Pathologically originates from columnar epithelium with glandular dysplasia. Treatment options: In addition to surgery and chemo-radiotherapy, targeted therapies (*e.g.*, anti-human epidermal growth factor receptor 2 drugs) show promising results. Molecular characteristics: Frequently involves TP53, ERBB2 mutations, and alterations in the epidermal growth factor receptor/human epidermal growth factor receptor 2 signaling pathway[47,48]. These findings emphasize the distinct etiological, pathological, molecular, and therapeutic differences between esophageal squamous cell carcinoma and EAC, underscoring the importance of subtype-specific treatment strategies in clinical practice.

The most significant highlight of this study is the introduction of frequency domain information, an innovative approach that enables deep learning models to capture and recognize subtle changes in pathological images that may otherwise be difficult to detect. While traditional deep learning models demonstrate considerable advantages in processing large-scale image data, they often exhibit limitations in recognizing minor changes, particularly the gradual transitions between different stages of esophageal cancer progression. The frequency domain features obtained through wavelet transform allow the model to extract more detailed image information from various frequency dimensions, significantly enhancing its sensitivity to pathological features. This is especially crucial in the diagnosis of early lesions, making early detection of esophageal cancer possible.

Another significant value of this study lies in the selection and application of the dataset. This project utilizes the Hyper Kvasir and other publicly available datasets, which contain a large number of high-quality esophageal pathology images annotated by professional endoscopists, covering multiple pathological stages from esophagitis and Barrett's esophagus to EAC. The use of this dataset not only ensures the quality of the training data for the model but also guarantees its generalization ability and practicality through validation with extensive real clinical data. The model's excellent performance in both training and validation demonstrates the broad applicability of deep learning technology in complex medical image processing, laying a solid foundation for future larger-scale clinical applications.

From a clinical perspective, this study provides a novel tool for the precise diagnosis and personalized treatment of esophageal cancer. The introduction of deep learning models not only enhances the accuracy of pathological classification and staging but also reduces the workload for physicians through automated diagnostics, shortening diagnostic times and improving clinical efficiency. Additionally, Wave-ViT's analytical approach enables physicians to make precise assessments at earlier stages of lesions, thereby providing a more scientific basis for personalized treatment plans. This advancement not only helps to lower the mortality rate associated with esophageal cancer but also significantly improves patient treatment outcomes and quality of life.

CONCLUSION

In summary, this project demonstrates that the application of deep learning technology in the pathological classification and staging of esophageal cancer not only achieves a dual enhancement of diagnostic accuracy and efficiency but also establishes a new technological pathway for early detection, precision medicine, and personalized treatment of esophageal cancer. This research holds significant implications and broad clinical application prospects.

FOOTNOTES

Author contributions: Zhang XL and Wang HZ contributed to the experimental conception and design; Wang LL, Wen JL, and Han X conducted the experiments; Wei W and Liu Q collected and assembled the experimental data; Wang LL, Wen JL, and Han X contributed to data analysis and interpretation; Zhang XL and Wang HZ wrote the article. All authors approved the final manuscript. Wang LL, Wen JL, and Han X contributed equally to this work.

Institutional review board statement: This study did not involve human subjects or living animals.

Informed consent statement: Not applicable.

Conflict-of-interest statement: All the authors report no relevant conflicts of interest for this article.

Data sharing statement: All data can be provided as needed.

Country of origin: China

ORCID number: Wei Wei 0009-0008-1766-5216.

S-Editor: Wang JJ
L-Editor: A
P-Editor: Zhao S

REFERENCES

1 **Khan R**, Saha S, Gimpaya N, Bansal R, Scaffidi MA, Razak F, Verma AA, Grover SC. Outcomes for upper gastrointestinal bleeding during the first wave of the COVID-19 pandemic in the Toronto area. *J Gastroenterol Hepatol* 2022; **37**: 878-882 [PMID: 35174540 DOI: 10.1111/jgh.15804]

2 **Aburasain RY**. Esophageal Cancer Classification in Initial Stages Using Deep and Transfer Learning. Proceedings of the 2024 IEEE International Conference on Advanced Systems and Emergent Technologies (IC_ASET); 2024 Apr 27-29; Hammamet, Tunisia. United States: Institute of Electrical and Electronics Engineers, 2024

3 **Tong T**. Complete Tumor Response of Esophageal Cancer: How Much Imaging Can Do? *Ann Surg Oncol* 2024; **31**: 4161-4162 [PMID: 38652195 DOI: 10.1245/s10434-024-15276-y]

4 **Fang S**, Xu P, Wu S, Chen Z, Yang J, Xiao H, Ding F, Li S, Sun J, He Z, Ye J, Lin LL. Raman fiber-optic probe for rapid diagnosis of gastric and esophageal tumors with machine learning analysis or similarity assessments: a comparative study. *Anal Bioanal Chem* 2024; **416**: 6759-6772 [PMID: 39322799 DOI: 10.1007/s00216-024-05545-w]

5 **Cao K**, Zhu J, Lu M, Zhang J, Yang Y, Ling X, Zhang L, Qi C, Wei S, Zhang Y, Ma J. Analysis of multiple programmed cell death-related prognostic genes and functional validations of necroptosis-associated genes in oesophageal squamous cell carcinoma. *EBioMedicine* 2024; **99**: 104920 [PMID: 38101299 DOI: 10.1016/j.ebiom.2023.104920]

6 **Zhang H**, Wen H, Zhu Q, Zhang Y, Xu F, Ma T, Guo Y, Lu C, Zhao X, Ji Y, Wang Z, Chu Y, Ge D, Gu J, Liu R. Genomic profiling and associated B cell lineages delineate the efficacy of neoadjuvant anti-PD-1-based therapy in oesophageal squamous cell carcinoma. *EBioMedicine* 2024; **100**: 104971 [PMID: 38244291 DOI: 10.1016/j.ebiom.2024.104971]

7 **Jiang P**, Li Y, Wang C, Zhang W, Lu N. A deep learning based assisted analysis approach for Sjogren's syndrome pathology images. *Sci Rep* 2024; **14**: 24693 [PMID: 39433593 DOI: 10.1038/s41598-024-75925-w]

8 **Hachache R**, Yahyaouy A, Riffi J, Tairi H, Abibou S, Adoui ME, Benjelloun M. Advancing personalized oncology: a systematic review on the integration of artificial intelligence in monitoring neoadjuvant treatment for breast cancer patients. *BMC Cancer* 2024; **24**: 1300 [PMID: 39434042 DOI: 10.1186/s12885-024-13049-0]

9 **Pusterla O**, Heule R, Santini F, Weikert T, Willers C, Andermatt S, Sandkühler R, Nyilas S, Latzin P, Bieri O, Bauman G. MRI lung lobe segmentation in pediatric cystic fibrosis patients using a recurrent neural network trained with publicly accessible CT datasets. *Magn Reson Med* 2022; **88**: 391-405 [PMID: 35348244 DOI: 10.1002/mrm.29184]

10 **Tsai MC**, Yen HH, Tsai HY, Huang YK, Luo YS, Kornelius E, Sung WW, Lin CC, Tseng MH, Wang CC. Artificial intelligence system for the detection of Barrett's esophagus. *World J Gastroenterol* 2023; **29**: 6198-6207 [PMID: 38186865 DOI: 10.3748/wjg.v29.i48.6198]

11 **Ohmori M**, Ishihara R, Aoyama K, Nakagawa K, Iwagami H, Matsuura N, Shichijo S, Yamamoto K, Nagaike K, Nakahara M, Inoue T, Aoi K, Okada H, Tada T. Endoscopic detection and differentiation of esophageal lesions using a deep neural network. *Gastrointest Endosc* 2020; **91**: 301-309.e1 [PMID: 31585124 DOI: 10.1016/j.gie.2019.09.034]

12 **Iwagami H**, Ishihara R, Aoyama K, Fukuda H, Shimamoto Y, Kono M, Nakahira H, Matsuura N, Shichijo S, Kanesaka T, Kanzaki H, Ishii T, Nakatani Y, Tada T. Artificial intelligence for the detection of esophageal and esophagogastric junctional adenocarcinoma. *J Gastroenterol Hepatol* 2021; **36**: 131-136 [PMID: 32511793 DOI: 10.1111/jgh.15136]

13 **Cui R**, Wang L, Lin L, Li J, Lu R, Liu S, Liu B, Gu Y, Zhang H, Shang Q, Chen L, Tian D. Deep Learning in Barrett's Esophagus Diagnosis: Current Status and Future Directions. *Bioengineering (Basel)* 2023; **10**: 1239 [PMID: 38002363 DOI: 10.3390/bioengineering10111239]

14 **Jain S**, Dhingra S. Pathology of esophageal cancer and Barrett's esophagus. *Ann Cardiothorac Surg* 2017; **6**: 99-109 [PMID: 28446998 DOI: 10.21037/acs.2017.03.06]

15 **Botros M**, de Boer OJ, Cardenas B, Bekkers EJ, Jansen M, van der Wel MJ, Sánchez CI, Meijer SL. Deep Learning for Histopathological Assessment of Esophageal Adenocarcinoma Precursor Lesions. *Mod Pathol* 2024; **37**: 100531 [PMID: 38830407 DOI: 10.1016/j.modpat.2024.100531]

16 **Bouzid K**, Sharma H, Killcoyne S, Castro DC, Schwaighofer A, Ilse M, Salvatelli V, Oktay O, Murthy S, Bordeaux L, Moore L, O'Donovan M, Thieme A, Nori A, Gehrung M, Alvarez-Valle J. Enabling large-scale screening of Barrett's esophagus using weakly supervised deep learning in histopathology. *Nat Commun* 2024; **15**: 2026 [PMID: 38467600 DOI: 10.1038/s41467-024-46174-2]

17 **Jian M**, Tao C, Wu R, Zhang H, Li X, Wang R, Wang Y, Peng L, Zhu J. HRU-Net: A high-resolution convolutional neural network for esophageal cancer radiotherapy target segmentation. *Comput Methods Programs Biomed* 2024; **250**: 108177 [PMID: 38648704 DOI: 10.1016/j.cmpb.2024.108177]

18 **Souza LA Jr**, Passos LA, Santana MCS, Mendel R, Rauber D, Ebigbo A, Probst A, Messmann H, Papa JP, Palm C. Layer-selective deep representation to improve esophageal cancer classification. *Med Biol Eng Comput* 2024; **62**: 3355-3372 [PMID: 38848031 DOI: 10.1007/s11517-024-03142-8]

19 **Iyer PG**, Sachdeva K, Leggett CL, Codipilly DC, Abbas H, Anderson K, Kisiel JB, Asfahan S, Awasthi S, Anand P, Kumar M P, Singh SP, Shukla S, Bade S, Mahto C, Singh N, Yadav S, Padhye C. Development of Electronic Health Record-Based Machine Learning Models to Predict Barrett's Esophagus and Esophageal Adenocarcinoma Risk. *Clin Transl Gastroenterol* 2023; **14**: e00637 [PMID: 37698203 DOI: 10.14309/ctg.0000000000000637]

20 **Yao T**, Pan Y, Li Y, Ngo CW, Mei T. Wave-ViT: Unifying Wavelet and Transformers for Visual Representation Learning. 2022 Preprint. Available from: arXiv:2207.04978 [DOI: 10.48550/arXiv.2207.04978]

21 **Zhu Z**, Soricut R. Wavelet-Based Image Tokenizer for Vision Transformers. 2024 Preprint. Available from: arXiv:2405.18616 [DOI: 10.48550/arXiv.2405.18616]

22 **Shoji Y**, Koyanagi K, Kanamori K, Tajima K, Ogimi M, Ninomiya Y, Yamamoto M, Kazuno A, Nabeshima K, Nishi T, Mori M. Immunotherapy for esophageal cancer: Where are we now and where can we go. *World J Gastroenterol* 2024; **30**: 2496-2501 [PMID: 38817664 DOI: 10.3748/wjg.v30.i19.2496]

23 **Borgli H**, Thambawita V, Smedsrud PH, Hicks S, Jha D, Eskeland SL, Randel KR, Pogorelov K, Lux M, Nguyen DTD, Johansen D, Griwodz C, Stensland HK, Garcia-Ceja E, Schmidt PT, Hammer HL, Riegler MA, Halvorsen P, de Lange T. HyperKvasir, a comprehensive multi-class image and video dataset for gastrointestinal endoscopy. *Sci Data* 2020; **7**: 283 [PMID: 32859981 DOI: 10.1038/s41597-020-00622-y]

24 **Rukundo O**. Effects of Image Size on Deep Learning. *Electronics* 2023; **12**: 985 [DOI: 10.3390/electronics12040985]

25 **He K**, Zhang X, Ren S, Sun J. Deep Residual Learning for Image Recognition. Proceedings of the 2016 IEEE Conference on Computer Vision and Pattern Recognition (CVPR); 2016 Jun 27-30; Las Vegas, NV, United States. United States: Institute of Electrical and Electronics Engineers, 2016

26 **Liu S**, Tian G, Xu Y. A novel scene classification model combining ResNet based transfer learning and data augmentation with a filter. *Neurocomputing* 2019; **338**: 191-206 [DOI: 10.1016/j.neucom.2019.01.090]

27 **Liu Y**, Zhang Y, Wang Y, Hou F, Yuan J, Tian J, Zhang Y, Shi Z, Fan J, He Z. A Survey of Visual Transformers. *IEEE Trans Neural Netw Learn Syst* 2024; **35**: 7478-7498 [PMID: 37015131 DOI: 10.1109/TNNLS.2022.3227717]

28 **Xu Y**, Wei H, Lin M, Deng Y, Sheng K, Zhang M, Tang F, Dong W, Huang F, Xu C. Transformers in computational visual media: A survey. *Comp Visual Med* 2022; **8**: 33-62 [DOI: 10.1007/s41095-021-0247-3]

29 **He X**, Chen Y, Lin Z. Spatial-Spectral Transformer for Hyperspectral Image Classification. *Remote Sens* 2021; **13**: 498 [DOI: 10.3390/rs13030498]

30 **Yang X**, Cao W, Lu Y, Zhou Y. Hyperspectral Image Transformer Classification Networks. *IEEE Trans Geosci Remote Sens* 2022; **60**: 1-15 [DOI: 10.1109/TGRS.2022.3171551]

31 **Zhang W**, Shen X, Zhang H, Yin Z, Sun J, Zhang X, Zou L. Feature importance measure of a multilayer perceptron based on the presingle-connection layer. *Knowl Inf Syst* 2024; **66**: 511-533 [DOI: 10.1007/s10115-023-01959-7]

32 **Tolstikhin I**, Houlsby N, Kolesnikov A, Beyer L, Zhai X, Unterthiner T, Yung J, Steiner A, Keysers D, Uszkoreit J, Lucic M, Dosovitskiy A.

MLP-Mixer: An all-MLP Architecture for Vision. 2021 Preprint. Available from: arXiv:2105.01601 [DOI: 10.48550/arXiv.2105.01601]

33 **Liang J**. Image classification based on RESNET. *J Phys Conf Ser* 2020; **1634**: 012110 [DOI: 10.1088/1742-6596/1634/1/012110]

34 **Chen J**, Lu Y, Yu Q, Luo X, Adeli E, Wang Y, Lu L, Yuille AL, Zhou Y. TransUNet: Transformers Make Strong Encoders for Medical Image Segmentation. 2021 Preprint. Available from: arXiv:2102.04306 [DOI: 10.48550/arXiv.2102.04306]

35 **Mallat SG**. A theory for multiresolution signal decomposition: the wavelet representation. *IEEE Trans Pattern Anal Machine Intell* 1989; **11**: 674-693 [DOI: 10.1109/34.192463]

36 **Lewis JR**, Pathan S, Kumar P, Dias CC. AI in Endoscopic Gastrointestinal Diagnosis: A Systematic Review of Deep Learning and Machine Learning Techniques. *IEEE Acc* 2024; **12**: 163764-163786 [DOI: 10.1109/ACCESS.2024.3483432]

37 **Min JK**, Kwak MS, Cha JM. Overview of Deep Learning in Gastrointestinal Endoscopy. *Gut Liver* 2019; **13**: 388-393 [PMID: 30630221 DOI: 10.5009/gnl18384]

38 **Selvaraju RR**, Cogswell M, Das A, Vedantam R, Parikh D, Batra D. Grad-CAM: Visual Explanations from Deep Networks *via* Gradient-Based Localization. *Int J Comput Vis* 2020; **128**: 336-359 [DOI: 10.1007/s11263-019-01228-7]

39 **Hong Z**, Xiong J, Yang H, Mo YK. Lightweight Low-Rank Adaptation Vision Transformer Framework for Cervical Cancer Detection and Cervix Type Classification. *Bioengineering (Basel)* 2024; **11**: 468 [PMID: 38790335 DOI: 10.3390/bioengineering11050468]

40 **Umamaheswari T**, Babu YMM. ViT-MAENB7: An innovative breast cancer diagnosis model from 3D mammograms using advanced segmentation and classification process. *Comput Methods Programs Biomed* 2024; **257**: 108373 [PMID: 39276667 DOI: 10.1016/j.cmpb.2024.108373]

41 **Sidana V**, Lnu R, Davenport A, Lekharaju V. Primary Oesophageal Lymphoma: A Diagnostic Dilemma. *Cureus* 2024; **16**: e73751 [PMID: 39677107 DOI: 10.7759/cureus.73751]

42 **Kamtam DN**, Lin N, Liou DZ, Lui NS, Backhus LM, Shrager JB, Berry MF. Radiation therapy does not improve survival in patients who are upstaged after esophagectomy for clinical early-stage esophageal adenocarcinoma. *JTCVS Open* 2025; **23**: 290-308 [PMID: 40061535 DOI: 10.1016/j.xjon.2024.11.001]

43 **Zhao YX**, Zhao HP, Zhao MY, Yu Y, Qi X, Wang JH, Lv J. Latest insights into the global epidemiological features, screening, early diagnosis and prognosis prediction of esophageal squamous cell carcinoma. *World J Gastroenterol* 2024; **30**: 2638-2656 [PMID: 38855150 DOI: 10.3748/wjg.v30.i20.2638]

44 **Espino A**, Cirocco M, Dacosta R, Marcon N. Advanced imaging technologies for the detection of dysplasia and early cancer in barrett esophagus. *Clin Endosc* 2014; **47**: 47-54 [PMID: 24570883 DOI: 10.5946/ce.2014.47.1.47]

45 **Geboes K**, Van Eyken P. The diagnosis of dysplasia and malignancy in Barrett's oesophagus. *Histopathology* 2000; **37**: 99-107 [PMID: 10931231 DOI: 10.1046/j.1365-2559.2000.00960.x]

46 **Gao W**, Liu S, Wu Y, Wei W, Yang Q, Li W, Chen H, Luo A, Wang Y, Liu Z. Enhancer demethylation-regulated gene score identified molecular subtypes, inspiring immunotherapy or CDK4/6 inhibitor therapy in oesophageal squamous cell carcinoma. *EBioMedicine* 2024; **105**: 105177 [PMID: 38924839 DOI: 10.1016/j.ebiom.2024.105177]

47 **Zhao N**, Zhang Z, Wang Q, Li L, Wei Z, Chen H, Zhou M, Liu Z, Su J. DNA damage repair profiling of esophageal squamous cell carcinoma uncovers clinically relevant molecular subtypes with distinct prognoses and therapeutic vulnerabilities. *EBioMedicine* 2023; **96**: 104801 [PMID: 37725855 DOI: 10.1016/j.ebiom.2023.104801]

48 **Zhang G**, Yuan J, Pan C, Xu Q, Cui X, Zhang J, Liu M, Song Z, Wu L, Wu D, Luo H, Hu Y, Jiao S, Yang B. Multi-omics analysis uncovers tumor ecosystem dynamics during neoadjuvant toripalimab plus nab-paclitaxel and S-1 for esophageal squamous cell carcinoma: a single-center, open-label, single-arm phase 2 trial. *EBioMedicine* 2023; **90**: 104515 [PMID: 36921563 DOI: 10.1016/j.ebiom.2023.104515]

World Journal of Gastroenterology

Submit a Manuscript: https://www.f6publishing.com

World J Gastroenterol 2025 May 21; 31(19): 105283

DOI: 10.3748/wjg.v31.i19.105283

ISSN 1007-9327 (print) ISSN 2219-2840 (online)

ORIGINAL ARTICLE

Retrospective Study

Serum calcium-based interpretable machine learning model for predicting anastomotic leakage after rectal cancer resection: A multi-center study

Bo-Yu Kang, Yi-Huan Qiao, Jun Zhu, Bao-Liang Hu, Ze-Cheng Zhang, Ji-Peng Li, Yan-Jiang Pei

Specialty type: Gastroenterology and hepatology

Provenance and peer review: Unsolicited article; Externally peer reviewed.

Peer-review model: Single blind

Peer-review report's classification

Scientific Quality: Grade A, Grade A, Grade A, Grade B, Grade B

Novelty: Grade A, Grade A, Grade A, Grade B, Grade B

Creativity or Innovation: Grade A, Grade A, Grade A, Grade B, Grade B

Scientific Significance: Grade A, Grade A, Grade A, Grade B, Grade B

P-Reviewer: Abdelsamad A; Li JT; Xu DW

Received: January 17, 2025

Revised: March 27, 2025

Accepted: April 27, 2025

Published online: May 21, 2025

Processing time: 124 Days and 13.2 Hours

Bo-Yu Kang, Yi-Huan Qiao, Jun Zhu, Ze-Cheng Zhang, Ji-Peng Li, Department of Digestive Surgery, Xijing Hospital of Digestive Diseases, Xi'an 710032, Shaanxi Province, China

Jun Zhu, Department of General Surgery, The Southern Theater Air Force Hospital, Guangzhou 510000, Guangdong Province, China

Bao-Liang Hu, Yan'an Medical College, Yan'an University, Yan'an 716000, Shaanxi Province, China

Ji-Peng Li, Department of Experiment Surgery, Xijing Hospital, Xi'an 710032, Shaanxi Province, China

Yan-Jiang Pei, Department of Digestive Surgery, Honghui Hospital, Xi'an Jiaotong University, Xi'an 710032, Shanxi Province, China

Co-first authors: Bo-Yu Kang and Yi-Huan Qiao.

Co-corresponding authors: Ji-Peng Li and Yan-Jiang Pei.

Corresponding author: Yan-Jiang Pei, MD, PhD, Professor, Department of Digestive Surgery, Honghui Hospital, Xi'an Jiaotong University, No. 555 Youyi East Road, Beilin District, Xi'an 710032, Shanxi Province, China. 15829329200@126.com

Abstract

BACKGROUND

Despite the promising prospects of utilizing artificial intelligence and machine learning (ML) for comprehensive disease analysis, few models constructed have been applied in clinical practice due to their complexity and the lack of reasonable explanations. In contrast to previous studies with small sample sizes and limited model interpretability, we developed a transparent eXtreme Gradient Boosting (XGBoost)-based model supported by multi-center data, using patients' basic information and clinical indicators to forecast the occurrence of anastomotic leakage (AL) after rectal cancer resection surgery. The model demonstrated robust predictive performance and identified clinically relevant thresholds, which may assist physicians in optimizing perioperative management.

AIM
To develop an interpretable ML model for accurately predicting the occurrence probability of AL after rectal cancer resection and define our clinical alert values for serum calcium ions.

METHODS
Patients who underwent anterior resection of the rectum for rectal carcinoma at the Department of Digestive Surgery, Xijing Hospital of Digestive Diseases, Air Force Medical University, and Shaanxi Provincial People's Hospital, were retrospectively collected from January 2011 to December 2021,. Ten ML models were integrated to analyze the data and develop the predictive models. Receiver operating characteristic (ROC) curves, calibration curve, decision curve analysis, accuracy, sensitivity, specificity, positive predictive value, negative predictive value, and F1 score were used to evaluate model performance. We employed the SHapley Additive exPlanations (SHAP) algorithm to explain the feature importance of the optimal model.

RESULTS
A total of ten features were integrated to construct the predictive model and identify the optimal model. XGBoost was considered the best-performing model with an area under the ROC curve (AUC) of 0.984 (95%confidence interval: 0.972-0.996) in the test set (accuracy: 0.925; sensitivity: 0.92; specificity: 0.927). Furthermore, the model achieved an AUC of 0.703 in external validation. The interpretable SHAP algorithm revealed that the serum calcium ion level was the crucial factor influencing the predictions of the model.

CONCLUSION
A superior predictive model, leveraging clinical data, has been crafted by employing the most effective XGBoost from a selection of ten algorithms. This model, by predicting the occurrence of AL in patients after rectal cancer resection, has identified the significant role of serum calcium ion levels, providing guidance for clinical practice. The integration of SHAP provides a clear interpretation of the model's predictions.

Key Words: Machine learning; Rectal cancer; Anastomotic leakage; SHapley Additive exPlanations algorithms

Core Tip: Ten machine learning models were established using ten factors and interpreted using the SHapley Additive exPlanations model. Through model evaluation and comparison, we selected the best prediction model and performed external validation in multiple centers. We found for the first time that perioperative serum calcium ion level plays an important role in the occurrence of anastomotic leakage (AL) after anterior resection of rectal cancer, and proposed that preoperative serum calcium level lower than 2.1 and postoperative calcium level lower than 2.2 are clinical warning values for the occurrence of AL.

Citation: Kang BY, Qiao YH, Zhu J, Hu BL, Zhang ZC, Li JP, Pei YJ. Serum calcium-based interpretable machine learning model for predicting anastomotic leakage after rectal cancer resection: A multi-center study. *World J Gastroenterol* 2025; 31(19): 105283
URL: https://www.wjgnet.com/1007-9327/full/v31/i19/105283.htm
DOI: https://dx.doi.org/10.3748/wjg.v31.i19.105283

INTRODUCTION

Colorectal cancer is recognized as a critical public health issue, being the third most common cancer and the second leading cause of cancer-related mortality worldwide[1]. Rectal cancer is one of the most common and severe diseases that threatens human health worldwide as well[2]. And the global burden of rectal cancer is expected to increase by 2040[3]. Up to 20% of patients undergoing low anterior resection for rectal cancer experience anastomotic leakage (AL)[4]. AL is a severe complication after rectal cancer surgery, leading to increased permanent stoma formation and cancer recurrence[5,6]. Therefore, it is of great importance to investigate the risk factors for AL to reduce its incidence.

Machine learning (ML), an artificial intelligence (AI)-based predictive tool, holds significant advantages in dealing with the complex relationships between diseases and contributing factors in the medical field[7,8]. Currently, ML is extensively employed for predicting diseases and survival outcomes, aiding physicians in making precise clinical decisions[9-12]. SHapley Additive exPlanations (SHAP) is a tool for explaining predictions made by ML models. By leveraging the SHAP algorithm to analyze and interpret individual model predictions, as well as to provide a more comprehensive view of the impact of inputs on the output, the model gains increased clinical value. Currently, this type of interpretable predictive model has been successfully applied across various medical fields, such as predictions for sepsis and hepatocellular carcinoma[13,14].

Despite the promising prospects of utilizing AI and ML for comprehensive disease analysis, few models have been applied in clinical practice due to their complexity and the lack of reasonable explanations[15,16]. In contrast to previous studies with small sample sizes and limited interpretability, we developed a transparent eXtreme Gradient Boosting (XGBoost)-based model supported by multi-center data, using patients' basic information and clinical indicators to forecast the occurrence of AL after rectal cancer resection. The model demonstrated robust predictive performance and identified clinically relevant thresholds, which may assist physicians in optimizing perioperative management.

MATERIALS AND METHODS

Data and participants

This study encompassed 1818 patients diagnosed with rectal cancer, all of whom underwent anterior resection of the rectum for rectal carcinoma at the Department of Digestive Surgery, Xijing Hospital of Digestive Diseases, Air Force Medical University, from January 2011 to December 2021. The external validation data was collected from Shaanxi Provincial People's Hospital, encompassing 60 cases of patients who underwent anterior resection for rectal cancer from January 2021 to January 2024. The implementation of radical resection for rectal carcinoma strictly adhered to the treatment guidelines of the corresponding period, with standard surgical procedures employed. The case information came from electronic medical records. This study was a secondary analysis of retrospective data and was a retrospective, multi-cohort, observational study using de-identified data. Therefore, informed consent and research ethics committee approval were not required. The study protocol adhered to the ethical guidelines of the 1995 Declaration of Helsinki, and the previous study was approved by the ethics committee of the First Affiliated Hospital of Air Force Military Medical University (approval No. KY20212211-N-1).

Inclusion and exclusion criteria

Inclusion criteria: (1) Age ≥ 18 years; (2) Patients with confirmed AL after anterior resection of the rectum for rectal cancer; and (3) Primary rectal carcinoma confirmed by preoperative pathology.

Exclusion criteria: (1) Non-unifocal primary cancer lesions; (2) Development of rectourethral or rectovaginal leakage; (3) Incomplete clinical data; (4) Abnormal or unclear clinical data; (5) All cases with severe heart, lung, and brain diseases or serious infections; and (6) All cases with coagulation dysfunction or severe blood disorders. The flowchart of patient selection and model construction is illustrated in Figure 1.

Definitions and data preprocessing

The diagnosis of rectal cancer was based on the 2021 guidelines from the National Comprehensive Cancer Network for the diagnosis and treatment of rectal cancer. The definition of AL adopted the criteria proposed by The International Study Group of Rectal Cancer in 2009, and patients with three grades of A, B, and C were included in the study[17]. Based on 28 continuous variables, the median was taken as the cutoff value for dichotomization and 11 categorical variables were analyzed in dummy form. Preoperative and postoperative patient data were collected three days prior to surgery and one day after surgery, respectively, and subsequently entered into the electronic medical records. The data did not contain missing values.

Study variables

Based on patient information, clinical variables, and hematological indicators, we included 39 variables for analysis and screened for important factors using least absolute shrinkage and selection operator (LASSO) regression, stepwise Logistic regression, and Boruta regression. By employing LASSO regression, we used the optimal regularization lambda parameters, divided the entire dataset into 10 folds, and sequentially incorporated each variable into the model, ceasing the addition when the area under the receiver operating characteristic (ROC) curve (AUC) no longer increased, thereby conducting feature selection. Nine variables were considered significant in all regression analyses. Preoperative and postoperative serum creatinine levels, as well as postoperative cystatin C, were considered to be of significant importance in both regression models. These three variables all reflect renal function. To minimize potential interactions and considering that postoperative serum creatinine is more commonly used in clinical practice, we selected postoperative serum creatinine for inclusion in the model construction.

Model construction and validation

The patients (n = 1818) were randomly assigned to training and testing datasets in a 7:3 ratio. To evaluate the impact of data imbalance, models were constructed and evaluated using both raw data and SMOTE resampled data (n = 3721), and the most effective data processing method was selected. Additionally, the efficacy of the model will be rigorously evaluated through external validation processes to guarantee the precision and dependability of its prognostic capabilities. Subsequently, an optimal predictive model was developed utilizing 10 distinct ML algorithms: Logistic regression, support vector machine, gradient boosting machines, neural network, random forest, XGBoost, K-nearest neighbors, AdaBoost, light gradient boosting machine, and CatBoost. The performance of the models was rigorously assessed employing ROC curves, calibration curve, decision curve analysis (DCA), accuracy, sensitivity, specificity, positive predictive value (PPV), negative predictive value (NPV), and F1 score.

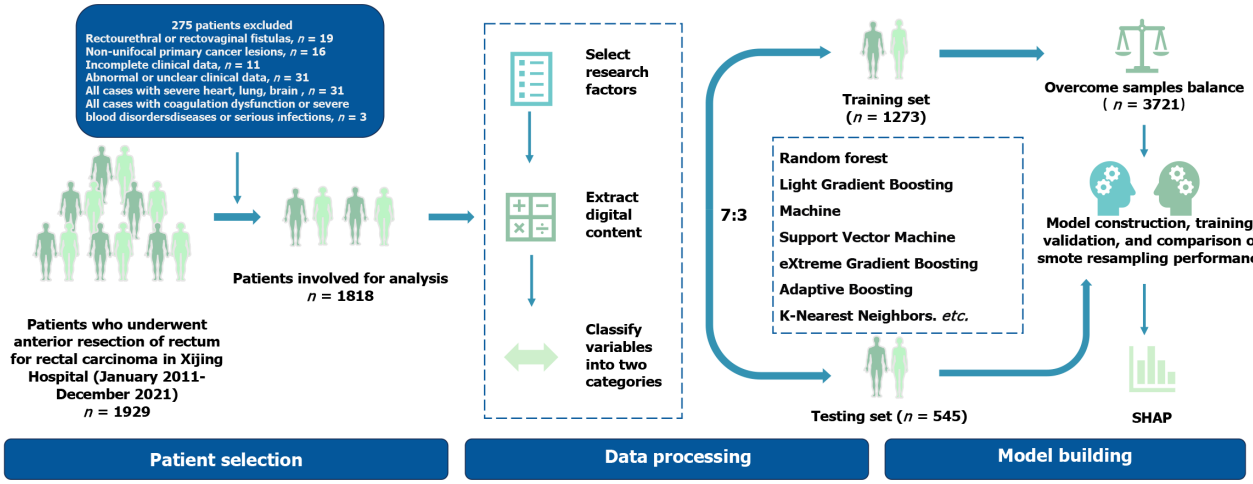

Figure 1 Flowchart of study procedure. SHAP: SHapley Additive exPlanations.

Evaluating predictive factors using SHAP values

SHAP, originally developed by Lee, is an approach grounded in cooperative game theory for elucidating ML models[18]. By assigning SHAP values that quantify the contribution of each predictor variable, SHAP creates a consistent framework ideal for assessing variable contributions within predictive models, thus mitigating the challenge of model opacity. Distinct from alternative methodologies, SHAP values offer local interpretability, enhancing the comprehension of model intricacies. Positive SHAP values indicate that the variable is more instrumental in predicting patients with AL, while negative values suggest that the variable is more conducive to predicting patients without AL.

Statistical analysis

Statistical analyses were performed by using R, version 4.4.1 (R, Foundation for Statistical Computing). SMOTE resampling was calculated using the R package DMwR. LASSO regularization model, Boruta regression, and Logistic regression were calculated using the R packages Boruta and glmnet. Ten ML models were calculated using the R packages e1071, gbm, caret, XGBoost, nnet, Adaboost, lightgbm, and Catboost. ROC curve, DCA, and calibration curve were calculated using the R packages pROC and rmda and risk regression. All continuous variables in this study were converted into categorical variables by median, and all categorical variables appeared in frequency and percentage form. The χ^2 test was used to compare the differences between groups, and $P < 0.05$ was considered statistically significant. The kernelshap and shiny packages in R were utilized to ascertain the significance and hierarchy of variables within the model. The directional influence of each variable on the outcome was established based on SHAP values and detailed visual explanations were generated at the individual observation level.

RESULTS

Patients' baseline characteristics

This retrospective study included 1818 patients (average age, 61.6 years; range, 20-89 years) from January 2011 to December 2021, including 1119 males and 699 females, of whom 86 (4.73%) suffered from AL. The baseline data of included patients are shown in Table 1. Baseline data for the training set, validation set, and external validation are shown in Supplementary Tables 1-3.

There was no significant difference in age, location, or other aspects between the AL group and NAL group ($P = 0.433$, $P = 0.517$). In the univariate analysis, significant differences ($P < 0.05$) were observed between the AL group and the NAL group with respect to family history, tobacco and alcohol history, CD34, T stage, preoperative and postoperative blood calcium levels, preoperative platelet count, preoperative plasma albumin and globulin levels, positive lymph node count (rLNs), and neoadjuvant therapy. Upon further multivariate analysis, significant differences were observed between the AL group and the NAL group in family history, tobacco and alcohol history, CD34, T stage, preoperative and post-operative blood calcium levels, preoperative platelet count, rLNs, and neoadjuvant therapy. These factors also emerged as common key variables across the three multivariate analysis results. Based on statistical analysis and clinical experience, we ultimately selected ten variables, namely, family history, tobacco and alcohol history, CD34, T stage, preoperative and postoperative blood calcium levels, preoperative platelet count, postoperative creatinine, rLNs, and neoadjuvant therapy, as parameters for the ML model (Supplementary Figure 1). Correlation coefficients between these variables are presented as a correlation matrix (Figure 2) and all the correlation coefficients were below 0.8, which demonstrated no serious collinearity. At this point, we identified the significant impact of serum calcium ion, as both preoperative and postoperative levels are important determinants of AL.

Table 1 Baseline characteristics of patients with and without anastomotic leakage, *n* (%)

	NAL (*n* = 1732)	AL (*n* = 86)	*P* value
Sex = male	1055 (60.9)	64 (74.4)	0.016
Tobacco or alcohol			< 0.001
No	1256 (72.5)	46 (53.5)	
Tobacco	258 (14.9)	18 (20.9)	
Alcohol	25 (1.4)	1 (1.2)	
All	193 (11.1)	21 (24.4)	
T stage			< 0.001
T1	192 (11.1)	2 (2.3)	
T2	453 (26.2)	17 (19.8)	
T3	995 (57.4)	43 (50.0)	
T4	92 (5.3)	24 (27.9)	
N stage			0.025
N0	291 (16.8)	12 (14.0)	
N1	1260 (72.7)	57 (66.3)	
N2	181 (10.5)	17 (19.8)	
Histological type			< 0.001
Adenocarcinoma	36 (2.1)	0 (0.0)	
Adenosquamouscarcinoma	0 (0.0)	6 (7.0)	
Others	1663 (96.0)	80 (93.0)	
Multi	1 (0.1)	0 (0.0)	
Neuroendocrine	17 (1.0)	0 (0.0)	
Stromal	15 (0.9)	0 (0.0)	
Family = yes	32 (1.8)	10 (11.6)	< 0.001
CD34 = yes	647 (37.4)	67 (77.9)	< 0.001
FOBT = M1	1276 (73.7)	64 (74.4)	0.978
Location = others	76 (4.4)	2 (2.3)	0.517
Age = high	871 (50.3)	39 (45.3)	0.433
Neoadjuvant = yes	142 (8.2)	57 (66.3)	< 0.001

NAL: Non-anastomotic leakage; AL: Anastomotic leakage.

Comparative performance analysis of ML models for predicting risk of AL

We trained 10 different ML prediction models on a dataset of 1273 raw samples and a dataset of 3721 samples, which were balanced using the SMOTE (Synthetic Least Squares) method and focused on 10 key factors. The performance of each model in the test set is shown in Table 2.

Most models demonstrated satisfactory predictive performance in terms of accuracy, sensitivity, specificity, PPV, NPV, and F1 score. When comparing the models derived from the raw dataset and the SMOTE-resampled dataset, it was observed that while the resampled group exhibited higher accuracy, the F1 score and calibration curve were inferior. The F1 score, as the harmonic mean of precision and recall, accurately shows a model's ability to predict minority classes[19]. The calibration curve, which compares predicted and actual outcomes, indicates how well the model performs in real-world scenarios[20]. When early stopping was applied, SMOTE resampling of the data led to worse F1 scores and calibration curves for AL patients. This suggests that resampling the minority data amplifies the noise and raises the risk of overfitting. XGBoost, Logistic regression, and Neural Network performed well on the ROC curve, with the highest AUC values of 0.988, 0.986 and 0.984, respectively, signifying their robust predictive capacity for AL. In terms of calibration curves and F1 scores, XGBoost outperformed the other two models, leading us to conclude that XGBoost is the optimal model in terms of performance for predicting AL occurrence, with the best PPV (0.92) and NPV (0.927). DCA is a method for evaluating the potential impact of predictive models on clinical decision-making and it assesses the clinical

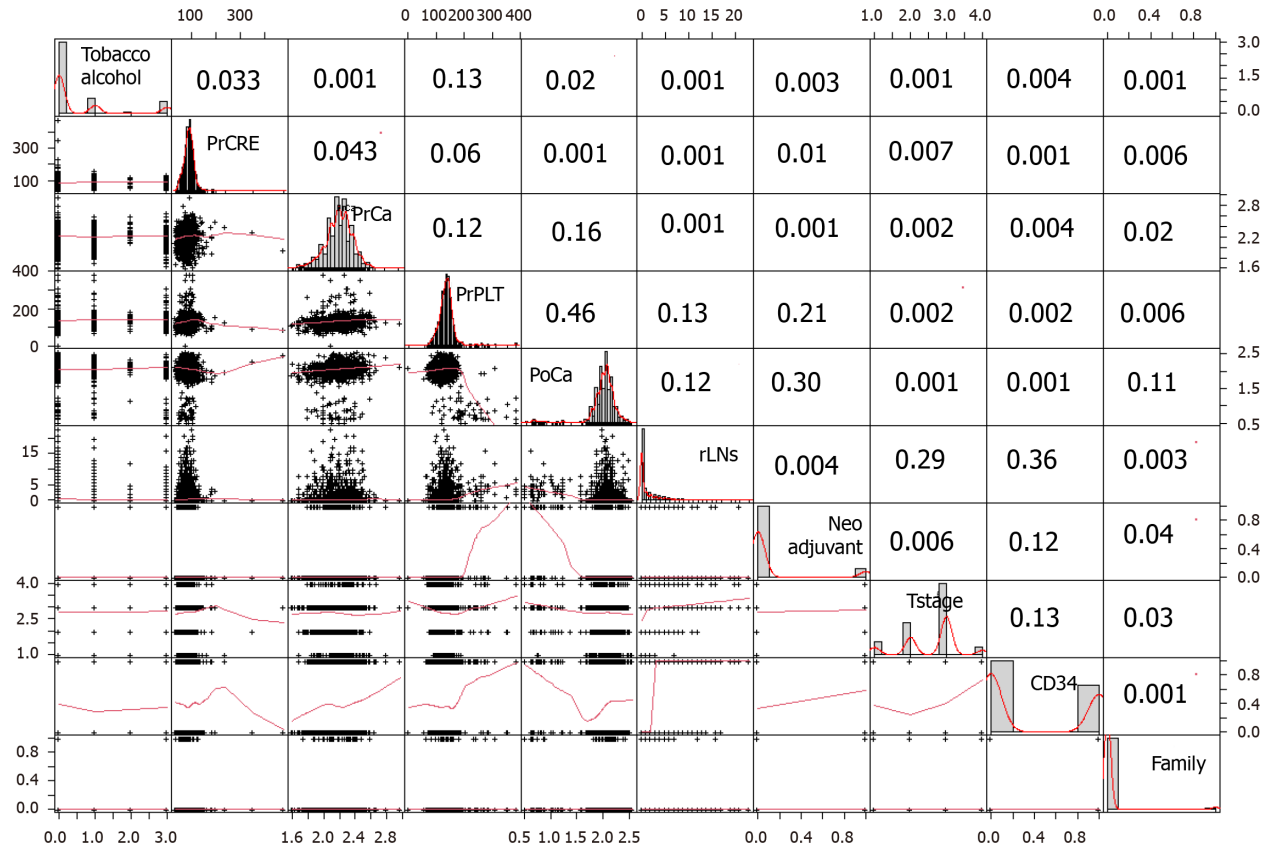

Figure 2 Interaction between variables in a correlation matrix. PrCa: Prstoperative calcium ion concentration; PrCRE: Preoperative serum creatinine concentration; PoCa: Postoperative calcium ion concentration; rLNs: Positive lymph node count; PrPLT: Preoperative platelet concentration.

utility of a model by comparing the net benefits of different threshold probabilities for treatment decisions[21]. The calibration curve in predictive modeling serves as a graphical representation that delineates the agreement between the predicted probabilities and the observed outcomes, thereby assessing the model's accuracy[22]. Therefore, to further evaluate the fitting effect of the XGBoost model, we drew its DCA curve and calibration curve. The DCA curve shows that the XGBoost model can provide profitable predictive performance within a threshold probability range of around 0.05 to 0.9. Despite the presence of data imbalance, the model demonstrated good performance in calibration curves, ROC curves, and confusion matrices, indicating that it indeed possesses high predictive performance (Figures 3 and 4).

External validation of the model

Although the model exhibited satisfactory predictive performance in the training and validation cohorts, the generalizability of findings from a single-center study is inherently constrained. To bolster the evidence for the model's predictive utility and to underscore the pivotal role of serum calcium ion concentrations, we pursued external validation. This rigorous assessment culminated in an AUC of 0.703 (95% confidence interval: 0.525 to 0.881) (Figure 5).

The SHAP to model interpretation

While ML models can achieve high predictive accuracy, their decision-making processes are often opaque, limiting their interpretability in clinical contexts. The application of SHAP has effectively demystified the "black box" nature of ML models, endowing them with interpretability. Through the lens of SHAP, we are able to gain a deeper comprehension of the predictive processes and, consequently, enhance the reliability of our models[23]. This approach allows for a more transparent understanding of how features contribute to the output and the individual characteristics of patients, which is crucial for the credibility and effectiveness of ML applications. In this study, we employed SHAP values to quantify the contribution of each variable to the predictive outcomes for patients (Figure 6). The greater the SHAP value, the more significant the increase in the incidence of AL that the variable was associated with. This method provided a robust framework for understanding the impact of individual factors on AL risk. Therefore, we analyzed one AL patient and one NAL patient separately (Figure 7). By using the interaction of significant factors diagram, we can clarify the effects of different factor combinations on the model and gain a deeper understanding of its behavior (Figure 8).

DISCUSSION

AL is a serious complication after anterior resection of rectal cancer, with a clinical incidence ranging from 3% to 20%, and

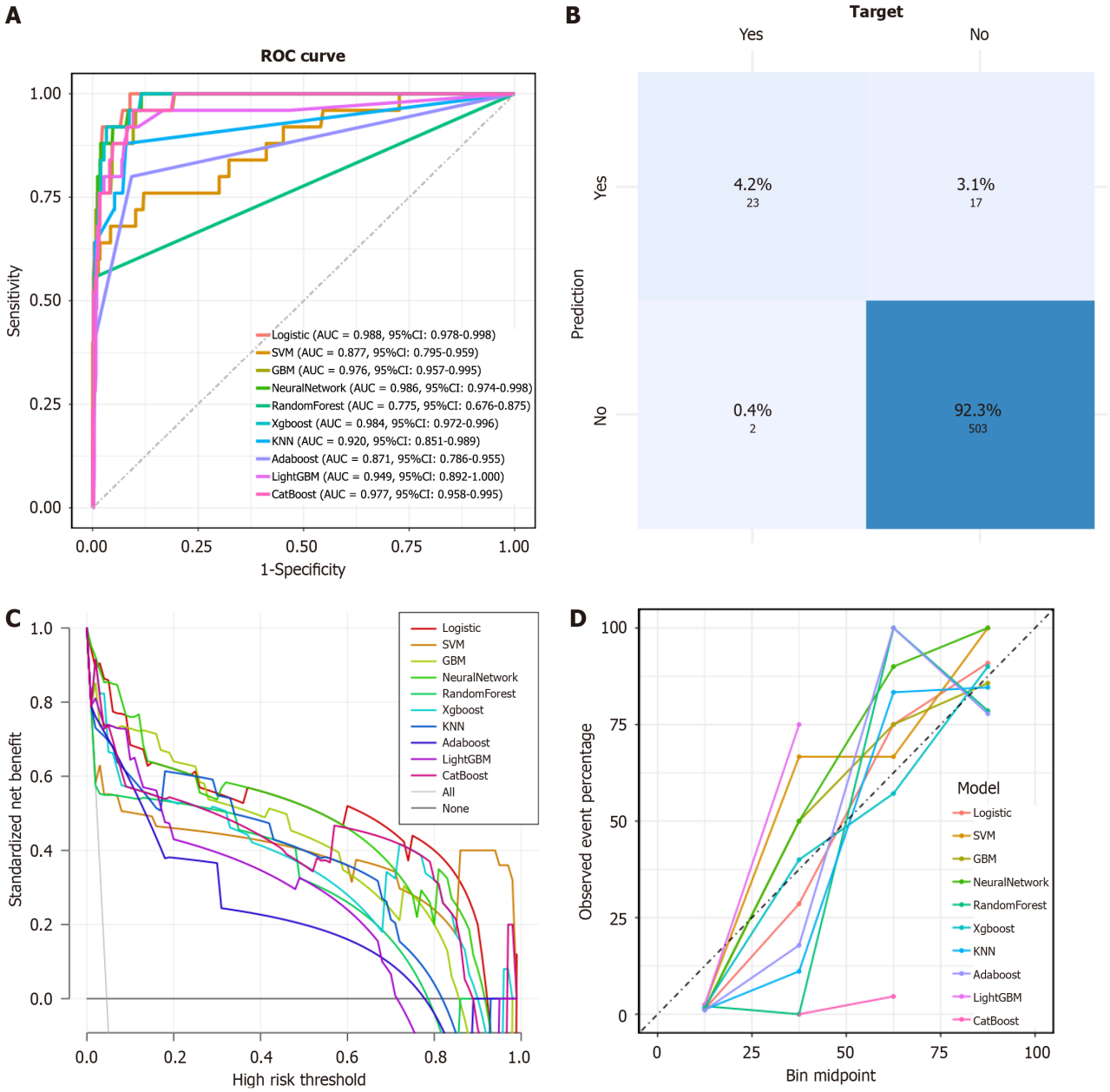

Figure 3 Testing and evaluation of eXtreme Gradient Boosting model based on raw data. A: Area under the receiver operating characteristic curve comparison between models; B: The confusion matrix of eXtreme Gradient Boosting model; C: Comparison of decision curve analysis curves between models; D: Comparison of calibration curves between models. AUC: Area under the receiver operating characteristic curve; ROC: Receiver operating characteristic; SVM: Support vector machine; GBM: Gradient boosting machines; KNN: K-nearest neighbors; LightGBM: Light gradient boosting machine.

can lead to severe mortality and poor prognosis[24]. In recent studies, AL has been confirmed to be associated with poor overall survival and disease-free survival[25]. Although new surgical methods have been recognized to be able to improve surgical outcomes[26], the occurrence of AL still poses a significant threat to patients. Therefore, reducing the occurrence of AL or intervening early in AL becomes a top priority.

In this study, to better predict the occurrence of AL and clarify the risk threshold for its development, we divided the clinical information, hematological indicators, and surgical details of 1818 patients into binary variables for analysis and external validation among 60 patients. This approach not only refined the model's predictive capabilities but also provides a clearer benchmark for clinical decision-making and perioperative care. And this study included 86 cases of AL, which is a larger number of positive cases compared to previous studies. This increased sample size of affected individuals contributes to a more accurate and reliable model. In the selection of patients, with the criterion that missing values should be less than 10%, we opted to exclude those with incomplete clinical data to ensure the most authentic dataset. To ensure data authenticity and minimize potential biases, we opted not to impute missing values and instead excluded incomplete records.

From a methodological perspective, in order to improve the accuracy of the model variables, we used three variable importance assessment methods and selected variables that are deemed significant by at least two of these methods for the construction of our ML model. Furthermore, to mitigate issues such as noise amplification and overfitting that may

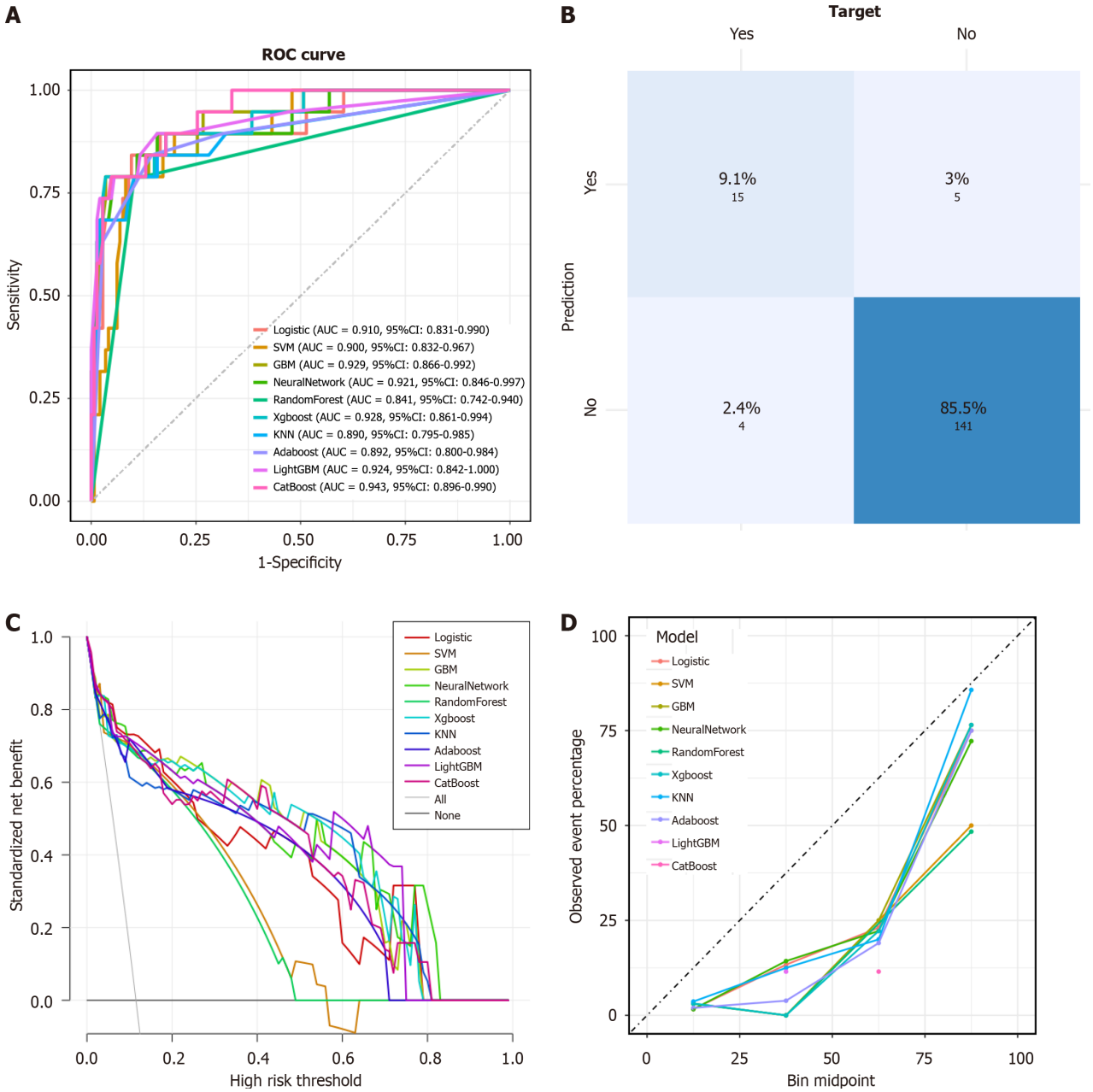

Figure 4 Testing and evaluation of eXtreme Gradient Boosting model based on SMOTE-resampled data. A: Area under the receiver operating characteristic curve comparison between models; B: The confusion matrix of eXtreme Gradient Boosting model; C: Comparison of decision curve analysis curves between models; D: Comparison of calibration curves between models. AUC: Area under the receiver operating characteristic curve; ROC: Receiver operating characteristic; SVM: Support vector machine; GBM: Gradient boosting machines; KNN: K-nearest neighbors; LightGBM: Light gradient boosting machine.

arise from SMOTE resampling, we constructed models using two sets of data: One before and one after SMOTE resampling. This approach enhanced the quality of the data, ensuring a more robust and reliable model. In the realm of ML, this study incorporated 10 distinct mainstream ML models. We employed a validation set to assess the models, conducting a comprehensive comparison that considered both graphical representations and data metrics. Ultimately, we determined that the XGBoost ML model demonstrated optimal performance across all assessed metrics. Moreover, this model demonstrated commendable predictive performance on imbalanced datasets as well, which aligned with the clinical reality of the low incidence of AL. Although the occurrence of AL is highly correlated with the medical environment and the surgical team at the time of surgery, the construction of this model can serve two main purposes. On the one hand, it allows for the estimation of the likelihood of an anastomotic leak in patients, guiding the medical team to pay closer attention to those at risk. On the other hand, it helps in identifying significant factors and determining clinical alert values, thereby improving patients outcomes.

From the importance ranking of features displayed by SHAP, which was used to assess the risk factors for the development of anastomotic leaks. the number of positive lymph nodes was considered the most significant prognostic factor, which was associated with tumor spread and metastasis, indicating the need for a more extensive lymph node dissection. In terms of hematological indicators, preoperative and postoperative serum calcium ion levels and preoperative platelet level were identified as the primary contributors. By synthesizing previous research and clinical

Table 2 Evaluation indicators in testing set of 10 machine learning models

Model	Accuracy	Sensitivity/PPV	Specificity/NPV	F1
Logistic.R	0.916	0.98	0.912	0.521
SVM.R	0.873	0.76	0.879	0.355
GBM.R	0.901	0.96	0.898	0.471
NeuralNetwork.R	0.89	0.98	0.885	0.455
RandomForest.R	0.974	0.56	0.994	0.667
XGBoost.R	0.925	0.92	0.927	0.708
KNN.R	0.919	0.88	0.921	0.5
Adaboost.R	0.903	0.8	0.908	0.43
LightGBM.R	0.916	0.92	0.915	0.5
CatBoost.R	0.906	0.96	0.904	0.485
Logistic.S	0.914	0.98	0.91	0.515
SVM.S	0.952	0.92	0.954	0.639
GBM.S	0.956	0.96	0.956	0.667
NeuralNetwork.S	0.958	0.96	0.958	0.676
RandomForest.S	0.95	0.76	0.96	0.585
XGBoost.S	0.939	0.96	0.938	0.593
KNN.S	0.952	0.84	0.958	0.618
Adaboost.S	0.804	0.92	0.798	0.301
LightGBM.S	0.927	0.96	0.925	0.545
CatBoost.S	0.943	0.96	0.942	0.608

Models denoted with 'S' are established using data post-SMOTE resampling, while those denoted with 'R' are constructed from the original data set. PPV: Positive predictive value; NPV: Negative predictive value; SVM: Support vector machine; GBM: Gradient boosting machines; XGBoost: eXtreme Gradient Boosting; KNN: K-nearest neighbors; LightGBM: Light gradient boosting machine.

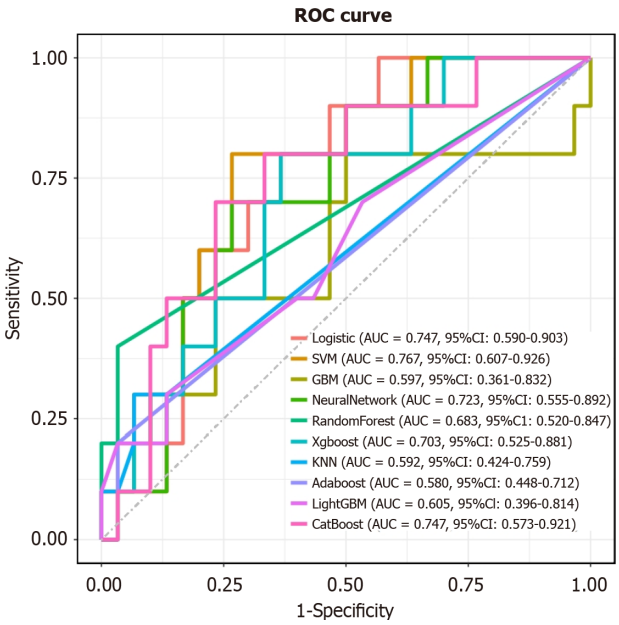

Figure 5 Receiver operating characteristic curve analysis of the eXtreme Gradient Boosting model based on the external validation dataset. AUC: Area under the receiver operating characteristic curve; ROC: Receiver operating characteristic; SVM: Support vector machine; GBM: Gradient

boosting machines; KNN: K-nearest neighbors; LightGBM: Light gradient boosting machine.

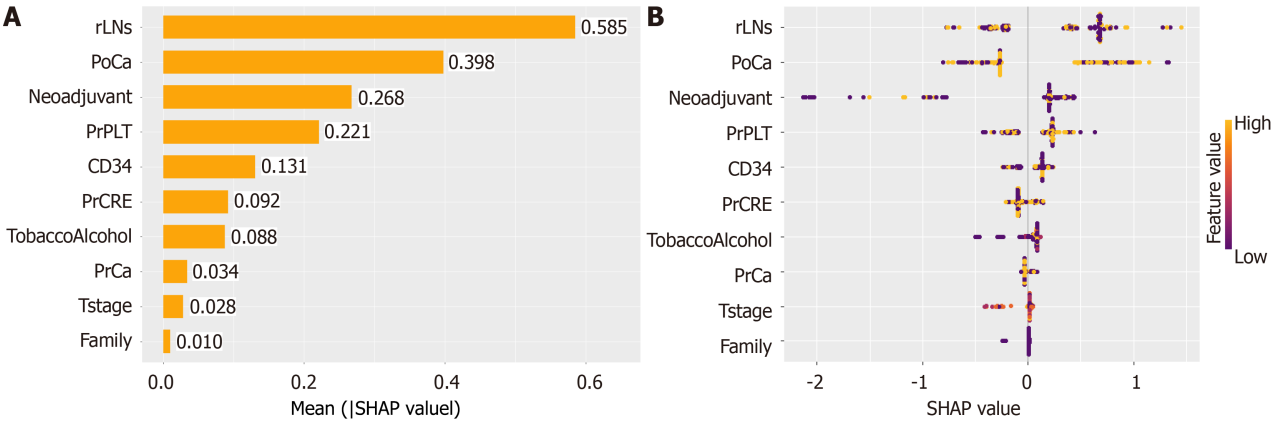

Figure 6 Interpretation of the eXtreme Gradient Boosting model using SHapley Additive exPlanations. A: Mean importance ranking of features displayed by SHapley Additive exPlanations (SHAP); B: Bee colony diagram of characterization attributes in SHAP. SHAP: SHapley Additive exPlanations.

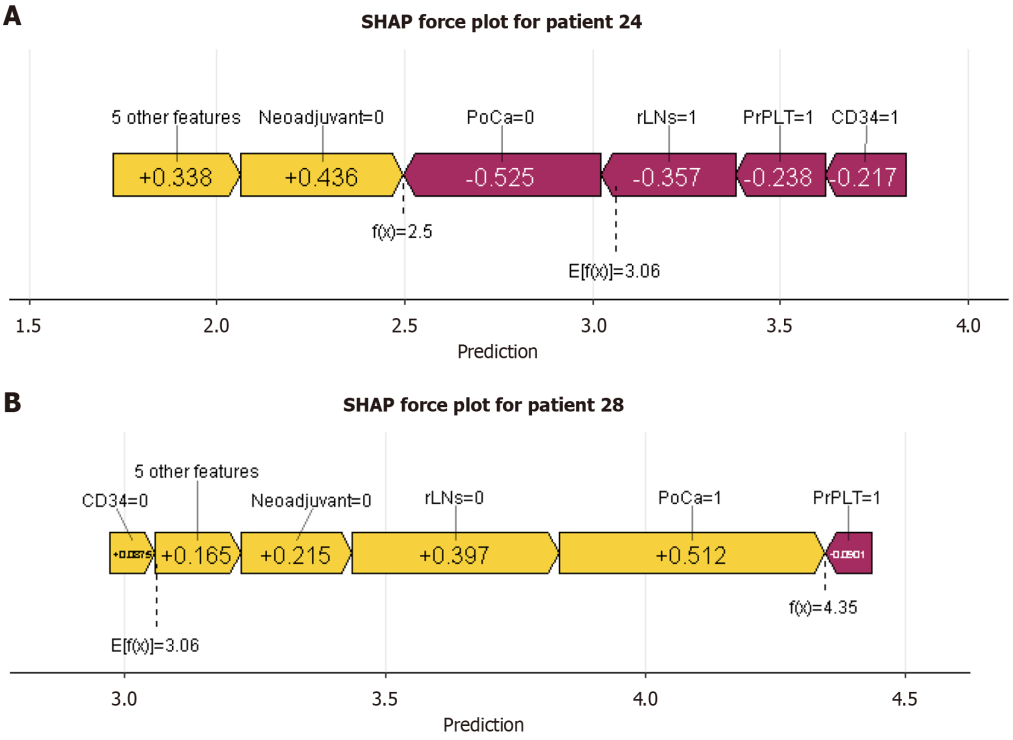

Figure 7 Interpretation of the light gradient boosting machine model using SHapley Additive exPlanations. A: A patient who did not develop anastomotic leakage; B: A patient who developed anastomotic leakage. SHAP: SHapley Additive exPlanations; PoCa: Postoperative calcium ion concentration; rLNs: Positive lymph node count; PrPLT: Preoperative platelet concentration.

experience, it is posited that both of these factors are intricately linked to the processes of infection and healing at the anastomotic site. A study in 2021 demonstrated that postoperative serum calcium ion level may be used to identify patients at risk for AL, and postoperative low serum calcium ion level can represent a risk factor for AL in digestive surgery[27]. In our study, we found that postoperative serum calcium ion levels have a greater impact on AL compared to preoperative serum calcium ion levels. On the other hand, this also highlights the importance of continuous blood calcium monitoring. In the context of coagulation, calcium ions, also known as clotting factor IV, can activate the intrinsic pathway of blood coagulation in conjunction with other coagulation factors, thereby accelerating the formation and activation of thrombin[28].

From a mechanistic perspective, existing studies have demonstrated that local calcium can modulate keratinocytes and fibroblasts, as well as contribute to the formation of the stratum corneum lipid barrier through signal transduction and gene expression[29]. Further research indicates that calcium flash (rapid calcium waves) dependent on TRP channels is

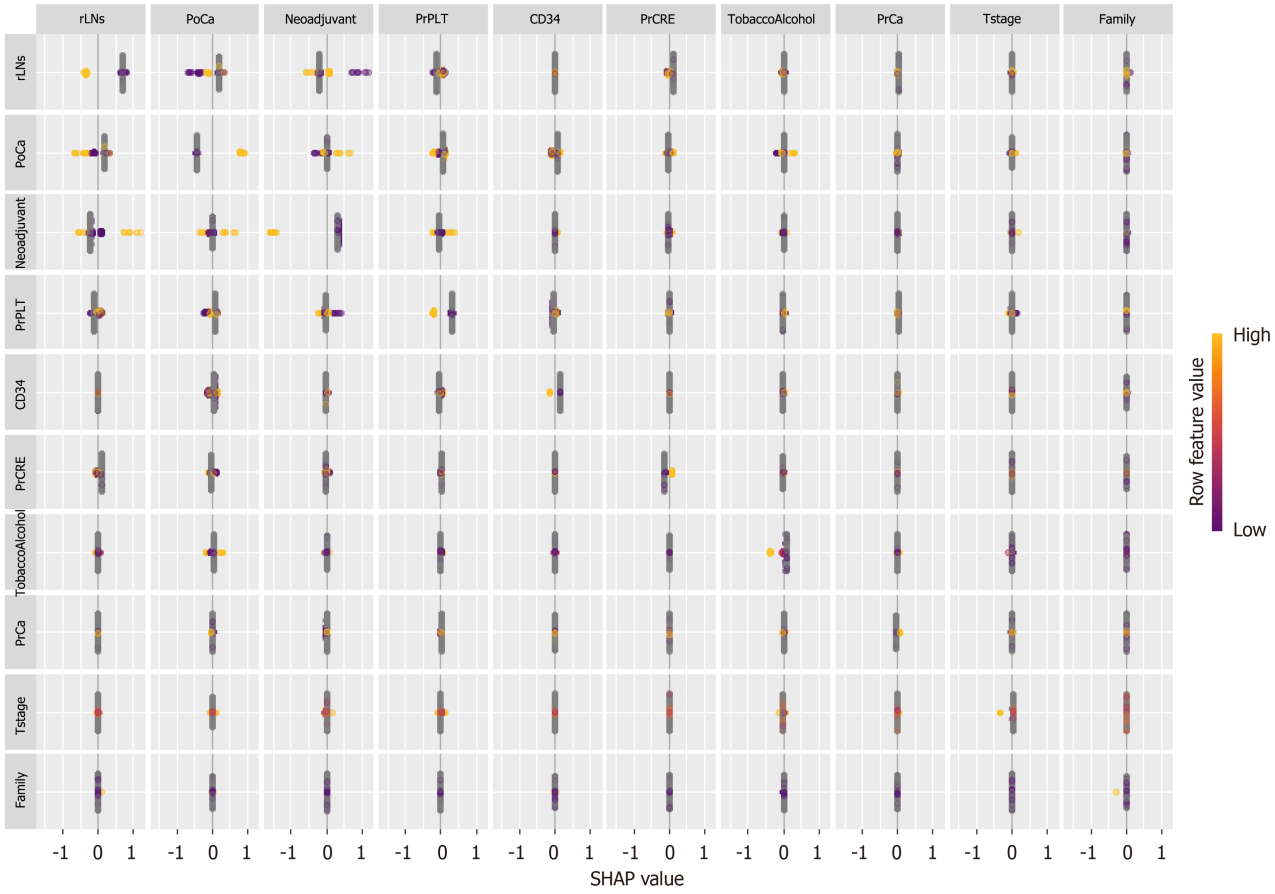

Figure 8 Interaction of significant factors based on SHapley Additive exPlanations. SHAP: SHapley Additive exPlanations; PrCa: Preoperative calcium ion concentration; PrCRE: Preoperative serum creatinine concentration; PoCA: Postoperative calcium ion concentration; rLNs: Positive lymph node count; PrPLT: Preoperative platelet concentration.

involved in the early stages of wound healing, which could partially explain the poor intestinal anastomosis associated with low calcium levels[30]. Building on the aforementioned theories, researchers have utilized calcium silicate ceramics to stimulate adipose-derived stem cells, thereby promoting angiogenesis and enhancing skin wound healing, as confirmed in animal models[31]. Beyond these functions, calcium ions can also enhance the antimicrobial activity of antimicrobial dressings by damaging and destroying bacterial cell membranes, as well as by oxidizing bacterial media, which further contributes to bacterial killing[32,33]. Clinical applications bestow greater significance upon basic research, and studies on the role of calcium in wound healing have been performed in animal models[34]. Therefore, in response to the present clinical practice, we can initially maintain the normal serum calcium ion levels in patients to minimize the risk of anastomotic leaks. In the future, it may be possible to further develop calcium-rich dressings or sutures to promote the healing of anastomotic sites in patients. Preoperative systemic immune-inflammation index (SII) in patients with colorectal cancer is considered a marker for evaluating the systemic inflammatory status of patients and associated with patient prognosis[35]. SII is calculated with the formula SII = (P × N)/L, where P, N, and L refer to platelet, neutrophil, and lymphocyte counts, respectively. Therefore, we believe that elevated preoperative platelet counts may indicate a heightened systemic inflammatory response, which could increase the risk of AL in patients and reduce their prognosis.

In this research, we found that neoadjuvant therapy is a risk factor for anterior resection of rectal cancer, which is consistent with previous studies[36]. A new significant risk factor was identified: Perioperative serum calcium ion levels. Patients with preoperative serum calcium ion levels below 2.2 or postoperative serum calcium ion levels below 2.06 are considered to be at risk for AL. This finding can not only aid clinicians in identifying high-risk populations for AL, but also provide clinical alert values. We posit that calcium plays a crucial role in anastomotic healing by exerting antimicrobial effects, promoting hemostasis, and enhancing the function of keratinocytes and fibroblasts. Consequently, hypocalcemia significantly impacts the risk of AL in patients post-proctectomy for rectal cancer.

Our multicenter study has constructed an ML predictive model that exhibits superior predictive accuracy, demonstrating commendable performance in both internal and external validation processes. Furthermore, the dichotomization of variables within our model has yielded clinically relevant threshold values for alerting purposes. With the aim of enhancing clinical utility and facilitating widespread adoption across a broad spectrum of hospitals, we have engineered an intuitive user interface (UI) designed for medical practitioners. This interface empowers clinicians to conduct real-time assessments of patients' risk for AL, thereby enabling them to modify treatment strategies in a timely and informed manner. At present, we have collected the survival data of 963 patients, and further survival analysis is expected.

However, our study was not without its limitations. Primarily, our retrospective study was inevitably subject to information bias, which included omissions and errors in data collection. Additionally, during the data processing phase, factors such as missing data also came into play. In addition, due to the limitations of our center's database, some important factors may be overlooked in model construction and multicenter validation, such as body mass index and the distance from the lower edge of the tumor to the dentate line. The lower AUC in the external validation may be attributed to the following reasons: (1) The external validation dataset is relatively small and there are differences in the baseline characteristics of patients from different centers; and (2) Variations exist in the testing conditions of hematological indicators across different centers, and during the study period, the testing techniques for hematological indicators have evolved. This omission may result in a less comprehensive model and could diminish its accuracy and stability. Finally, while this study provided an interactive, physician-friendly UI, there was still a gap before it meets clinical application standards. Therefore, we plan to develop a related app based on this model to facilitate its widespread use in clinical practice.

CONCLUSION

We have developed an ML predictive model based on perioperative serum calcium ion levels and other indices, which has shown excellent performance in predicting the occurrence of AL following anterior resection for rectal cancer. The application of SHAP has significantly enhanced the model's interpretability, playing a crucial role in both understanding the model and facilitating its clinical application. During the model construction, we have also identified the significant role of perioperative serum calcium ion and defined clinical alert values, which aids in the early warning of AL and provides prognostic information for patients.

FOOTNOTES

Author contributions: Kang BY and Qiao YH contributed equally to this study as co-first authors; Li JP and Pei YJ contributed equally to this study as co-corresponding authors; Kang BY was responsible for study conceptualization and design, data acquisition, analysis, and interpretation, and manuscript drafting, review, and editing; Qiao YH was responsible for study conceptualization and design, data acquisition, analysis, and interpretation, and manuscript review and editing; Zhu J was responsible for data acquisition, analysis, and interpretation, statistical analysis, and manuscript review and editing; Hu BL was responsible for data analysis and interpretation, and statistical analysis. Li JP and Pei YJ were responsible for manuscript review and editing.

Supported by National Natural Science Foundation of China, No. 82172781; and Shaanxi Health Scientific Research Innovation Team Project, No. 2024TD-06.

Institutional review board statement: The previous study was approved by the ethics committee of the First Affiliated Hospital of Air Force Military Medical University (approval No. KY20212211-N-1).

Informed consent statement: This study was a secondary analysis of retrospective data and was a retrospective, multi-cohort, observational study using de-identified data. Therefore, consent and research ethics committee approval was not required.

Conflict-of-interest statement: The authors declare that the research was conducted in the absence of any commercial or financial relationships that could be construed as a potential conflict of interest.

Data sharing statement: The data that support the findings of this study are available from the corresponding author upon reasonable request.

Country of origin: China

ORCID number: Bo-Yu Kang 0009-0001-1758-8627; Ji-Peng Li 0000-0001-8822-1518; Yan-Jiang Pei 0009-0009-4899-9312.

S-Editor: Lin C
L-Editor: Wang TQ
P-Editor: Zhao S

REFERENCES

1 **Thomas CE**, Lin Y, Kim M, Kawaguchi ES, Qu C, Um CY, Lynch BM, Van Guelpen B, Tsilidis K, Carreras-Torres R, van Duijnhoven FJB,

Sakoda LC, Campbell PT, Tian Y, Chang-Claude J, Bézieau S, Budiarto A, Palmer JR, Newcomb PA, Casey G, Le Marchandz L, Giannakis M, Li CI, Gsur A, Newton C, Obón-Santacana M, Moreno V, Vodicka P, Brenner H, Hoffmeister M, Pellatt AJ, Schoen RE, Dimou N, Murphy N, Gunter MJ, Castellví-Bel S, Figueiredo JC, Chan AT, Song M, Li L, Bishop DT, Gruber SB, Baurley JW, Bien SA, Conti DV, Huyghe JR, Kundaje A, Su YR, Wang J, Keku TO, Woods MO, Berndt SI, Chanock SJ, Tangen CM, Wolk A, Burnett-Hartman A, Wu AH, White E, Devall MA, Díez-Obrero V, Drew DA, Giovannucci E, Hidaka A, Kim AE, Lewinger JP, Morrison J, Ose J, Papadimitriou N, Pardamean B, Peoples AR, Ruiz-Narvaez EA, Shcherbina A, Stern MC, Chen X, Thomas DC, Platz EA, Gauderman WJ, Peters U, Hsu L. Characterization of Additive Gene-environment Interactions For Colorectal Cancer Risk. *Epidemiology* 2025; **36**: 126-138 [PMID: 39316822 DOI: 10.1097/EDE.0000000000001795]

2 **Lian J**, Li J, Liu C, Luan B, Miao Y. Research progress of robot and laparoscope in postoperative complications of rectal cancer. *J Robot Surg* 2024; **18**: 135 [PMID: 38520491 DOI: 10.1007/s11701-024-01872-3]

3 **de'Angelis N**, Schena CA, Azzolina D, Carra MC, Khan J, Gronnier C, Gaujoux S, Bianchi PP, Spinelli A, Rouanet P, Martínez-Pérez A, Pessaux P; Association Française de Chirurgie (AFC). Histopathological outcomes of transanal, robotic, open, and laparoscopic surgery for rectal cancer resection. A Bayesian network meta-analysis of randomized controlled trials. *Eur J Surg Oncol* 2025; **51**: 109481 [PMID: 39581810 DOI: 10.1016/j.ejso.2024.109481]

4 **Penna M**, Hompes R, Arnold S, Wynn G, Austin R, Warusavitarne J, Moran B, Hanna GB, Mortensen NJ, Tekkis PP; International TaTME Registry Collaborative. Incidence and Risk Factors for Anastomotic Failure in 1594 Patients Treated by Transanal Total Mesorectal Excision: Results From the International TaTME Registry. *Ann Surg* 2019; **269**: 700-711 [PMID: 29315090 DOI: 10.1097/SLA.0000000000002653]

5 **Zarnescu EC**, Zarnescu NO, Costea R. Updates of Risk Factors for Anastomotic Leakage after Colorectal Surgery. *Diagnostics (Basel)* 2021; **11** [PMID: 34943616 DOI: 10.3390/diagnostics11122382]

6 **Su Y**, Li Y, Zhang H, Yang W, Liu M, Luo X, Liu L. Machine learning model for prediction of permanent stoma after anterior resection of rectal cancer: A multicenter study. *Eur J Surg Oncol* 2024; **50**: 108386 [PMID: 38776864 DOI: 10.1016/j.ejso.2024.108386]

7 **Hu W**, Jin T, Pan Z, Xu H, Yu L, Chen T, Zhang W, Jiang H, Yang W, Xu J, Zhu F, Dai H. An interpretable ensemble learning model facilitates early risk stratification of ischemic stroke in intensive care unit: Development and external validation of ICU-ISPM. *Comput Biol Med* 2023; **166**: 107577 [PMID: 37852108 DOI: 10.1016/j.compbiomed.2023.107577]

8 **Ngiam KY**, Khor IW. Big data and machine learning algorithms for health-care delivery. *Lancet Oncol* 2019; **20**: e262-e273 [PMID: 31044724 DOI: 10.1016/S1470-2045(19)30149-4]

9 **Shao S**, Zhao Y, Lu Q, Liu L, Mu L, Qin J. Artificial intelligence assists surgeons' decision-making of temporary ileostomy in patients with rectal cancer who have received anterior resection. *Eur J Surg Oncol* 2023; **49**: 433-439 [PMID: 36244844 DOI: 10.1016/j.ejso.2022.09.020]

10 **Chen KA**, Goffredo P, Butler LR, Joisa CU, Guillem JG, Gomez SM, Kapadia MR. Prediction of Pathologic Complete Response for Rectal Cancer Based on Pretreatment Factors Using Machine Learning. *Dis Colon Rectum* 2024; **67**: 387-397 [PMID: 37994445 DOI: 10.1097/DCR.0000000000003038]

11 **Stanzione A**, Verde F, Romeo V, Boccadifuoco F, Mainenti PP, Maurea S. Radiomics and machine learning applications in rectal cancer: Current update and future perspectives. *World J Gastroenterol* 2021; **27**: 5306-5321 [PMID: 34539134 DOI: 10.3748/wjg.v27.i32.5306]

12 **Liu Y**, Shi J, Liu W, Tang Y, Shu X, Wang R, Chen Y, Shi X, Jin J, Li D. A deep neural network predictor to predict the sensitivity of neoadjuvant chemoradiotherapy in locally advanced rectal cancer. *Cancer Lett* 2024; **589**: 216641 [PMID: 38232812 DOI: 10.1016/j.canlet.2024.216641]

13 **Ma J**, Bo Z, Zhao Z, Yang J, Yang Y, Li H, Yang Y, Wang J, Su Q, Wang J, Chen K, Yu Z, Wang Y, Chen G. Machine Learning to Predict the Response to Lenvatinib Combined with Transarterial Chemoembolization for Unresectable Hepatocellular Carcinoma. *Cancers (Basel)* 2023; **15** [PMID: 36765583 DOI: 10.3390/cancers15030625]

14 **Hu C**, Li L, Huang W, Wu T, Xu Q, Liu J, Hu B. Interpretable Machine Learning for Early Prediction of Prognosis in Sepsis: A Discovery and Validation Study. *Infect Dis Ther* 2022; **11**: 1117-1132 [PMID: 35399146 DOI: 10.1007/s40121-022-00628-6]

15 **Rajkomar A**, Dean J, Kohane I. Machine Learning in Medicine. *N Engl J Med* 2019; **380**: 1347-1358 [PMID: 30943338 DOI: 10.1056/NEJMra1814259]

16 **Kagawa Y**, Smith JJ, Fokas E, Watanabe J, Cercek A, Greten FR, Bando H, Shi Q, Garcia-Aguilar J, Romesser PB, Horvat N, Sanoff H, Hall W, Kato T, Rödel C, Dasari A, Yoshino T. Future direction of total neoadjuvant therapy for locally advanced rectal cancer. *Nat Rev Gastroenterol Hepatol* 2024; **21**: 444-455 [PMID: 38485756 DOI: 10.1038/s41575-024-00900-9]

17 **Kulu Y**, Ulrich A, Bruckner T, Contin P, Welsch T, Rahbari NN, Büchler MW, Weitz J; International Study Group of Rectal Cancer. Validation of the International Study Group of Rectal Cancer definition and severity grading of anastomotic leakage. *Surgery* 2013; **153**: 753-761 [PMID: 23623834 DOI: 10.1016/j.surg.2013.02.007]

18 **Islam MM**, Rahman MJ, Rabby MS, Alam MJ, Pollob SMAI, Ahmed NAMF, Tawabunnahar M, Roy DC, Shin J, Maniruzzaman M. Predicting the risk of diabetic retinopathy using explainable machine learning algorithms. *Diabetes Metab Syndr* 2023; **17**: 102919 [PMID: 38091881 DOI: 10.1016/j.dsx.2023.102919]

19 **Buchan K**, Filannino M, Uzuner Ö. Automatic prediction of coronary artery disease from clinical narratives. *J Biomed Inform* 2017; **72**: 23-32 [PMID: 28663072 DOI: 10.1016/j.jbi.2017.06.019]

20 **Brien WF**, Crawford L, Raby A, Richardson H. In-house calibration of the international sensitivity index or calibration curve for determination of the international normalized ratio. *Arch Pathol Lab Med* 2004; **128**: 308-312 [PMID: 14987157 DOI: 10.5858/2004-128-308-ICOTIS]

21 **Van Calster B**, Wynants L, Verbeek JFM, Verbakel JY, Christodoulou E, Vickers AJ, Roobol MJ, Steyerberg EW. Reporting and Interpreting Decision Curve Analysis: A Guide for Investigators. *Eur Urol* 2018; **74**: 796-804 [PMID: 30241973 DOI: 10.1016/j.eururo.2018.08.038]

22 **Moosavi SM**, Ghassabian S. Linearity of Calibration Curves for Analytical Methods: A Review of Criteria for Assessment of Method Reliability. In: Stauffer MT, editor. Calibration and Validation of Analytical Methods - A Sampling of Current Approaches London: Intech Open, 2018 [DOI: 10.5772/intechopen.72932]

23 **Ladbury C**, Zarinshenas R, Semwal H, Tam A, Vaidehi N, Rodin AS, Liu A, Glaser S, Salgia R, Amini A. Utilization of model-agnostic explainable artificial intelligence frameworks in oncology: a narrative review. *Transl Cancer Res* 2022; **11**: 3853-3868 [PMID: 36388027 DOI: 10.21037/tcr-22-1626]

24 **Liu Y**, Wan X, Wang G, Ren Y, Cheng Y, Zhao Y, Han G. A scoring system to predict the risk of anastomotic leakage after anterior resection for rectal cancer. *J Surg Oncol* 2014; **109**: 122-125 [PMID: 24318774 DOI: 10.1002/jso.23467]

25 **Wang S**, Liu J, Wang S, Zhao H, Ge S, Wang W. Adverse Effects of Anastomotic Leakage on Local Recurrence and Survival After Curative Anterior Resection for Rectal Cancer: A Systematic Review and Meta-analysis. *World J Surg* 2017; **41**: 277-284 [PMID: 27743072 DOI: 10.1007/s00268-016-3761-1]

26 **Abdelsamad A**, Elsheikh A, Eltantawy M, Othman AM, Arif F, Atallah H, Elderiny H, Zayed H, Alshal MM, Ali MM, Elmorsi AH, Rashad S, Elagezy F, Gebauer F, Langenbach MR, Hamdy NM. A battle of surgical strategies: Clinically enlarged lateral lymph nodes in patients with locally advanced rectal cancer; extended mesorectal excision (e-TME) versus traditional surgery (TME-alone) a meta-analysis. *Pathol Res Pract* 2025; **269**: 155874 [PMID: 40073644 DOI: 10.1016/j.prp.2025.155874]

27 **Budin C**, Staniloaie D, Vasile D, Ilco A, Balan DG, Popa CC, Stiru O, Tulin A, Enyedi M, Miricescu D, Georgescu DE, Georgescu TF, Badiu DC, Mihai DA. Hypocalcemia: A possible risk factor for anastomotic leak in digestive surgery. *Exp Ther Med* 2021; **21**: 523 [PMID: 33815596 DOI: 10.3892/etm.2021.9955]

28 **Furie B**, Furie BC. Thrombus formation in vivo. *J Clin Invest* 2005; **115**: 3355-3362 [PMID: 16322780 DOI: 10.1172/JCI26987]

29 **Pastar I**, Stojadinovic O, Yin NC, Ramirez H, Nusbaum AG, Sawaya A, Patel SB, Khalid L, Isseroff RR, Tomic-Canic M. Epithelialization in Wound Healing: A Comprehensive Review. *Adv Wound Care (New Rochelle)* 2014; **3**: 445-464 [PMID: 25032064 DOI: 10.1089/wound.2013.0473]

30 **Subramaniam T**, Fauzi MB, Lokanathan Y, Law JX. The Role of Calcium in Wound Healing. *Int J Mol Sci* 2021; **22** [PMID: 34204292 DOI: 10.3390/ijms22126486]

31 **Wang M**, Zhan H, Wang J, Song H, Sun J, Zhao G. Calcium silicate-stimulated adipose-derived stem cells promote angiogenesis and improve skin wound healing. *Aging (Albany NY)* 2023; **15**: 4746-4756 [PMID: 37263631 DOI: 10.18632/aging.204760]

32 **Souad G**, Baghdadi C. Effect of calcium phosphate synthesis conditions on its physico-chemical properties and evaluation of its antibacterial activity. *Mater Res Express* 2020; **7**: 015040

33 **Tang NFR**, Armynah B, Tahir D. Structural and optical properties of alginate-based antibacterial dressing with calcium phosphate and zinc oxide for biodegradable wound painting applications. *Int J Biol Macromol* 2024; **276**: 133996 [PMID: 39032876 DOI: 10.1016/j.ijbiomac.2024.133996]

34 **Zhou Q**, Kang H, Bielec M, Wu X, Cheng Q, Wei W, Dai H. Influence of different divalent ions cross-linking sodium alginate-polyacrylamide hydrogels on antibacterial properties and wound healing. *Carbohydr Polym* 2018; **197**: 292-304 [PMID: 30007617 DOI: 10.1016/j.carbpol.2018.05.078]

35 **Chen JH**, Zhai ET, Yuan YJ, Wu KM, Xu JB, Peng JJ, Chen CQ, He YL, Cai SR. Systemic immune-inflammation index for predicting prognosis of colorectal cancer. *World J Gastroenterol* 2017; **23**: 6261-6272 [PMID: 28974892 DOI: 10.3748/wjg.v23.i34.6261]

36 **Spinelli A**, Foppa C, Carvello M, Sacchi M, De Lucia F, Clerico G, Carrano FM, Maroli A, Montorsi M, Heald RJ. Transanal Transection and Single-Stapled Anastomosis (TTSS): A comparison of anastomotic leak rates with the double-stapled technique and with transanal total mesorectal excision (TaTME) for rectal cancer. *Eur J Surg Oncol* 2021; **47**: 3123-3129 [PMID: 34384655 DOI: 10.1016/j.ejso.2021.08.002]

World Journal of Gastroenterology

Submit a Manuscript: https://www.f6publishing.com

World J Gastroenterol 2025 May 21; 31(19): 106644

DOI: 10.3748/wjg.v31.i19.106644

ISSN 1007-9327 (print) ISSN 2219-2840 (online)

ORIGINAL ARTICLE

Retrospective Study

Pescadillo ribosomal biogenesis factor 1 and programmed death-ligand 1 in gastric and head and neck squamous cell carcinoma

Xiao-Nan Hu, Chun-Feng Li, Si-Meng Huang, Chun-Lei Nie, Rui Pang

Specialty type: Gastroenterology and hepatology

Provenance and peer review: Unsolicited article; Externally peer reviewed.

Peer-review model: Single blind

Peer-review report's classification

Scientific Quality: Grade B, Grade B

Novelty: Grade B, Grade C

Creativity or Innovation: Grade B, Grade C

Scientific Significance: Grade C, Grade C

P-Reviewer: Ohtsuka M; Saiura A

Received: March 7, 2025

Revised: April 7, 2025

Accepted: April 23, 2025

Published online: May 21, 2025

Processing time: 74 Days and 20.5 Hours

Xiao-Nan Hu, Department of Head and Neck Radiotherapy Ward, Harbin Medical University Cancer Hospital, Harbin 150081, Heilongjiang Province, China

Chun-Feng Li, Department of Gastrointestinal Surgical Ward, Harbin Medical University Cancer Hospital, Harbin 150081, Heilongjiang Province, China

Si-Meng Huang, Chun-Lei Nie, Rui Pang, Department of Head and Neck Surgery, Harbin Medical University Cancer Hospital, Harbin 150081, Heilongjiang Province, China

Co-first authors: Xiao-Nan Hu and Chun-Lei Nie.

Corresponding author: Rui Pang, Deputy Director, Department of Head and Neck Surgery, Harbin Medical University Cancer Hospital, No. 150 Haping Road, Harbin 150081, Heilongjiang Province, China. 3151@hrbmu.edu.cn

Abstract

BACKGROUND

Gastric cancer (GC) and head and neck squamous cell carcinoma (HNSCC) are common malignancies with high morbidity and mortality rates. Traditional treatments often yield limited efficacy, especially in advanced cases. Recent advancements in immunotherapy, particularly immune checkpoint inhibitors targeting programmed death-ligand 1 (PD-L1), have shown promise. However, the expression and interaction of pescadillo ribosomal biogenesis factor 1 (PES1) and PD-L1 in these cancers remain unclear. Understanding their roles could provide new insights into tumor biology and improve therapeutic strategies.

AIM

To investigate the expression levels of PES1 and PD-L1 in tumor tissues of patients with GC and HNSCC.

METHODS

A total of 58 cases of GC and HNSCC undergoing surgical resection were selected from January 2022 to January 2024. Paraffin specimens of GC and HNSCC tissues were taken from the patients, and the sections were subjected to staining with immunohistochemistry and hematoxylin-eosin staining, and the protein expression of PES1 and PD-L1 was observed microscopically.

RESULTS
Among 58 GC and HNSCC tissues, 30 cases were positive and 28 cases were negative for PES1 expression, and 34 cases were positive and 24 cases were negative for PD-L1 expression. The positive expression rates of PES1 and PD-L1 were 51.72% and 58.62%, respectively. PES1 expression was correlated with the TNM stage, lymph node metastasis, and the depth of infiltration ($P < 0.05$), and PD-L1 expression was correlated with the differentiation degree, lymph node metastasis, and infiltration depth ($P < 0.05$).

CONCLUSION
PES1 and PD-L1 were positively expressed in GC and HNSCC tissues and correlated with clinical features. They may serve as potential biomarkers for immune-targeted therapies.

Key Words: Pescadillo ribosomal biogenesis factor 1; Programmed death-ligand 1; Gastric cancer; Head and neck squamous cell carcinoma; Expression level

Core Tip: This study investigated the expression of pescadillo ribosomal biogenesis factor 1 (PES1) and programmed death-ligand 1 (PD-L1) in tumor tissues from patients with gastric cancer and head and neck squamous cell carcinoma. We found that both proteins exhibited significant positive expression rates (51.72% for PES1 and 58.62% for PD-L1) and were associated with clinical features such as TNM stage and lymph node metastasis. Our results suggest that PES1 and PD-L1 may play critical roles in tumor progression and immune escape, potentially serving as biomarkers for immune-targeted therapies.

Citation: Hu XN, Li CF, Huang SM, Nie CL, Pang R. Pescadillo ribosomal biogenesis factor 1 and programmed death-ligand 1 in gastric and head and neck squamous cell carcinoma. *World J Gastroenterol* 2025; 31(19): 106644
URL: https://www.wjgnet.com/1007-9327/full/v31/i19/106644.htm
DOI: https://dx.doi.org/10.3748/wjg.v31.i19.106644

INTRODUCTION

Gastric cancer (GC) and head and neck squamous cell carcinoma (HNSCC) are common malignant tumors that pose a grave menace to human health worldwide[1,2]. GC is ranked fifth in tumor frequency across the globe and is the fifth-leading cause of cancer-related deaths, especially in China where its incidence and mortality rates remain high[3]. This scenario not only presents a significant danger to the well-being of patients but also imposes a substantial strain on the societal public health infrastructure. The high morbidity and mortality of GC requires continuous innovation and breakthroughs in treatment strategies, especially for patients with advanced and/or recurrent disease in which existing treatments, such as chemotherapy and radiotherapy, have limited efficacy.

Meanwhile, head and neck tumors are a part of the most common and widespread malignant tumors worldwide. HNSCC is the most frequently occurring head and neck tumor. The effectiveness of conventional treatments, especially in patients with advanced or recurrent disease, is still limited, and there is a pressing necessity to identify novel treatment approaches, particularly for patients who are resistant to chemotherapy or experience recurrence[4].

In recent years, with the rise of immunotherapy, especially the clinical application of immune checkpoint inhibitors, new hope has been brought to tumor treatment. Among them, programmed death-ligand 1 (PD-L1), as an important immune checkpoint molecule, is strongly expressed in a spectrum of tumor tissues and inhibits T cell activity by binding to programmed death 1 (PD-1), leading to tumor immune escape[5,6]. The PD-L1/PD-1 pathway is a cornerstone of regulating immune response and maintaining immune tolerance, and its inhibitors can block this pathway and restore T cell activity, thus enhancing immune response and inhibiting tumor growth.

PD-L1 has been demonstrated to be highly elevated in GC and HNSCC, with its expression level being significantly in line with clinicopathological features and patient outcomes. In GC, the expression of PD-L1 was closely linked to the depth of infiltration of tumor cells, the degree of differentiation, and the survival of patients. In HNSCC, PD-L1 expression was also closely in line with clinical stage. Additionally, patients with PD-L1 positivity had a higher likelihood of deriving benefits from anti-PD-1/PD-L1 treatment[7-10]. Although the important role of PD-L1 in tumor immunotherapy has been widely recognized, much remains unknown about its expression mechanism and interaction with other immune molecules.

Pescadillo ribosomal biogenesis factor 1 (PES1), as a new biomarker, has not yet been intensively investigated in terms of its expression in tumor tissues and its relationship with PD-L1[11]. Therefore, the purpose of this study was to detect the expression of PES1 and PD-L1 in tumor tissues of patients with GC and HNSCC, to explore the differences in their expression in different pathological grades and clinical stages, to provide theoretical and experimental bases for the immune-targeted therapy of GC and HNSCC, and to provide new ideas for the future immunotherapeutic strategies.

MATERIALS AND METHODS

Patient selection

A total of 58 cases of GC and HNSCC admitted to our hospital for surgical resection between January 2022 and January 2024 were selected, all of which were definitively diagnosed as GC or HNSCC by pathology. Among them, there were 37 male patients and 21 female patients. The age range was 39 to 72 years with a mean of 52.33 ± 8.29 years. Surgical resection specimens were used for analysis, and other relevant clinical data were taken from patients' pathology reports and medical records. The utilization of the specimens for clinical purposes in this study was examined and sanctioned by the hospital's Ethics Committee.

Inclusion criteria were: (1) Patients and their families have signed informed consent; (2) Patients have not received radiotherapy, chemotherapy, or immunotherapy for tumors; and (3) All specimens were fixed in 40 g/L formaldehyde and embedded in paraffin within 60 min after removal from the body, and the thickness of the tissue sections was 4 μm. Exclusion criteria were: (1) Patients with metastatic tumors or recurrent tumors; (2) Patients with severe consciousness disorders; (3) Patients with combined cardiac, pulmonary, and renal function abnormalities; (4) Patients with pathological conditions; and (5) Patients with incomplete pathological and clinical data. The research was endorsed by the hospital's Ethics Committee, and all participants provided informed consent.

Reagents and instruments

Reagents: (1) PES1 antibody. Select a highly specific and sensitive PES1 monoclonal antibody for detecting PES1 expression in tumor tissues; (2) PD-L1 antibody. Select a highly specific and sensitive PD-L1 monoclonal antibody for detecting PD-L1 expression in tumor tissues; (3) Immunohistochemistry staining kit. Contains all necessary stains such as hematoxylin, eosin, *etc*, reagents, antibody diluent, fixative, dehydrating agent, transparency agent, *etc.*, for immunohistochemical staining of tumor tissues; (4) PBS. Use to wash the samples and remove excess antibodies and stains; (5) Sealing agent. Use to seal the samples, protect the samples, and prevent discoloration; and (6) Pipette. Use for the precise addition of samples, such as antibodies and staining solutions.

Instruments: (1) Microscope. For observing the results of immunohistochemical staining and evaluating the expression of PES1 and PD-L1 in tumor tissues; (2) Thermostatic incubator. For temperature control during fixation, dehydration, transparency, and staining of the samples; (3) Paraffin slicer. For cutting paraffin-embedded tumor tissue blocks into thin slices; and (4) Tissue dehydrator. For the gradual transition of the tissue samples from a watery state to solvents such as alcohol and xylene to facilitate paraffin embedding.

Sample collection

Representative tumor tissues from patients with GC and HNSCC were obtained under sterile conditions by surgical resection or biopsy. Surgically resected tumor tissues were immediately placed in formalin fixative, and the fixation time was usually 24-48 h. After fixation, the tissue samples were processed into paraffin blocks through dehydration, clarification, wax immersion, and embedding procedures and stored in a 4 °C refrigerator for a long time. Before immunohistochemical testing, 4-6 μm thick slices were cut out from the paraffin blocks, attached to anti-detachment slides, and dried at 60 °C.

Immunohistochemical testing

Sections were immersed twice in xylene for 10 min each time to remove paraffin and then sequentially hydrated by passing through a gradient of 1000 g/L, 950 g/L, 900 g/L, 800 g/L, and 700 g/L ethanol for 5 min each time. Finally, the sections were washed with distilled water to remove any residual ethanol.

Antigen repair

Sections were positioned in citrate buffer (pH 6.0) and thermally repaired with antigen using a microwave oven or an autoclave to increase antigen exposure and antibody binding efficiency. After repair was completed, the sections were allowed to cool to ambient temperature and subsequently rinsed with PBS three times, each for a duration of 5 min.

Sections were treated with 30 g/L hydrogen peroxide solution and incubated at room temperature for 10 min to quench endogenous peroxidase activity, followed by rinsing with PBS three times, each for 5 min. Sections were closed using 50 g/L goat serum or bovine serum albumin and incubated at ambient temperature for a duration of 30 min to minimize nonspecific binding.

Appropriate dilution ratios of PES1 and PD-L1 specific primary antibodies were added dropwise to the sections, ensuring that the antibodies covered the tissue area evenly. The sections were placed in a wet box and incubated overnight at 4 °C or for 1-2 h at ambient temperature. The sections were washed with PBS three times, each time for 5 min to remove the unbound primary antibody.

Horseradish peroxidase-labeled secondary antibody was added dropwise on the sections and incubated at room temperature for 30 min to allow the reaction to proceed. The sections were washed with PBS 3 times for 5 min each time. Freshly prepared DAB staining solution was added by drops on the sections. The staining was observed under the microscope and immediately rinsed with distilled water to terminate the staining when a brown precipitate appeared.

Sections were re-stained using hematoxylin to color the nuclei, followed by hydrochloric acid alcohol differentiation and ammonia return to blue. Sections were subjected to graded ethanol dehydration (700 g/L, 800 g/L, 900 g/L, 950 g/L, 1000 g/L) and xylene transparency. Neutral gum was used to seal the sections, ensuring that the sections were flat and free of air bubbles. The slices were observed under a microscope, and the staining of PES1 and PD-L1 was recorded. The

positive expression rate was evaluated according to the staining intensity and distribution range.

Observation indicators

(1) Expression of PES1 and PD-L1 in GC and HNSCC tissues; and (2) Association between PES1 and PD-L1 expression levels and the clinical characteristics of GC and HNSCC.

Statistical analysis

Statistical analysis was conducted using SPSS 25.0. Measurement data that followed a normal distribution were presented as mean ± SD. Comparisons between groups were made using the *t* test. Counting data were represented as *n* (%), with the χ^2 test employed for analysis. The immunohistochemical staining expression of PES1 and PD-L1 proteins in GC and HNSCC tissues was evaluated using Fisher's discriminant method (Fisher's test). Statistical signi-ficance was set at $P < 0.05$.

RESULTS

Expression of PES1 and PD-L1 in GC and HNSCC tissues

Among 58 cases of GC and HNSCC, 30 cases were positive and 28 cases were negative for PES1 expression. In addition, 34 cases were positive and 24 cases were negative for PD-L1 expression. The positive expression rates of PES1 and PD-L1 were 51.72% and 58.62%, respectively (Table 1).

Association between PES1 and PD-L1 expression levels and the clinical characteristics of GC and HNSCC

PES1 expression correlated with TNM stage, lymph node metastasis, and infiltration depth ($P < 0.05$), while it was not correlated with gender, age, degree of differentiation, tumor diameter, and diabetes mellitus ($P > 0.05$). PD-L1 expression was correlated with degree of differentiation, lymph node metastasis, and infiltration depth ($P < 0.05$) but was not correlated with gender, age, TNM stage, tumor diameter, and diabetes ($P > 0.05$) (Tables 2 and 3).

DISCUSSION

GC ranks as one of the foremost causes of cancer-related fatalities on a global scale[12,13]. The majority of patients with GC are in advanced stages at the time of diagnosis and have shorter survival times and poor overall quality of life[14]. Traditional treatments include surgery, radiotherapy, and chemotherapy, but for advanced GC the cure rate of surgery is low, and the efficacy of radiotherapy is poor. Over the past few years, the development of immunotherapy and the achievement of certain clinical efficacy have made it a new treatment mode, in which immune checkpoint inhibitors play an important role[15-17].

PES1 is a nucleolin protein and has gradually been paid attention to in recent years[18]. It has been noted that in GC cell lines (AGS and N87) inhibition of PES1 expression leads to cell cycle arrest in the G1 phase, a finding that implies that low expression levels of PES1 play a part in inhibiting cell proliferation[19]. However, PES1 has not received sufficient attention within the field of GC research, and its specific significance in the clinical diagnosis and prognostic assessment of GC remains unclear.

HNSCC is a routine malignant tumor that is highly heterogeneous[20]. Although classical tumor TNM staging has been widely used for clinical diagnosis and to assist in clinical treatment decisions, TNM staging is based only on the tumor itself and fails to accurately predict the projection of patients with HNSCC. More and more studies have shown that various immune cells in the tumor microenvironment, especially B cells, contribute significantly to tumor progression and prediction of outcomes[21-24]. However, the presentation of PES1 in HNSCC and its relationship with immune infiltration have not been clarified.

In view of this, GC and HNSCC were chosen as the subjects of this study, covering two common malignant tumors, thus expanding the scope of the study. For the detection method, we used monoclonal antibodies with high specificity and sensitivity for immunohistochemical detection, which improved the accuracy of the results. In addition, this study explored the relationship between PES1 and PD-L1 for the first time, which provided new ideas for future research on the synergistic role of both in tumor immune escape.

In this study, 58 GC and HNSCC tissues were examined, and the experiments established that PES1 and PD-L1 had positive expression rates of 51.72% and 58.62%, respectively, in both tumor tissues. This finding suggests that PES1 and PD-L1 may contribute significantly to the development and progression of GC and HNSCC. Specifically, the expression level of PES1 may change with the increase of tumor malignancy and may be involved in the process of tumor invasion and metastasis. It has been shown that the high expression of PES1 in tumor tissues may be closely related to tumor development and progression, and as a potential biomarker for some tumors, it serves the purpose of early diagnosis, prognostic assessment, and monitoring of therapeutic efficacy[25-27].

PES1 is an important biomarker, and its aberrant expression has been in line with the onset and progression of a variety of cancers. In some tumors, high expression of PES1 tends to predict a more malignant, aggressive, and metastatic tumor. Therefore, PES1 may be a powerful indicator for assessing the prognosis of tumor patients. In addition, the expression of PES1 has certain specificity in the tissues of different tumors and makes its application in individualized therapy a great potential. In this study, we found that PES1 was contingent upon high expression rates in tumor tissues of

Table 1 Expression of pescadillo ribosomal biogenesis factor 1 and programmed death-ligand 1 in gastric cancer and head and neck squamous cell cancer tissues

	Negatives	Positive
PES1	28 (48.28)	30 (51.72)
PD-L1	24 (41.38)	34 (58.62)

Data are presented as *n* (%). PES1: Pescadillo ribosomal biogenesis factor 1; PD-L1: Programmed death-ligand 1.

Table 2 Relationship between pescadillo ribosomal biogenesis factor 1 expression and clinical features of gastric cancer and head and neck squamous cell carcinoma

Diagnostic trait	*n*	PES1		χ^2	*P* value
		Negative (*n* = 28)	Positive (*n* = 30)		
Sex				0.222	0.637
Male	37	17 (45.95)	20 (54.05)		
Women	21	11 (52.38)	10 (47.62)		
Age (years)				0.210	0.647
< 60	41	19 (46.34)	22 (53.66)		
≥ 60	17	9 (52.94)	8 (47.06)		
Degree of differentiation				0.672	0.412
Poorly differentiated	32	17 (53.13)	15 (46.88)		
Moderately to well differentiated	26	11 (42.31)	15 (57.69)		
TNM staging				8.312	0.004
I-II	28	19 (67.86)	9 (32.14)		
III	30	9 (30.00)	21 (70.00)		
Lymphatic node transfer				5.287	0.021
Yes	39	15 (38.46)	24 (61.54)		
No	19	13 (68.42)	6 (31.58)		
Infiltration depth				6.846	0.009
T1/T2	25	17 (68.00)	8 (32.00)		
T3/T4	33	11 (33.33)	22 (66.67)		
Tumor diameter (cm)				0.485	0.486
< 5	41	21 (51.22)	20 (48.78)		
≥ 5	17	7 (41.18)	10 (58.82)		
Diabetes				0.021	0.885
Yes	15	7 (46.67)	8 (53.33)		
No	43	21 (48.84)	22 (51.16)		

Data are presented as *n* (%). PES1: Pescadillo ribosomal biogenesis factor 1.

both GC and HNSCC, a result that further supports the value of PES1 as a potential biomarker.

In terms of PD-L1, the findings of this research indicated a substantial association between its expression and the degree of differentiation, lymph node metastasis, and depth of infiltration of the tumor ($P < 0.05$). This finding is in accordance with earlier studies and suggests that PD-L1 is vital to tumor immune escape. PD-L1 inhibits T cell activation and proliferation by binding to PD-1 on the surface of T cells, which in turn helps tumor cells to dodge surveillance and clearance by the immune system[28-30]. This immune escape mechanism enables tumors to continue to grow under the suppression of the immune system and exhibits strong invasiveness and metastatic ability. Therefore, high PD-L1 expression is usually highly tied to malignant biological behaviors of tumors, such as high tumor aggressiveness, high

Table 3 Relationship between programmed death-ligand 1 expression and clinical characteristics of gastric cancer and head and neck squamous cell carcinoma

Diagnostic trait	*n*	PD-L1		χ^2	*P* value
		Negative (*n* = 24)	Positive (*n* = 34)		
Sex				0.879	0.349
Male	37	17 (45.95)	20 (54.05)		
Women	21	7 (33.33)	14 (66.67)		
Age (years)				0.367	0.545
< 60	41	18 (43.90)	23 (56.10)		
≥ 60	17	6 (35.29)	11 (64.71)		
Degree of differentiation				6.508	0.011
Poorly differentiated	32	18 (56.25)	14 (43.75)		
Moderately to well differentiated	26	6 (23.08)	20 (76.92)		
TNM staging				0.049	0.825
I-II	28	12 (42.86)	16 (57.14)		
III	30	12 (40.00)	18 (60.00)		
Lymphatic node transfer				5.525	0.019
Yes	39	12 (30.77)	27 (69.23)		
No	19	12 (63.16)	7 (36.84)		
Infiltration depth				9.269	0.002
T1/T2	25	16 (64.00)	9 (36.00)		
T3/T4	33	8 (24.24)	25 (75.76)		
Tumor diameter (cm)				0.000	0.984
< 5	41	17 (41.46)	24 (58.54)		
≥ 5	17	7 (41.18)	10 (58.82)		
Diabetes				1.192	0.275
Yes	15	8 (53.33)	7 (46.67)		
No	43	16 (37.21)	27 (62.79)		

Data are presented as *n* (%). PD-L1: Programmed death-ligand 1.

metastatic capacity, and poor prognosis.

However, unlike PES1, PD-L1 expression showed no significant association with TNM staging ($P > 0.05$). This result suggests that more complex factors may need to be considered when assessing the clinical significance of PD-L1. For example, the tumor microenvironment, immune cell infiltration, and other immune escape mechanisms may have an impact on the expression level of PD-L1. Therefore, the independence of PD-L1 expression from TNM staging also suggests that relying solely on PD-L1 as a prognostic marker may have certain limitations and that multiple factors must be combined to more accurately predict patient prognosis.

In addition, this study also found that PD-L1 expression was independent of patient gender, age, tumor diameter, and diabetes mellitus status ($P > 0.05$), which further supported the exact function of PD-L1 in tumor immunomodulation. These results suggest that the important role played by PD-L1 in the immune escape process is not affected by these common clinical features and makes its potential and application value in tumor immunotherapy even more prominent.

Combined with the observations made in this research, we can speculate that PES1 and PD-L1 may serve as potential biomarkers for GC and HNSCC and that their high expression may be intertwined with tumor invasiveness, metastatic ability, and poor prognosis. Recent studies have shown that immune checkpoint molecules play a key role in tumor immune escape. PD-L1, as an important immune checkpoint molecule, inhibits the activation and proliferation of T cells by binding to PD-1 on the surface of T cells, which in turn helps tumor cells to evade the surveillance and clearance of the immune system.

The abnormal expression of PES1 in tumors may be related to immune regulation. In this study, we found that PES1 and PD-L1 had certain positive expression rates in GC and HNSCC tissues, and the expression of PES1 was related to TNM staging, lymph node metastasis and infiltration depth, while the expression of PD-L1 was related to differentiation

degree, lymph node metastasis, and infiltration depth. This suggests that PES1 and PD-L1 may interact with each other and participate in the immune escape process of the tumor. This finding provides new ideas and directions for clinical selection of appropriate therapies, especially in the context of immunotherapy, and PES1 and PD-L1 may provide valuable references for individualized treatment. However, more large-sample studies and in-depth mechanistic studies are needed to verify this hypothesis.

Notably, although this study revealed the expression of PES1 and PD-L1 in GC and HNSCC and their relationship with clinical features, their interaction has not been directly explored yet. In view of this, future studies could further explore the interaction mechanism between PES1 and PD-L1. From the theoretical analysis, PES1 may regulate the expression level of PD-L1 by affecting the signaling pathways in tumor cells and thus regulating the expression level of PD-L1. For example, PES1 may promote the transcription of the *PD-L1* gene by affecting the activity of certain transcription factors, thereby increasing the protein expression of PD-L1. In addition, PES1 may also indirectly affect the function of PD-L1 by influencing immune cell infiltration in the tumor microenvironment. For example, high expression of PES1 may attract more immune-suppressive cells to infiltrate into tumor tissues, and these immune-suppressive cells may enhance the immunosuppressive function of PD-L1 by secreting cytokines, thereby promoting immune escape from the tumor.

An in-depth study of the interaction between PES1 and PD-L1 will not only help to further reveal the mechanism of tumor immune escape but may also provide an important theoretical basis for the development of new tumor immunotherapy strategies. For example, if we can find the key targets to block the interaction between PES1 and PD-L1, it may provide new ideas for combination immunotherapy, thus improving the effectiveness of tumor treatment. In addition, exploring whether PES1 and PD-L1 can be used as biomarkers for joint prediction of tumor prognosis is also an important direction for future research. By gaining a deeper understanding of the roles of these two in tumor immunomodulation, we may be able to develop more precise and effective therapeutic strategies to further enhance the efficacy of tumor therapy and the quality of patient survival.

CONCLUSION

This study provided valuable information on the articulation of PES1 and PD-L1 in GC and HNSCC and their clinical significance. However, the present study has some limitations, such as a small sample size, which limits the generalizability and reliability of the findings. In addition, the current study only conducted univariate analysis and did not consider the effects of potential confounders such as age and gender. Therefore, future studies need to further expand the sample size and employ multifactorial regression analyses to more comprehensively reveal the roles of PES1 and PD-L1 in tumor biology to more accurately assess the relationship between their expression and the clinical features of GC and HNSCC.

FOOTNOTES

Author contributions: Hu XN, Li CF, Huang SM, and Nie CL contributed to the research design, data collection, data analysis, and paper writing; Pang R was responsible for the research design, funding application, data analysis, reviewing and editing, communication coordination, ethical review, copyright and licensing, and follow-up; All authors read and approved the final manuscript. Hu XN and Nie CL contributed equally to this work as co-first authors.

Institutional review board statement: The research was reviewed and approved by the Affiliated Cancer Hospital of Harbin Medical University.

Informed consent statement: All research participants or their legal guardians provided written informed consent prior to study registration.

Conflict-of-interest statement: No conflicts of interest were associated with this work.

Data sharing statement: No other data available.

Country of origin: China

ORCID number: Rui Pang 0000-0001-9015-9290.

S-Editor: Qu XL
L-Editor: Filipodia
P-Editor: Wang WB

REFERENCES

1 **Jin M**, Zhang G, Wang S, Zhao R, Zhang H. ISL1 and AQP5 complement each other to enhance gastric cancer cell stemness by regulating CD44 expression. *Transl Cancer Res* 2024; **13**: 5484-5496 [PMID: 39525012 DOI: 10.21037/tcr-24-248]

2 **Hadebe B**, Harry L, Gabela L, Masikane S, Patel M, Zwane S, Pillay V, Bipath P, Cebekhulu N, Nyakale N, Ramdass P, Msimang M, Aldous C, Sathekge M, Vorster M. Chemokine Receptor-4 Targeted PET/CT Imaging with (68)Ga-Pentixafor in Head and Neck Cancer-A Comparison with (18)F-FDG and CXCR4 Immunohistochemistry. *Diagnostics (Basel)* 2024; **14** [PMID: 39001265 DOI: 10.3390/diagnostics14131375]

3 **Deng C**, Deng G, Chu H, Chen S, Chen X, Li X, He Y, Sun C, Zhang C. Construction of a hypoxia-immune-related prognostic panel based on integrated single-cell and bulk RNA sequencing analyses in gastric cancer. *Front Immunol* 2023; **14**: 1140328 [PMID: 37180146 DOI: 10.3389/fimmu.2023.1140328]

4 **Zebene ED**, Lombardi R, Pucci B, Medhin HT, Seife E, Di Gennaro E, Budillon A, Woldemichael GB. Proteomic Analysis of Biomarkers Predicting Treatment Response in Patients with Head and Neck Cancers. *Int J Mol Sci* 2024; **25** [PMID: 39684225 DOI: 10.3390/ijms252312513]

5 **Nakamura K**, Yaguchi T, Murata M, Ota Y, Mikoshiba A, Kiniwa Y, Okuyama R, Kawakami Y. Tumor eradication by triplet therapy with BRAF inhibitor, TLR 7 agonist, and PD-1 antibody for BRAF-mutated melanoma. *Cancer Sci* 2024; **115**: 2879-2892 [PMID: 38894534 DOI: 10.1111/cas.16251]

6 **Chen H**, Wei J, Zhu Z, Hou Y. Multifaceted roles of PD-1 in tumorigenesis: From immune checkpoint to tumor cell-intrinsic function. *Mol Carcinog* 2024; **63**: 1436-1448 [PMID: 38751009 DOI: 10.1002/mc.23740]

7 **Oualla K**, Castelo Branco L, Nouiyakh L, Amaadour L, Benbrahim Z, Arifi S, Mellas N. Therapeutic Approaches With Immune Checkpoint Inhibitors in Head and Neck Cancers and the Role of PD-L1 as a Biomarker. *Cancer Control* 2021; **28**: 10732748211004878 [PMID: 33827280 DOI: 10.1177/10732748211004878]

8 **Elbehi AM**, Anu RI, Ekine-Afolabi B, Cash E. Emerging role of immune checkpoint inhibitors and predictive biomarkers in head and neck cancers. *Oral Oncol* 2020; **109**: 104977 [PMID: 32853912 DOI: 10.1016/j.oraloncology.2020.104977]

9 **Novoplansky O**, Jagadeeshan S, Prasad M, Yegodayev KM, Marripati D, Shareb RA, Greenshpan Y, Mathukkada S, Ben-Lulu T, Bhattacharya B, Porgador A, Kong D, Brägelmann J, Gutkind JS, Elkabets M. Dual inhibition of HERs and PD-1 counteract resistance in KRAS(G12C)-mutant head and neck cancer. *J Exp Clin Cancer Res* 2024; **43**: 308 [PMID: 39567998 DOI: 10.1186/s13046-024-03227-0]

10 **Laban S**, Remark R, Idel C, Ribbat-idel J, Krupar R, Schröck A, Klümper N, Döscher J, Sikora A, Abou Kors T, von Witzleben A, Vahl J, Grages A, Sonntag M, Brunner C, Hoffmann T, Gnjatic S. 915P Longer OS and RFS for CD3high/PD-L1+ head and neck squamous cell carcinoma (HNSCC) patients. *Ann Oncol* 2024; **35**: S643 [DOI: 10.1016/j.annonc.2024.08.976]

11 **Yuan S**, Xu N, Yang J, Yuan B. Emerging role of PES1 in disease: A promising therapeutic target? *Gene* 2025; **932**: 148896 [PMID: 39209183 DOI: 10.1016/j.gene.2024.148896]

12 **Li XQ**, Yang J, Liu B, Han SM. Disitamab vedotin combined with apatinib in gastric cancer: A case report and review of literature. *World J Clin Oncol* 2024; **15**: 1351-1358 [PMID: 39473863 DOI: 10.5306/wjco.v15.i10.1351]

13 **Liu Y**, Yu X, Shen H, Hong Y, Hu G, Niu W, Ge J, Xuan J, Qin JJ, Li Q. Mechanisms of traditional Chinese medicine in the treatment and prevention of gastric cancer. *Phytomedicine* 2024; **135**: 156003 [PMID: 39305742 DOI: 10.1016/j.phymed.2024.156003]

14 **Tang L**, He Y, Pang Y, Su Z, Zhou Y, Wang Y, Lu Y, Jiang Y, Han X, Song L, Wang L, Li Z, Lv X, Wang Y, Yao J, Liu X, Zhou X, He S, Zhang Y, Song L, Li J, Wang B. Suicidal ideation in advanced cancer patients without major depressive disorder. *Psychooncology* 2022; **31**: 1941-1950 [PMID: 36109867 DOI: 10.1002/pon.6033]

15 **Yang T**, Xu R, You J, Li F, Yan B, Cheng JN. Prognostic and clinical significance of HER-2 low expression in early-stage gastric cancer. *BMC Cancer* 2022; **22**: 1168 [PMID: 36371187 DOI: 10.1186/s12885-022-10262-7]

16 **Araruna GF**, Ribeiro HSC, Torres SM, Diniz AL, Godoy AL, Farias IC, Costa WL Jr, Coimbra FJF. Impact of Minimally Invasive Surgery on Early and Late Outcomes of Patients With Gastric Cancer Treated Using Neoadjuvant Chemotherapy. *J Surg Oncol* 2024; **130**: 776-784 [PMID: 39295557 DOI: 10.1002/jso.27904]

17 **Zhou Y**, Wang Q, Deng H, Xu B, Zhou Y, Liu J, Liu Y, Shi Y, Zheng X, Jiang J. N6-methyladenosine demethylase FTO promotes growth and metastasis of gastric cancer *via* m(6)A modification of caveolin-1 and metabolic regulation of mitochondrial dynamics. *Cell Death Dis* 2022; **13**: 72 [PMID: 35064107 DOI: 10.1038/s41419-022-04503-7]

18 **Li YZ**, Zhang C, Pei JP, Zhang WC, Zhang CD, Dai DQ. The functional role of Pescadillo ribosomal biogenesis factor 1 in cancer. *J Cancer* 2022; **13**: 268-277 [PMID: 34976188 DOI: 10.7150/jca.58982]

19 **Li J**, Zhou X, Lan X, Zeng G, Jiang X, Huang Z. Repression of PES1 expression inhibits growth of gastric cancer. *Tumour Biol* 2016; **37**: 3043-3049 [PMID: 26423399 DOI: 10.1007/s13277-015-4069-8]

20 **Bhat AA**, Yousuf P, Wani NA, Rizwan A, Chauhan SS, Siddiqi MA, Bedognetti D, El-Rifai W, Frenneaux MP, Batra SK, Haris M, Macha MA. Tumor microenvironment: an evil nexus promoting aggressive head and neck squamous cell carcinoma and avenue for targeted therapy. *Signal Transduct Target Ther* 2021; **6**: 12 [PMID: 33436555 DOI: 10.1038/s41392-020-00419-w]

21 **Toh J**, Reitsma AJ, Tajima T, Younes SF, Ezeiruaku C, Jenkins KC, Peña JK, Zhao S, Wang X, Lee EYZ, Glass MC, Kalesinskas L, Ganesan A, Liang I, Pai JA, Harden JT, Vallania F, Vizcarra EA, Bhagat G, Craig FE, Swerdlow SH, Morscio J, Dierickx D, Tousseyn T, Satpathy AT, Krams SM, Natkunam Y, Khatri P, Martinez OM. Multi-modal analysis reveals tumor and immune features distinguishing EBV-positive and EBV-negative post-transplant lymphoproliferative disorders. *Cell Rep Med* 2024; **5**: 101851 [PMID: 39657667 DOI: 10.1016/j.xcrm.2024.101851]

22 **Wang B**, Liu W, Song B, Li Y, Wang Y, Tan B. Targeting LINC00665/miR-199b-5p/SERPINE1 axis to inhibit trastuzumab resistance and tumorigenesis of gastric cancer *via* PI3K/AKt pathway. *Noncoding RNA Res* 2025; **10**: 153-162 [PMID: 39399377 DOI: 10.1016/j.ncrna.2024.07.004]

23 **Mi D**, Li C, Li Y, Yao M, Li Y, Hong K, Xie C, Chen Y. Discovery of novel BCL6-Targeting PROTACs with effective antitumor activities against DLBCL in vitro and in vivo. *Eur J Med Chem* 2024; **277**: 116789 [PMID: 39208743 DOI: 10.1016/j.ejmech.2024.116789]

24 **Low JT**, Christie M, Ernst M, Dumoutier L, Preaudet A, Ni Y, Griffin MDW, Mielke LA, Strasser A, Putoczki TL, O'Reilly LA. Loss of NFKB1 Results in Expression of Tumor Necrosis Factor and Activation of Signal Transducer and Activator of Transcription 1 to Promote Gastric Tumorigenesis in Mice. *Gastroenterology* 2020; **159**: 1444-1458.e15 [PMID: 32569771 DOI: 10.1053/j.gastro.2020.06.039]

25 **Yao X**, Lu C, Shen J, Jiang W, Qiu Y, Zeng Y, Li L. A novel nine gene signature integrates stemness characteristics associated with prognosis in hepatocellular carcinoma. *BIOCELL* 2021; **45**: 1425-1448 [DOI: 10.32604/biocell.2021.017289]

26 **He Y**, Xiang J, Li Y, Huang W, Gu F, Wang Y, Chen R. PES1 is a biomarker of head and neck squamous cell carcinoma and is associated with the tumor microenvironment. *Cancer Med* 2023; **12**: 12622-12638 [PMID: 37076985 DOI: 10.1002/cam4.5948]

27 **Fu Z**, Jiao Y, Li YQ, Ke JJ, Xu YH, Jia BX, Liu B. PES1 In Liver Cancer: A Prognostic Biomarker With Tumorigenic Roles. *Cancer Manag Res* 2019; **11**: 9641-9653 [PMID: 31814761 DOI: 10.2147/CMAR.S226471]

28 **Albrecht T**, Brinkmann F, Albrecht M, Lonsdorf AS, Mehrabi A, Hoffmann K, Kulu Y, Charbel A, Vogel MN, Rupp C, Köhler B, Springfeld C, Schirmacher P, Roessler S, Goeppert B. Programmed Death Ligand-1 (PD-L1) Is an Independent Negative Prognosticator in Western-World Gallbladder Cancer. *Cancers (Basel)* 2021; **13** [PMID: 33918309 DOI: 10.3390/cancers13071682]

29 **Fokter Dovnik N**, Smyth EC. Changes in the therapeutic landscape of oesophago-gastric cancers. *Curr Opin Oncol* 2021; **33**: 362-367 [PMID: 33720069 DOI: 10.1097/CCO.0000000000000728]

30 **Bansal A**, Srinivasan R, Rohilla M, Rai B, Rajwanshi A, Suri V, Chandra Saha S. Immunotyping in tubo-ovarian high-grade serous carcinoma by PD-L1 and CD8+ T-lymphocytes predicts disease-free survival. *APMIS* 2021; **129**: 254-264 [PMID: 33455015 DOI: 10.1111/apm.13116]

World Journal of Gastroenterology

Submit a Manuscript: https://www.f6publishing.com

World J Gastroenterol 2025 May 21; 31(19): 103727

DOI: 10.3748/wjg.v31.i19.103727

ISSN 1007-9327 (print) ISSN 2219-2840 (online)

LETTER TO THE EDITOR

Limitations and suggestions for emphysematous pancreatitis: Diagnosis, treatment, and prognosis

Xiang Li, Hong-Juan Li, Wei-Yao-Zhen He, Hai-Yan Fu

Specialty type: Gastroenterology and hepatology

Provenance and peer review: Unsolicited article; Externally peer reviewed.

Peer-review model: Single blind

Peer-review report's classification

Scientific Quality: Grade B, Grade B

Novelty: Grade B, Grade B

Creativity or Innovation: Grade B, Grade B

Scientific Significance: Grade B, Grade B

P-Reviewer: Zhang YG

Received: November 28, 2024

Revised: March 16, 2025

Accepted: April 1, 2025

Published online: May 21, 2025

Processing time: 173 Days and 22.8 Hours

Xiang Li, Department of Radiology, The Third People's Hospital of Kunming, Yunnan Clinical Medicine Center for Infectious Diseases, Kunming 650200, Yunnan Province, China

Hong-Juan Li, Hai-Yan Fu, Hospice Care Center, The Third People's Hospital of Kunming, Yunnan Clinical Medicine Center for Infectious Diseases, Kunming 650200, Yunnan Province, China

Wei-Yao-Zhen He, Department of Ultrasound Intervention, The Third People's Hospital of Kunming, Yunnan Clinical Medicine Center for Infectious Diseases, Kunming 650200, Yunnan Province, China

Corresponding author: Hai-Yan Fu, MD, Postdoctoral Fellow, Associate Chief Physician, Hospice Care Center, The Third People's Hospital of Kunming, No. 319 Wujing Road, Guandu District, Kunming 650200, Yunnan Province, China. fuhaiyan0622@163.com

Abstract

We read with great interest the article by Cao *et al* on 15 cases of emphysematous pancreatitis (EP). The study highlights the high mortality rate associated with EP and emphasizes the role of next-generation sequencing (NGS) in identifying its etiology. Additionally, it suggests treatment strategies such as antimicrobial therapy and early percutaneous catheter drainage, which may improve patient outcomes. However, we have identified certain limitations related to case selection, the evaluation of NGS technology, and the timing of computed tomography scans. To enhance the study's findings, we recommend expanding the study population, systematically evaluating the role of NGS in EP, and providing a more detailed analysis of the antibiotic initiation and duration. Furthermore, specifying the timing of computed tomography scans would improve clarity. Addressing these concerns could strengthen the study's contribution to the evidence-based management of EP, offering valuable insights for clinical practice.

Key Words: Emphysematous pancreatitis; Next-generation sequencing; Computed tomography; Diagnosis; Treatment

Core Tip: The results section of the abstract states that 5 cases of extensive emphysematous pancreatitis accounted for 33.3%, not 66.7%, and 7 cases of early-onset emphysematous pancreatitis accounted for 46.7%, not 47.1%. We recommend including details on the timing of antibiotic initiation and duration, as well as the timing of EP detection by computed tomography.

Citation: Li X, Li HJ, He WYZ, Fu HY. Limitations and suggestions for emphysematous pancreatitis: Diagnosis, treatment, and prognosis. *World J Gastroenterol* 2025; 31(19): 103727
URL: https://www.wjgnet.com/1007-9327/full/v31/i19/103727.htm
DOI: https://dx.doi.org/10.3748/wjg.v31.i19.103727

TO THE EDITOR

We read with great interest the recent publication by Cao *et al*[1], which retrospectively examines the diagnosis, treatment, and prognosis of 15 cases of emphysematous pancreatitis (EP). The study highlights the alarmingly high mortality rate of EP and emphasizes the role of next-generation sequencing (NGS) in its etiological diagnosis. Furthermore, it introduces potential treatment strategies, including antimicrobial therapy and early percutaneous catheter drainage, which may significantly improve patient prognosis. While this work provides valuable insights, we would like to highlight some important limitations that warrant further discussion.

First, the study reported a mortality rate of 60% (9 of 15 cases), which is notably higher than the rates observed in previous studies[2]. This raises concerns about potential case selection bias. Clarification of the inclusion criteria would help contextualize these findings. Second, EP is characterized by the presence of gas within or around necrotic pancreatic tissue, often due to gas-forming bacterial infections or enteric pancreatic fistulas. Considering that patients with EP may have diabetes or immune disorders, single bacterial cultures may fail to detect all pathogens. Although NGS enhances pathogen identification, it is important to consider the potential presence of conditional pathogens. Additionally, previous studies emphasize the necessity of timely antibiotic administration targeting gram-negative bacteria[3]. However, the study did not provide details on antibiotic initiation or duration, which are critical for optimizing treatment. Although NGS was performed in cases 1 to 5, three of these patients succumbed to the disease, reinforcing the importance of early recognition and timely intervention.

Third, computed tomography (CT) imaging remains the gold standard for diagnosing EP due to its high specificity and sensitivity in detecting intraparenchymal and free gas around the pancreas[4]. However, the study did not specify the timing of the initial CT scan. Delayed CT evaluations may contribute to diagnostic delays, potentially missing the optimal therapeutic window and leading to increased mortality[5]. Timely CT assessment, followed by immediate empirical antibiotic therapy targeting gram-negative bacteria (most commonly, *Escherichia coli*), is crucial[5]. NGS should be used concurrently to identify causative pathogens, allowing for subsequent antibiotic adjustments to improve outcomes[6]. An integrated approach that combines imaging and molecular diagnostics could optimize EP management. Finally, the management of EP necessitates a multidisciplinary team, involving radiologists, gastroenterologists, infectious disease specialists, critical care physicians, and emergency surgeons[5].

In conclusion, this study provides valuable insights into EP but could be further strengthened by addressing the aforementioned limitations. Expanding the study population, providing more detail on antibiotic administration, and specifying CT timing would enhance the robustness of the findings and further contribute to the evidence-based management of EP. We greatly appreciate the authors' contributions to this critical area of research.

FOOTNOTES

Author contributions: Fu HY conceptualized this study and drafted manuscript; Li X and Li HJ participated in the discussion; Li X and He WYZ revised the manuscript; and all authors had read and agreed to the final version of the manuscript.

Conflict-of-interest statement: All the authors report no relevant conflicts of interest for this article.

Country of origin: China

ORCID number: Hai-Yan Fu 0000-0003-0885-6180.

S-Editor: Wei YF
L-Editor: A

P-Editor: Zhao S

REFERENCES

1 **Cao LJ**, Lu ZH, Zhang PJ, Yang X, Yu WL, Sun Y. Emphysematous pancreatitis: Diagnosis, treatment, and prognosis. *World J Gastroenterol* 2024; **30**: 4929-4936 [PMID: 39679309 DOI: 10.3748/wjg.v30.i46.4929]

2 **Chou CY**, Su YJ, Yang HW, Chang CW. Risk factors for mortality in emphysematous pancreatitis. *J Drug Assess* 2020; **9**: 1-7 [PMID: 31893161 DOI: 10.1080/21556660.2019.1684927]

3 **Bul V**, Yazici C, Staudacher JJ, Jung B, Boulay BR. Multiorgan Failure Predicts Mortality in Emphysematous Pancreatitis: A Case Report and Systematic Analysis of the Literature. *Pancreas* 2017; **46**: 825-830 [PMID: 28609373 DOI: 10.1097/MPA.0000000000000834]

4 **McCloskey M**, Low VH. CT of pancreatic gas gangrene. *Australas Radiol* 1996; **40**: 75-76 [PMID: 8838895 DOI: 10.1111/j.1440-1673.1996.tb00351.x]

5 **Darawsha B**, Mansour S, Fahoum T, Azzam N, Kluger Y, Assalia A, Khuri S. Fulminant Emphysematous Pancreatitis: Diagnosis Time Counts. *Gastroenterology Res* 2024; **17**: 32-36 [PMID: 38463147 DOI: 10.14740/gr1671]

6 **Zuo YH**, Wu YX, Hu WP, Chen Y, Li YP, Song ZJ, Luo Z, Ju MJ, Shi MH, Xu SY, Zhou H, Li X, Jie ZJ, Liu XD, Zhang J. The Clinical Impact of Metagenomic Next-Generation Sequencing (mNGS) Test in Hospitalized Patients with Suspected Sepsis: A Multicenter Prospective Study. *Diagnostics (Basel)* 2023; **13**: 323 [PMID: 36673134 DOI: 10.3390/diagnostics13020323]

World Journal of Gastroenterology

Submit a Manuscript: https://www.f6publishing.com

World J Gastroenterol 2025 May 21; 31(19): 105617

DOI: 10.3748/wjg.v31.i19.105617

ISSN 1007-9327 (print) ISSN 2219-2840 (online)

LETTER TO THE EDITOR

Obesity paradox role in the immunosuppressive treatment of hepatocellular carcinoma

Leandro Sierra, Mohamad-Noor Abu-Hammour, Arjun Chatterjee, C Roberto Simons-Linares

Specialty type: Gastroenterology and hepatology

Provenance and peer review: Unsolicited article; Externally peer reviewed.

Peer-review model: Single blind

Peer-review report's classification

Scientific Quality: Grade A, Grade A, Grade B, Grade B

Novelty: Grade A, Grade A, Grade B, Grade B

Creativity or Innovation: Grade A, Grade B, Grade C, Grade C

Scientific Significance: Grade A, Grade B, Grade B, Grade B

P-Reviewer: Cao KD; Lin R; Wang JK

Received: January 30, 2025

Revised: March 15, 2025

Accepted: April 1, 2025

Published online: May 21, 2025

Processing time: 111 Days and 12 Hours

Leandro Sierra, Mohamad-Noor Abu-Hammour, Department of Internal Medicine, Cleveland Clinic Foundation, Cleveland, OH 44195, United States

Arjun Chatterjee, C Roberto Simons-Linares, Department of Gastroenterology and Hepatology, Cleveland Clinic Foundation, Cleveland, OH 44195, United States

Corresponding author: C Roberto Simons-Linares, MD, Senior Researcher, Department of Gastroenterology and Hepatology, Cleveland Clinic Foundation, 9500 Euclid Avenue, Cleveland, OH 44195, United States. simonsc@ccf.org

Abstract

The "obesity paradox" in hepatocellular carcinoma (HCC) suggests patients with obesity may experience better treatment outcomes compared to patients without obesity. Wang *et al* highlighted this paradox in HCC immunotherapy, demonstrating superior progression-free survival and overall survival in patients with overweight and obesity treated with lenvatinib and camrelizumab, focusing on hepatitis B virus-related HCC. Mechanisms such as better nutritional reserves, leptin-mediated immune modulation, and reduced protein breakdown may explain these outcomes. Obesity's role in anti-programmed cell death protein-1 therapy appears could have a benefit, while its effects on other treatments, such as anti-vascular endothelial growth factor therapy, may reduce efficacy. Further research is needed to explore how obesity influences the effectiveness of other most common immunotherapies like nivolumab, pembrolizumab, and bevacizumab, and whether weight loss as well as weight-loss related sarcopenia impacts these benefits.

Key Words: Obesity paradox; Hepatocellular carcinoma; Immunotherapy; Anti-programmed death-1 therapy; Leptin; Anti-vascular endothelial growth factor therapy

Core Tip: The "obesity paradox" in hepatocellular carcinoma suggests better outcomes in patients with obesity undergoing immunotherapy, potentially due to leptin-driven immune modulation and enhanced nutritional reserves. While promising, these findings have only been demonstrated with lenvatinib and camrelizumab, and have not yet been observed with more commonly used immunotherapy treatments for hepatocellular carcinoma, such as nivolumab, pembrolizumab, or bevacizumab. Although intriguing, this phenomenon remains limited by the scope of current studies.

Citation: Sierra L, Abu-Hammour MN, Chatterjee A, Simons-Linares CR. Obesity paradox role in the immunosuppressive treatment of hepatocellular carcinoma. *World J Gastroenterol* 2025; 31(19): 105617
URL: https://www.wjgnet.com/1007-9327/full/v31/i19/105617.htm
DOI: https://dx.doi.org/10.3748/wjg.v31.i19.105617

TO THE EDITOR

The "obesity paradox" in liver disease refers to the observation that, contrary to the general expectation that obesity worsens health outcomes, patients with obesity with certain liver diseases may have better survival rates and treatment responses compared to patients without obesity. The study by Wang *et al*[1] provides further insight into this underexplored issue, examining the impact of body mass index (BMI) on outcomes of lenvatinib plus camrelizumab treatment in advanced hepatocellular carcinoma (HCC). This study highlights the "obesity paradox" in immunotherapy for HCC and suggests its potential applicability to other liver diseases in various contexts. The purpose of our brief communication is to expand the understanding of immunosuppressant treatment strategies for individuals with obesity and HCC, providing insights that may guide clinical decisions. Additionally, it will be pivotal for further research studying the role of obesity in other immunotherapies, as well as their role in other liver diseases.

Main findings and limitations of the study

Wang *et al*[1] demonstrated that overweight patients and those with obesity (BMI ≥ 25 kg/m²) achieved superior progression-free survival (8.53 months *vs* 6.30 months, $P < 0.001$) and overall survival (OS, 15.30 months *vs* 11.90 months, $P = 0.001$) compared to their non-overweight counterparts. Subgroup analyses further revealed that patients with obesity (BMI ≥ 30 kg/m²) had the best progression-free survival (10.00 months, hazard ratio 0.13, 95% confidence interval: 0.06-0.31) and OS (16.60 months, hazard ratio 0.28; 95% confidence interval: 0.14-0.57) compared to patients without obesity [1]. This paradoxical relationship suggests that the metabolic and immunological changes associated with obesity may enhance the efficacy of certain immune checkpoint inhibitors. Notably, the study was conducted in a subset of the population with hepatitis B virus-related HCC and did not include other causes of HCC, such as hepatitis C virus, metabolic-associated fatty liver disease, or alcohol-related liver disease. Additionally, the study focused solely on treatment with lenvatinib plus camrelizumab, excluding other commonly used anti-programmed death-1 (PD-1) therapies for HCC, such as nivolumab or pembrolizumab. This limitation makes it challenging to extrapolate the findings to routine clinical practice.

Obesity role in liver disease

Multiple studies have shown that the presence of obesity may improve inpatient mortality in cirrhotic patients[2-4]. For instance, a study by Karagozian *et al*[2] found that cirrhotic patients with obesity had a lower crude mortality rate (2.7% *vs* 3.5%, $P = 0.02$) compared to cirrhotic patients without obesity, despite having longer hospital stays and higher healthcare costs[2]. One key factor is the enhanced nutritional reserve in patients with obesity, which may provide a buffer against the catabolic stress of acute illness. The degradation of fatty acids in critically ill patients releases 3-hydroxybutyrate, which significantly decreases phenylalanine-to-tyrosine degradation and reduces net forearm phenylalanine release, leading to a reduction in protein breakdown and enhanced muscle regeneration post-hospitalization[5,6]. In HCC, studies have demonstrated that lean patients with metabolic-associated fatty liver disease-associated HCC have poorer long-term surgical outcomes compared to overweight and obese patients, suggesting an obesity paradox in this subgroup. Specifically, in one study, lean patients exhibited a 5-year OS of 55.4% and recurrence-free survival of 35.1%, whereas overweight patients had a 5-year OS of 71.3% and recurrence-free survival of 55.6%[7]. Another study using data from the Korean Central Cancer Registry indicated that overweight males with HCC had better OS compared to normal-weight males, particularly after transarterial chemoembolization[8].

Role of obesity in HCC immunotherapy

Adipose cells cause an increase in leptin, which is a proinflammatory adipokine believed to be the primary factor responsible for differences in the effectiveness of immunotherapy for HCC. Leptin enhances the efficacy of anti-PD-1 checkpoint therapy through several mechanisms. It repolarizes tumor-associated macrophages to an inflammatory type 1 macrophages-like phenotype with antitumor activity. Leptin also downregulates the immunosuppressive function of regulatory T-cells, boosting $CD8^+$ T-cell activity. Additionally, it activates natural killer cells and enhances the migratory and stimulatory capacity of dendritic cells, further promoting antitumor immunity (Figure 1). However, while these mechanisms benefit anti-PD-1 therapy, obesity may reduce the effectiveness of other treatments. For instance, 5-fluorouracil may be less effective in HCC patients with obesity due to reduced dihydropyrimidine dehydrogenase

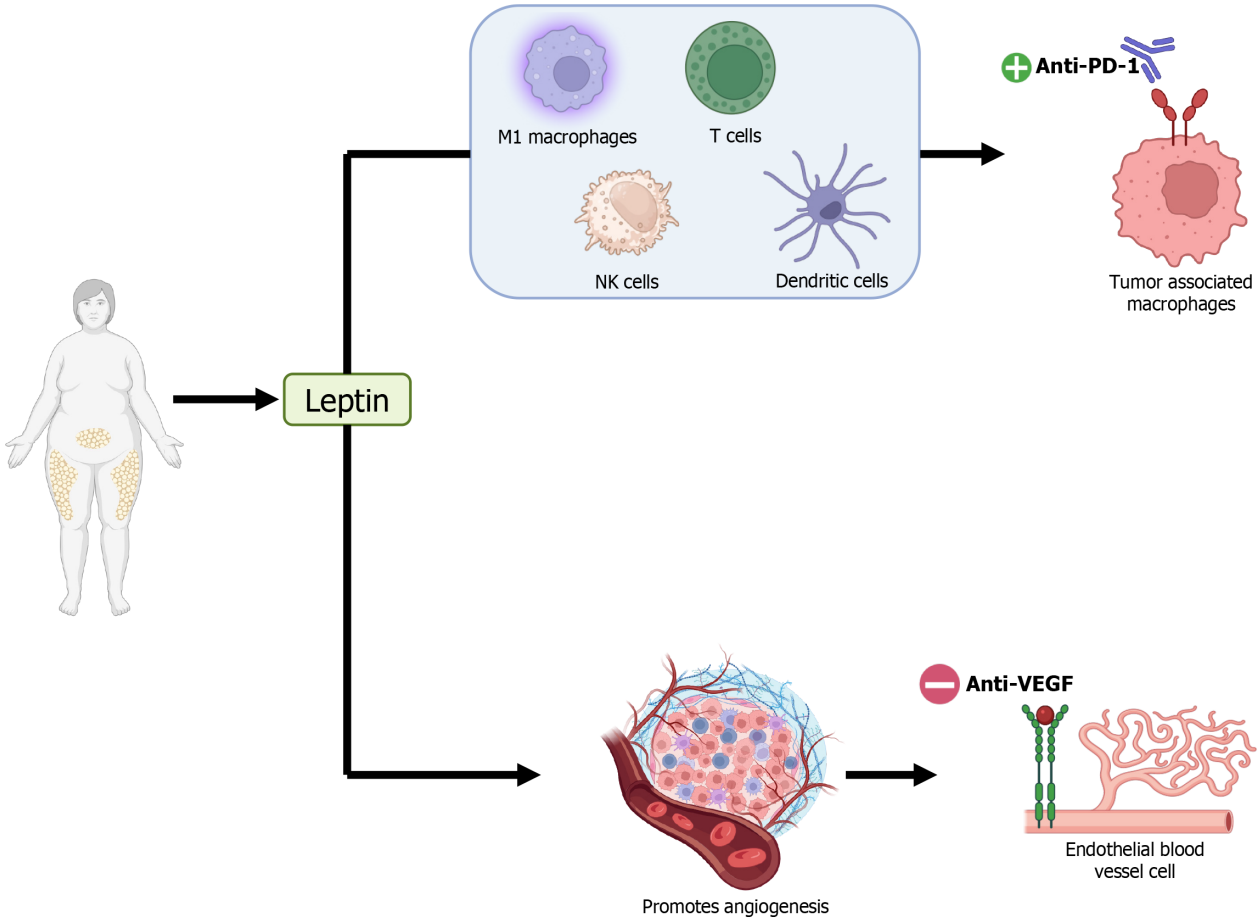

Figure 1 Mechanism of obesity in the role of immunosuppressants for hepatocellular carcinoma. M1 macrophages: Type 1 macrophages; NK cells: Natural killer cells; PD-1: Programmed Death-1; VEGF: Vascular endothelial growth factor.

activity, which exacerbates toxicity. Similarly, anti-vascular endothelial growth factor (VEGF) treatments like bevacizumab may be less effective in patients with obesity. Obesity increases the production of alternative proangiogenic factors, such as interleukin-6 and fibroblast growth factor 2, which promote angiogenesis independently of VEGF, reducing the efficacy of anti-VEGF therapies (Figure 1).

Conclusion

The impact of immunosuppressants on HCC patients with obesity remains largely unexplored. In fact, the article by Wang *et al*[1] is the first to study this intervention in a real-world population. However, the treatment analyzed is not one of the most commonly used immunotherapies, leaving an opportunity for further research on how obesity influences the effectiveness of treatments such as nivolumab, pembrolizumab, or bevacizumab for HCC. Additionally, it is unclear whether the benefits diminish once a patient loses weight through interventions such as lifestyle modification, glucagon-like peptide-1 therapy, or bariatric surgery. Further research on this subject is crucial to guide clinicians in tailoring treatments based on individual patient characteristics.

FOOTNOTES

Author contributions: Sierra L contributed to conceptualization, project administration, formal analysis, and visualization; Abu-Hammour MN contributed to formal analysis; Sierra L, Abu-Hammour MN, and Chatterjee A contributed to data curation, and wrote the original draft; Simons-Linares CR contributed to conceptualization, methodology, supervision, validation, and visualization; and all authors have reviewed, and edited the draft, read and agreed to the published version of the manuscript.

Conflict-of-interest statement: All the authors report no relevant conflicts of interest for this article.

Country of origin: United States

ORCID number: Leandro Sierra 0000-0002-7148-5450; Mohamad-Noor Abu-Hammour 0000-0001-5579-9807; Arjun Chatterjee 0000-0003-4707-988X; C Roberto Simons-Linares 0000-0002-5586-3722.

S-Editor: Wei YF
L-Editor: A
P-Editor: Zhao S

REFERENCES

1 **Wang YQ**, Pan D, Yao ZY, Li YQ, Qu PF, Wang RB, Gu QH, Jiang J, Han ZX, Liu HN. Impact of baseline body mass index on the long-term prognosis of advanced hepatocellular carcinoma treated with immunotherapy. *World J Gastroenterol* 2024; **30**: 4132-4148 [PMID: 39474397 DOI: 10.3748/wjg.v30.i37.4132]

2 **Karagozian R**, Bhardwaj G, Wakefield DB, Baffy G. Obesity paradox in advanced liver disease: obesity is associated with lower mortality in hospitalized patients with cirrhosis. *Liver Int* 2016; **36**: 1450-1456 [PMID: 27037497 DOI: 10.1111/liv.13137]

3 **Jiang H**, Li M, Yu H, Huang Y, Yang B, Wu B, Yang Y. Body mass index and waist-to-height ratio effect on mortality in non-alcoholic fatty liver: revisiting the obesity paradox. *Front Endocrinol (Lausanne)* 2024; **15**: 1419715 [PMID: 39713050 DOI: 10.3389/fendo.2024.1419715]

4 **Endo K**, Kakisaka K, Abe T, Yusa K, Nakaya I, Watanabe T, Suzuki A, Yoshida Y, Oikawa T, Miyasaka A, Kuroda H, Matsumoto T. Positive impact of obesity on the prognosis of liver cirrhosis. *J Gastroenterol Hepatol* 2024; **39**: 1663-1672 [PMID: 38700075 DOI: 10.1111/jgh.16590]

5 **Goossens C**, Weckx R, Derde S, Dufour T, Vander Perre S, Pauwels L, Thiessen SE, Van Veldhoven PP, Van den Berghe G, Langouche L. Adipose tissue protects against sepsis-induced muscle weakness in mice: from lipolysis to ketones. *Crit Care* 2019; **23**: 236 [PMID: 31262340 DOI: 10.1186/s13054-019-2506-6]

6 **Swierczynski J**, Sledzinski T, Slominska E, Smolenski R, Sledzinski Z. Serum phenylalanine concentration as a marker of liver function in obese patients before and after bariatric surgery. *Obes Surg* 2009; **19**: 883-889 [PMID: 18431611 DOI: 10.1007/s11695-008-9521-z]

7 **Zhang W**, Li MY, Li ZQ, Diao YK, Liu XK, Guo HW, Wu XC, Wang H, Wang SY, Zhou YH, Lu J, Lin KY, Gu WM, Chen TH, Li J, Liang YJ, Yao LQ, Wang MD, Li C, Yin DX, Pawlik TM, Lau WY, Shen F, Chen Z, Yang T. Long-term outcomes following hepatectomy in patients with lean non-alcoholic fatty liver disease-associated hepatocellular carcinoma versus overweight and obese counterparts: A multicenter analysis. *Asian J Surg* 2024 [PMID: 39054140 DOI: 10.1016/j.asjsur.2024.07.089]

8 **Cha B**, Yu JH, Jin YJ, Suh YJ, Lee JW. Survival Outcomes According to Body Mass Index in Hepatocellular Carcinoma Patient: Analysis of Nationwide Cancer Registry Database. *Sci Rep* 2020; **10**: 8347 [PMID: 32433488 DOI: 10.1038/s41598-020-65460-9]

World Journal of Gastroenterology

Submit a Manuscript: https://www.f6publishing.com

World J Gastroenterol 2025 May 21; 31(19): 105888

DOI: 10.3748/wjg.v31.i19.105888

ISSN 1007-9327 (print) ISSN 2219-2840 (online)

LETTER TO THE EDITOR

Characterization of subepithelial tumors of upper gastrointestinal tract by endoscopic ultrasound

Santosh Shenoy

Specialty type: Gastroenterology and hepatology

Provenance and peer review: Invited article; Externally peer reviewed.

Peer-review model: Single blind

Peer-review report's classification
Scientific Quality: Grade B, Grade C
Novelty: Grade C, Grade D
Creativity or Innovation: Grade C, Grade D
Scientific Significance: Grade C, Grade D

P-Reviewer: Hakim GD; Zhang YQ

Received: February 11, 2025
Revised: March 5, 2025
Accepted: March 21, 2025
Published online: May 21, 2025
Processing time: 101 Days and 0.5 Hours

Santosh Shenoy, Department of General Surgery, Kansas City VA Medical Center, University of Missouri, Kansas City, MO 64128, United States

Corresponding author: Santosh Shenoy, MD, FACS, Professor, Department of General Surgery, Kansas City VA Medical Center, University of Missouri, 4801 E Linwood, Kansas City, MO 64128, United States. shenoy2009@hotmail.com

Abstract

In this article we comment on the paper by Xu *et al* describing retrospective data on endoscopic treatment outcome of esophageal gastrointestinal stromal tumors (GISTs). Esophageal GIST is a rare type of mesenchymal tumor. GISTs originate from the interstitial cells of Cajal, which are pacemaker cells involved in gut motility. GISTs are most commonly found in the stomach and small intestine, but esophageal involvement is rare. Esophageal GISTs account for < 1% of all GISTs. Endoscopic resection remains the mainstay for small, localized tumors with excellent outcomes. However, larger tumors may require multidisciplinary strategies to provide the best oncological outcomes. Here, we discuss the usefulness of endoscopic ultrasound (EUS) of subepithelial tumors of the upper gastrointestinal tract. EUS is a crucial tool in the diagnosis, staging, and management of subepithelial masses. Given the subepithelial nature of these tumors, standard endoscopy is not adequate, making EUS essential for a comprehensive assessment. EUS provides accurate tumor size assessment and enables fine needle aspirations guided biopsy, for treatment planning.

Key Words: Subepithelial tumors; Esophageal gastrointestinal stromal tumors; Endoscopic ultrasound; Artificial intelligence; Endoscopic resection

Core Tip: Esophageal gastrointestinal stromal tumor (GIST) is a rare type of mesenchymal tumor. Esophageal GISTs account for < 1% of all GISTs. Endoscopic resection remains the mainstay for small, localized tumors with excellent outcomes. Endoscopic ultrasound (EUS) is a crucial tool in the diagnosis, staging, and management of esophageal GIST. Given the submucosal nature of these tumors, standard endoscopy is not adequate, making EUS essential for a comprehensive assessment. EUS provides accurate tumor sizing, and enables fine needle aspiration guided biopsy of carefully selected large inoperable tumors or where diagnosis is in doubt, which is critical for risk stratification and treatment planning.

Citation: Shenoy S. Characterization of subepithelial tumors of upper gastrointestinal tract by endoscopic ultrasound. *World J Gastroenterol* 2025; 31(19): 105888
URL: https://www.wjgnet.com/1007-9327/full/v31/i19/105888.htm
DOI: https://dx.doi.org/10.3748/wjg.v31.i19.105888

TO THE EDITOR

In this article we comment on the paper describing retrospective data on endoscopic treatment outcome of esophageal gastrointestinal stromal tumors (GISTs) by Xu *et al*[1] in *World Journal of Gastroenterology*. The authors performed endoscopic resection of the esophageal subepithelial lesions with optimal outcomes (R0 resection). However, it is not clear if the authors performed endoscopic ultrasound (EUS) prior to the planned resection to assess the tumor size and other aspects necessary for surgical planning. We discuss some salient points associated with esophageal GISTs and the role of EUS in treatment of these tumors. The common subepithelial tumors of the upper gastrointestinal tract are GISTs, lipomas, leiomyoma, carcinoid tumors and ectopic pancreatic tissue. These lesions are diagnosed and differentiated based on their unique histochemical staining and the gastrointestinal layer of origin. Most lesions are identified incidentally and considered benign; however, some tumors such as GISTs and carcinoids have a strong propensity for malignant transformation[2,3].

Esophageal GIST is a rare type of mesenchymal tumor. GISTs originate from the interstitial cells of Cajal, which are pacemaker cells involved in gut motility. These tumors are most commonly found in the stomach and small intestine, and esophageal involvement is rare. Esophageal GISTs account for < 1% of all GISTs. They typically occur in the lower esophagus and are characterized by spindle or epithelioid cells. Most GISTs, including of the esophagus, display mutations in the *c-KIT* (*CD117*) or *PDGFRA* genes. Certain rare molecular, familial types such as neurofibromatosis neurofibromin 1, succinate dehydrogenase, *BRAF* or *NTRK* genes are also associated with GISTs and generally show primary resistance to standard tyrosine kinase inhibitors (TKIs)[4,5]. Common symptoms include dysphagia, sensation of food stuck in the esophagus, chest pain or discomfort. This may lead to weight loss. Erosion of the overlying mucosa may cause hematemesis. Smaller lesions may be asymptomatic[3,6].

Diagnostic modalities and tumor markers

Diagnostic modalities include upper gastrointestinal endoscopy, which may detect a submucosal bulge into the esophageal lumen and may have superficial ulcerations. Biopsy is usually not necessary as it may lead to capsule disruption and tumor spread. EUS helps assess tumor size, morphology and depth[6,7]. However current endoscopic imaging tools struggle to differentiate GISTs from leiomyomas. Recently, a few studies have demonstrated that incorporation of real-time artificial intelligence (AI) systems during EUS examinations can assist endoscopists in rapidly and accurately differentiating various types of subepithelial tumors of the upper GI tract, facilitating improved diagnostic and therapeutic decision-making. A cohort of 59 participants with subepithelial tumors was prospectively enrolled and compared to that of endoscopists to assess the real-time clinical application of the AI system. The AI system was superior in differentiating between GISTs and leiomyomas diagnosis, respectively, markedly surpassing endoscopists[8].

Similarly, an automatically optimized radiomics modeling system (AORMS) based on EUS images was evaluated for the diagnosis and the risk stratification of gastric GIST. A total of 205 patients with EUS images of small (< 2 cm) gastric GISTs were retrospectively enrolled in the development phase of AORMS and compared to 178 patients with images obtained by endoscopists from different centers. The performance of AORMS was compared to that of endoscopists in the development set and evaluated in the independent testing set. AORMS outperformed endoscopists by > 20% in diagnosing small gastric GISTs[9]. A computed tomography scan of the abdomen and pelvis is necessary for assessment of the size of the mass, regional lymphadenopathy (although uncommon with GIST) and local extraluminal abutment associated with these tumors. The characteristic biomarkers associated differentiating these tumors from other mesenchymal tumors of the gastrointestinal tract include immunochemistry markers positive for c-KIT (CD117), discovered on GIST 1 (DOG 1), and smooth muscle actin[3-5].

Esophageal GISTs are subepithelial tumors and out of reach of conventional biopsy forceps and pose a diagnostic challenge for gastroenterologists. Standard upper endoscopy is inadequate, making EUS essential for a comprehensive assessment[7-9]. EUS is indispensable in diagnosing and managing subepithelial gastrointestinal tumors. It provides detailed imaging, enables guided biopsy, aids in risk assessment, and helps guide treatment decisions. EUS provides accurate tumor sizing and delineates tumor borders with high resolution, which is critical for risk stratification and treatment planning. EUS is useful to confirm the layer of origin, as these tumors arise from the muscularis propria or submucosa which is typical for GISTs. Benign small tumors are generally hypoechoic with well-delineated borders.

Heterogeneous echotexture may indicate necrosis or malignancy. Use of contrast-enhanced EUS has demonstrated the ability to differentiate GISTs with early and clear enhancement from leiomyomas that displays little or no enhancement[6,10].

EUS-fine needle aspiration (FNA) enables histological and immunohistochemical analysis [CD117, discovered on GIST (DOG-1) *etc.*] to confirm the diagnosis. However, some studies have demonstrated that EUS-FNA tissue acquisition does not reliably reflect the mitotic index and GIST proliferation[11]. Smaller lesions (< 2 cm) have a poor diagnostic yield with EUS-FNA. Biopsy is generally not necessary for smaller tumors as it may lead to capsule disruption and tumor spread and it may be feasible to proceed immediately with endoscopic resection for histological diagnosis. Pre-resection EUS, however, will help assess tumor size and depth. Resection of small subepithelial lesions of ≤ 2 cm can be accomplished *en bloc* with an endoscopic cap band mucosectomy device[6,7].

If FNA is inconclusive, EUS-guided core biopsy may be needed. It is especially useful when distinguishing GISTs from other submucosal lesions such as leiomyomas, schwannomas and malignant sarcomas. For larger lesions, tissue diagnosis is necessary. For larger lesions of the fourth hypoechoic layer, EUS-FNA and core biopsy are safe and have a good diagnostic yield. EUS features, suggestive of high malignant potential include heterogeneous mass with irregular borders, ulceration of overlying mucosa, size > 5 cm, and presence of enlarged lymph nodes[7].

Management modalities

The primary treatment for localized esophageal GIST < 3 cm is surgical resection with a disease-free, 1-mm margin, *i.e.*, R0 resection. In carefully selected patients this may be accomplished by endoscopic enucleation as is demonstrated by Xu *et al*, with optimal results and excellent prognosis[1]. Larger lesions may pose a significant problem due to their location and abutment into the periesophageal tissues and organs and require a careful multidisciplinary approach. Minimally invasive approaches, *i.e.*, robotic-assisted abdominal laparoscopy or thoracoscopy, can be considered for resection. There is no indication routinely to perform lymph node dissection, as most GISTs do not metastasize to lymph nodes with the possible exception of some succinate-dehydrogenase-deficient GISTs, which may metastasize to lymph nodes. Esophagectomy is usually not necessary; however, it may be required if the tumor is larger and does not respond to neoadjuvant therapy[4,5,7]. Targeted therapy with TKIs is necessary as first-line treatment for unresectable, metastatic, or high-risk GISTs. Imatinib (400 mg daily orally for 6 months) is most commonly used to shrink large locally invasive tumors and make them amenable for resection. However, there remains a proportion of patients with tumors resistant to imatinib and other newer second- and third-generation TKIs are recommended, *i.e.*, sunitinib and regorafenib, respectively, as well as the new broad-spectrum TKI ripretinib[4,5].

Prognosis

The prognosis of esophageal GIST depends on several factors, including tumor size, mitotic index, nongastric site, tumor rupture and presence of metastases[4]. Esophageal GISTs are rare and tend to have a worse prognosis compared to GISTs from other parts of the gastrointestinal tract. The prognosis depends on several factors, including tumor size, mitotic rate, molecular mutations, and resectability. In general, smaller tumors < 2 cm with a low mitotic index have an excellent prognosis after complete resection. Tumor size (≥ 10 cm) and high mitotic rate (> 5/5 mm^2) with deletion mutation in KIT exon 11 involving codons 557–558 and a positive microscopic margin are associated with increased risk for recurrence and metastasis[12]. *KIT*/*PDGFRA* mutations may influence response to therapy. Some *PDGFRA* mutations are resistant to imatinib. For large tumors with a high mitotic index, adjuvant therapy with imatinib 400 mg daily for 3 years is recommended to reduce recurrence[3,5,7]. The 5-year survival rates vary; for localized disease (completely resected, small tumors with low mitotic index) it is greater than 70%–80%. For higher risk features, *i.e.*, large tumors with high mitotic index, the 5-year survival decreases to 30%–50%, while for metastatic or unresectable tumors, the survival is < 20%. The overall 5-year disease-free survival and disease-specific survival were 65.1% and 65.9%, respectively[13]. Surveillance with computed tomography scan or magnetic resonance imaging is recommended every 6 mo to yearly for 5 years[3,5,7].

Conclusion

Esophageal GIST is a rare type of mesenchymal tumor. Esophageal GISTs account for < 1% of all GISTs. Endoscopic resection remains the mainstay for small, localized tumors, with excellent outcomes. EUS is a useful tool in the diagnosis, staging and management of esophageal GIST. Given the submucosal nature of these tumors, standard endoscopy is inadequate, making EUS essential for a comprehensive assessment. EUS provides accurate tumor sizing, and enables FNA-guided biopsy for carefully selected large inoperable tumors or where diagnosis is in doubt, which is critical for risk stratification and treatment planning.

FOOTNOTES

Author contributions: Shenoy S designed the overall concept and outline of the manuscript and the writing, discussion, editing the manuscript, and review of literature.

Conflict-of-interest statement: The author reports no relevant conflicts of interest for this article.

Country of origin: United States

ORCID number: Santosh Shenoy 0000-0001-6117-1151.

S-Editor: Wei YF
L-Editor: Kerr C
P-Editor: Zhao S

REFERENCES

1 **Xu EP**, Qi ZP, Zhang JW, Li B, Ren Z, Cai MY, Cai SL, Lv ZT, Chen ZH, Liu JY, Zhong YS, Zhou PH, Shi Q. Endoscopic treatment outcome of oesophageal gastrointestinal stromal tumours. *World J Gastroenterol* 2025; **31**: 102393 [PMID: 40093666 DOI: 10.3748/wjg.v31.i10.102393]

2 **Menon L**, Buscaglia JM. Endoscopic approach to subepithelial lesions. *Therap Adv Gastroenterol* 2014; **7**: 123-130 [PMID: 24790643 DOI: 10.1177/1756283X13513538]

3 **Shenoy S**. Small bowel sarcoma: Tumor biology and advances in therapeutics. *Surg Oncol* 2015; **24**: 136-144 [PMID: 26278844 DOI: 10.1016/j.suronc.2015.08.002]

4 **Blay JY**, Kang YK, Nishida T, von Mehren M. Gastrointestinal stromal tumours. *Nat Rev Dis Primers* 2021; **7**: 22 [PMID: 33737510 DOI: 10.1038/s41572-021-00254-5]

5 **Judson I**, Jones RL, Wong NACS, Dileo P, Bulusu R, Smith M, Almond M. Gastrointestinal stromal tumour (GIST): British Sarcoma Group clinical practice guidelines. *Br J Cancer* 2025; **132**: 1-10 [PMID: 38840030 DOI: 10.1038/s41416-024-02672-0]

6 **Costa F**, Casaca R, Monteiro C, Ramos P. Oesophageal GIST. *BMJ Case Rep* 2020; **13**: e238058 [PMID: 33130586 DOI: 10.1136/bcr-2020-238058]

7 **Franco MC**, Schulz RT, Maluf-Filho F. Opinion: How to manage subepithelial lesions of the upper gastrointestinal tract? *World J Gastrointest Endosc* 2015; **7**: 1262-1267 [PMID: 26675266 DOI: 10.4253/wjge.v7.i18.1262]

8 **Dong Z**, Zhao X, Zheng H, Zheng H, Chen D, Cao J, Xiao Z, Sun Y, Zhuang Q, Wu S, Xia J, Ning M, Qin B, Zhou H, Bao J, Wan X. Efficacy of real-time artificial intelligence-aid endoscopic ultrasonography diagnostic system in discriminating gastrointestinal stromal tumors and leiomyomas: a multicenter diagnostic study. *EClinicalMedicine* 2024; **73**: 102656 [PMID: 38828130 DOI: 10.1016/j.eclinm.2024.102656]

9 **Cai M**, Song B, Deng Y, Gao P, Cai S, Yalikong A, Xu E, Zhong Y, Yu J, Zhou P. Automatically optimized radiomics modeling system for small gastric submucosal tumor (<2 cm) discrimination based on EUS images. *Gastrointest Endosc* 2024; **99**: 537-547.e4 [PMID: 37956896 DOI: 10.1016/j.gie.2023.11.006]

10 **Pesenti C**, Bories E, Caillol F, Ratone JP, Godat S, Monges G, Poizat F, Raoul JL, Ries P, Giovannini M. Characterization of subepithelial lesions of the stomach and esophagus by contrast-enhanced EUS: A retrospective study. *Endosc Ultrasound* 2019; **8**: 43-49 [PMID: 30264741 DOI: 10.4103/eus.eus_89_17]

11 **Ricci R**, Chiarello G, Attili F, Fuccio L, Alfieri S, Persiani R, Di Pietro S, Martini M, Costamagna G, Larocca LM, Larghi A. Endoscopic ultrasound-guided fine needle tissue acquisition biopsy samples do not allow a reliable proliferation assessment of gastrointestinal stromal tumours. *Dig Liver Dis* 2015; **47**: 291-295 [PMID: 25596931 DOI: 10.1016/j.dld.2014.12.011]

12 **Kang G**, Kang Y, Kim KH, Ha SY, Kim JY, Shim YM, Heinrich MC, Kim KM, Corless CL. Gastrointestinal stromal tumours of the oesophagus: a clinicopathological and molecular analysis of 27 cases. *Histopathology* 2017; **71**: 805-812 [PMID: 28644569 DOI: 10.1111/his.13292]

13 **Feng F**, Tian Y, Liu Z, Xu G, Liu S, Guo M, Lian X, Fan D, Zhang H. Clinicopathologic Features and Clinical Outcomes of Esophageal Gastrointestinal Stromal Tumor: Evaluation of a Pooled Case Series. *Medicine (Baltimore)* 2016; **95**: e2446 [PMID: 26765432 DOI: 10.1097/MD.0000000000002446]

World Journal of Gastroenterology

Submit a Manuscript: https://www.f6publishing.com

World J Gastroenterol 2025 May 21; 31(19): 108304

DOI: 10.3748/wjg.v31.i19.108304

ISSN 1007-9327 (print) ISSN 2219-2840 (online)

CORRECTION

Correction to "CMA down-regulates p53 expression through degradation of HMGB1 protein to inhibit irradiation-triggered apoptosis in hepatocellular carcinoma"

Jing-Hua Wu, Zhi-Yong Yuan

Specialty type: Gastroenterology and hepatology

Provenance and peer review: Unsolicited article; Externally peer reviewed.

Peer-review model: Single blind

Peer-review report's classification

Scientific Quality: Grade B

Novelty: Grade B

Creativity or Innovation: Grade B

Scientific Significance: Grade B

P-Reviewer: Kotlyarov S

Received: April 10, 2025

Revised: April 17, 2025

Accepted: April 25, 2025

Published online: May 21, 2025

Processing time: 41 Days and 2.7 Hours

Jing-Hua Wu, Medical Laboratory, Tangshan Maternal and Child Health Care Hospital, Tangshan 063000, Hebei Province, China

Zhi-Yong Yuan, Department of Radiotherapy, Tianjin Medical University Cancer Institute and Hospital, National Clinical Research Center for Cancer, Key Laboratory of Cancer Prevention and Therapy, Tianjin's Clinical Research Center for Cancer, Tianjin 300000, China

Corresponding author: Zhi-Yong Yuan, Professor, Department of Radiotherapy, Tianjin Medical University Cancer Institute and Hospital, National Clinical Research Center for Cancer, Key Laboratory of Cancer Prevention and Therapy, Tianjin's Clinical Research Center for Cancer, Huanhu West Road, Tianjin 300000, China. zhiyong0524@163.com

Abstract

Correction to "CMA down-regulates p53 expression through degradation of HMGB1 protein to inhibit irradiation-triggered apoptosis in hepatocellular carcinoma. *World J Gastroenterol* 2017; 23: 2308-2317 [PMID: 28428710 DOI: 10.3748/wjg.v23.i13.2308]". Due to the high number of images, the Tubulin bands intended for Figure 2D were incorrectly stored in the folder for Figure 3D, resulting in the wrong image being used for the Tubulin bands in Figure 3D.

Key Words: Correction; *World Journal of Gastroenterology*

Core Tip: This manuscript is to add a correction note to "CMA down-regulates p53 expression through degradation of HMGB1 protein to inhibit irradiation-triggered apoptosis in hepatocellular carcinoma. *World J Gastroenterol* 2017; 23: 2308-2317 [PMID: 28428710 DOI: 10.3748/wjg.v23.i13.2308]".

Citation: Wu JH, Yuan ZY. Correction to "CMA down-regulates p53 expression through degradation of HMGB1 protein to inhibit irradiation-triggered apoptosis in hepatocellular carcinoma". *World J Gastroenterol* 2025; 31(19): 108304
URL: https://www.wjgnet.com/1007-9327/full/v31/i19/108304.htm
DOI: https://dx.doi.org/10.3748/wjg.v31.i19.108304

CORRECTION

In this correction, we wish to address an error identified in our published manuscript titled "CMA down-regulates p53 expression through degradation of HMGB1 protein to inhibit irradiation-triggered apoptosis in hepatocellular carcinoma" in the *World Journal of Gastroenterology*[1].

During figure preparation, the Tubulin bands intended for Figure 2D were inadvertently misplaced in the folder for Figure 3F, resulting in an incorrect image being used for the Tubulin bands in Figure 3F. This error arose solely from image misplacement and does not affect the scientific validity or conclusions of the paper. Additionally, Figure 3D and 3F derive from the same experimental batch (HMGB1 knockdown). For clarity, Figure 3D (Clone formation assay after HMGB1 knockdown) includes HMGB1 and Tubulin bands, which are also shown in Figure 3F (see Figure 1 in this correction). Similarly, Figure 2D and Figure 4A originate from the same experiment (LAMP-2a knockdown), in which the expression levels of p53, p21, HMGB1, and Tubulin proteins were simultaneously detected by Western blot. To more clearly present our findings, we separately display the relevant protein expression results in Figures 2D and 4A (Figure 2D: Changes in p53 and p21 protein levels after LAMP-2a knockdown; Figure 4A: Changes in HMGB1 protein levels after LAMP-2a knockdown).

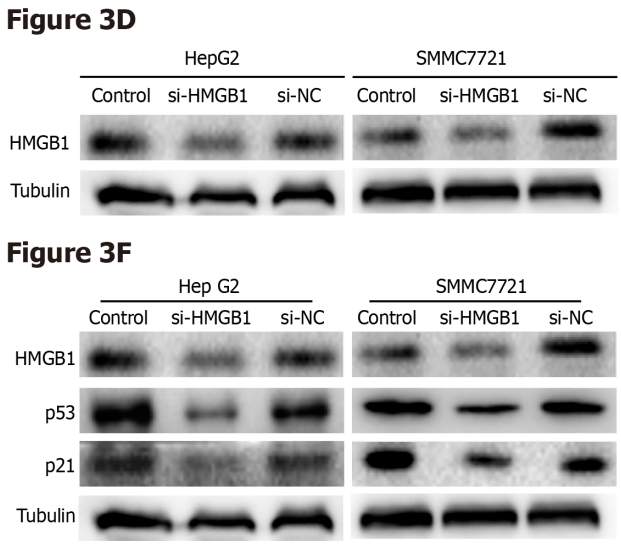

Figure 1 Corrected Figure 3D and F. A: Corrected Figure 3D; B: Corrected Figure 3F.

We apologize for the error in our published article[1]. However, we believe that this correction ensures the accuracy and integrity of the paper.

FOOTNOTES

Author contributions: All authors drafted and revised this correction.

Conflict-of-interest statement: We have no conflict of interest to disclose.

Country of origin: China

ORCID number: Jing-Hua Wu 0000-0002-0811-784X; Zhi-Yong Yuan 0000-0002-4745-6895.

S-Editor: Liu H
L-Editor: Wang TQ
P-Editor: Zhao S

REFERENCES

1 **Wu JH**, Guo JP, Shi J, Wang H, Li LL, Guo B, Liu DX, Cao Q, Yuan ZY. CMA down-regulates p53 expression through degradation of HMGB1 protein to inhibit irradiation-triggered apoptosis in hepatocellular carcinoma. *World J Gastroenterol* 2017; **23**: 2308-2317 [PMID: 28428710 DOI: 10.3748/wjg.v23.i13.2308]

Published by **Baishideng Publishing Group Inc**
7041 Koll Center Parkway, Suite 160, Pleasanton, CA 94566, USA
Telephone: +1-925-3991568
E-mail: office@baishideng.com
Help Desk: https://www.f6publishing.com/helpdesk
https://www.wjgnet.com